

IR 1997



INDEPENDENT RESEARCH 1997 ANNUAL REPORT

SPAWAR



*Systems Center
San Diego*

TECHNICAL DOCUMENT 2987
April 1998

Independent Research 1997 Annual Report

Approved for public release;
distribution is unlimited.



Space and Naval Warfare Systems Center
San Diego, CA 92152-5001

CONTENTS

INTRODUCTION	3
FY 97 TRANSITIONED PROJECTS	5
Faster-Than-Real-Time Synthetic Forces Simulation	7
Broadband-Fiber-Source Power and Spectrum Dependence on Reflectance and Filter Properties	7
Constant Envelope Modulation Techniques for UHF SATCOM	8
Stochastic Resonance Detectors	8
SELECTED INDEPENDENT RESEARCH PROJECTS	11
Enhanced Magnetic Signal Detection by Using Stochastic Resonance in a Radio Frequency (rf) Superconducting Quantum Interference Device (SQUID)	13
Decision Theory Augmented by Natural Event Metrics with Applications to Data Fusion	29
Performance Analysis of Multichannel Adaptive Equalization (MAEQ) for Line-of-Sight Digital Radio	49
ACCOMPLISHMENTS AND IMPACTS	57
Fiber-Optic Device Research	59
Matched-Field Acoustic Processing for Antisubmarine Warfare	61
Bioluminescence as a Flow Diagnostic	62
PROJECT SUMMARIES	63
COMMAND AND CONTROL	65
Enhancing SmartNet for Scheduling Network Traffic	67
Important Perceptual Features for Speaker Identity	68
Faster-Than-Real-Time Synthetic Forces (FTRT SF) Simulation	71
Reflective Memory on Standard Local Area Networks	74
COMMUNICATIONS	77
Resonantly Enhanced EHF Optoelectronic Transceiver Components	79
H^∞ Waves: A New Approach to Estimating Electromagnetic Fields	82
Algebraic-Geometric Error Control Coding for Improved Performance of Naval High-Data-Rate Line-of-Sight and Satellite Communications Systems	85
Constant Envelope Modulation Techniques for UHF SATCOM	89

SURVEILLANCE	93
Generalized Higher Order Crossings Theory and Practice	95
Array Processing with Three-Dimensional Bathymetry	98
Inverse Synthetic Aperture Radar (ISAR) Scatter Location for Complex Targets via Direction-Finding/Beamforming Methods	101
Active Matched-Field Tracking	104
Acoustic Data Analysis Using Fourth-Order Cumulants	106
Impulsive Snap-through Acoustic Projector (ISnAP)	111
Solid-State Blue Laser Development	115
High-Modulation-Rate, Solid-State Surveillance Laser	119
OTHER LEADERSHIP AREAS	121
Development of Ultramicroelectrode (UME) Arrays for Use in a Remote Probe	123
Investigation of Shallow Momentumless Wakes	126
Exact Diagonalization of Many Body Hamiltonians	129
Sparse Complete Orthogonal Factorization as Applied to Bistatic Target-Strength Prediction	131
Segmentation of Independent Motion via Pattern Recognition of Motion Flow in the Log-Polar Transformed Domain	135
Broadband-Fiber-Source Power and Spectrum Dependence on Reflectance and Filter Properties	137
Propwash/Wake Resuspension in San Diego Bay—The Grand Plan	140
Surface-Plasmon, Flat-Panel Display	142
Biosonar Ensonification of Buried Mines	145
Computational Modeling of Sediment Resuspension	147
PUBLICATIONS AND PRESENTATIONS	151
REFEREED JOURNALS, BOOKS/CHAPTERS, AND DISSERTATIONS (PUBLISHED/ACCEPTED)	153
Refereed Journals	153
Books/Chapters	154
REFEREED JOURNALS, BOOKS/CHAPTERS, AND DISSERTATIONS (SUBMITTED)	155
SSC SAN DIEGO (FORMERLY NRaD) PUBLICATIONS	155
PRESENTATIONS TO PROFESSIONAL MEETINGS	156

HONORS AND AWARDS	161
PATENT ACTIVITY	167
INDEPENDENT RESEARCH	
Patents Issued	169
Statutory Invention Registration (SIR) Issued	171
Claims Allowed; Notice of Allowance	171
Patent Applications Filed	172
Invention Disclosures Authorized	176
Invention Disclosures Submitted	177
INDEPENDENT EXPLORATORY DEVELOPMENT	
Claims Allowed; Notice of Allowance	181
Patent Applications Filed	181
PROJECT TABLES	183
NRaD (now SSC San Diego) FY 97 Independent Research Database	185
SSC San Diego FY 98 Independent Research Database	188
GLOSSARY	191

INTRODUCTION

INTRODUCTION

New and innovative ideas proposed by the scientists and engineers of the Space and Naval Warfare (SPAWAR) Systems Center, San Diego (SSC San Diego)* are supported and encouraged through the Independent Research (IR) Program, which is sponsored by the Office of Naval Research (ONR). The IR program is implemented at SSC San Diego under the authority of the Deputy Executive Director for Science, Technology, and Engineering and managed by the Science and Technology Office. This program supports basic research in several areas of interest to the Navy, including command and control, communications, surveillance, and navigation.

The FY 97 IR projects were selected under the direction of the Deputy for Science, Dr. Alan Gordon. The program began with the March 1996 call for proposals in four IR Thrust Areas. These areas are Command and Control, Communications, Surveillance, and Other Leadership Areas. Scientists and engineers responded with 81 written proposals. These proposals were screened for scientific merit and Navy relevance and then evaluated by panels of experts. These panels included Dr. Gordon, line management for each principal investigator, SSC San Diego technical experts, faculty members from local universities, and visiting professors on the ONR–ASEE (American Society for Engineering Education) Summer Faculty Research Program. Based on evaluations by these panels and an administrative review, 29 projects were selected. Total funding of \$2,521K was available for the FY 97 IR Program. Dr. Gordon retired in October 1996, and Dr. Eric Hendricks became the SSC San Diego IR Program Manager. Continuation of the FY 97 program was coordinated by Dr. Larry Flesner under the direction of Dr. Hendricks.

This report contains tables that provide information on active and multisponsored projects and lists of publications and patents. Although the Independent Exploratory Development (IED) program terminated at the end of FY 93, this report includes information on patents that resulted from the IED program after the FY 94 report. The bulk of this report contains short descriptions of the FY 97 IR projects that highlight their objectives and accomplishments. In addition, three IR projects are featured with more detailed descriptions. The featured projects were selected based on the exemplary results obtained.

The three featured projects are:

“Magnetic Signal Detection by Using Stochastic Resonance in a Radio Frequency (rf) Superconducting Quantum Interference Device (SQUID),” by A. R. Bulsara and M. E. Inchiosa. The authors studied the detection of very weak direct current (dc) or cyclic magnetic signals via a single-junction rf SQUID by using variants of the stochastic resonance (SR) effect.

“Decision Theory Augmented by Natural Event Metrics with Applications to Data Fusion,” by I. R. Goodman and G. F. Kramer. This project considered the extension of the standard theory of decision making (ETDM) with emphasis on hypotheses testing to include the testing for similarity of disparate probability-functional models. Applications to data-fusion problems were exhibited, and basic numerical experiments were conducted verifying the potential for significant increase of efficiency when ETDM is employed compared to standard approaches.

*Formerly Naval Command, Control and Ocean Surveillance Center (NCCOSC) RDT&E Division (NRaD).

“Performance Analysis of Multichannel Adaptive Equalization (MAEQ) for Line-of-Sight Digital Radio,” by M. Reuter. An MAEQ structure was analyzed for conditions common to the line-of-sight digital radio environment of interest to the Navy. The goal was to improve digital radio receiver performance over traditional single-antenna receivers.

Fiscal Year	Independent Research					Independent Exploratory Development				
	93	94	95	96	97	93	94	95	96	97
Funding (\$K)	2,278	2,312	2,463	2,763	2,521	834	—	—	—	—
Number of projects	27	28	29	31	29	12	—	—	—	—
Professional work-years	15	14	15.3	15.6	14.5	7	—	—	—	—
Refereed journals, books, and dissertations (published/accepted)	26	13	26	19	19	2	—	—	—	—
Refereed journals, books, and dissertations (submitted)	N/A	10	9	9	10	N/A	—	—	—	—
NRaD/SSC San Diego publications	5	5	3	4	2	3	1	—	—	—
Presentations to professional meetings	66	25	60	38	50	6	—	—	—	—
Patents issued	4	7	5	6	7	6	3	2	—	—
Statutory Invention Registration	—	—	—	—	1	—	—	—	—	—
Claims allowed, pending issue	—	2	2	—	2	4	—	—	3	2
Patent applications filed	14	6	6	11	12	7	5	4	2	2
Invention disclosures authorized	4	—	5	6	4	2	1	1	1	—
Invention disclosures submitted	—	7	7	7	10	—	1	—	—	—
Percent of completed projects transitioned	36	25	54	24	25	10	—	—	—	—

FY 97 TRANSITIONED PROJECTS

Faster-Than-Real-Time Synthetic Forces Simulation

Principal Investigator: Jeffrey Wallace

The purpose of SSC San Diego project number ZU38 was to investigate software architectures for realistic, very high speed computer simulation of military forces. The goal was to achieve simulation speeds that exceed real-time simulation (i.e., simulation time equal to physical time). This process is referred to as faster-than-real-time simulation (e.g., execution of 2 days of simulation time within a period of several hours).

The main accomplishment of the project was the identification of two software architectures and a single software abstraction layer that achieve the desired goal of faster-than-real-time simulation of realistic military forces and equipment. This objective was accomplished at both the electronic-circuit level for military equipment and at the theater level for military forces. These capabilities have been demonstrated and accepted for transition into fleet programs.

The primary transition of this work has been to the Joint Simulation System (JSIMS). JSIMS is a \$600M program and is currently the largest military-forces simulation program. The simulation architecture identified by this IR work has been adopted for use in the JSIMS program. SSC San Diego received \$6.8M in FY 98 funds under the JSIMS program.

The simulation architectures identified by this IR project have also been adopted for use in two 6.3 projects sponsored by the Director, Defense Research and Engineering (DDR&E) High-Performance Computing Modernization Program (HPCMP). These projects are the Forces Modeling and Simulation for Training; and the High-Performance, High-Level Architecture Runtime Infrastructure projects. The funding amounts for these projects at SSC San Diego are \$1.2M in FY 98, \$1.4M in FY 99, and \$700K in FY 00.

Broadband-Fiber-Source Power and Spectrum Dependence on Reflectance and Filter Properties

Principal Investigator: Richard Orazi

SSC San Diego project number ZU49 was an investigation of rare-earth doped optical-fiber light sources. A goal of the project was to devise novel methods to improve performance. Optical-fiber sources are the most promising light source for interferometric fiber-optic gyroscopes (IFOGs). Because of high sensitivity, physical robustness, and potential low cost, IFOGs are a leading candidate for next-generation tactical- and navigation-grade gyroscopes for a wide variety of military and civilian systems.

A key component for IFOGs is the optical source. Requirements for the optical source are high power, wide spectrum, wavelength stability, low cost, and small size. Rare-earth doped optical-fiber amplified spontaneous emission (ASE) sources are the most promising technology to achieve these requirements. However, a current limitation of ASE sources is inadequate wavelength stability, particularly as affected by temperature. The instability results primarily from gain competition

between emission wavelength peaks and can be substantially mitigated by implementation of an optical filter in the ASE source. A major achievement of this project was to demonstrate a simple, potentially low-cost optical filter based upon fused-fiber-coupler technology.

This IR project has transitioned by incorporation into an ongoing Defense Advanced Research Projects Agency (DARPA)-sponsored Manufacturing Technology (MANTECH) program for IFOGs. Due in part to early results from the IR project, SSC San Diego project number ET22 was established in FY 97. The project received \$100,000 in FY 97 and is expected to receive \$120,000 in FY 98. The DARPA program manager is Lt. Col. Beth Kaspar, DARPA/Sensor Technology Office (STO), (703) 696-2320, bkaspar@darpa.mil.

Constant Envelope Modulation Techniques for UHF SATCOM

Principal Investigator: Bruce Watkins

The original title of SSC San Diego project number ZU23 was “Adaptive Predistortion for the Linearization of RF Amplifiers.” The title was revised to reflect a change of direction in the research effort. The objective of this program was to investigate modulation techniques resistant to signal distortion caused by nonlinear amplifiers and communication channel effects.

Major accomplishments of this effort were the identification and development of novel combinations of pulse shape and code modulation that are highly resistant to the nonlinearities occurring in Ultra-High-Frequency Satellite Communications (UHF SATCOM) systems, thereby enabling a large increase in data-rate capabilities.

This project has transitioned by incorporation of results into a program sponsored by SPAWAR Systems Command to develop standards for Medium-Data-Rate UHF SATCOM systems. The program is directed by SPAWAR Code 176-3, LCDR Eric Lantto, (619) 524-7986, lanttoe@spawar.navy.mil. The program manager at SSC San Diego is Frank Tirpak, Jr., (619) 553-2526, ftirpak@spawar.navy.mil.

Modulation and waveform standards resulting from this project will also be integrated into a new SPAWAR Digital Modular Radio system as an option in FY 99. In addition, great interest in the improved modulation methods has been expressed by many Navy groups (including participants in the Information Technology for the 21st Century [IT-21] effort) seeking to achieve increased data rates to surface and subsurface combatants via acoustic as well as electromagnetic communication systems.

Stochastic Resonance Detectors

Principal Investigator: Adi Bulsara

SSC San Diego project number ZU03 was an investigation of novel signal-detection methods in Superconducting Quantum Interference Devices (SQUIDs) based on the phenomenon of stochastic resonance. A principal goal of this effort was to develop SQUID detectors that would be robust in the presence of high levels of background noise.

Although conventional SQUID magnetic detectors are highly sensitive, they have characteristics that severely limit their applications. One limitation is that conventional superconductors require

expensive cryogenic cooling apparatus, and a second limitation is that the “slew” rate, or ability to respond to rapidly varying fields, is restricted by the feedback system employed in radio-frequency modulated SQUIDs. Both of these limitations can potentially be circumvented by developing novel detection methods that exploit stochastic-resonance phenomena. A noise-robust SQUID could use high-temperature superconductors to alleviate the expense of cryogenic cooling. In addition, a noise-robust system could be used outside the shielded environments in which laboratory SQUID detectors are normally employed.

A principal accomplishment of this project has been to develop a SQUID detection scheme that shifts the detection of a low-frequency magnetic signal out of the $1/f$ noise regime, while maintaining high slew-rate capability. This accomplishment has enabled the project to transition into exploratory commercial development under a Naval Air Systems Command (NAVAIR)-sponsored Phase II Small Business Innovation Research (SBIR) program with Quantum Magnetics, Inc. The program manager at Quantum Magnetics is Dr. Andrew Hibbs.

SELECTED INDEPENDENT RESEARCH PROJECTS

Enhanced Magnetic Signal Detection by Using Stochastic Resonance in a Radio Frequency (rf) Superconducting Quantum Interference Device (SQUID)

A. R. Bulsara and M. E. Inchiosa

We study the detection of very weak direct current (dc) or cyclic magnetic signals via a single-junction radio frequency (rf) Superconducting Quantum Interference Device (SQUID) by using variants of the stochastic resonance (SR) effect. Two distinct regimes of operation of the SQUID are taken into account. For the SQUID in its hysteretic (or bistable) mode of operation, a weak dc target signal may be detected by pre-biasing the device with a known cyclic signal. The dc signal skews the potential energy function of the SQUID. In turn, the even harmonics of the cyclic signal appear in the output power spectral density. The spectral amplitudes of all the harmonics are found to exhibit maxima as functions of the noise intensity and the dc signal; the maxima can be shown to depend on matchings of characteristic deterministic and stochastic time scales. A phenomenological description based on a generic bistable system is followed by actual calculations of the first two spectral amplitudes for the hysteretic SQUID. This behavior underlies a recently proposed “frequency-shifting” technique for circumventing detector noise limitations that would otherwise constrain the detection of very-low-amplitude signals. When the SQUID is operated as a nonhysteretic device, the input–output transfer characteristic can be “tuned” via a control parameter to yield the optimal response to a cyclic or dc signal in the presence of fixed background noise. In both the non-hysteretic and hysteretic operating regimes, the theoretical calculations are found to be in excellent agreement with simulations and with experiments (carried out at Quantum Magnetics, Inc., under a Naval Air Systems Command [NAVAIR]-funded Phase II Small Business Innovation Research [SBIR]).

INTRODUCTION

Periodically modulated stochastic systems have received considerable attention recently [1]; these systems, which can generally be described by the “particle-in-potential” paradigm

$$\frac{dx}{dt} = -\frac{\partial U(x)}{\partial x} + S(t) + N(t),$$
 exhibit a richness of noise-mediated resonance behavior in the spectral measures (e.g., the output signal-to-noise ratio, [SNR]) of the response. In these systems, $S(t)$ and $N(t)$ denote a deterministic signal (often taken to be time-periodic) and noise (usually taken to be Gaussian). The potential function $U(x)$ is even (often bistable), resulting in an output power spectral density (PSD) consisting of *odd* multiples of the signal frequency, ω , superimposed on a Lorentzian noise background. Among the noise-mediated cooperative effects that can occur in such systems, stochastic resonance (SR) has received considerable attention lately.

Stochastic resonance is a cooperative phenomenon whereby small amounts of noise in a nonlinear dynamic system or sensor can enhance the response of the system to deterministic time-varying signals. The effect has been investigated for periodic signals in broadband noise; however, there are indications that it would work for more complex (aperiodic) signals. The hallmark of SR is a plot of the output SNR (measured at the fundamental of the applied frequency) vs. noise; this curve passes through a maximum at a critical value of noise—a value that can be calculated in terms of the system

and signal parameters. For signal-processing applications involving fixed noise, one may obtain the previously mentioned SNR enhancement by varying other system control parameters that are easier to adjust. It is important to state at the outset that SR *cannot* (at least for the simple case of a known signal in broadband noise) deliver an output SNR in excess of the input. It may, however, enhance the detectability of signals under certain conditions. For more complex signals, SR may provide a valuable signal-processing tool; however, little or no research has been carried out in this area.

However, real-world nonlinear dynamic systems are often asymmetric, with the dynamics containing even and odd functions of the state variable. The simplest route to asymmetry in the above dynamics is to incorporate a small dc term x_0 into the signal $S(t)$ or, equivalently, a term $-xx_0$ into $U(x)$. The output PSD of asymmetric systems contains contributions from *all* the harmonics of the periodic signal frequency; hence, the appearance and change in the magnitudes, as a function of x_0 , of peaks at even multiples of ω (this would, of course, be accompanied by a concomitant change in the spectral amplitudes at odd multiples) could be taken as quantifying measures of the asymmetry-producing signal. Asymmetric dynamic systems of the above form with Gaussian white noise have been studied [2]. The spectral amplitudes of the harmonics of the periodic signal, in the output PSD, pass through maxima as a function of noise intensity. It has been suggested that this behavior might be a manifestation of the well-known SR effect at higher orders [3].

For detection of static magnetic signatures (e.g., from mines or submarines), the idea introduced above provides a novel means of bypassing low-frequency noise limitations that constrain conventional sensors. The idea consists of biasing the detector (in this case, a single-junction rf Superconducting Quantum Interference Device [SQUID]) with a deterministic periodic magnetic signal of known amplitude, and known frequency, ω . This will lead to the usual SR effect wherein the SNR at the fundamental frequency, ω , passes through a maximum, and the PSD contains only the odd harmonics, ω , 3ω , 5ω , etc. Now, the dc signal that is to be detected is applied to the SQUID. This has the effect of making the potential asymmetric, and the even harmonics, 2ω , 4ω , etc., will appear in the output PSD. The strengths of these harmonics will be a function of the applied dc signal as well as the known signal of frequency, ω , and the SQUID parameters. So, a matched filter (for example), set to detect the second harmonic, 2ω , would effectively be detecting and determining the strength of the unknown dc signal. Note that by adjusting the system and reference signal parameters, the strength of this harmonic can also be made to pass through a maximum at a critical value of the applied noise, or some other control parameter. By setting the matched filter to detect the frequency 2ω and suitably selecting ω , we would effectively shift the detection out of the $1/f$ noise regime of the PSD.

In fact, for more complex operating scenarios, if a “clean” window is known to exist in a particular regime of the PSD, we can choose the reference frequency ω to carry out our detection in that window. This technique, which is impossible in a linear system, makes no attempt to eliminate low-frequency noise or to enhance the output SNR in the conventional sense; it merely shifts the detection to a more acceptable part of the frequency spectrum. It is clear, also, that this “nonlinear heterodyning” idea will work only if the low-frequency noise that constrains the sensor operation is uncorrelated with the signals of interest; this is often the case.

The above idea was tested in FY 95–96 laboratory experiments. It affords a novel technique that can be applied to SQUIDS (particularly high-temperature [HT] SQUIDS, which have higher levels of LF noise) as well as other nonlinear dynamic sensors (e.g., conventional fluxgate magnetometers) that

are noise-constrained. It is worth pointing out that recent experiments have shown that SR can, in fact, render SQUIDs far more robust to noise: Signals that are below the noise level and virtually undetectable by conventional SQUIDs can easily be detected and amplified by SQUIDs operating as SR devices. This has potentially important ramifications for HT SQUIDs, which have greater noise problems than their helium counterparts; it is now believed that SR offers a way to implement HT SQUIDs in practice. HT SQUIDs are far easier to operate and have less stringent cryogenic requirements than helium-cooled SQUIDs; hence, SR represents a means of further simplifying an extremely complex technology.

The goal of the Independent Research project was to mate the observations of the FY 95 experiment to a theory that could enhance our understanding of the physics of the problem and lead to detailed analyses of the performance of the sensor, under various operating scenarios of interest to specific application. In particular, the dependence of the output SNR on the internal sensor parameters was investigated; such “design” information is critical to the construction of the optimal sensor for a given application.

In this work, we outline a systematic treatment of the resonant behavior of the spectral amplitudes at $k\omega$ ($k = 1, 2, 3, \dots$). The resonant behavior depends on a new control parameter, the degree of asymmetry, and can be interpreted at all orders k , via a matching of deterministic and stochastic time scales reminiscent of recent interpretations of SR in integrate-fire model neurons [4] and bistable dynamic systems [5] as a *bona fide* resonance. We start with a purely deterministic phenomenological theory that shows the occurrence of multiple maxima in the spectral amplitudes in a generic asymmetric system; we then introduce characteristic stochastic time scales (these critically depend on the asymmetry, as well as the spectral characteristics of the noise) and argue that a precise and elegant matching of these time scales must occur for all k for there to be resonance behavior in the spectral amplitudes of the harmonics when the noise is turned on. The phenomenological development is followed by a theoretical computation of the first two spectral amplitudes ($k = 1, 2$) on a rf SQUID loop; results in line with recent experimental observations are obtained, and the resonance behavior as a function of the noise variance (for fixed asymmetry) is also discussed. The details of the calculations outlined in this report have been published in two recent journal articles [6, 7].

Finally, we note that SQUIDs may be operated as multistable, or hysteretic, devices (corresponding to a potential energy function that has well-defined maxima and minima), or as dispersive (i.e., nonhysteretic) devices, wherein the potential energy function is almost parabolic (i.e., it admits of a single global minimum); in the latter case, the dynamics are more easily characterized via an input-output transfer characteristic, whence the output PSD can be calculated. The transition of the SQUID from a hysteretic to nonhysteretic device occurs via a pitchfork bifurcation controlled by a “design parameter.” In a single-junction or rf SQUID, this parameter is fixed by the fabrication process and cannot be easily controlled in an experiment. However, recent calculations using a two-junction or dc SQUID have shown that an externally controllable parameter can control the bifurcation in this device. Experiments carried out using a dc SQUID yield a rich noise-mediated cooperative behavior in the output PSD and the SNR at the fundamental of an applied periodic signal. In the presence of an asymmetrizing dc bias, we obtain specific regimes where the output SNR is maximal, and other regimes where the SQUID performance is degraded. A calculation on a single-junction rf SQUID yields remarkably similar behavior, with the control parameter being the above-mentioned design

parameter. For simplicity, we confine our attention to the response at the fundamental only, although it is readily apparent that all the harmonics of the cyclic signal will appear in the output PSD. We outline the results of the calculation and note that it is always beneficial to operate the SQUID in the nonhysteretic regime where the spectral response is better than in the hysteretic regime, hence the importance of such a calculation. We also note that the calculation may be used to predict the response of the device to a cyclic or dc magnetic signal; we return to this point in the final section. Finally, we observe that the calculations and experiments using dc SQUIDS afford a means of “tuning” the stochastic resonance to achieve optimal signal-detection performance by using the externally controllable *deterministic* bias parameter; the noise level is *not* adjusted (it is the internal noise of the device). The bias parameter allows one to deform and adjust the transfer characteristic of the device, effectively optimizing its dynamic range to the signal and noise.

THE rf SQUID IN THE HYSTERETIC REGIME

Phenomenological Description

We start with a simple phenomenological model of a purely deterministic situation. Consider a periodic signal, $A \sin \omega t$, applied to a generic bistable potential, $U(x)$. The signal is assumed to be of amplitude barely sufficient to achieve switching between the two stable states of the potential, which we assume to be asymmetric. We shall be concerned only with the dichotomous output, $f(t)$, over a single period, T , of the signal, where we define

$$\begin{aligned} f(t) &= f_0 \quad 0 \leq t < \Theta \\ &= 0 \quad \Theta \leq t < T. \end{aligned} \quad (1)$$

Clearly, the residence times, Θ and $T - \Theta$, in the two stable states are functions of the asymmetry of the system: for a symmetric potential, $\Theta = T/2$. We now Fourier analyze $f(t)$:

$$f(t) = \frac{a_0}{2} + \sum_{k=1}^{\infty} \{a_k \cos k\omega t + b_k \sin k\omega t\}, \quad (2)$$

where we readily compute

$$\begin{aligned} a_0 &\equiv \frac{2}{T} \int_0^T f(t) dt = \frac{2f_0\Theta}{T} \\ a_k &\equiv \frac{2}{T} \int_0^T f(t) \cos k\omega t dt = \frac{f_0}{\pi k} \sin k\omega\Theta \\ b_k &\equiv \frac{2}{T} \int_0^T f(t) \sin k\omega t dt = \frac{f_0}{\pi k} (1 - \cos k\omega\Theta). \end{aligned}$$

Clearly, for a symmetric potential ($\Theta = T/2$), only the odd multiples of ω will be present. From the above expressions, the spectral amplitude at $k\omega$ is given by

$$M_k = \frac{f_0}{\pi k} \left[\sin^2 k\omega\Theta + (1 - \cos k\omega\Theta)^2 \right]^{1/2} = \frac{2f_0}{\pi k} \sin \frac{k\omega\Theta}{2}, \quad (3)$$

where we will be interested in the absolute value only. A plot (figure 1) of $|M_k|$ over the interval $T/2 \leq \Theta \leq T$ reveals multiple maxima with the number of maxima being $k/2$ and $(k+1)/2$ for even and odd k , respectively. The locations of these maxima are readily found from the condition $k\omega\Theta = n\pi$ (n odd). We observe that the fundamental ($k = 1$) has a single maximum for $\Theta = \Theta_1 = T/2$ corresponding to the symmetric case; the first harmonic ($k = 2$) has a single maximum for $\Theta = \Theta_2 = 3T/4$; the $k = 3$ harmonic has maxima at $\Theta = \Theta_3 = 5T/6, T/2$; the $k = 4$ harmonic at $\Theta = \Theta_4 = 7T/8, 5T/8$, and so on. Note (see figure 1) that the spectral amplitudes with odd k have a maximum at $\Theta = T/2$ (corresponding to the symmetric potential case), while ones with even k vanish in this case.

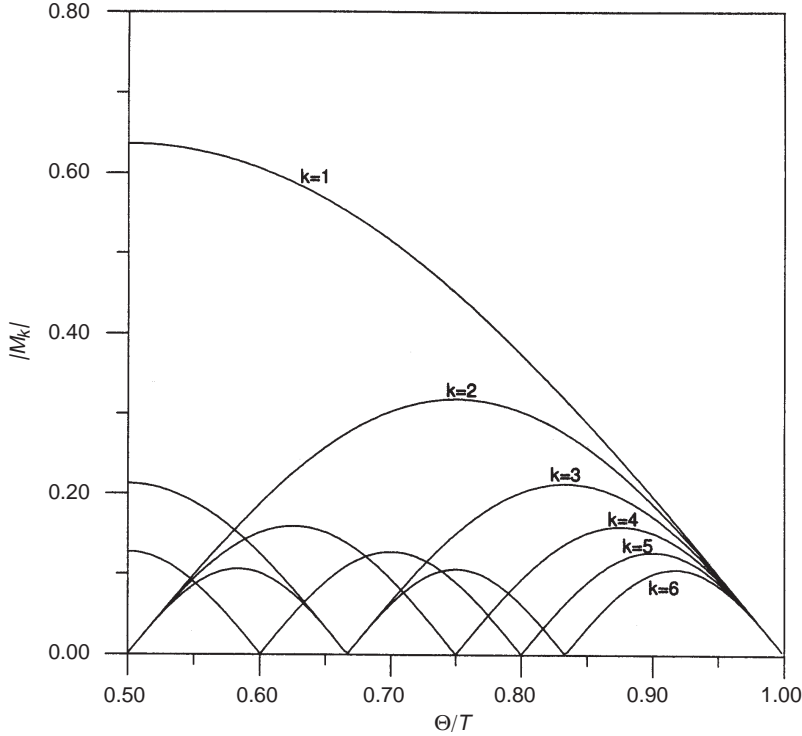


Figure 1. Spectral amplitudes at frequency $k\omega$, $k = 1, 2, \dots, 6$ in the output PSD for the purely deterministic case, as computed from the phenomenological theory (eqn. (3)) with $f_0 = 1$. The horizontal scale represents the degree of asymmetry as quantified by the ratio, Θ/T .

The extension to the noisy case is achieved by introducing the mean residence times, $\langle t_l \rangle$ and $\langle t_r \rangle$, in the left and right states of the potential (the left well has the shallower minimum). For convenience, these may be computed in the absence of the periodic signal; the presence of the signal affects these mean times only slightly [6] for weak signal amplitudes. We then postulate that to achieve a maximum in a given spectral amplitude, $|M_k|$, (assuming the output to be approximately periodic), we must achieve $\langle t_r \rangle = \Theta_k$ and $\langle t_l \rangle = T - \langle t_r \rangle$. For the first few harmonics, this yields immediately $\langle t_l \rangle = T/2 = \langle t_r \rangle$ for $k = 1$ (this is the classical frequency-matching condition for stochastic resonance), $\langle t_l \rangle = T/4$, and $\langle t_r \rangle = 3T/4$ for $k = 2$, etc. In fact, we find a precise matching of stochastic and deterministic time scales for every frequency $k\omega$ whenever the spectral amplitude $|M_k|$ possesses a maximum. At frequency $k\omega$, we may write the general conditions for these “resonances” as:

$$\langle t_l \rangle = \frac{nT}{k2}, \quad \langle t_r \rangle = T - \langle t_l \rangle, \quad \frac{\langle t_l \rangle}{\langle t_r \rangle} = \frac{n/2k}{1 - n/2k}, \quad (4)$$

where n is odd and $1 \leq n \leq k$. This leads to an elegant pattern of numbers which exposes a precise matching of stochastic (the mean residence times) and deterministic (the signal period) time scales that must exist to obtain the (multiple) resonances (as a function of asymmetry) at the frequencies $k\omega$ when the system is noisy. We now explore the resonance behavior in a specific system, the rf SQUID loop operated in the hysteretic regime.

The rf SQUID Loop

The standard rf SQUID loop is a superconducting loop into which a single Josephson junction has been inserted [7]. The dynamics are multistable with the magnetic flux through the superconducting loop being quantized in units of the flux quantum, $\Phi_0 \equiv h/2e$. In the presence of the junction, the magnetic flux Φ through the loop, in response to an applied time-dependent magnetic flux, Φ_ϵ , evolves according to the dynamics [7],

$$\left(LC \frac{d^2}{dt^2} + \tau_L \frac{d}{dt} + 1 \right) \frac{\Phi(t)}{\Phi_0} + \frac{\beta}{2\pi} \sin \frac{2\pi\Phi(t)}{\Phi_0} = \frac{\Phi_\epsilon(t)}{\Phi_0}, \quad (5)$$

where L and C are the loop inductance and capacitance, $\tau_L \equiv L/R_J$ (R_J being the normal state resistance of the junction), and the parameter $\beta \equiv 2\pi I_c / \Phi_0$ (I_c is the junction critical current) controls the hysteretic behavior of the device: The SQUID output is hysteretic for $\beta > 1$, i.e., the steady-state Φ vs. Φ_ϵ curves are multivalued. In most practical applications, the SQUID loop is shunted by a low resistance in order to remove hysteresis in the voltage-current characteristic of the junction [7]; this process effectively renders the link capacitance, C , extremely small so that the inertial term in (5) may be neglected. Transforming to the normalized state variable, $x(t) \equiv \Phi(t)/\Phi_0$, we may write the dynamics (5) in the ‘‘particle-in-a-potential’’ form

$$\tau_L \frac{dx}{dt} = - \frac{\partial U(x)}{\partial x} + n(t) + y(t), \quad (6)$$

where the potential function

$$U(x) = \frac{1}{2}(x - x_0)^2 - \frac{\beta}{4\pi^2} \cos 2\pi x \quad (7)$$

is multistable when $\beta > \beta_{sc}$, where $\beta_{sc} = 1$ for $x_0 = 0$. We have expressed the (normalized) external flux, Φ_ϵ/Φ_0 , as the sum of three terms: a symmetry-breaking dc term, x_0 , (which we incorporate into $U(x)$); an AC term, $n(t) = A \sin(\omega t + \theta)$ with θ being a (often-assumed random) phase factor; and a noise term, $y(t)$. Typically, the time constant $\tau_L \approx 10^{-12}$ seconds, so that with the exception of the (internal) thermal noise, which is assumed negligible for the purposes of this paper, any externally applied noise will usually have a bandwidth far smaller than the SQUID bandwidth, τ_L^{-1} . This is even more the case in experimental setups wherein a resistive shunt must often be placed across the SQUID to filter out high-frequency noise. The LR circuit formed by the shunt resistance and the loop inductance results in a low-pass filter that decreases the input noise bandwidth even further [8].

Hence, we must take $y(t)$ to be zero-mean Gaussian *exponentially correlated* noise; it may be modeled via a white-noise-driven Ornstein–Uhlenbeck (O–U) process [9]:

$$\frac{dy}{dt} = -\tau^{-1}y + \sigma F(t), \quad (8)$$

where $F(t)$ is zero-mean “white” noise with autocorrelation $\langle F(t)F(t+s) \rangle_t = \delta(s)$, and τ is the correlation time of the “colored” noise, $y(t)$. Then, one easily verifies [9] that $y(t)$ has zero mean and autocorrelation function $\langle y(t)y(t+s) \rangle_t = \langle y^2 \rangle e^{-|s|/\tau}$, whence the “white” limit, corresponding to delta-correlated noise, is realized when $\tau \rightarrow 0$. The colored noise has variance $\langle y^2 \rangle = \sigma^2\tau/2$ (we reiterate that $y(t)$ has units of normalized magnetic flux).

It is convenient to pre-bias the SQUID loop so that the potential (7), for $\beta > 1$, is centrally bistable with possible outlying metastable states. This is accomplished [8] by incorporating a dc bias $m/2$ (m odd) in the potential: We replace x_0 by $x_0 + m/2$. Assuming the signal and noise to be very slow compared to the well-relaxation time (the standard adiabatic assumption), we may incorporate the signal, $n(t)$, and the noise, $y(t)$, into the potential function, $U(x)$, as well, writing (6) in the form

$\tau_L \frac{dx}{dt} = -\frac{\partial U_\epsilon(x)}{\partial x}$ where the potential function U_ϵ is now given by

$$U_\epsilon(x(t)) = \frac{1}{2} \left(x - x_0 - \frac{m}{2} - y(t) - n(t) \right)^2 - \frac{\beta}{4\pi^2} \cos 2\pi x. \quad (9)$$

It is worthwhile to note that for the very small time constants, τ_L , that characterize real SQUIDs, the adiabatic assumption is expected to be a very good one, breaking down for input signals or input noise with power at very high frequencies (approaching τ_L^{-1}). The thermal background noise in the sensor is indeed broadband [7] but far smaller in magnitude than ambient environmental noise that limits practical SQUIDs. The environmental noise usually has a bandwidth less than τ_L^{-1} . As already stated, we neglect the thermal background noise throughout this work. Finally, we assume that the signal amplitude, A , is too weak to allow switching between the stable states of the potential to occur in the absence of the noise.

SR, defined in the conventional way via the maximum (as a function of input noise power) in the output power SNR at the fundamental frequency ω , has been observed in an experiment performed in 1992 [8]. Two separate experiments carried out in 1994 [10, 11] have observed such resonance behavior in the spectral amplitudes of higher harmonics (including the even ones) when the symmetry-breaking dc signal x_0 is present. Numerical simulations that determined the output power in the $k = 1 - 4$ harmonics of the SQUID model (6) were recently presented, along with an approximate theoretical computation of this output power for the $k = 1, 2$ harmonics [6]. Very good agreement was found between theory and numerical simulations. In what follows, we present a much fuller account of the theoretical calculation of the output power as well as new results that provide a guide for using the resonance behavior depicted in figure 1 in practical nonlinear dynamic devices.

We now outline (see [6] for details) an approximate theoretical calculation of the first two spectral amplitudes in the output PSD. We model the SQUID as a two-state system with a hysteretic input–output characteristic having state probabilities, $p_{1,2}(t)$, and master equations

$$\begin{aligned}\frac{\partial p_1}{\partial t} &= W_{21}(t)p_2(t) - W_{12}(t)p_1(t) \\ \frac{\partial p_2}{\partial t} &= W_{12}(t)p_1(t) - W_{21}(t)p_2(t),\end{aligned}\tag{10}$$

where $p_1 + p_2 = 1$, and $W_{ik}(t)$ denotes the transition rate from state i to state k . These rates are the approximate inverses of the mean passage times, $\langle t_l \rangle$ and $\langle t_r \rangle$, introduced earlier. The transition rates are computed by solving [9] the first passage problem for the O–U process (underpinning the noise) between the values y_{c1} and y_{c2} . We can write down [6],

$$W_{12}^{-1} \approx T_{12} = 2\sigma^{-2} \int_{y_{c2}}^{y_{c1}} \epsilon^{z^2/\sigma^2\tau} dz \int_{-\infty}^z \epsilon^{-z'^2/\sigma^2\tau} dz' = 2\tau \sqrt{\pi} \int_{u_{c2}}^{u_{c1}} \epsilon^{u^2} \Psi(u) du, \tag{11}$$

where we define

$$y_{c1,2} = x_{i1,2} - x_0 - \frac{m}{2} - n(t) + \frac{\beta}{2\pi} \sin 2\pi x_{i1,2} \tag{12}$$

and

$$\begin{aligned}\kappa_{i1} &= \frac{m-1}{2} + \frac{1}{2\pi} \cos^{-1}(-\beta^{-1}) \\ \kappa_{i2} &= \frac{m+1}{2} - \frac{1}{2\pi} \cos^{-1}(-\beta^{-1}).\end{aligned}\tag{13}$$

A corresponding expression may be obtained for W_{21} :

$$W_{21}^{-1} \approx T_{21} = 2\tau \sqrt{\pi} \int_{u_{c2}}^{u_{c1}} \epsilon^{u^2} \Psi(-u) du. \tag{14}$$

We have defined $\Psi(u) \equiv \frac{1}{2}[1 + \text{erf}(u)]$ and $u_{c1,2} \equiv y_{c1,2}/(\sigma\sqrt{\tau})$; further, we have, for later notational convenience, set $T_{12} \equiv \langle t_l \rangle$ and $T_{21} \equiv \langle t_r \rangle$. As expected, for $x_0 = 0$, we find $y_{c2} = -y_{c1}$ and $T_{12} = T_{21}$. The integrals in (11,14) may be expressed in terms of the imaginary error function $\text{erfi}(z) = \text{erf}(iz)/i$ and the generalized hypergeometric function ${}_pF_q(a_1, \dots, a_p; b_1, \dots, b_q; z)$:

$$\int_{u_{c2}}^{u_{c1}} \epsilon^{u^2} \Psi(\pm u) du = \left[\frac{1}{4} \sqrt{\pi} \text{erfi}(u) \pm \frac{{}_2F_2\left(1, 1; \frac{3}{2}, 2; u^2\right) u^2}{2\sqrt{\pi}} \right]_{u_{c2}}^{u_{c1}}.$$

To compute the PSD of the SQUID output, we must first solve the system (10) for the state probabilities $p_{1,2}(t)$. Then, the two-state dynamics that characterize the SQUID may be well-approximated by the global probability density function

$$P(x, t) \approx p_1(t) \delta(x - x_{10}) + p_2(t) \delta(x - x_{20}), \tag{15}$$

where $x_{1,20} \equiv x_{1,2}|_{A=0}$ are the locations of the minima of the *unperturbed* potential (7). The mean value $\langle x(t) \rangle$ is obtained from

$$\langle x(t) \rangle = \int x P(x, t) dx = x_{10} p_1(t) + x_{20} p_2(t). \quad (16)$$

A general solution of (10) is beyond the scope of this paper. However, we are interested in the spectral amplitudes of the first two peaks ($k = 1, 2$) in the output PSD. Accordingly, we are interested only in an expansion of $\langle x(t) \rangle$ to include terms up to second order (i.e., the $k = 2$ harmonic):

$$\langle x(t) \rangle = M_0 + M_1 \cos(\omega t + \phi_1) + M_2 \cos(2\omega t + \phi_2), \quad (17)$$

where $\phi_{1,2}$ are phases that may have random components, and the amplitudes, M_i , are as yet undetermined. The autocorrelation function of the output is

$$K(s) \equiv \langle \langle x(t)x(t+s) \rangle \rangle_t \rightarrow \frac{1}{T} \int_0^T \langle x(t) \rangle \langle x(t+s) \rangle dt \quad (18)$$

in the $s \rightarrow \infty$ limit, $T = 2\pi/\omega$ being the signal period. Using (17) we readily find

$$K(s) = M_0^2 + \frac{M_1^2}{2} \cos \omega s + \frac{M_2^2}{2} \cos 2\omega s, \quad (19)$$

so that the powers at the frequencies ω and 2ω in the output PSD are, respectively, $M_1^2/2$ and $M_2^2/2$.

We solve the system (10) after expanding the transition rates to $O(A^2)$. Specifically, we define $u_{c1,20} \equiv u_{c1,2}|_{n(t)=0}$ and set

$$u_{c1,2} = u_{c1,20} - \eta'(t), \quad \eta'(t) \equiv A' \sin(\omega t + \theta), \quad (20)$$

with $A' \equiv A/\sqrt{2y^2}$ being a natural (and convenient) perturbation expansion parameter; we expect the theory to be valid for $A' \ll 1$ and within the realm of the adiabatic approximation (see above). We now expand the transition rates as

$$\begin{aligned} W_{12} &\approx \alpha_0 + \alpha_1 \eta'(t) + \alpha_2 \eta'^2(t) \\ W_{21} &\approx \beta_0 + \beta_1 \eta'(t) + \beta_2 \eta'^2(t), \end{aligned} \quad (21)$$

the expansion coefficients being obtained through a straightforward expansion of the transition rates [6]. Once the coefficients have been obtained, the expansions (23) can be substituted into (10) and the integration formally carried out, whence we compute the quantities M_1 and M_2 .

In figures 2 and 3 we show the powers $M_1^2/2$ and $M_2^2/2$ in the first two peaks ($k = 1, 2$) in the output PSD as functions of the dc offset, x_0 , and the input noise parameter, σ^2 . The known signal amplitude is held constant, as is the SQUID nonlinearity parameter, β ; this results in a constant ratio, $A/\Delta U_0$, where ΔU_0 is the height of the potential barrier of the central bistability of our problem, in the absence of any skewing (i.e., for $x_0 = 0$). In $M_1^2/2$ (the SQUID output power at frequency ω), the

basic SR effect is readily visible: For $x_0 = 0$, the power displays a clear maximum as a function of the input noise power. The power in the first harmonic, $M_2^2/2$, vanishes as $x_0 \rightarrow 0$ as expected. However, for $x_0 \neq 0$, this power, like the power at the fundamental, displays a maximum as a function of the input noise power; also, a maximum is seen as a function of x_0 , and the location of this maximum depends on the noise power. The curves do not display a strong dependence on ω ; however, the adiabatic approach does require that $f \equiv \frac{\omega}{2\pi} \ll \tau^{-1}, \tau_L^{-1}$. It is important to note that the central bistable structure of the potential disappears for $x_0 = 1/2$; therefore, close to this point, the bistable model upon which our theoretical calculation is based begins to break down. Figures 2 and 3 may be compared with numerical simulations of the SQUID dynamics [6]; the agreement is excellent.

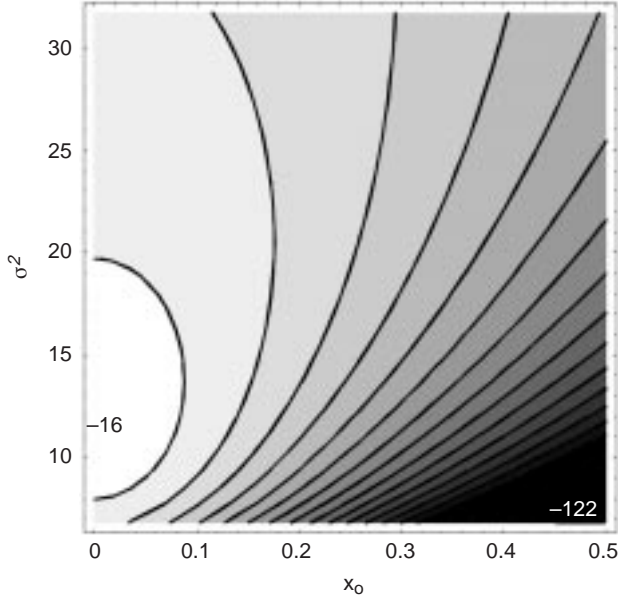


Figure 2. Contour plot of SQUID output power $M_1^2/2$ at the driving frequency ω vs. asymmetrizing dc signal x_0 and noise parameter (in units of sec^{-1}) σ^2 . Other parameters: $\beta = 5$, $A = 0.1$, $\omega = 10$, $\tau = 0.01$, $m = 1$. Numbers within contour plot mark the maximum and minimum power points (in dB).

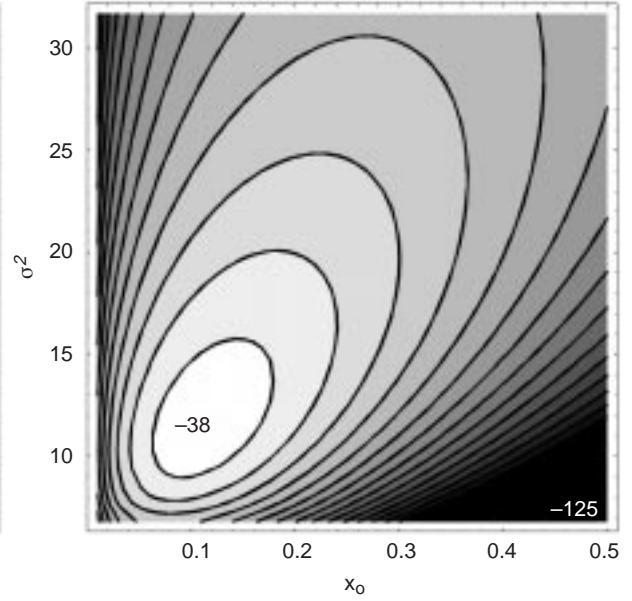


Figure 3. Contour plot of SQUID output power $M_2^2/2$ (in dB) at frequency 2ω vs. asymmetrizing dc signal x_0 and noise parameter (in units of sec^{-1}) σ^2 . Other parameters as in figure 2. Numbers within contour plot mark the maximum and minimum power points (in dB).

THE rf SQUID AS A “STATIC” NONLINEAR AND NONHYSTERETIC DEVICE

We now consider [14], the case $0 \leq \beta < 1$ for which the SQUID potential function is monostable (approaching a parabola, corresponding to linearity, as $\beta \rightarrow 0$). In this regime, we characterize the SQUID as a *non*-dynamical element, characterized by an input–output transfer characteristic; such a description is possible because of the large bandwidth (or the small time constant, τ_L , in (6)) of the device. As before, we assume an evolution equation $\tau_L \dot{x} = -U'(x) + x_\epsilon$ for the dimensionless magnetic flux, $x(t)$, in the loop. We apply an external magnetic flux, $x_\epsilon(t) = x_i(t) + x_0$, where x_0 is a dc bias flux and $x_i(t) \equiv A \cos(\omega_0 t + \phi_0) + y(t)$ represents an input signal consisting of a sine wave (with a random initial phase) plus noise $y(t)$ assumed to be exponentially correlated as defined in (8).

The SQUID output measured is the “shielding flux,” $x_s(t) \equiv x(t) - x_e(t)$. We obtain the quasi-static input–output transfer characteristic, $g(x_i(t)) = x_s(t)$, by setting $\tau_L \dot{x} = 0$ in the equation of motion and solving for x_s as a function of x_i . In the nonhysteretic regime ($0 \leq \beta < 1$), a Fourier–Bessel expansion has been obtained for x_s [7]:

$$g(x_i) = x_s = \lim_{n'_{\max} \rightarrow \infty} \sum_{n'=1}^{n'_{\max}} M_{n'}(\beta) \sin[2\pi n'(x_i + x_0)]; \quad (22)$$

$$M_{n'} \equiv \frac{(-1)^{n'}}{n'\pi} J_{n'}(n'\beta).$$

Figure 4 shows one period of the transfer characteristic, with $x_0 = 1/2$ (modifying x_0 simply translates the curve horizontally). Small ripples visible in the right half of the plot for $\beta = 1$ (solid curve) show the result of truncating (22) after 40 terms. We retained 200 terms when generating the smooth curves in the left half of the plot. The summation approaches the true transfer characteristic more quickly for lower β values. For $\beta = 0.5$ (dashed curve) the truncation error with 40 terms is less than 10^{-10} . As β is increased from 0 (not shown) to 1, the distance Δx_i from a minimum of the transfer characteristic to the next (higher x_i) maximum *decreases* linearly from 0.5 to 0.18. The minima and maxima heights vary linearly with β and vanish as $\beta \rightarrow 0$.

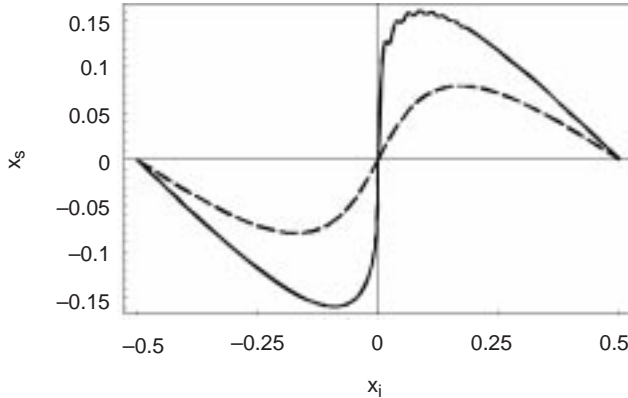


Figure 4. rf SQUID transfer characteristic $x_s = g(x_i)$ for $\beta = 0.5$ (dashed) and $\beta = 1$ (solid). Right half of plot calculated using $n'_{\max} = 40$, left half using $n'_{\max} = 200$. Bias flux $x_0 = 1/2$.

We compute the power spectral density via the second moment of the output, $\langle x_s(t)x_s(t + \tau) \rangle_t$. We then calculate the output SNR and display its maximization for the specific case of the SQUID loop; however, the properties we will discuss are generic to systems with similar transfer characteristics.

Applying Stratonovich’s general formula [15] for the second moment of a zero-memory nonlinear transformation of a sine wave plus Gaussian noise, we obtain

$$\begin{aligned} \langle x_s(t)x_s(t + \tau) \rangle_t &= \sum_{n=0}^{\infty} \sum_{k=0}^{\infty} \left[\frac{\sigma^n}{2\pi} \int_{-\infty}^{\infty} \int_{-\infty}^{\infty} g(x_i) \epsilon^{-ix_i \Omega} dx_i J_k(A\Omega) \epsilon^{-\sigma^2 \Omega^2 / 2} \Omega^n d\Omega \right]^2 \\ &\quad \frac{(-1)^{n+k}}{n!} \epsilon_k R^n(\tau) \cos(k\omega_o \tau), \end{aligned} \quad (23)$$

where $\epsilon_{k=0} \equiv 1$, $\epsilon_{k>0} \equiv 2$. From this, the one-sided power spectral density is computed [14] by using $S(\omega) = 2 \int_{-\infty}^{\infty} \langle x_s(t)x_s(t + \tau) \rangle_t \epsilon^{i\omega\tau} d\tau$, whence the SNR at the frequency, ω , may be computed. The power spectrum consists of δ -functions superimposed on a smooth noise background. Rapid convergence of the summation over k occurs for $k \gg 2\pi n'_{\max} A$. The summation over n will converge quickly if, $2\pi n'_{\max} \langle y^2 \rangle \ll 1$, with slower convergence if this condition is not met.

We consider the case of arbitrary bias flux. If $x_0 \neq 1/2$, the input signal will not be centered between a transfer characteristic minimum and maximum, and the output SNR may be affected. In fact, the output SNR at the sine-wave frequency exhibits a deep trough for input signals centered on one of the extrema of the transfer characteristic. Plotted as a function of x_0 and β , the SNR will exhibit a pattern of spreading troughs as the locations of the transfer characteristic extrema spread with decreasing β . (The SNR surface will be even and periodic in x_0 with period one.)

The dc SQUID [7] consists of a superconducting loop interrupted by *two* Josephson junctions. Experiments using a high- β dc SQUID generated transfer characteristics qualitatively similar to those discussed above for the rf SQUID. However, it is not necessary to use a set of different dc SQUIDs with differing β 's to study a family of transfer characteristics. Instead, the transfer characteristic of the dc SQUID may be modified over a family of curves very similar to those of the rf SQUID by applying various amounts of dc bias current, I_b , across the Josephson junctions. Recall that β depends on the junction critical current I_c : $\beta \equiv 2\pi L I_c / \Phi_0$. The bias current applied across the junctions can be thought of as effectively changing the junction critical currents. This results in plots analogous to those discussed in the preceding paragraph, but with I_b taking the role of β .

For the rf SQUID, Δx_i decreases linearly with increasing β . For the dc SQUID, experimental data show a linear increase of Δx_i with I_b over the range of Δx_i values possible in the rf SQUID ($0.18 \leq \Delta x_i \leq 0.5$). Inverting these relations, we can use Δx_i as a common scale for comparing rf SQUID results at various β 's with dc SQUID results at various I_b 's. In figure 5, we plot the theoretically calculated output SNR R_{out} [14] beside a plot of *experimental* output SNR data from a high- β dc SQUID. The theoretical plot reproduces the experimentally observed pattern of maxima centered at half-integral values of x_0 and surrounded by diverging troughs.

In the experiment, the output noise power fell below the measurement system noise floor for $\Delta x_i > 0.3$. Therefore, we added a fixed noise floor to the calculated rf SQUID output noise power as well. Without a noise floor, deep troughs still occur in the theoretical output SNR, but they are narrower. The troughs are therefore *not* due simply to the very small slope near the transfer characteristic extrema reducing the output signal power relative to a fixed noise floor. Rather, nonlinear response is modifying the output signal and noise powers by different amounts.

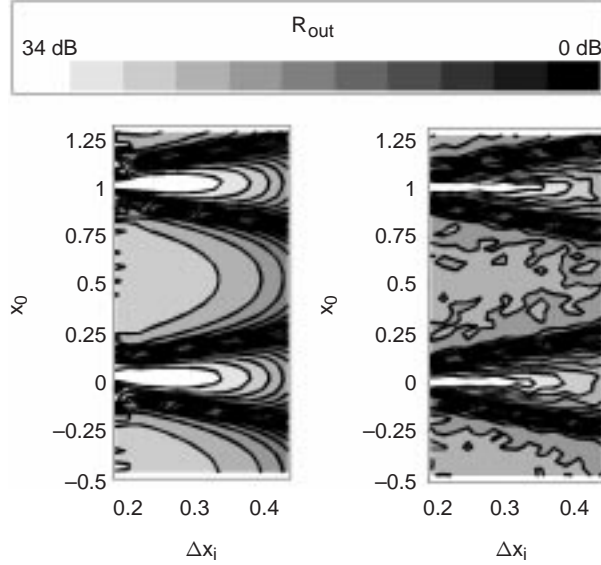


Figure 5. Theoretical (left) and experimental (right) output SNR as a function of x_0 and Δx_i , with $A = 0.001$, input SNR $R_{in} = 34$ dB, $n'_{max} = 40$.

DISCUSSION

This article summarizes published work (theoretical and experimental) describing the response of a single junction rf SQUID to a very weak “target” dc magnetic field, in the presence of background noise and a *known* cyclic magnetic field with which the device is pre-biased. The response of the device to the cyclic field is altered by the dc signal, and this provides a means toward detecting and quantifying the target signal.

The results for the hysteretic SQUID (which explain very well the experimental observations of [10] and [11]) should be applicable to generic bistable and (in special situations such as described here in connection with the SQUID) multistable systems with broken symmetry. Many nonlinear detectors suffer from significant low-frequency noise limitations (the noise may be internal, e.g., $1/f$, or external). By carefully selecting the frequency, ω , of the *known* bias signal, the detection may be shifted to a more acceptable part of the frequency spectrum. Then, in a detector that has an *a priori* symmetric potential, the appearance of the even multiples of ω in the output PSD, together with the change in the spectral amplitudes, M_k , in the presence of the symmetry-breaking signal (which may be dc or have a single frequency, in which case one looks at the properties of combination tones in the output PSD), may be used to detect or estimate the weak target signal. This idea was, in fact, demonstrated in laboratory experiments carried out with a specially designed “SR-SQUID” [10] assuming only internal white noise, as well as a conventional rf SQUID [11] using externally applied correlated noise. In actual remote-sensing applications, one often knows *a priori* the spectral characteristics of the background noise. In this case, it is clearly of benefit to be able to adjust the potential barrier height, ΔU_0 , and/or the amplitude of the known bias signal so as to achieve the highest possible sensitivity. In fact, the peak powers in figures 3 and 4 increase as the ratio $A/\Delta U_0$ increases; hence, for optimum detection, it might be advisable to adjust the bias signal amplitude, A , such that it is

almost at the threshold for deterministic switching, with the barrier height already selected to maximize the output SNR. The barrier height may be adjusted by either fabricating a SQUID with a certain nonlinearity parameter, β , (in turn, this parameter depends on the junction critical current, I_c , and the loop inductance, L) or by introducing an asymmetrizing dc flux, x_0 , as discussed here. It is important to note that theory predicts the best possible output SNR at the fundamental for zero barrier height, corresponding to the linear system case; however, other practical considerations may render this mode of detection impractical in real devices, e.g., the rf SQUID detector, wherein background noise and a low slew-rate make detection of very weak signals via conventional techniques difficult in the presence of even moderate amounts of noise. For practical applications, it would be desirable to be able to compute *a priori* the receiver operating characteristics (ROCs) of the sensor [13], which are plots of detection vs. false alarm probabilities for different detection thresholds. This calculation is currently in progress. Note also that the frequency-shifting idea that is the focus of this work applies exclusively to nonlinear systems; a linear sensor, for example, would not display this phenomenon.

For the case of the nonhysteretic device, we have followed a slightly different tack: We assume that the transfer characteristic for an applied (and, presumably, known) dc signal is known or has been measured via an experiment. Then, the response to a target periodic signal is calculated and shown in figure 4. It is immediately apparent that this approach permits a solution to the inverse problem: Given figure 4 and a *known* cyclic bias signal, one may read off the SQUID response for any (unknown) dc target signal. Clearly, the important problem to consider, when evaluating the actual performance of real devices, is the signal-detection performance (quantified, for example, by the ROCs) of the device under different operating scenarios; this is currently being investigated.

The nonlinearity parameter, β , (or the bias current in the experimental setup involving a two-junction SQUID) serves as a “tuning” parameter that is *independent* of the input SNR and that can be used to optimize the response of the device. Increasing β leads one into the hysteretic regime where the transfer characteristic is multivalued with respect to the input and can no longer be tuned by adjusting β . Our work shows that the effects described in the preceding section may be generic to nonlinear, nonhysteretic dynamic systems that respond via transfer characteristics of the type shown in figure 4; such characteristics are typical products of experiments on nonlinear devices. No assumptions regarding the existence of a threshold or an *a priori* form for a crossing rate have been made. It is worth reiterating that the parameter, β , is a fabrication parameter in rf SQUIDs and cannot be adjusted during an experiment. For this reason, the two-junction or dc SQUID, in which an *adjustable* bias current (for fixed β) controls the response, may be the device of choice for practical signal-detection applications.

ACKNOWLEDGMENT

Much of this work was carried out in collaboration with Dr. Luca Gammaitoni (University degli Studi di Perugia, Italy) with additional funding from the Office of Naval Research and a NATO Collaborative Research Grant.

REFERENCES

1. Jung, P. 1993. "Periodically Modulated Stochastic Processes," *Physics Reports*, vol. 234, pp. 175ff, (good overview).
2. Bartussek, R., P. Jung, and P. Hanggi. 1996. *Physical Review E*, vol. 49, pp. 3930;
Jung, P. and R. Bartussek. 1996. Article in *Fluctuations and Order: The New Synthesis*, ed. M. Millonas, Springer-Verlag, NY;
Lorincz, K., Z. Gingl, L. Kiss, and A. Bulsara. 1996. "Higher Order Stochastic Resonance in a Level Crossing Detector," submitted to *Physical Review E*.
3. Wiesenfeld, K. and F. Moss. 1995. *Nature*, vol. 373, pp. 33–36, (good overview);
Bulsara, A. and L. Gammaitoni. 1996. "Tuning in to Noise," *Physics Today*, vol. 49, no. 3, pp. 39–45, (good overview).
4. Bulsara, A., S. Lowen, D. Rees. 1994. "Cooperative Behavior in the Periodically Modulated Wiener Process: Noise-Induced Complexity in a Model Neuron," *Physical Review E*, vol. 49, pp. 4989–5000;
Bulsara, A., T. Elston, C. Doering, S. Lowen, and K. Lindenberg. 1996. "Cooperative Behavior in Periodically Driven Noisy Integrate-Fire Models of Neuronal Dynamics," *Physical Review E*, vol. 53, pp. 3958–3969.
5. Gammaitoni, L., F. Marchesoni, and S. Santucci. 1995. "Stochastic Resonance as a Bona Fide Resonance," *Physical Review Letters*, vol. 74, pp. 1052ff.
6. Bulsara, A., M. Inchiosa, and L. Gammaitoni. 1996. "Noise Controlled Resonance Behavior in Nonlinear Dynamical Systems with Broken Symmetry," *Physical Review Letters*, vol. 77, pp. 2162–2165;
Inchiosa, M., A. Bulsara, and L. Gammaitoni. 1997. "Higher Order Resonant Behavior in Asymmetric Nonlinear Stochastic Systems," *Physical Review E*, vol. 55, pp. 4049–4056.
7. Barone, A. and G. Paterno. 1982. *Physics and Applications of the Josephson Effect*, J. Wiley, NY.
8. Hibbs, A., A. Singaas, E. Jacobs, A. Bulsara, J. Bekkedahl, and F. Moss. 1995. "Stochastic Resonance in a Superconducting Loop with a Josephson Junction," *Journal of Applied Physics*, vol. 77, pp. 2582–2590.
9. (see, e.g.) Gardiner, C. 1983. *Handbook of Stochastic Methods*, Springer-Verlag, Berlin.
10. Rouse, R., S. Han, and J. Lukens. 1995. *Applied Physics Letters*, vol. 66, (108).
11. Quantum Magnetics, Inc. 1995. *New Type of Magnetic Flux Sensor based on Stochastic Resonance in a Flux Quantized Superconducting Loop*, Final Report. 7740 Kenemar Ct., San Diego, CA.
12. Gammaitoni, L., F. Marchesoni, E. Menichaella-Saetta, and S. Santucci. 1989. *Physical Review Letters*, vol. 62, pp. 349+;
McNamara, B. and K. Wiesenfeld. 1989. *Physical Review A*, vol. 39, pp. 4854ff.

13. Inchiosa, M. E. and A. R. Bulsara. 1996. "Signal Detection Statistics of Stochastic Resonators," *Physical Review E*, vol. 53, pp. 2021R–2042R;
Inchiosa, M. E. and A. R. Bulsara. 1998. "DC Signal Detection via Dynamical Asymmetry in a Nonlinear Device," *Physical Review E*, in press.
14. Inchiosa, M. E., A. R. Bulsara, A. D. Hibbs, and B. Whitecotton. 1998. "Signal Enhancement in a Nonlinear Transfer Characteristic," *Physical Review Letters*, vol. 80, 16 February, p. 1381.
15. Stratonovich, R. 1963. *Topics in the Theory of Random Noise, vol. 1*, Gordon and Breach, NY.

Principal Investigator:
Dr. Adi Bulsara

0601152N
ZU03

Decision Theory Augmented by Natural Event Metrics with Applications to Data Fusion

I.R. Goodman and G.F. Kramer

Probability-functional models are models of perceived situations in the form of functions of probabilities of contributing events that can also be represented as probabilities of single (yet possibly quite complicated) events. Such events may be given in explicit or implicit form. Examples of the former include models in the form of overall conditional probabilities or as weighted sums of probabilities; examples of the latter include large classes of fuzzy logic models of linguistic-based information. The standard development of probability and decision theory has (1) ignored the general issue of establishing a comprehensive approach to the comparison and combination of probability-functional models; (2) been limited to ad hoc or situation-specific applications for particular aspects of the problem; and (3) not been applied to develop a unified sound viewpoint of the issue. An example of the first situation is the standard treatment of conditional information where no natural extension of hypotheses testing has been developed for determining the degree of similarity of one conditional expression with another, when the state and uncertainty of each can be represented as conditional probabilities. An example of the second situation is the consideration of information modeled initially as formal functions of probabilities (other than conditional probabilities) such as weighted averages or particular nonlinear functions of probabilities. An example of the third situation is the separate development of fuzzy logic from probability theory to treat natural language information, rather than taking a unified point of view. This project considered the extension of the standard theory of decision making (ETDM) with emphasis on hypotheses testing, to include the testing for similarity of disparate probability-functional models. The approach taken in developing ETDM acting upon such models was a threefold one. In the first phase, it was shown that for a large class of probability-functional models, each is actually representable as a corresponding single "relational" event lying in some Boolean or sigma algebra, which properly extends the initial one containing the contributory events. Natural event or probability metrics are legitimate distance functions (and hence measures of event similarity or dissimilarity) that are derived from probability evaluations. Such metrics, until recently, have only been of limited interest, such as in the construction of certain probability spaces, where only the standard one based on the probability of the Boolean symmetric difference has been in use. In light of the above remarks, the second phase of work developed new probability metrics, compared them to the standard one, and applied all to the imbedded probability-functional models as events. In the third phase, under a uniform assumption on the higher order probability distribution of the relevant relative atomic probabilities, each probability metric evaluated over a pair of given models, if desired, could itself be considered as a random variable with a computable distribution. Each probability metric could also be used as a test statistic for hypotheses testing for sameness of the models and related problems. ETDM encompasses, as special cases, extended Bayesian decision making and extended likelihood procedures. Applications to data-fusion problems were exhibited and basic numerical experiments were conducted verifying the potential for significant increase of efficiency when ETDM is employed compared to standard approaches.

INTRODUCTION: BOOLE'S IDEA

Among the many contributing factors over the past 200 years that have shaped the standard evolution of probability theory, two, in particular, have contributed to an unnecessary restriction of its applicability to real-world problems: the rejection of Boole's ideas on representing conditional probabilities algebraically and the gradual overwhelming emphasis of probability theory upon numerical-based relations.

The first, chronologically, was the almost outright refusal by the probability community of the time (mid- and late nineteenth century) [1] to consider seriously Boole's ideas that it is meaningful to treat the argument $(a|b)$ that appears in the expression for conditional probability

$$P(a|b) = P(a)/P(b), \quad (1)$$

as a stand-alone quantity, where in eq.(1), it is assumed that $a \leq b$, i.e., a is a subevent of b and $P(b) > 0$ [2]. That is, Boole tacitly assumed that one could extend the initial Boolean algebra B of events a, b, \dots and given probability measure P over B somehow so that (using the same notation for the extension of P)

$$P((a|b)) = P(a|b). \quad (2)$$

Combining eqs.(1) and (2), Boole considered a possible solution $(a|b)$ of

$$P((a|b)) = P(a)/P(b). \quad (3)$$

If the thesis behind eq.(2) (or eq.(3)) could be realized, then one could possibly go farther and manipulate algebraically/logically such entities and, in turn, evaluate them by probabilities, such as, for given ordinary events a, b, c, d in B , determine $P((a|b) \& (c|d))$ or $P((a|b)' \vee (c|d)) \& (e|f)$ completely in terms of the (assumed known) joint probability evaluations of a, b, c, d, e, f . Here, the standard Boolean/logical connectives—and their extension to $(a|b)$, $(c|d)$, $(e|f)$ —are indicated by the notation $\&$ for conjunction, \vee for disjunction, $()'$ for negation, etc. We call any such $(a|b)$, $(c|d)$, $(e|f), \dots$ a “conditional event” (Boole called each a “division of events” due to the division of probability it naturally corresponds to) and interpret, e.g., $(a|b)$ linguistically as “ a , given b ” or “if b , then a ,” etc. However, Boole, possibly in light of the criticism heaped upon him, did not carry the idea of conditional events very far, never developing any kind of calculus of logical operations acting upon them, but did consider some formal Boolean normal form expansions and their use in “probability-inverse” problems. (See Hailperin's expositions on Boole's work [3], [4].)

Unfortunately, except for a handful of researchers (who, until recently, worked independently) the idea of conditional events and conditional event algebra (CEA) remained a topic bypassed by the mainstream probability community. (See e.g., Goodman's detailed history of the issue until 1991 [5] and Nguyen and Walker's more updated comments [6].)

A MOTIVATING EXAMPLE AND THE CONDITIONAL EVENT ALGEBRA PROBLEM

One basic motivation for attempting to extend ordinary (relatively unconditional) events to a conditional setting and establish a corresponding CEA is to compare conditional information. For example, one might wish to determine whether two inference rules really represent the same concept, up

to some reasonable degree. Although redundancy is, in general, a good thing, it may also invoke unnecessary cost, such as when the above-stated simple problem is magnified hundreds or thousands of times apropos to a complex real-world-oriented expert diagnosis system such as MYCIN [7] or PROSPECTOR [8].

This brings us to the basic problem of testing hypotheses for sameness for two conditional expressions “if b, then a” vs. “if d, then c,” whose uncertainties are modeled according to eq.(3); i.e., the reliability of these rules are given as $P(a|b)$, $P(c|d)$, respectively. Any of the events a, b, c, d may be logical compounds of certain common contributing events and/or may be related in other ways.

Example 1. Two rules may be in the form of “correlating” or making a decision concerning whether two apparent targets of interest I, II really represent the same target:

$$R_1 = \text{“if } (A \vee B \& C), \text{ then } (D \vee E)\text{”} \quad (4)$$

vs.

$$R_2 = \text{“if } (A \vee F \& C), \text{ then } (D \vee G)\text{”} \quad (5)$$

where, e.g., we have the interpretations

A = “present radar sensors indicate distance between I and II is \leq threshold k_o ,”

B = “human-based sensors indicate I and II are of the same friendly or neutral nationality,”

C = “past type T sensor system information indicates (vector) velocity difference between I and II \leq (vector) threshold j_o ,”

D = “I and II represent same target,”

E = “I and II are to be considered serious candidates for correlation, pending further input data,”

F = “present type T sensor system information indicates an emitting pattern for I and II belonging to X or Y (but not necessarily same) nationality,”

G = “I and II are moderate candidates for correlation, pending further input data.” (6)

By inspection of eqs.(4) and (5), a certain similarity of structure holds between R_1 and R_2 . In addition, we see from the definitions in eq.(6) that there is some similarity and difference within corresponding event pair (B,F) and within (E,G). Is there a systematic way to obtain a quantitative means to test whether R_1 and R_2 are significantly different or similar, assuming the occurrences/nonoccurrences of the relevant events A, B, C, D, E, F, G are: (1) not necessarily certain and (2) governed by a probability measure P, so that all finite combinations of events are determined consistently according to the laws of probability and some primitive set of probability combination values?

Suppose then, a Boolean (or sigma) algebra B_o could be found extending the original one B containing A,B,...,G, with B_o also containing R_1 and R_2 as (conditional) events and suppose initial probability P over B can be extended to a probability measure, say P_o over B_o , yielding relations for $P_o(R_1)$ and $P_o(R_2)$, analogous to eq.(3). That is, letting

$$a = D \vee E, \quad b = A \vee B \& C, \quad c = D \vee G, \quad d = A \vee F \& C, \quad (7)$$

we suppose

$$R_1 = (a|b) \text{ and } R_2 = (c|d) \text{ all lie in } B_0 \quad (8)$$

and

$$P_0(R_1) = P(a|b), \quad P_0(R_2) = P(c|d), \quad (9)$$

provided $P(b), P(d) > 0$. Then, we can use any of several natural *probability metrics* that any probability space possesses to test how close the events R_1 and R_2 are to each other. For example, the function $d_{P,2}: B_0^2 \rightarrow [0,1]$ is a legitimate and well-known metric (see e.g., Kappos [9]), where for any two events, say a and b in B_0 ,

$$\begin{aligned} d_{P,2}(a,b) &= P_0(a \& b' \vee a' \& b) \text{ (probability of Boolean symmetric difference)} \\ &= P_0(a \& b') + P_0(a' \& b) = P_0(a) + P_0(b) - 2P_0(a \& b). \end{aligned} \quad (10)$$

Inspection of eq.(10) shows that to determine $d_{P,2}(a,b)$ explicitly, we need to be able to determine the probabilities of, at the very least, the conjunctive probability of a and b .

For the problem at hand, this translates into being able to determine conjunctive probabilities of both conditional events R_1 and R_1 . *That is, we need to be able to establish a CEA over B to obtain these computations.* See also additional discussion in a later section of this article. (For detailed background, see the recent monograph [10], sections 10 *et passim*. Additional details can be found [11] on how other related problems can be addressed.) ■

It should also be mentioned at this point that an alternate, and temporally first, approach to the modeling of conditional expressions is through the *material conditional* operator \Rightarrow , one of the 16 possible binary Boolean operators, defined for any two events a, b in B as

$$b \Rightarrow a = b' \vee a = b' \vee a \& b. \quad (11)$$

But, it is readily seen that \Rightarrow is not compatible with conditional probability, i.e., in general

$$P(b \Rightarrow a) = 1 - P(b) + P(a \& b) < P(a|b). \quad (12)$$

(See e.g., [12], chapter 1 for a history of the discrepancy between the material conditional and the probability conditional.)

All of the above leads to two basic issues: (1) How do we construct CEAs? and (2) What guidelines can be established for choosing the most appropriate CEAs for a given problem?

OTHER MOTIVATING EXAMPLES AND THE RELATIONAL EVENT ALGEBRA PROBLEM

The second factor leading to the reduced scope of applicability of probability theory cannot be identified with a single source. Instead, the thrust of the scope of probability gradually developed with an emphasis on numerically based concepts rather than algebraic ones. Take, for example, the richness of the standard literature concerning maximum likelihood techniques, Bayesian analysis, Markov

chaining, diffusion theory, and mathematical statistics as a whole. (As a test, the reader is invited to peruse any typical volume of one of the leading sources for documenting articles on probability and its applications, *Mathematical Reviews*.) Of course, there are some exceptions where algebraic concepts are utilized, such as in invariant theory of estimation and hypotheses testing [13] or in qualitative or ordered-choice probability [14]. But, as a whole, the algebraic underpinnings of probability theory have been, for the most part, ignored in attempting to apply the theory (as is evident in the case of CEA discussed above).

It is not difficult to see that the idea behind eq.(3) generalizes to the following problem: Given a function f and probabilities of, say, three ordinary events, for purpose of simplicity, $P(a)$, $P(b)$, $P(c)$, where $f(P(a),P(b),P(c))$ lies between 0 and 1, as probability certainly does. Find a Boolean algebra B_o , extending the initial Boolean algebra B containing the ordinary events a , b , c ,... and a probability P_o over B_o extending any given probability P over B and find a “relational” event $f(a,b,c)$, formally extending the domain of definition for f , such that $f(a,b,c)$ lies in B_o , such that the analogue of eq.(3) holds. Here, arithmetic division is replaced by f and the $(\cdot|.)$ notation replaced by the f notation, and we have the commutative or homomorphic relation if such a relational event exists:

$$P_o(f(a,b,c)) = f(P(a),P(b),P(c)). \quad (13)$$

It is understood that eq.(13) (just as eq.(3)) is to hold for all possible well-defined P and events a,b,c , subject to any given prior constraints (such as partial ordering, etc.). (See figure 1 illustrating the general relational event algebra problem [which includes the conditional event algebra problem as a special case when f is arithmetic division] and its application to possible comparison of probability-functional models.)

Example 2. One example of an f occurring on the right-hand side of eq. (13) includes *the linear weighting case*, where

$$f(P(a), P(b), P(c)) = w_1P(a) + w_2P(b) + w_3P(c), \quad (14)$$

where the w_j are constant real weights not depending on the particular P and a,b,c chosen. Note that we do not restrict a,b,c to be mutually disjoint or exhaustive. ■

Example 3. Another example of f is the nonlinear weighted exponential model of two variables where, for simplicity, we assume either a,b are P -independent or disjoint:

$$f(P(a),P(b)) = w_1(P(a))^r + w_2(P(b))^s, \quad (15)$$

where r,s are positive real constants and w_1 and w_2 are constant real weights. ■

Example 4. Yet another type of example of f arises from fuzzy logic (see e.g., [15] for background), where, at first, no probability connections may seem apparent. Consider, for example, the sentence

$$Q = \text{“The ship is very long or the sea state is not quite high.”} \quad (16)$$

Letting

$$L = \text{“ship is long,” } M = \text{“sea state is medium,”} \quad (17)$$

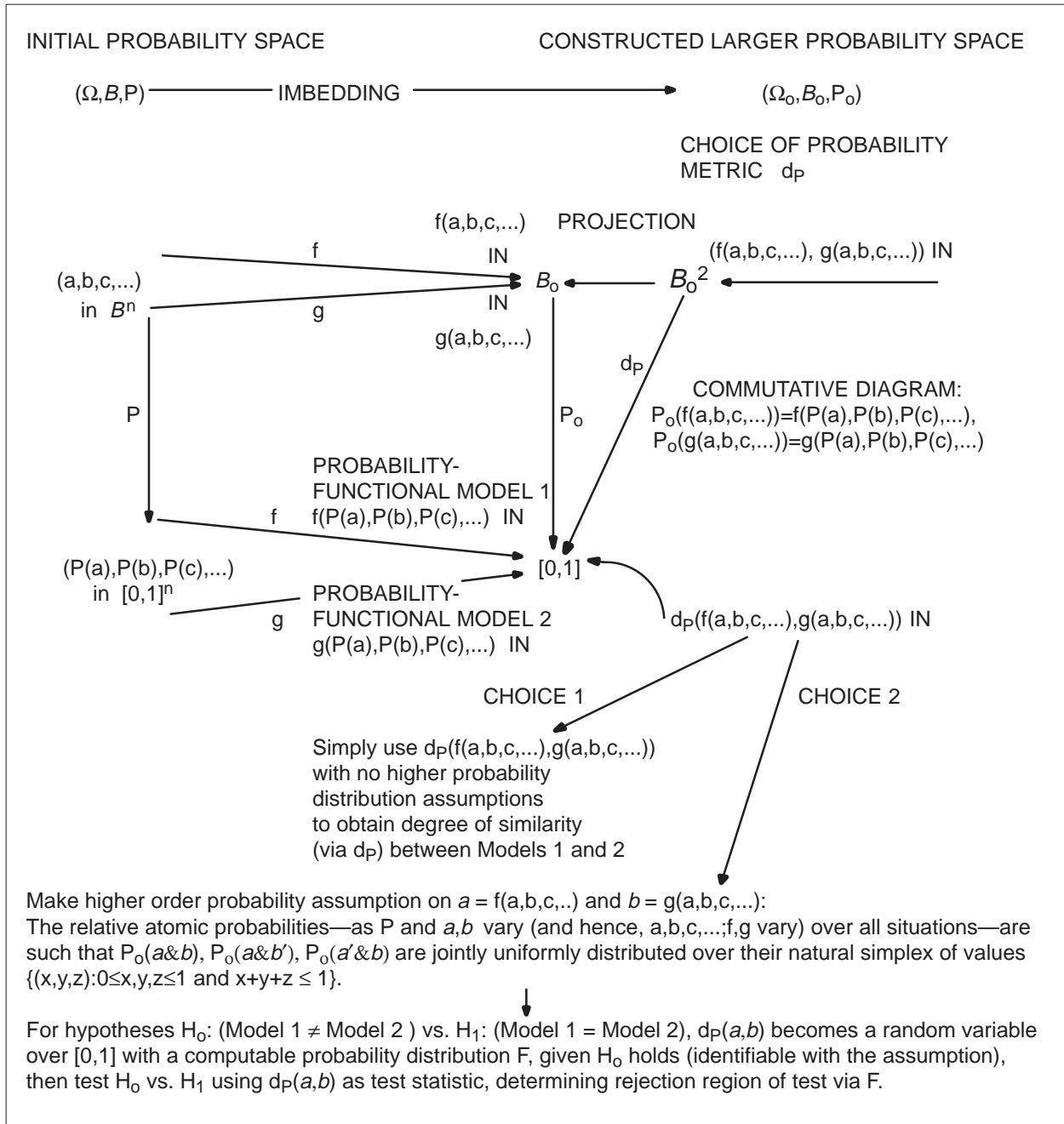


Figure 1. Approach to the basic problem of comparing probability-functional models via relational events and, in turn, ETDM.

a common fuzzy logic interpretation of Q in eq.(16) is in terms of the “truth” function of Q , $t(Q)$, which, unlike the classical logic case, can be any real number between 0 and 1 and is given in truth-functional form, i.e., as a function g of the separate truth evaluations of the components L , M :

$$t(Q) = g(t(L), t(M)). \tag{18}$$

A typical choice of g leads to

$$t(Q) = \text{probsum}((t(L))^2, 1 - (t(M))^{3/2}) = (t(L))^2 + 1 - (t(M))^{3/2} - [((t(L))^2 \cdot (1 - (t(M))^{3/2}))] \quad (19)$$

where, letting

$$x = \text{actual length of ship, } y = \text{actual sea-state level,} \quad (20)$$

which in general are not known,

$$t(L) = L(x), \quad t(M) = M(y). \quad (21)$$

In eq.(18), L and M are now identified with their fuzzy set membership functions $L:D_1 \rightarrow [0,1]$ and $M:D_2 \rightarrow [0,1]$, where the domains of L and M are, say,

$$D_1 = [0', 1', 2', \dots, 300', \dots, 1000'], \quad D_2 = \{0, 1, 2, \dots, 10\}. \quad (22)$$

Note also the dependency of $t(L)$, $t(M)$ on x , y , respectively, in eq.(21). It is assumed that fuzzy set membership functions L , M are obtainable by empirical and/or other methods (see e.g., the now-classic work of Dubois and Prade [16], pp. 255–264). Note that the exponentials 2 and 3/2 in eq.(19) correspond roughly to the intensifiers “very” and “quite high,” while $1 - ()$ corresponds to negation, and probsum to “or.” Of course, other interpretations are possible (see again [15], [16] for background). Since, at least theoretically, x and y can vary freely over their respective domains D_1 and D_2 , putting together eqs.(18), (19), (21), and indicating the appropriate functional dependency on x , y , we have

$$t(Q)(x,y) = \text{probsum}((L(x))^2, 1 - (M(y))^{3/2}), \text{ all } x \text{ in } D_1, y \text{ in } D_2. \quad (23)$$

Now, for the connection to probability: It has been demonstrated by Goodman, Nguyen, Hohle, and others that a natural connection between fuzzy logic and probability is furnished via the one-point coverages of appropriately constructed random sets. (See e.g., [17] for general background and [18] for a recent algebraic characterization.) In particular, this implies that eq.(21) can be rewritten as,

$$L(x) = P(x \text{ in } S(L)), \quad M(y) = P(y \text{ in } S(M)), \text{ all } x \text{ in } D_1, \text{ all } y \text{ in } D_2, \quad (24)$$

where $S(L)$ and $S(M)$ are appropriately chosen random subsets of domains D_1 and D_2 , respectively, and P is an appropriately chosen probability measure. Finally, recognizing that we can also rewrite eq.(24) in the form

$$L(x) = P(a_x), \quad M(y) = P(b_y), \quad (25)$$

where events

$$a_x = (x \text{ in } S(L)), \quad b_y = (y \text{ in } S(M)), \text{ all } x \text{ in } D_1, \text{ all } y \text{ in } D_2, \quad (26)$$

lie in some Boolean (or sigma) algebra B , eq.(23) becomes the final desired probability-functional form(s):

$$t(Q)(x,y) = \text{probsum}((P(a_x))^2, 1 - (P(b_y))^{3/2}), \text{ all } x \text{ in } D_1, y \text{ in } D_2. \quad (27)$$

■

Example 5. As a final example, consider f as any analytic function of one variable that has all coefficients in its power series expansion about zero forming either weights or deficient weights. That is, there are real constants τ_j such that for any a in B , and probability P over B ,

$$f(P(a)) = \sum_{j=0}^{+\infty} (P(a))^j \cdot w_j, \quad 0 \leq w_j \leq 1, \quad \sum_{j=0}^{+\infty} w_j \leq 1. \quad (28)$$

■

Again, as in the case of the conditional event problem, if we desire to compare quantitatively competing models describable in the form of functions of probabilities (such as in any of the above examples) we need to be able to extend the given probability space of events to a larger one (i.e., extend the Boolean algebra of events and probability measure) with computable probabilities of operations among the events. We then can apply probability metrics, as in the case of conditional expressions discussed above to test hypotheses for similarity. See figure 1 again for a summary of the general relational and conditional event algebra problem and its possible solutions in terms of “commutative” diagrams.

A SOLUTION SCHEME FOR THE GENERAL RELATIONAL EVENT ALGEBRA PROBLEM

With all of the necessary basic concepts established, it is of some interest to see just what specific forms relational and conditional events take. The basic principal in discovering such events begins actually as an extension of Boole’s and others’ thinking connecting algebraic or event operators and relations to numerical ones in a natural way where arithmetic addition, subtraction, and multiplication corresponds to event disjoint disjunction, difference, and Cartesian product. Noting that analytic functions—equivalently, infinite power series—play a key role in numerical analysis, it is natural to extrapolate the above relations between numerical and event operators so that we seek a general event representation of an infinite series, restricted so that their constant coefficients all lie in the unit interval. Roughly speaking, in carrying out the general program to obtain relational events, we go through three aspects: First, the conditional event algebra problem is provided a solution that fits into the above analogy. This is then specialized to the problem of obtaining “constant-probability” events (explained below), corresponding to the constant coefficients of the power series functions. Finally, a suitable transform is applied to the original numerical function or power series, so that the corresponding algebraic form consists of disjoint terms, each term being the Cartesian product of a constant-probability event and an integer power event, or Cartesian product of such events, each corresponding to an appropriately iterated Cartesian product of an event.

SOLUTION FOR THE CONDITIONAL EVENT ALGEBRA PROBLEM

The arithmetic division of one number s in $[0,1]$ by a larger number t in $[0,1]$, s/t , is represented in terms of the three other arithmetic operators most simply by the usual, and necessarily infinite, power series

$$s/t = s \cdot (1/t') = \sum_{j=0}^{+\infty} (t')^j \cdot s, \quad t' = 1 - t. \quad (29)$$

Thus, following the above basic principle of correspondence between arithmetic and algebraic operators, the natural analogue of eq.(29) is simply

$$(a|b) = \bigvee_{j=0}^{+\infty} (b')^j \times a, \quad (30)$$

where we use the integer exponential (repeated Cartesian product) notation for events to be

$$(b')^j \times a = \begin{cases} \underbrace{b' \times \dots \times b'}_{j \text{ factors}}, & \text{if } j = 1, 2, \dots \\ a, & \text{if } j = 0. \end{cases} \quad (31)$$

Eq.(30) means that the Boolean algebra required to contain $(a|b)$ must have at least a countable infinity of factor spaces, each identical to B , the initial Boolean algebra containing a, b, \dots . In fact, if P is the initial given probability measure over B , and we denote Ω as the space of points or universal event in B , so that (Ω, B, P) represents the initial probability space of unconditional events, then it readily follows that the product probability space, say (Ω_0, B_0, P_0) consisting of a countably infinite number of factor probability spaces, each identical to (Ω, B, P) , is sufficient to do the job. That is, not only does $(a|b)$ lie in B_0 (with the obvious identification of each of its disjoint terms $(b')^j \times a$ with $(b')^j \times a \times \Omega_0$), but also we have as a check for eq.(3) holding:

$$P_0((a|b)) = P_0\left(\bigvee_{j=0}^{+\infty} (b')^j \times a\right) = \sum_{j=0}^{+\infty} (P(b'))^j \cdot P(a) = (1/(1 - P(b')))P(a) = P(a|b). \quad (32)$$

Following the above definition and exploiting the basic recursive relationship

$$(a|b) = ab \vee (b' \times (a|b)), \quad (33)$$

valid for each conditional event, we can obtain closed-form expressions for all finite Boolean/logical combinations in B_0 of any conditional events, as well as their corresponding probability evaluations under P_0 . For example (see [19] for details of the resulting calculus of operations), assuming $a \leq b$, $c \leq d$ in B , and $P(b), P(d) > 0$,

$$\begin{aligned} P_0((a|b) \& (c|d)) &= [P(a\&c) + P(a\&d')P(c|d) + P(cb')P(a|b)] / P(b \vee d), \\ P_0((a|b) \vee (c|d)) &= P(a|b) + P(c|d) - P_0((a|b) \& (c|d)), \\ (a|b)' &= (a'|b) \text{ and } P_0((a|b)') = 1 - P(a|b). \end{aligned} \quad (34)$$

Because (Ω_0, B_0, P_0) forms an ordinary probability space, all laws and results from the standard development of probability theory are immediately applicable here. Hence the bottom two parts of eq.(34) are not unexpected! Note how (Ω, B, P) is naturally imbedded in (Ω_0, B_0, P_0) as a first factor space.

In addition, it is shown in [19] that this product space approach to conditional event algebra leads to a number of desirable properties, beyond having a legitimate probability space, including being able to obtain all higher order conditionals analogously, obtaining a natural relation with the standard conditioning of random variables, and a full characterization of this approach via a reasonable independence assumption, among others.

SOLUTION OF THE CONSTANT-PROBABILITY EVENT PROBLEM

The constant-probability event problem may best be stated and a solution provided through the following example for the representation of $2/3$: Let c be any event in Boolean algebra B so that $P(c) > 0$ for all probability measures P over B of interest. Then, if we let

$$a = (b \times b \times b') \vee (b \times b' \times b), \quad b = (b \times b \times b') \vee (b \times b' \times b) \vee (b' \times b \times b), \quad (35)$$

clearly a, b are in B_3 , part of 3-factor product probability space (Ω^3, B_3, P_3) (with identical factors being (Ω, B, P)), with the identical evaluation

$$P_3(b \times b \times b') = P_3(b \times b' \times b) = P_3(b' \times b \times b) = P(b')(P(b))^2, \quad (36)$$

so that conditional event $(a|b)$ is in $(B_3)_o$, part of the product probability space construction given above, corresponding to full probability space $((\Omega^3)_o, (B_3)_o, (P_3)_o)$. Thus, eqs.(32), (35), (36) show here

$$(P_3)_o((a|b)) = [2P(b')(P(b))^2] / [3P(b')(P(b))^2] = 2/3, \quad (37)$$

for all such P that $0 < P(c) < 1$; it is also not dependent upon the specific c chosen.

A similar procedure can be carried out for any rational number, but this brings about four basic issues: (1) What form does the calculus of logical operations take with respect to constant-probability events among themselves and among ordinary events or other conditional events? (2) Which constant-probability representation of a given rational number do we choose, such as $2/3$ vs. $4/6$ vs. $6/9$ vs...? (3) How can we handle simultaneously rationals with larger and larger irreducible denominators? (4) Can we take limits in some rigorous way of the rational number representations to obtain arbitrary real representations for any real number in the unit interval? While the answer to (1) is readily seen to be essentially min and max for conjunction and disjunction, respectively, with a reverse-like interval form holding for negations among constant-probability events, and that conjunction of a constant-probability event with an ordinary event reduces to a Cartesian product relation [11], only recently, a full satisfactory solution to the remaining issues has been obtained and is provided in the upcoming publication [20]. From now on, for any real t , $0 \leq t \leq 1$, denote the constant-probability event corresponding to t as $\theta(t)$, noting by convention,

$$\theta(0) = \emptyset_o, \quad \theta(1) = \Omega_o. \quad (38)$$

USE OF CONSTANT-PROBABILITY EVENTS IN DEVELOPING SOLUTIONS TO THE RELATIONAL EVENT ALGEBRA PROBLEM

As stated above, constant-probability events play a key role in obtaining relational events. A listing of solutions to a wide variety of relational event algebra problems is provided in [10], section III. Here, we present relational events for the five examples shown in table 1.

Table 1. Relational events corresponding to the five examples.

Example	Given Probability-Functional Form $f(P(a),P(b),P(c),\dots)$	Corresponding Relational Event $f(a,b,c,\dots)$
Conditional Event (Ex. 1)	$f(P(a),P(b)) = P(a)/P(b) = P(a b),$ $a \leq b$ in B ; $P(b) > 0$	$f(a, b) = 'a/b' = (a b)$ $= \bigvee_{j=0}^{+\infty} (b')^j \times a$
Linear Weighted Event (Ex. 2)	$f(P(a),P(b),P(c)) = w_1P(a) + w_2P(b) + w_3P(c),$ w_j constant real weights, a,b,c in B arbitrary (not necessarily disjoint or exhaustive)	$f(a,b,c) = 'w_1a + w_2b + w_3c'$ $= abc \vee ((a\&b\&c') \times \theta(w_1+w_2))$ $\vee ((a\&b'\&c) \times \theta(w_1+w_3)) \vee ((a'\&b\&c) \times \theta(w_2+w_3))$ $\vee ((a\&b'\&c') \times \theta(w_1)) \vee ((a'\&b\&c') \times \theta(w_2))$ $\vee ((a'\&b'\&c) \times \theta(w_3))$
Nonlinear: Weighted Exponential (Two Arguments) (Ex. 3)	$f(P(a),P(b)) = w_1(P(a))^r + w_2(P(b))^s,$ w_j constant real weights, r,s positive real constants; a, b P-independent or disjoint allows simpler computations when combining these functions	$f(a, b) = 'w_1a^r + w_2b^s'$ $= (a^r\&b^s) \vee ((a^r\&(b^s)') \times \theta(w_1))$ $\vee (((a^r)'\&b^s) \times \theta(w_2));$ $a^r = a^{[r]} \times a^{\{r\}},$ [[.]] greatest integer function, {.} fractional excess function, $a^t = \bigvee_{j=0}^{+\infty} (a')^j \times a \times \theta(\lambda_{j,t}),$ and for any $t, 0 \leq t < 1,$ $\lambda_{j,t} = \begin{cases} 1, & \text{if } j = 0, \\ ((1-t)(2-t)\dots(j-t))/j!, & \text{if } j = 1, 2, \dots \end{cases}$
Fuzzy Logic (Ex. 4)	t (The ship is very long or the sea state is not quite high) $= \text{probsum}((t(L)(x))^2, 1 - (t(M)(y))^{3/2})$ $= f(P(a_x), P(b_y))$ $= \text{probsum}((P(a_x))^2, 1 - (P(b_y))^{3/2}),$ $a_x = (x \text{ in } S(L)), b_y = (y \text{ in } S(M)),$ all x in D_1, y in D_2	$f(a_x, b_y) = 'probsum(a_x^2, (b_y^{3/2})'$ $= a_x^2 \boxtimes (b_y^{3/2})'$ (Cartesian sum) $= ((a_x^2)' \times (b_y^{3/2})')$ $= a_x^2 \vee [((a_x \times a_x') \vee a_x') - (((a_x \times a_x') \vee a_x') \times b_y^{3/2})]$ (further simplifiable)
Analytic Function of One Variable (Ex.5)	$f(P(a)) = \sum_{j=0}^{+\infty} (P(a))^j \cdot w_j,$ $0 \leq w_j \leq 1, \sum_{j=0}^{+\infty} w_j \leq 1$	$f(a) = ' \sum_{j=0}^{+\infty} a^j \cdot w_j '$ $= \bigvee_{j=0}^{+\infty} (a^j \times a' \times \theta(w_1 + \dots + w_j))$

PROBABILITY METRICS AND THEIR USE IN TESTING HYPOTHESES FOR SAMENESS OF PROBABILITY-FUNCTIONAL MODELS

During FY 97, a full solution to the set of possible probability metrics was established together with a theory showing the compatibility of algebraic-based metrics with their numerical counterparts established. (See [10], especially chapter 14.) In brief, the three possible generating natural event metrics corresponding to Boolean operator form for consequent and antecedent are (recalling that any subadditive nondecreasing function composed with a given metric is always a metric), given any initial probability space (Ω, B, P) and any two events a, b in B , using notation compatible with [10]:

$$d_{P,2}(a,b) = P(a \& b' \vee a' \& b) , \quad (39)$$

the probability of the Boolean symmetric difference, the standard one mentioned earlier, and

$$d_{P,3}(a,b) = P(a \& b' \vee a' \& b \mid a \vee b) , \quad (40)$$

$$d_{P,4}(a,b) = P(a \& b' \vee a' \& b \mid a' \vee b') . \quad (41)$$

Other probability metrics exist but are not in the Boolean forms as in eqs.(39)–(41). For example, the “naive” (and non-Boolean) metric

$$d_{P,1}(a,b) = |P(a) - P(b)| \quad (42)$$

is a legitimate distance function, but obviously is not a satisfactory one, since it can yield low values, with a and b being quite dissimilar. In turn, we make the higher order probability assumption—also identifiable with the null hypothesis $H_0: a \neq b$ —that formally $P(a \& b)$, $P(a' \& b)$, $P(a \& b')$ are jointly uniformly distributed over their natural domain (the remaining relative atomic probability $P(a' \& b')$ being fully determined by the other three as the complement of their sum), taking into account all the possible variations from situation to situation of $P, a, b, c, \dots; f, g$. We then can obtain closed-form distributions for each of the above four metrics, *now interpreted as random variables under the hypothesis $H_0: a \neq b$, as opposed to hypothesis $H_1: a = b$* . Table 2 summarizes the cumulative probability distribution functions F_j corresponding to each $d_{P,j}$ distribution, under H_0 .

Table 2. Tabulation of cumulative probability distributions for a class of probability metrics.

Probability Metric $d_{P,j}$	Corresponding Cumulative Probability Distribution Function F_j of $d_{P,j}$ under H_0 (and Basic Uniform Distribution Assumption for the Relative Atomic Probabilities)
$d_{P,1}(a,b) = P(a) - P(b) $, all a, b in B	$F_1(t) = 1 - (1 - t)^3$, $0 \leq t \leq 1$
$d_{P,2}(a,b) = P(a \& b' \vee a' \& b)$ $= P(a \& b') + P(a' \& b)$, all a, b in B	$F_2(t) = t^2 \cdot (3 - 2t)$, $0 \leq t \leq 1$
$d_{P,3}(a,b)$ $= P(a \& b' \vee a' \& b \mid a \vee b)$ $= d_{P,2}(a,b) / P(a \vee b)$, all a, b in B	$F_3(t) = t^2$, $0 \leq t \leq 1$
$d_{P,4}(a,b) = d_{P,3}(a', b')$ $= P(a \& b' \vee a' \& b \mid a' \vee b')$ $= d_{P,2}(a,b) / P(a' \vee b')$, all a, b in B	$F_4(t) = t^2$, $0 \leq t \leq 1$

In brief, we carry out the standard route to testing hypotheses, only using as a testing statistic the selected probability metric $d_{P,j}$ and its appropriate evaluation at constructed relational events a, b . Thus, choosing any significance level α , $0 < \alpha \ll 1$,

$$\text{Accept } H_0 \text{ (and Reject } H_1) \text{ iff } d_{P,j}(a,b) \geq C_\alpha, \quad (43)$$

$$\text{Reject } H_0 \text{ (and Accept } H_1) \text{ iff } d_{P,j}(a,b) < C_\alpha,$$

where threshold C_α is determined from F_j as :

$$\begin{aligned} \alpha &= \text{Prob}(\text{Test here rejects } H_0 \mid H_0 \text{ really true}) = \text{Prob}(d_{P,j}(a,b) < C_\alpha \mid H_0 \text{ really true}) \\ &= F_j(C_\alpha), \end{aligned} \quad (44)$$

whence

$$C_\alpha = F_j^{-1}(\alpha). \quad (45)$$

Alternatively, and especially useful when F_j is not readily functionally inverted, is the variable significance approach, whereby, instead of fixing α beforehand, we simply use as the threshold the value of $d_{P,j}(a,b)$ at hand and compute

$$\alpha = \text{Prob}(\text{Test here rejects } H_0 \mid H_0 \text{ really true}) = F_j(d_{P,j}(a,b)), \quad (46)$$

where $d_{P,j}(a,b)$ in the argument of F_j is considered the actual evaluation, not the random variable behind it. (See again [10], chapter 14 for more details.) A number of numerical tests according to this procedure were carried out with results to be published separately [21]. (See also [11] for details of a general numerical experiment applicable to exponential probability-functional models.)

DEVELOPMENT OF ETDM AND OUTLINE OF A SCHEME FOR VERIFYING IMPROVEMENT THROUGH ITS USE OVER STANDARD APPROACHES

Figure 2 presents an outline of the general approach to comparing the use of relational events via the choice of probability metric $d_{P,2}$ (others could just as well be chosen) versus the situation where no use is made of relational events. The idea is simply to combine the standard Fréchet–Hailperin bounds on conjunctive probability ([10], section III) together with a nondecreasing property of the evaluated metric in $P_o(a\&b)$, where a and b are the relational events representing the probability-functional models of interest. Figure 3 specializes the procedure to Example 2 modified to two arguments, while figure 4 considers likewise Example 1 in the form of identical consequences, a . The latter situation can be interpreted as the problem of comparing (but not yet combining!) two posterior probability descriptions of the same parameter event of interest. In all of these cases, via the Fréchet–Hailperin bounds, we obtain lower knowledge and total knowledge differences between making full use of the representing relational (or conditional) events and ignoring them. In fact, N. Rowe concluded tacitly in his book ([22], section 8) that while the problem of obtaining specific forms for conditional events was apparently intractable (obviously erroneous in light of our results), nevertheless one could apply bounds such as the Fréchet–Hailperin. (His tacit assumption was that whatever form conditional events took, they did lie in a legitimate probability space connected with the unconditional events and were subject to all standard laws and properties of probabilities.)

1. Given:

Common Probability Space (Ω, B, P) ; Events a, b, c, \dots in B ,
 Probability-Functional Model 1: $M_1 = f(P(a), P(b), P(c), \dots)$,
 Probability-Functional Model 2: $M_2 = g(P(a), P(b), P(c), \dots)$,

2. Goal: Knowledge Ordering and Improvement Relative to Specific Use of Relational Events vs. Their Non-Use

- Imbed (Ω, B, P) into appropriate and larger probability space (Ω_0, B_0, P_0) and obtain relational event algebra solution $f(a, b, c, \dots)$ in B_0 to M_1 and $g(a, b, c, \dots)$ in B_0 to M_2 :

$$M_1 = P_0(f(a, b, c, \dots)), \quad M_2 = P_0(g(a, b, c, \dots)); \quad (*)$$

all a, b, c, \dots in B (subject to possible constraint), all well-defined P

- Let $Q = \{(a, b): \text{all possible } a, b \text{ formally satisfying eq. (*) in place of actual relational events } (f(a, b, c, \dots), g(a, b, c, \dots)), \text{ respectively, but where no knowledge of the structure of } a, b \text{ is assumed (in same spirit as N. Rowe [22])}\}$

3. Ordering of Probability Metrics

- $d_{P,1}(a, b) = |M_1 - M_2| = |P_0(a) - P_0(b)| = |P_0(a \& b') - P_0(a' \& b)|$
 — No knowledge of evaluation of $P_0(a \& b)$, etc. needed –
 $\leq d_{P,2}(a, b) = P_0(a \& b' \vee a' \& b) = P_0(a \& b') + P_0(a' \& b) = M_1 + M_2 - 2P_0(a \& b)$
 — Requires, equivalently, knowledge of $P_0(a \& b)$
 and is decreasing in $P_0(a \& b)$, for Q holding, i.e.,
 M_1, M_2 fixed
 $\leq d_{P,3}(a, b) = P_0(a \& b' \vee a' \& b \mid a \vee b) = d_{P,2}(a, b) / P(a \vee b)$
 $= (M_1 + M_2 - 2P_0(a \& b)) / (M_1 + M_2 - P_0(a \& b))$
 — Requires, equivalently, knowledge of $P_0(a \& b)$
 and is decreasing in $P_0(a \& b)$, for Q holding, i.e.,
 M_1, M_2 fixed
- Fréchet–Hailperin knowledge bounds on $P_0(a \& b)$ in general with Q holding

$$\text{MAX}(M_1 + M_2 - 1, 0) = \text{MIN}_{\underset{Q}{P_0(a \& b)}} \leq P_0(a \& b) \leq \text{MAX}_{\underset{Q}{P_0(a \& b)}} = \text{MIN}(M_1, M_2)$$

Use of Frechet–Hailperin knowledge bounds and decreasing function of $P_0(a \& b)$ property of $d_{P,2}(a \& b)$, $d_{P,3}(a \& b)$:

$$|M_1 - M_2| = \text{MIN}_{\underset{Q}{d_{P,2}(a \& b)}} \leq d_{P,2}(a \& b) \leq \text{MAX}_{\underset{Q}{d_{P,2}(a \& b)}} = \text{MIN}(M_1 + M_2, 1)$$

4. General Lower Knowledge and Total Knowledge Differences (KD) Between Use of Relational Events via $d_{P,2}$ vs. Their Non-Use

- $0 \leq \text{Lower KD} = d_{P,2}(a, b) - |M_1 - M_2| = \text{MIN}(M_1, M_2) - P_0(a \& b)$
 $\leq \text{Total KD} = \text{MIN}(M_1 + M_2, 1) - |M_1 - M_2| = \text{MIN}(M_1, M_2, 1 - M_1, 1 - M_2) \leq 1$

Figure 2. Outline of steps leading to quantitative measures of potential knowledge improvement using relational events via probability metric $d_{P,2}$. The reader should note the distinction between the italic a, b and the nonitalic a, b, c, \dots

1. Given: Example 2 with Two Arguments

Common Probability Space (Ω, B, P) ; Events a, b, c, \dots in B ,

Probability-Functional Model 1:

$$M_1 = f(P(a), P(b)) = w_1 P(a) + (1 - w_1) P(b),$$

Probability-Functional Model 2:

$$M_2 = g(P(a), P(b)) = w_2 P(a) + (1 - w_2) P(b),$$

$0 \leq w_1, w_2 \leq 1$ Constant Real Numbers

2. Obtain Relational Events

Imbed (Ω, B, P) into larger probability space (Ω_0, B_0, P_0)

$$a = f(a, b) = a \& b \vee ((a \& b') \times \theta(w_1)) \vee ((a' \& b) \times \theta(1 - w_1)),$$

$$b = g(a, b) = a \& b \vee ((a \& b') \times \theta(w_2)) \vee ((a' \& b) \times \theta(1 - w_2)),$$

Satisfying for all a, b in B , all P ,

$$P_0(a) = M_1, \quad P_0(b) = M_2$$

3. Computation of Two Probability Metrics

$$d_{P,1}(a, b) = |M_1 - M_2| = |P(a \& b') - P(a' \& b)| \cdot |w_1 - w_2|,$$

$$d_{P,2}(a, b) = P_0(a \& b') + P_0(a' \& b) = (P(a \& b') + P(a' \& b)) \cdot |w_1 - w_2|$$

$d_{P,2}(a, b)$, in turn, can then be used to make nontrivial comparisons between the models (see figure 1)

4. Lower Knowledge and Total Knowledge Differences (KD) Between Use of Relational Events via $d_{P,2}$ vs. Their Non-Use

$$0 \leq \text{Lower KD} = d_{P,2}(a, b) - |M_1 - M_2| = 2 \text{MIN}(P(a \& b'), P(a' \& b)) \cdot |w_1 - w_2| \\ \leq \text{Total KD} = \text{MIN}(M_1, M_2, 1 - M_1, 1 - M_2) \leq 1$$

Figure 3. Outline of implementation of quantitative measures of potential knowledge improvement using relational events for Example 2 modified for the two argument case.

1. Given: Example 1 with Consequences Identical

This is identifiable with problem of testing for similarity two posterior probability descriptions of same parameter of interest, a , via information, b , vs. information, d : common Probability Space (Ω, B, P) ; Events a, b, c, \dots in B ,

Probability-Functional Model 1:

$$M_1 = f(P(a), P(b), P(d)) = P(a|b)$$

Probability-Functional Model 2:

$$M_2 = g(P(a), P(b), P(d)) = P(c|d)$$

2. Obtain Relational Events, i.e., Conditional Events Here

Imbed (Ω, B, P) into larger Probability Space (Ω_0, B_0, P_0) ,

$$a = f(a, b) = (a|b), \quad b = g(a, b) = (a|d)$$

Satisfying for all a, b in B , all P , with $P(b), P(d) > 0$,

$$P_0(a) = M_1 = P(a|b), \quad P_0(b) = M_2 = P(c|d)$$

3. Computation of Two Probability Metrics

$$d_{P,1}(a, b) = | P(a|b) - P(a|d) | = | P_0((a|b) \& (a'|d)) - P_0((a'|b) \& (a|d)) | ,$$

$$d_{P,2}(a, b) = P_0((a|b) \& (a'|d)) + P_0((a'|b) \& (a|d)) ,$$

$d_{P,2}(a, b)$, in turn, can then be used to make nontrivial comparisons between the models (see figure 1)

4. Lower Knowledge and Total Knowledge Differences (KD) Between Use of Relational Events via $d_{P,2}$ vs. Their Non-Use

$$0 \leq \text{Lower KD} = d_{P,2}(a, b) - |M_1 - M_2| = 2 \text{MIN} (P_0((a|b) \& (a'|d)), P_0((a'|b) \& (a|d))) \\ \leq \text{Total KD} = \text{MIN} (P(a|b), P(a|d), P(a'|b), P(a'|d)) \leq 1$$

where the calculus of Boolean operators on conditional events yields:

$$P_0((a|b) \& (a'|d)) = [P(a \& b \& d')P(a'|d) + P(a' \& d \& b')P(a|b)] / P(b \vee d),$$

$$P_0((a'|b) \& (a|d)) = [P(a' \& b \& d')P(a|d) + P(a \& d \& b')P(a'|b)] / P(b \vee d)$$

Figure 4. Application of ETDM to the comparison of posterior probabilities referring to the same event parameter of interest.

ADDITIONAL AREAS OF RESEARCH COVERED

A number of issues concerning the establishment of a general ETDM based upon probability metrics are discussed in further detail in [23] and [24]. A preliminary version of certain aspects of the development of ETDM as given in [10] was presented in [25]. In a related vein (see again Example 4), [26] presents the general relational event algebra interpretation of natural language information via initial fuzzy logic description followed by one-point random set coverage theory, together with illustrative examples. [27] is a preliminary version of [28], whereby additional examples are provided of fuzzy logic models converted to probability-functional ones—with emphasis on homomorphic-like preservation of fuzzy logic modifiers using exponentiation. New research on

unifying disparate approaches to CEA and relating it further to the conditioning of random variables was presented in [29] and future publications will document this development further.

SUMMARY AND CONCLUSIONS

Conditional event algebra was fully extended to the more general form of relational event algebra, which proved useful in addressing a large class of information models—the probability-functional ones. More specifically, it was demonstrated that probability metrics, as well as the standard Fréchet–Hailperin bounds on the probability evaluations of logical operations, could be applied to relational event algebra to: produce sound measures of model similarity; fully test hypotheses for sameness of the models; and apropos to procedures that use relational events and those which do not, obtain quantitative knowledge differences, either in closed-form or in a suitable structure for numerical implementation. In turn, the above results form the basis for an extended theory of decision making that now includes probability-functional models. In addition, for the first time, relational event algebra was also shown to be directly applicable to natural language modeling via two levels of connectors: fuzzy logic and one-point random set theory. The problem of establishing a comprehensive theory of constant-probability events (a key building block in constructing relational events) was also addressed successfully.

Interest in conditional and relational event algebra has been gradually growing—as attested to by the contributions of a number of other researchers to edited books such as [30]; the entire issue of the journal *IEEE Transactions on Systems, Man & Cybernetics* devoted to CEA [31]; the extensive references by Hailperin in the latter part of his recent work, [4]; and the convening of a number of meetings, workshops, and popular lectures on these subjects. Future work on probability-functional models must follow up this beginning and address the issues of estimation and deduction. In fact, recent progress has been made on connecting the Boolean-structured CEA proposed here with other candidate non-Boolean CEAs, and in particular, with Adams’ “high probability” deductive system [32]. On the other hand, a number of open questions still remain concerning the hypotheses testing aspect of this work, including uniqueness of representation; computability; improvement of relational event forms for certain classes of nonanalytic functions, including min and max; and characterizations of local independence properties.

REFERENCES

1. Jevons, W.S. 1879. *The Principles of Science: A Treatise on Logic and Scientific Method*, 3rd Ed., Macmillan Co., London; Dover Reprint, NY, 1958.
2. Boole, G. 1854. *An Investigation of the Laws of Thought*, Walton & Maberly, London; Dover Reprint, NY, 1951.
3. Hailperin, T. 1986. *Boole’s Logic and Probability*, 2nd Ed., North-Holland Press, Amsterdam.
4. Hailperin, T. 1996. *Sentential Probability Logic*, Lehigh University Press, Bethlehem, PA.
5. Goodman, I. R. 1991. “Evaluation of Combinations of Conditioned Information: A History,” *Information Sciences*, vols. 57–58, pp. 79–110.

6. Nguyen, H. T. and E. A. Walker. 1994. "A History and Introduction to the Algebra of Conditional Events and Probability Logic," *IEEE Transactions on Systems, Man, & Cybernetics*, vol. SMC 24, no. 12 (December), pp. 1671–1675.
7. Buchanan, B. G. and E. H. Shortliffe. 1984. *Rule-Based Expert Systems*, Addison–Wesley, Reading, MA.
8. Duda, R. O. 1980. "The PROSPECTOR System for Mineral Extraction," Final Report, SRI Project #8172, AI Center, SRI International, Menlo Park, CA.
9. Kappos, D. A. 1969. *Probability Algebras & Stochastic Spaces*, Academic Press, NY.
10. Goodman, I. R., R. P. Mahler, and H. T. Nguyen. 1997. *Mathematics of Data Fusion*, Kluwer Academic Publishers, Dordrecht, Holland.
11. Goodman, I. R. and G. F. Kramer. 1997. "Comparison of Incompletely Specified Models in C⁴I and Data Fusion Using Relational and Conditional Event Algebra," *Proceedings of the Third International Command and Control Research and Technology Symposium* (held at National Defense University, Washington, DC, 17 to 20 June), pp. 193–215.
12. Goodman, I. R., H. T. Nguyen, and E. A. Walker. 1991. *Conditional Inference and Logic for Intelligent Systems: A Theory of Measure-Free Conditioning*, North-Holland Press, Amsterdam.
13. Lehmann, E. L. 1959. *Testing Statistical Hypotheses*, John Wiley & Sons, Inc., NY.
14. Fine, T. L. 1973. *Theories of Probability: An Examination of Foundations*, Academic Press, NY.
15. Nguyen, H. T. and E. A. Walker. 1997. *A First Course in Fuzzy Logic*, CRC Press, Boca Raton, FL.
16. Dubois, D. and H. Prade. 1980. *Fuzzy Sets & Systems: Theory & Applications*, Academic Press, New York.
17. Goodman, I. R. and H. T. Nguyen. 1985. *Uncertainty Models for Knowledge-Based Systems*, North-Holland Press, Amsterdam.
18. Goodman, I. R. 1994. "A New Characterization of Fuzzy Logic Producing Homomorphic-Like Relations with One-Point Coverages of Random Sets," *Advances in Fuzzy Theory & Technology*, vol. 2 (P. P. Wang, ed.), Duke University, Durham, NC, pp. 133–159.
19. Goodman, I. R. and H. T. Nguyen. 1995. "Mathematical Foundations of Conditionals and Their Probabilistic Assignments," *International Journal of Uncertainty, Fuzziness Knowledge-Based Systems*, vol. 3, no. 3 (September), pp. 247–339.
20. Goodman, I. R. and H. T. Nguyen. "The Matching Problem for Functions of Probability and Its Application to Data Fusion," to be submitted for publication.
21. Goodman, I. R. and G. F. Kramer. "Numerical Experiments Connected with Relational Event Algebra and Subsequent Decision Making," to be submitted for publication.
22. Rowe, N. 1988. *Artificial Intelligence through PROLOG*, Prentice-Hall, Englewood Cliffs, NJ.

23. Goodman, I.R. and G.F. Kramer. 1996. "Extension of Relational Event Algebra to a Decision Making Setting," *Proceedings of the Conference on Intelligent Systems: A Semiotic Perspective*, (held at National Institute of Standards & Technology (NIST), Gaithersburg, MD, 20 to 23 October), pp. 103–108.
24. Goodman, I. R. and G. F. Kramer. 1997. "Decision-Making Relative to Functionally-Expressed Information in Terms of Probabilities or Possibilities," *Proceedings of 1997 IRIS National Symposium on Sensor and Data Fusion* (held at MIT Lincoln Laboratory, Lexington, MA, 14 to 17 April), vol. 1, pp. 89–108.
25. Goodman, I. R. and G. F. Kramer. 1997. "Combination of Evidence and Deduction Corresponding to Collections of Events Which Are Not Initially Probability Represented," presented at the 35th Annual Bayesian Research Conference, University of Southern California (USC), Los Angeles, CA, 19 to 22 April.
26. Goodman, I. R. and G. F. Kramer. 1997. "Extension of Relational and Conditional Event Algebra to Random Sets with Applications to Data Fusion," in book *Random Sets: Theory & Applications* (IMA volume in Mathematics & Its Applications # 97), J. Goutsias, R. P. Mahler, and H. T. Nguyen, eds., Springer–Verlag, Berlin, pp. 209–239.
27. Goodman, I. R. 1997. "Homomorphic-Like Random Set Representations for Fuzzy Logic Models Using Exponentiation with Applications to Data Fusion," *Proceedings of the Third Joint Conference on Information Sciences*, (held at Research Triangle Park, NC, 1 to 5 to March), pp. 271–274.
28. Goodman, I. R. "Applicability of Conditional and Relational Event Algebra to Expert Systems Theory and New Homomorphic-Like Random Set Representations for Fuzzy Logic Models Using Exponential Modifiers," to appear in book *Advances in Machine Intelligence & Soft Computing*, vol. V, P. P. Wang, ed., Duke University, NC.
29. Goodman, I. R. 1997. "Two New Results in Product Space Conditional Event Algebra (PS): A Characterization Relating all Three Major CEAs Through Deduction and A New Family That Extends PS and Includes Locally Dependent Densities for the Limiting Case of Point-Nested Antecedents," invited presentation to the Department of Electrical and Computer Engineering, University of Massachusetts at Amherst, MA, 15 April.
30. Goodman, I. R., M. M. Gupta, H. T. Nguyen, and G. S. Rogers. 1991. *Conditional Logic in Expert Systems*, North-Holland Press, Amsterdam.
31. Dubois, D., I. R. Goodman, and P. G. Calabrese (eds.). 1994. Special Issue on Conditional Event Algebra, *IEEE Transactions on Systems, Man, & Cybernetics*, vol. SMC 24, no. 12 (December).
32. Goodman, I. R. and H. T. Nguyen. "New Connections Between Product Space Conditional Event Algebra and Adams' High Probability Logic," to be submitted for publication.

Principal Investigator:
Dr. I. R. Goodman

0601152N
ZU07

Performance Analysis of Multichannel Adaptive Equalization (MAEQ) for Line-of-Sight Digital Radio

Michael Reuter

Multichannel adaptive equalization combines the concepts of spatial diversity and temporal equalization into a joint spatial-temporal filter that can be used to improve digital radio receiver performance over traditional single-antenna receivers. A multichannel adaptive equalizer structure is analyzed in this research project for conditions common to the line-of-sight (LOS) digital radio environment of interest to the Navy. This environment is characterized by flat and frequency-selective fading as well as by severe interference effects. The multichannel equalizer is ideally suited for this challenging environment.

NEED AND BACKGROUND

The Navy is interested in providing reliable line-of-sight (LOS) communications for ship-to-ship, ship-to-shore, and ship-to-air applications. Future high-data-rate LOS digital radios for mobile military applications must operate in a crowded spectrum and contend with intentional or unintentional jamming, co-channel signals, and time-varying propagation environments inducing both flat and frequency-selective fading (figure 1). Moreover, the spectrally efficient modulation formats such as M-ary phase shift keying (M-PSK) or M-ary quadrature amplitude modulation (M-QAM) that will be required to achieve the desired high data rates will further strain system performance issues. The time-varying spatial and temporal nature of this environment is ideally suited for adaptive equalization, particularly multichannel adaptive equalization (MAEQ).

MAEQ combines the spatial processing of adaptive narrowband beamformers with the temporal processing of single-channel adaptive equalizers into a joint spatial-temporal filter. MAEQ is capable of compensating for intersymbol interference induced by dispersive communication channels while simultaneously mitigating the effects of flat and frequency-selective channel fading and spatially correlated interference. Potentially, MAEQ is an important component of reliable high-data-rate LOS digital radio systems between mobile platforms.

RESEARCH GOAL

The MAEQ filter considered in this research project was originated by Monsen [1], [2] and is shown in figure 2. It has demonstrated significant performance improvements over both narrowband adaptive beamformers and single-channel adaptive equalizers. The structure consists of M isotropic antenna elements, each followed by a two-sided fractionally spaced transversal equalizer with oversampling factor O_s , and an N_3 -tap symbol-spaced decision feedback filter. Each fractionally spaced equalizer has N_1 precursor and N_2 postcursor taps. A carrier recovery loop follows each transversal filter. This structure is robust because it can do simultaneous signal acquisition, carrier synchronization, and channel equalization in an interference-dominated environment. Minimization of the mean square error (MMSE) is used as the optimization criterion.

Although multichannel equalization has received increased attention in recent years [3], [4], and [5], little or no analysis has been done on the effect of the combined spatial and temporal characteristics of the MAEQ on its performance in the LOS environment. Quantifying the performance of the

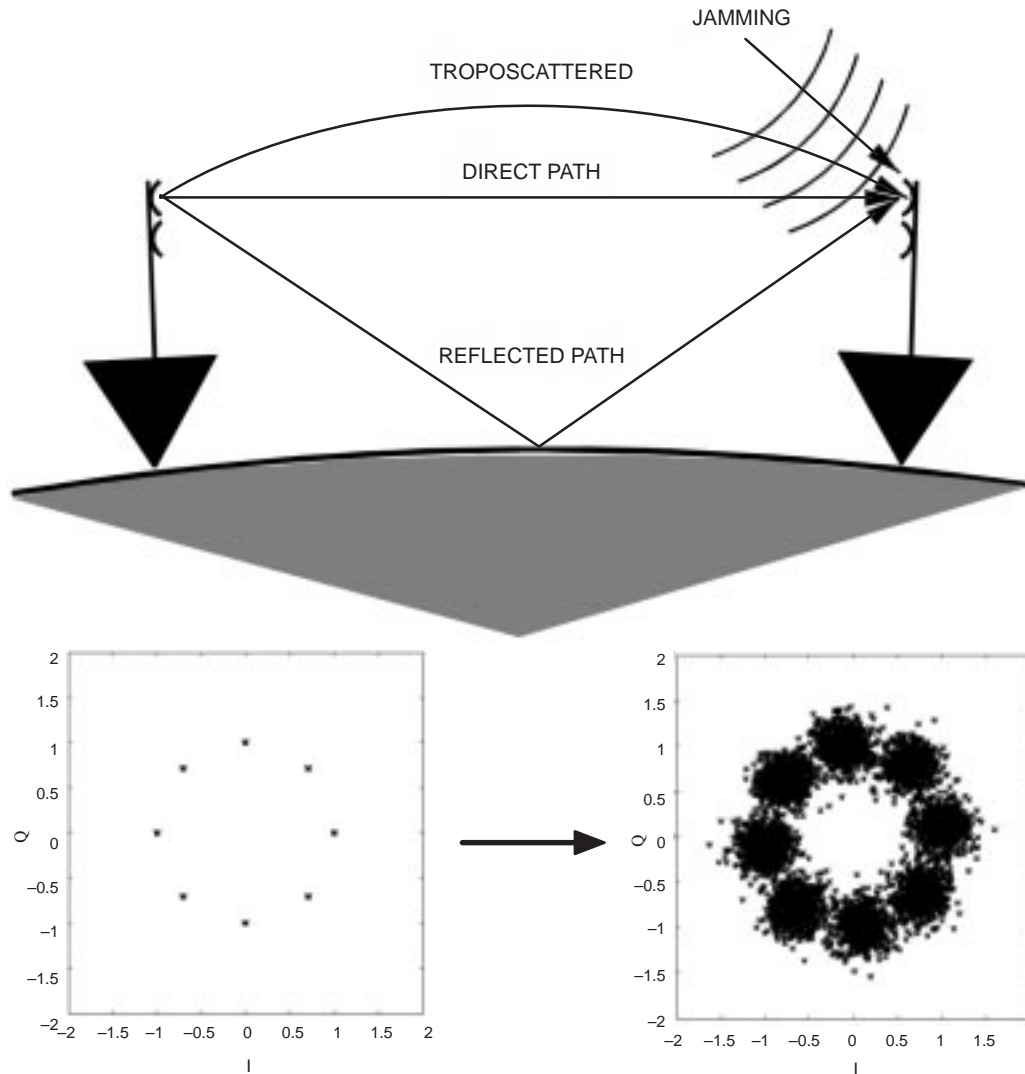


Figure 1. Ship-to-ship communication environment schematic.

MAEQ in terms of system and environmental parameters has important implications for designing reliable receivers such as determining required computational or hardware requirements, number of antennas, quality of filters, anti-jam performance, system capacity, etc. The goal of this research effort is to answer questions such as:

- Given an interference and propagation (channel) environment, what is the desired spatial distribution of antennas?
- What is the required receive signal-to-noise ratio?
- How many taps are required in the feedforward and feedback filters to adequately cancel interference as well as equalize the communication channel?
- Given some MAEQ structure, what is the worst-case environment (interference, multipath propagation, fading) that can be adequately equalized at some base performance level?

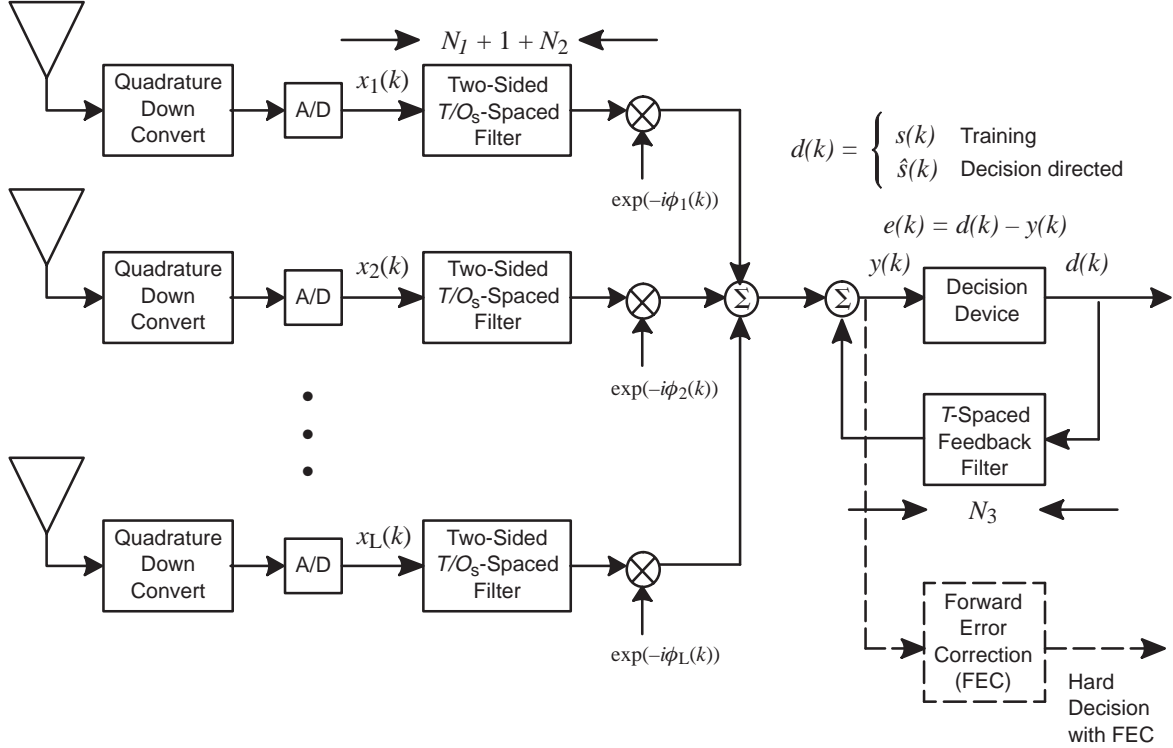


Figure 2. Multichannel adaptive equalizer structure.

MAEQ PERFORMANCE ANALYSIS

The steady-state Wiener filter of the MAEQ depicted in figure 2 has been derived for the LOS radio environment. Initial effort went to quantifying the anti-jam characteristics of the MAEQ as a function of system parameters such as equalizer length, spatial distribution of the antennas, transmit/receive filters, signal-to-noise ratio (SNR), and signal-to-interference ratio (SIR). These results have been presented in [6] and [7].

Two measures of performance for analyzing equalizers are of interest. The mean square error is important because it is independent of the modulation format and is the basis of the optimization criterion of the MAEQ considered in this research. Also, the probability of symbol error is an important measure, particularly from a communication theory standpoint. However, calculating the probability of error (P_e) for the MAEQ is a challenging problem because of the intersymbol interference induced by bandlimiting in the transmit and receive filtering, in the multipath propagation, and in the equalizer itself. To solve this problem, a computationally efficient technique to calculate P_e with intersymbol interference was developed. The method is very useful because it is applicable to two-dimensional modulation formats with arbitrary decision regions. This work was documented in [8].

Some numerical results will demonstrate the findings of this work. For all simulations, an evenly spaced, vertical antenna array with half-wave-wavelength spacing is used. Figures 3, 4, and 5 are the spatial-spectral beampatterns of the MAEQ with four antennas for scenarios with consecutively larger interferer bandwidths. A notch is observed to be centered at the interferer, effectively canceling it both spatially and spectrally. Also, as the bandwidth increases, this interference canceling

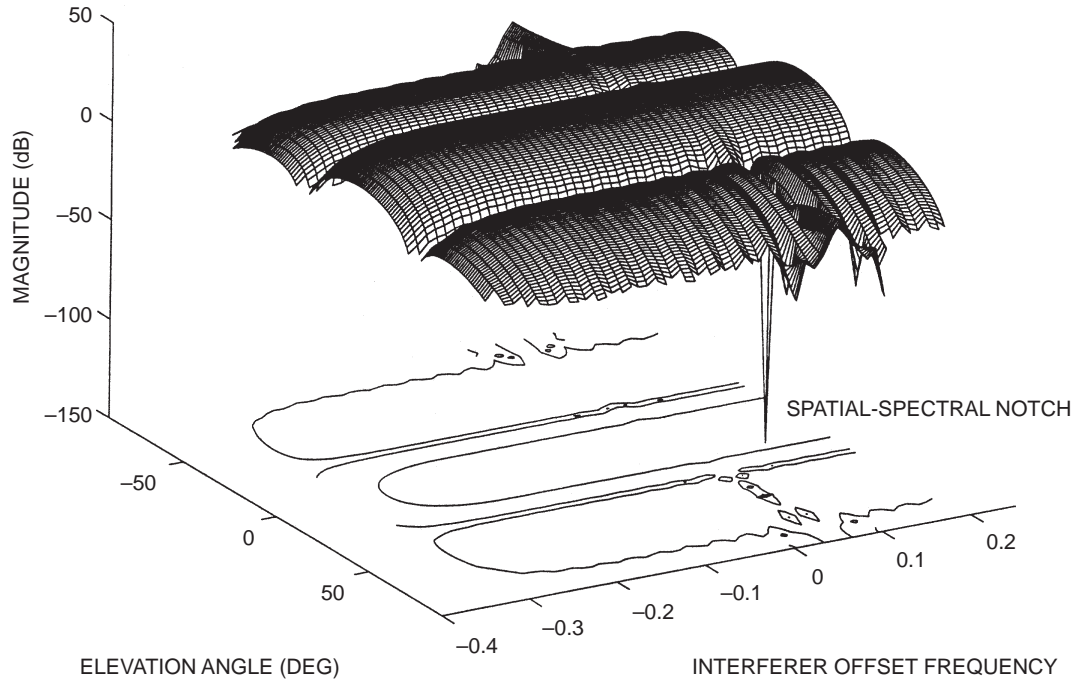


Figure 3. Beampattern for MAEQ with four antennas and a continuous wave (CW) interferer at 50° elevation and normalized offset frequency 0.05.

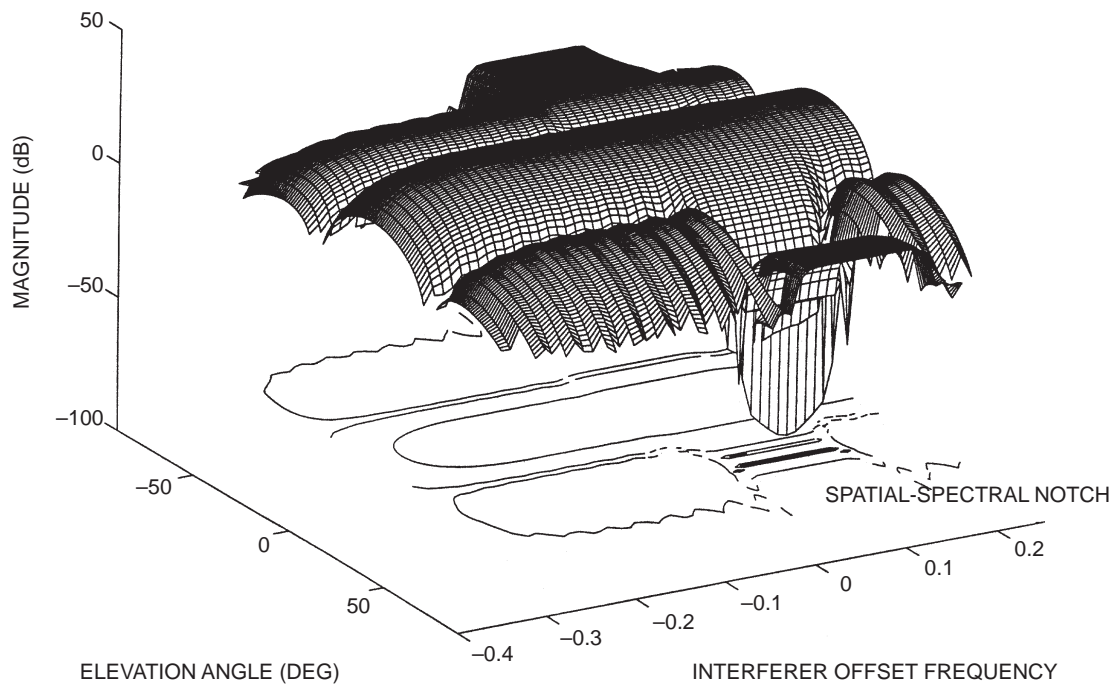


Figure 4. Beampattern for MAEQ with four antennas and an interferer at 50° elevation with normalized offset frequency 0.05 and bandwidth 0.10.

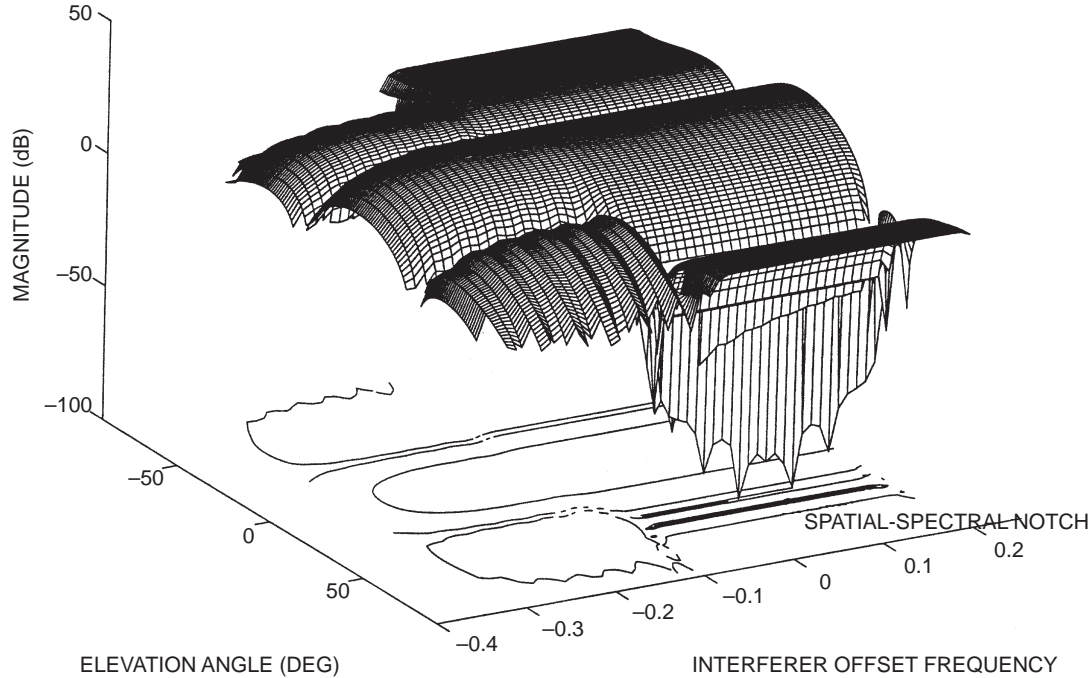


Figure 5. Beam pattern for MAEQ with four antennas and an interferer at 50° elevation with normalized offset frequency 0.05 and bandwidth 0.25.

comes at the price of increased distortion of the quiescent beam pattern of the MAEQ, resulting in possibly significant intersymbol interference.

Figure 6 plots P_e for 4-PSK and 16-PSK modulation formats and the corresponding MMSE versus SNR for arrays with one, two, four, and six antennas in which an interferer is arriving with elevation angle 10°, normalized bandwidth of 0.25, and SIR = -20 dB. Each equalizer is symmetric with $N_1 = N_2 = 30$ taps, and $N_3 = 15$ feedback taps. The symbol rate is the same for both formats. For the single equalizer case, an unrealistically high SNR is required to meet a specification of $P_e = 10^{-6}$ for 16-PSK. However, there is a dramatic drop in required SNR by adding just one more antenna. Conversely, there is only a modest improvement in performance between the four and six antenna arrays due to similar spatial nulling capabilities for this interference arrival angle. These plots also are useful in relating the MMSE to P_e . For unit variance symbols, a P_e of 10^{-6} requires a MMSE of approximately 0.040 for 4-PSK and 0.003 for 16-PSK for all antenna arrays. These MMSE requirements can be designed more easily into the MAEQ structure than can P_e .

Figure 7 demonstrates the effect the spatial beam pattern of a four-antenna array has on performance. P_e and MMSE are plotted versus interferer elevation angle for various interferer bandwidths and SNR = 10 dB for 4-PSK. The beam pattern structure is clearly visible. It is interesting to note that regardless of the bandwidth, the array spatially cancels the interference when it arrives off the main lobe of the antenna. However, as the interferer enters the main lobe, the temporal properties of the equalizers dominate. In this region, performance substantially degrades as the interferer bandwidth increases. The performance of the array is relatively insensitive to interferer elevation angle for the CW case.

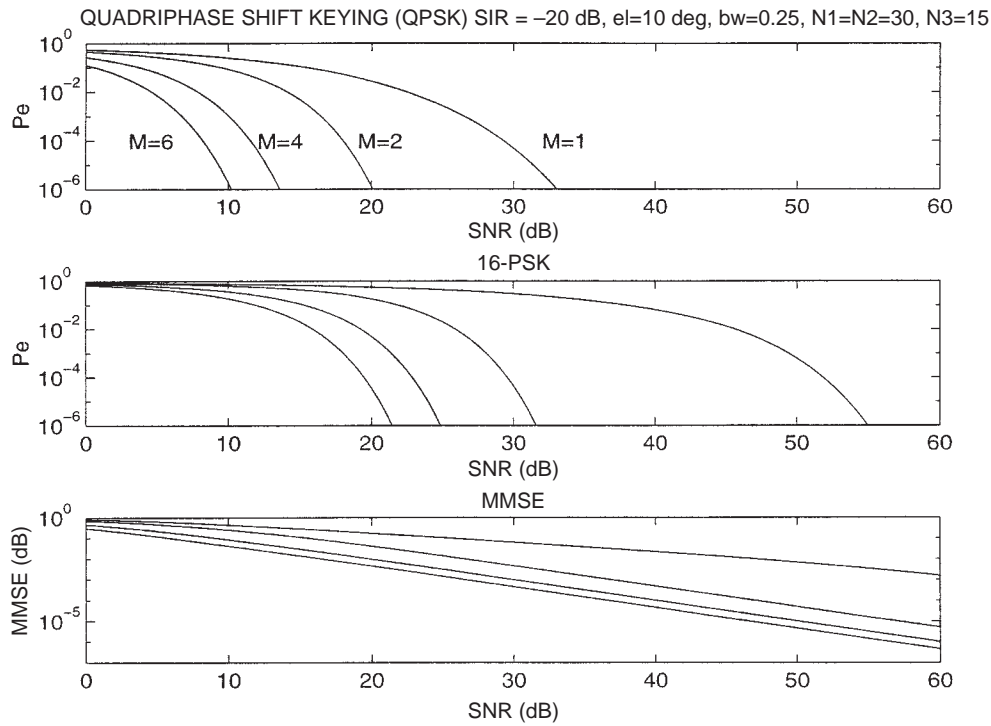


Figure 6. 4-PSK and 16-PSK for one, two, four, and six antennas with an interference elevation angle of 10° and bandwidth 0.25.

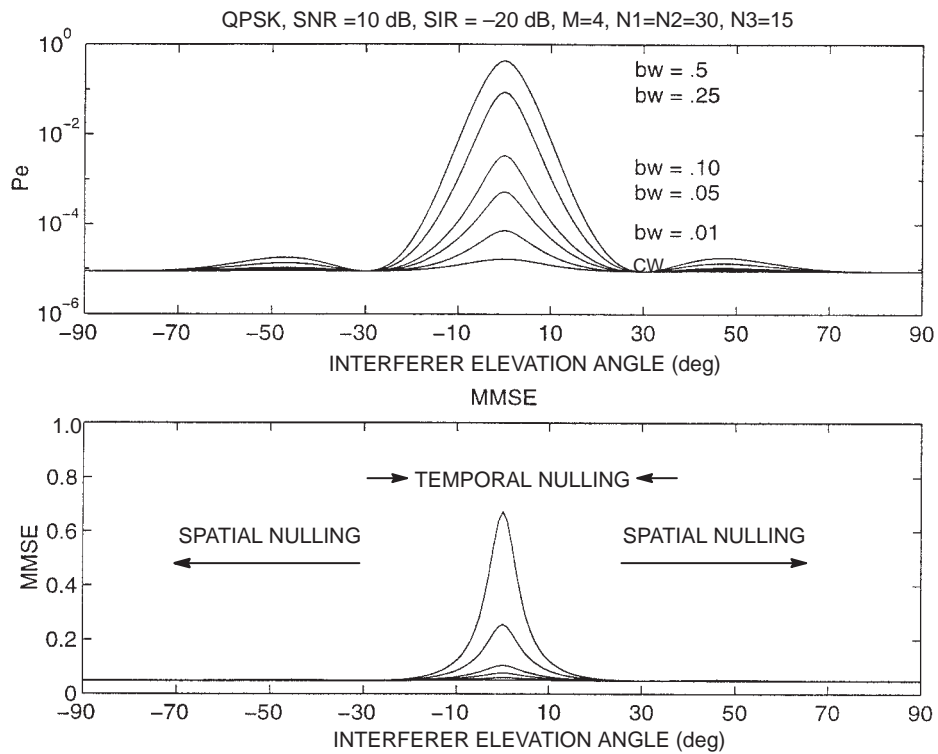


Figure 7. 4-PSK with various interferer bandwidths for four antennas.

Figure 8 shows the effect of varying the number of equalizer taps in a four-element array with SNR = 10 dB and 4-PSK modulation. The normalized interferer bandwidth is 0.01. The equalizers are symmetric with $N_1 = N_2 = N$ and $N_3 = N/2$ feedback coefficients. All arrays perform approximately equally when the interferer falls outside of the main lobe of the antenna due to the spatial nulling properties of the MAEQ. However, as the interferer arrival angle enters the main lobe, the temporal nulling effects of equalizers outperform those with fewer taps. This indicates that for CW or narrow-band interferers, increasing the number of taps can make the MAEQ relatively insensitive to the direction of the interference due to the temporal nulling capability of long equalizers. Then, the antenna geometry can be based upon other criteria such as mitigation of fading effects and not on interference nulling. This is not necessarily the case with very broadband interference or co-channel interference.

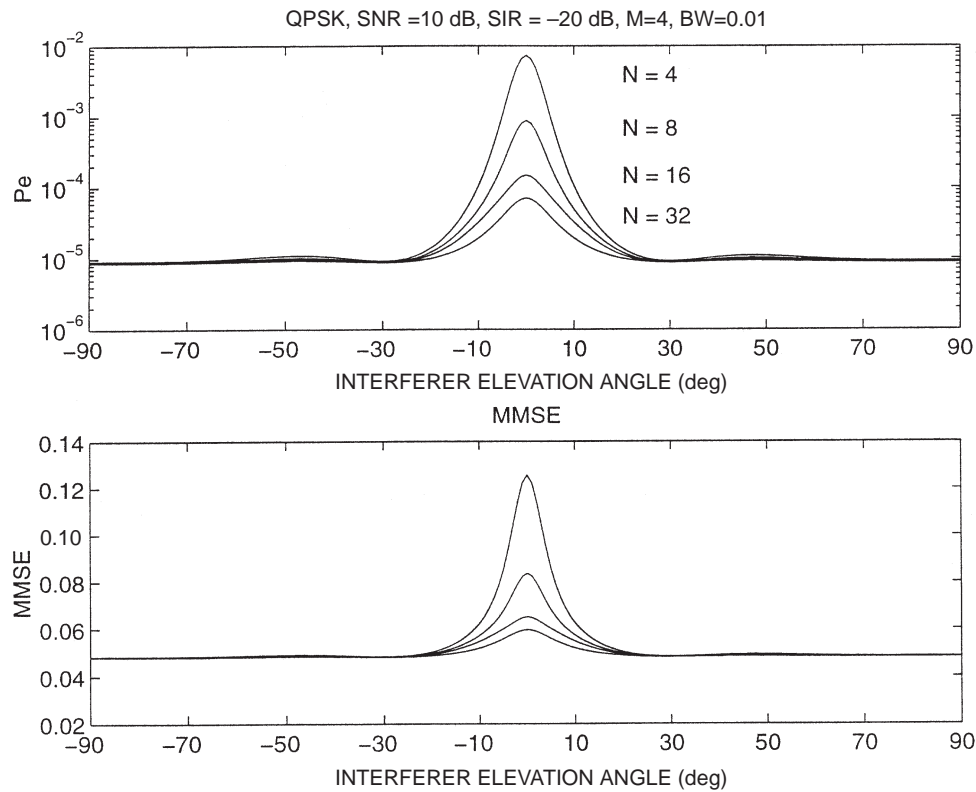


Figure 8. 4-PSK and symmetric equalizers for various equalizer lengths with four antennas and interference bandwidth 0.01.

FURTHER WORK

Although the MAEQ structure is very robust and should be an important component in a high-data-rate digital radio, additional robustness can be obtained by incorporating coding as is shown in figure 2. Recent results [9] indicate that by adding enough antennas to a receiver, a fading channel can be transformed into an additive white Gaussian noise (AWGN) channel. This has important implications for the MAEQ because if distortion caused by channel-induced dispersion and interference can be mitigated, simple codes that work well on the AWGN channel may considerably improve the performance of the MAEQ.

REFERENCES

1. Mosen, P. 1977. "Theoretical and Measured Performance of a DFE Modem on a Fading Multi-path Channel," *IEEE Transactions on Communications*, vol. COM-25, no. 10, pp. 1144–1153.
2. Mosen, P. 1984. "MMSE Equalization of Interference on Fading Diversity Channels," *IEEE Transactions on Communications*, vol. COM-32, no. 1, pp. 5–12.
3. Winters, J., J. Salz, and R. Gitlin. 1994. "The Impact of Antenna Diversity on the Capacity of Wireless Communications Systems," *IEEE Transactions on Communications*, vol. 42, no. 2/3/4, pp. 1740–1751.
4. Clark, M., L. Greenstein, W. Kennedy, and M. Shafi. 1994. "Optimum Linear Diversity Receivers for Mobile Communications," *IEEE Transactions on Vehicular Technology*, vol. VT-43, no. 1, pp. 47–56.
5. Lo, N., D. D. Falconer, and A. Sheikh. 1991. "Adaptive Equalization and Diversity Combining for Mobile Radio Using Interpolated Channel Estimates," *IEEE Transactions on Vehicular Technology*, vol. VT-40, no. 3, pp. 636–645.
6. Reuter, M., R. North, and J. Zeidler. 1995. "The Performance of Multichannel Adaptive Equalization for LOS Digital Communication Corrupted by Interference," *International Conference on Acoustic Speech and Signal Processing (ICASSP)*, pp. 1856–1859.
7. Reuter, M., R. North, and J. Zeidler. 1995. "Performance Analysis of a Multichannel Adaptive Equalizer for Line-of-Sight Digital Radio," *IEEE Military Communications Conference (MILCOM)*, pp. 597–601.
8. Reuter, M. 1997. "Numerically Efficient Fourier-Based Technique for Calculating Error Probabilities with Intersymbol Interference," *IEEE Transactions on Communications*, vol. 45, no. 6, pp. 629–632.
9. Ventura-Traveset, J., G. Caire, E. Biglieri, and G. Taricco. 1997. "Impact of Diversity Reception on Fading Channels with Coded Modulation—Part I: Coherent Detection," *IEEE Transactions on Communications*, (May), pp. 563–572.

Principal Investigator:
Michael Reuter

0601152N
ZU12

ACCOMPLISHMENTS AND IMPACTS

ACCOMPLISHMENTS AND IMPACTS

Fiber-Optic Device Research

Principal Investigators: Matt McLandrich and Richard Orazi

Background:

For several years, SSC San Diego has invested In-house Laboratory Independent Research (ILIR) (or simply IR) funds for research projects relating to fiber-optic devices. An example of this research can be found as a featured article entitled “Optical Fiber Devices Based on Index of Refraction Changes in Highly Overcoupled Fused-Fiber Couplers,” in the Independent Research 1996 Annual Report, NRaD TD 2933, pp. 11–22.

Scientific Accomplishments:

The basic research has focused primarily on the optical coupling that occurs between optical fibers when the fibers are fused together. The coupling mechanisms are dependent on many factors such as fiber properties and the fusing process, and the coupling can also be modified subsequent to fusion by mechanical stress or exposure to ultraviolet light. Methods for monitoring and controlling the optical coupling in fused fiber devices have resulted from this basic research.

Technology Impacts:

In the early 1990s, a proposal was made to the Distributed Surveillance Technology program [funded by ONR 321, SSC San Diego program manager Ken Rogers, (619) 553–1521] to develop a narrow-channel wavelength division multiplexer (WDM) operating in the 1550-nm region. The proposed application was long-haul, bi-directional, fiber-optic telemetry links for remote acoustic sensor arrays. In the course of this work, the problem of polarization dependence arose and was solved, leading to development of the Polarization Independent Narrow-Channel WDM (PINC WDM). Erbium-doped fiber-optical amplifiers were also investigated as part of this program.

While the PINC WDM satisfied the performance requirements for the intended application, the production of the devices was characterized by high cost and low yield, making them unsuitable for widespread application. Consequently, work was initiated under a Manufacturing Technology (MANTECH) effort to solve this deficiency. Funds were provided for 1 year via the Common All-Optical Towed Array (CAOTA) MANTECH program [sponsored by ONR, SSC San Diego program manager John Townsend, (619) 553–1382]. This effort resulted in increased production yield from 10% to greater than 80%, while the cost was reduced from more than \$1,000 to less than \$100.

A Cooperative Research and Development Agreement (CRADA) has been executed with SDL, Inc., the largest U.S. producer of laser diodes. The CRADA includes license agreements for a portfolio of SSC San Diego fused-coupler/PINC WDM patents. SDL has recently introduced three new products incorporating fiber-optic couplers based on inventions by Matt McLandrich and Richard Orazi. These commercial off-the-shelf (COTS) products will find applications in communication systems and other fiber-optic-based technologies, both military and civilian.

SSC San Diego is supporting the DARPA Global Positioning System (GPS) Guidance Package Program (GGP) and an associated Interferometric Fiber-Optic Gyroscope (IFOG) MANTECH program. In the course of these support activities, various technical issues related to gyro components (e.g., couplers) and subsystems (e.g., broadband light sources) have arisen. Recognizing that the unique SSC San Diego PINC WDM technology may offer solutions, DARPA has provided funds to investigate novel erbium-doped fiber-light-source components and architectures. This work is a transition of Richard Orazi's FY 97 IR project, detailed elsewhere in this report.

Numerous patents, journal publications, and awards have resulted from ILIR-sponsored fiber-optic research at SSC San Diego and from the transition programs that have followed.

Fleet Impacts:

The PINC WDM is an essential component of the electro-optic telemetry for fiber-optic-based anti-submarine warfare (ASW) sensors. It is also an essential component of the arrays in the All-Optical Deployable System (AODS), [managed by SPAWAR] and is useful in both towed arrays and planar hull-mounted arrays. Only a few hundred thousand dollars were invested in the PINC WDM workstation under CAOTA, and this is by far the most beneficial portion of the overall CAOTA effort.

Another potential fleet impact may result from collaboration with SSC San Diego personnel to explore further development of IFOG technology for subsurface marine navigation. Current IFOG technology is not adequate for this application, and inertial systems presently in use are too costly to purchase and maintain.

Finally, it should be noted that this technology has transitioned into commercial production and consequently, will find its way into fleet systems via use of COTS products.

Matched-Field Acoustic Processing for Antisubmarine Warfare

Principal Investigator: Dr. Homer Bucker

Background:

Matched-Field Processing (MFP) is a method of extracting information from acoustic data gathered by acoustic arrays in order to determine the direction, range, and depth of targets. The method was first developed and reported by Dr. Homer Bucker in 1975 under ILIR sponsorship at SSC San Diego (then Naval Ocean Systems Center). The pioneer reference in this field is:

H. P. Bucker, "Use of Calculated Sound Fields and Matched-Field Detection to Locate Sound Sources in Shallow Water," *J. Acoust. Soc. Am.*, vol. 59, pp. 368–373 (1976).

Scientific Accomplishments:

Since the mid 1970s, MFP has evolved into an active area of research in underwater acoustics with the *Journal of the Acoustical Society of America* adding matched-field processing as a subject category listing (43.30.W, "Passive Sonar Systems and Algorithms, Matched-Field Processing"). Much of this research has been driven by recent successes in applying the techniques in littoral waters to improve the passive detection of submarines with vertical and horizontal arrays. By searching in range, depth, and azimuth, MFP improves the signal-to-noise ratio by rejecting surface-generated noise while classifying a target as submerged by determining target depth.

Technology Impacts:

Several Navy laboratories, contractors, and universities have active research and development programs that are based on MFP technology. Some of the organizations include SSC San Diego, Naval Research Laboratory (NRL), Naval Undersea Warfare Center (NUWC), Science Applications International Corporation (SAIC), ORINCON, Scripps Institution of Oceanography (SIO), Duke University, University of Texas Applied Research Laboratory (APL), and University of Victoria in Canada.

MFP was the primary approach used in the High-Gain Initiative, a multimillion dollar Office of Naval Research program conducted between 1987 and 1991 that focused on deep-water applications. Since that time, experiments have demonstrated feasibility and improved performance in shallow water.

Fleet Impacts:

Performance improvements have been demonstrated using horizontal line arrays of the aperture that are currently in the Fleet, such as the Surveillance Towed Array Sensor System (SURTASS) and the submarine TB-23 towed array. Similar apertures are currently in development for the SPAWAR Advanced Deployable System project. The sponsors of these systems, SPAWAR and Naval Sea Systems Command (NAVSEA) Advanced Submarine Technology Office (ASTO), are currently evaluating proposals to develop adaptive MFP as an approach for providing target classification and improved detection in the forward sector, end-fire direction of their respective systems.

Bioluminescence as a Flow Diagnostic

Principal Investigator: Dr. James Rohr

Background:

From FY 93 to FY 95, an IR project was funded to investigate flow-induced stimulation of luminescent plankton for the purpose of flow visualization. This research was motivated, in part, by a belief that such luminescence occurred only in the presence of turbulent flow, and by references in the marine biology literature suggesting that dolphins were able to move through water laden with luminescent organisms without stimulating them. This phenomenon was ascribed to a conjecture that, through some unknown mechanism, the animal was able to maintain a laminar boundary layer at high speeds.

Scientific Accomplishments:

The ILIR-sponsored effort led to a collaborative transition via an ONR-funded effort with Dr. Michael Latz, a marine biologist at Scripps Institution of Oceanography, wherein related experiments were performed with cultured species of dinoflagellates. Comparisons between morphological structure and bioluminescence response to shear stress were made. Numerous publications and reports resulted from this collaboration.

In collaboration with Dr. Latz, the phenomenon of flow-induced bioluminescence for specific organisms was quantitatively defined. The bioluminescence threshold occurred in laminar flow at shear stresses of the order of 1 dyn/cm^2 . Also, at shear stresses greater than about 10 dyn/cm^2 (still laminar flow), the response of individual cells usually peak and remain nearly constant with further increase in shear stress.

This information was applied to predict the effects of flows around ships and animals. For example, according to calculations, even a laminar boundary layer at speeds well below 2 meters per second would exceed threshold levels of flow-induced luminescence.

Navy dolphins were filmed under conditions suitable to study dolphin-stimulated bioluminescence. It was found, as predicted, that bioluminescence can be observed along most of the animal, and the thickness of the boundary layer is the most important parameter determining the intensity of the bioluminescence.

Technology Impacts:

Civilian applications for development of medical devices are proposed in the following paper: J. Rohr, J. Allen, J. Losee, and M. I. Latz, "The Use of Bioluminescence As A Flow Diagnostic," *Physics Letters A.*, vol. 228, pp. 408–416 (1997).

Fleet Impacts:

Anticipated fleet impacts are primarily in surveillance. Examples include swimmer detection, signatures for ship motion, and effects of tidal flow around tethered mines. A potential route for exploitation would be development of hyperspectral sensing techniques that could reveal flow-induced bioluminescence in the presence of high-levels of ambient light.

PROJECT SUMMARIES

COMMAND AND CONTROL

Enhancing SmartNet for Scheduling Network Traffic

Objective(s): Effectively schedule computational tasks in light of the effects of network congestion.

Accomplishment(s): A method was developed and shown to adequately account for network delays when scheduling computational tasks on networks of heterogeneous computers.

The computational and network requirements of current command and control systems are continually increasing. It is assumed that forward-deployed forces will possess significant computational capabilities, such as personal computer (PC), Sun, and Hewlett-Packard (HP) workstations, and that these computers will be linked via satellite networks to databases and supercomputer centers throughout the world. In such an environment, scheduling is crucial to ensure that high-priority tasks receive appropriate computational resources and that network bandwidth, latency, and congestion are considered when allocating these resources. The SmartNet system is intended to perform this scheduling function.

Traditional approaches to task scheduling have relied on either balancing the load on the computers on the network, or on allowing users to decide *a priori* which computers to use for their tasks. SmartNet has been designed to consider both the rate at which each computer executes each task in isolation, as well as the load on each computer as it is assigned tasks. This work enhanced SmartNet to also consider network bandwidth, latency, and congestion when scheduling tasks.

Tests were performed simulating the operation of hundreds of different networks of computers running thousands of different mixes of tasks. These tests verified that the SmartNet scheduling system can accommodate the variations in task completion times due to network effects better than the traditional scheduling approaches.

REFERENCE

Freund, R. F., M. Gherrity, S. Ambrosius, M. Campbell, M. Halderman, D. Hensgen, E. Keith, T. Kidd, M. Kussow, J. Lima, F. Mirabile, L. Moore, B. Rust, and H. J. Siegel. "Scheduling Resources in Multi-User, Heterogeneous, Computing Environments," submitted to the *Journal of Parallel and Distributed Computing* and presented as an invited paper in the 1998 Heterogeneous Computing Workshop, Orlando, FL.

Principal Investigator:
Dr. Richard Freund

0601152N
ZU06

Additional Contact:
Michael Gherrity

Important Perceptual Features for Speaker Identity

Objective(s): Determine the most important acoustic features that affect human perception of voice identity for familiar and unfamiliar speakers. Specifically, the degree of familiarity was investigated and acoustic parameters were perturbed 25 percent in the first experiment, and candidate acoustic parameters were perturbed to match the target speaker in the second experiment.

Accomplishment(s): This research helped the speech projects currently in work at SSC San Diego. We are now writing a longer report and plan to write a proposal for continuing research. The actual factors that differentiate between familiar and unfamiliar speakers still need to be studied.

BACKGROUND

Speaker identification and signal-sorting algorithms have to add some perceptually based features to improve the performance of automatic speaker identification. At present, the spectrum (sometimes with a minimum of sequential information) is measured statistically. These methods do not encompass human perceptual features in identifying speakers. The inclusion of human perceptual features in computer algorithms could increase speaker identification accuracy. The present research studied the effect of various perceptual features on speaker identification accuracy.

The literature was reviewed in the previous research conducted on the potential factors that affect speaker identity. Earlier studies have shown that spectral characteristics, pitch contour, mean frequency, and segmental durations affect speaker identification (Higuchi & Hashimoto, 1995; Itoh & Saito, 1988; Kitamura & Akagi, 1995). The perception of voice identification is sensitive to the formant shift. Some studies have been conducted on the relevance of listener familiarity with the speakers. Identification of familiar speakers is very important in tactical communications that usually involve speakers who have been heard previously. Important communications require confirmation of identity before action is taken.

APPROACH

The Speaker Identification algorithm for comparing the results of human performance with computer identification was developed. A MATLAB* computer program was created to manipulate the speech parameters. The programmer developed the interface for the experiment and integrated the manipulated speech into the test programs. In the present research, two experiments were conducted. In the first experiment, pitch, formant shift, and speaking rate were tested. Based on the results of the first experiment, additional factors, singularly and in combination, were tested in the second experiment. The six parameters that were perturbed, singularly or in combination, were: formant shift, glottal

*MATLAB is a registered trademark of the The MathWorks, Inc.

excitation, energy, average pitch, pitch contour, and duration.** Table 1 identifies the parameters perturbed in each condition.

Table 1. Number of the speech condition corresponding to the parameters that were perturbed.

Number	Parameters Perturbed for each Speech Condition
1	Formant Shift
2	Glottal Excitation
3	Energy
4	Average Pitch
5	Pitch Contour
6	Duration
7	Normal (No parameters perturbed)
8	Formant Shift & Excitation
9	Formant Shift & Energy
10	Formant Shift & Average Pitch
11	Formant Shift & Pitch Contour
12	Formant Shift, Excitation, & Energy
13	Formant Shift, Energy, Average Pitch
14	Formant Shift, Excitation, Average Pitch, & Duration
15	Formant Shift, Excitation, Energy, Average Pitch, & Duration
16	All six parameters
17	Excitation, Energy, Average Pitch, & Duration
18	Excitation, Energy, Average Pitch, Pitch Contour, & Duration

Listener familiarity with the speakers was also tested. Problems of familiarity testing include measurement of degree of familiarity, choice of spoken material (read vs. spontaneous), and size of speaker set. In this research, degree of familiarity was measured and tested. Familiarity was divided into four groups. The first group of listeners (unfamiliar) had never met the speakers. The second group of listeners were slightly familiar with the speakers. "Slightly familiar" meant the listeners only spoke with the speakers briefly once or twice a week. The third group of listeners (very familiar) associated closely with the speakers. The fourth group of listeners (working familiar) not only associated closely with the speakers but also were aware of how the speech was manipulated. The speakers and all of the listeners in this group had worked closely together for a minimum of 4 years. Computer speaker identification was also compared to human speaker identification.

RESULTS

The results of the first experiment showed that speaking rate had no significant effect. However, pitch variation and formant shift significantly affected speaker identification accuracy. In the second experiment, speech condition was highly significant. Neuman-Keuls comparison tests showed that the normal condition (no parameters perturbed, condition 7 in table 1), energy alone (condition 3),

**Formants in the spectral envelope were shifted to resemble the target speaker for perturbations in the formant shift condition. The parameter excitation is defined as the residual wave form after taking out the spectral envelope. Energy is defined as the power of each pitch pulse averaged across the wave form. Average pitch referred to changing the range of pitch pulses over the entire sentence. Pitch contour referred to changing the contour of the pitch wave form to match the target speaker. Duration was the length of each phoneme.

and duration alone (condition 6) were significantly more accurate than any of the other speech conditions. In other words, the perturbation of duration or energy alone did not significantly influence listeners' perception of the identity of the speaker.

Conditions 2 (glottal excitation), 4 (average pitch), and 5 (pitch contour) did significantly increase errors when compared with the normal condition. Thus, speaker identity is affected by each of these parameters alone. However, except for formant shift, listeners were more accurate when a single parameter alone was perturbed than when a combination of parameters were perturbed. In the condition where the formants were shifted alone (condition 1), listeners had significantly more errors than any of the other single parameter conditions. Condition 1 also had significantly more errors than conditions 17 and 18 where formant shift was not included as a parameter. Excluding formant shift alone, conditions 17 and 18 had significantly more errors than the normal condition and the single parameter conditions. Listeners made significantly more errors in the conditions where two or more parameters were perturbed.

Familiarity was not significant. The factors tested in this research had no effect on accuracy between familiar and unfamiliar listeners. The comparison between human listeners and the computer speaker identification program showed some similarities. Overall, the human listeners identified speakers more accurately than the computer program except for Conditions 17 and 18 where the formants were not shifted.

REFERENCES

1. Higuchi, N. and M. Hashimoto. 1995. "Analysis of Acoustic Features Affecting Speaker Identification," *Eurospeech Proceedings*.
2. Itoh, K. and Saito, S. 1988. "Effects of Acoustical Feature Parameters on Perceptual Speaker Identity," *Review of the Electrical Communications Laboratories*, vol. 35, no. 1.
3. Kitamura, T. and M. Akagi. 1995. "Speaker Individualities in Speech Spectral Envelopes," *Journal of the Acoustical Society of Japan*, vol. 16, no. 5.

Principal Investigator:
Suzanne V. Bemis

0601152N
ZU20

Co-Investigator:
Stephen W. Nunn

Faster-Than-Real-Time Synthetic Forces (FTRT SF) Simulation

Objective(s): Research software architectures and methodologies that permit realistic, high-fidelity computer simulations of military forces and equipment which can be executed not only in real-time (i.e., simulation time equals wall-clock time), but permits execution at faster-than-real-time speeds (i.e., 2 days of simulation time can be executed in several hours).

Accomplishment(s): The main accomplishment has been the identification of two simulation architectures and a single software abstraction layer which allow realistic, high-fidelity simulations of military forces and equipment faster-than-real-time. This goal was achieved at both the electronic circuit-level for military equipment and the theater-level for military forces. These capabilities have been demonstrated to independent, interested DoD representatives.

Over the last two decades, researchers have attempted to develop large-scale simulations spanning many levels of system resolution. Models developed by operations researchers in support of DoD are an example. These efforts to develop simulations of large parts of reality, from switching circuits to human decision making, have made use of most of what is known about software technologies and techniques.

Declarative programming, for example, is typically used to model human decision making, while static portions of models are written in imperative languages for efficiency. However, most expert systems are designed as stand-alone packages and provide only loosely coupled interfaces to imperative languages. This is true of other software technologies and has hampered their general ability to address modeling and simulation in a consistent and integrated manner. Recent DARPA and DoD initiatives, such as the Synthetic Theater of War (STOW) advanced technology demonstration, have goals far beyond the use of these large simulations as single-user analytical tools. Ambitious efforts are underway to provide distributed interactive simulations using virtual reality for training, virtual prototyping of hardware, and analytical applications.

The Faster-Than-Real-Time Synthetic Forces (FTRT SF) IR project is a project of the Collaborative, Object-oriented Advanced Simulation Technology Research (COASTeR) group at SSC San Diego. The goal of FTRT SF is to research issues surrounding simulation architectures that are an enabling technology for intelligent, collaborative, simulation-based software engineering environments. The domain of interest is the construction of large-scale, complex simulations of military forces.

The approach taken in the FTRT SF project has been to research and evaluate existing simulation architectures, and in concert with other DoD development projects, suggest modifications to meet the above-stated goals and objectives. We have concerned ourselves with three simulation architectures, the Quick Threads Simulation Runtime (QTSR), the Synchronous Parallel Environment for Emulation and Discrete-Event Simulation (SPEEDES) framework, and the TEMPO simulation framework. (TEMPO is an extension of the language SIM⁺⁺ developed by Jade Technologies and used in the SimCore Simulation framework developed at Science Applications International Corporation (SAIC)). The SPEEDES simulation framework has received the bulk of our attention, since it is a Government-Off-The-Shelf (GOTS) product, and we are able to manipulate the computer source code. Our additions have been in the areas of communications protocol design, data distribution

management design, and abstraction layers to improve developer efficiency without sacrificing execution speed.

One of our primary concerns is the overhead required to perform the basic operation of time evolution, namely the time required to process a simulation event. Table 1 shows the time required for each framework to process an event. The time is in units of microseconds (10^{-6}).

Table 1. Simulation event processing times in microseconds.

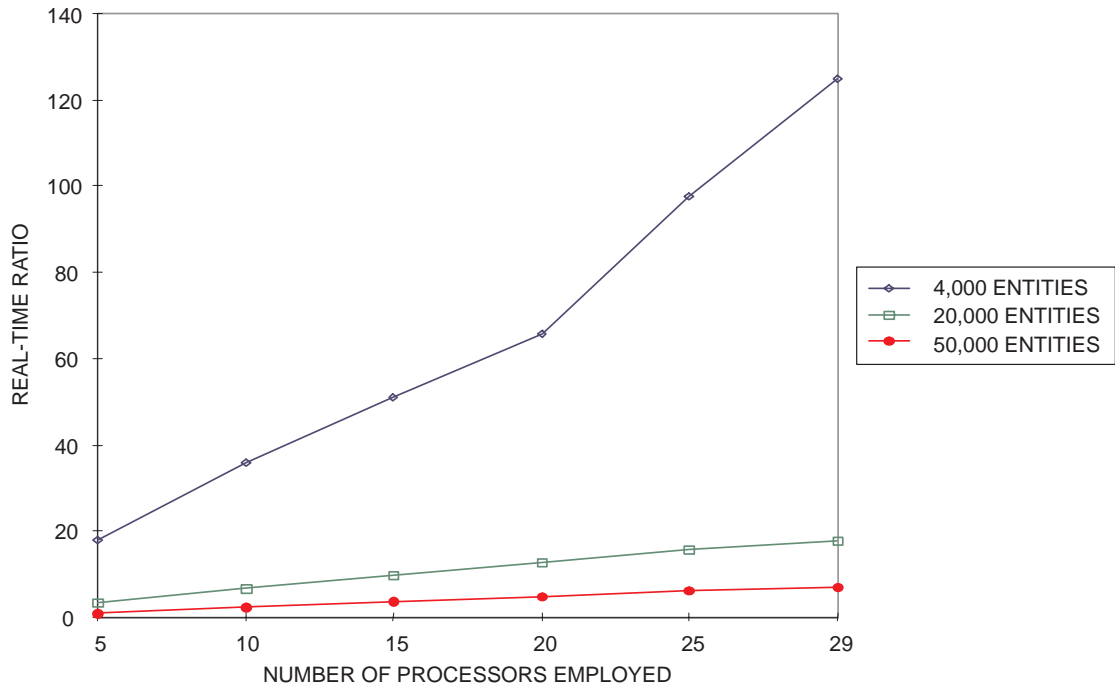
Simulation Framework	Event Processing Time
QTSR	6.5
TEMPO	10
SPEEDES	10 – 25

These results are consistent with the fact that the target hardware architectures are increasingly more general. The QTSR framework is designed for single central processing unit (CPU) execution; the TEMPO framework is designed for shared-memory multiprocessors or shared-memory clusters of computers; and the SPEEDES framework is designed for both parallel computers (shared-memory and distributed-memory computers) and networks of computers.

We have built several scalability-benchmarking simulation SPEEDES and executed them on a 32-processor Convex Exemplar enterprise server, and we present some of these results here. The Joint National Test Facility has been rigorously benchmarking SPEEDES on networks of workstations, but these results are not available at this writing. The initial results are very promising, yielding linear scalability.

Figure 1 shows our SPEEDES-based benchmarking results for constructive wargaming simulation for real-time command and control (C^2) training. The models were based on physics-oriented motion and sensor models from existing, operational wargames. To determine the range of simulation speeds available to an exercise controller, it is necessary to measure the achievable ratio of simulation time to wall-clock time for a given exercise size. The ratios achieved for various entity counts and processors are plotted on the vertical axis. The horizontal axis is a plot of the number of processors employed by the Convex Exemplar to execute the configuration. Note that the scalability is linear for light, moderate, and heavy loading.

The significance of these results is that we may now simulate much larger military scenarios with affordable computational resources. The fact that the SPEEDES simulation framework has been adopted for use in the largest DoD simulation program is evidence of the validity and usefulness of our results.



CONVEX EXEMPLAR, 20-s PERIOD FOR MOTION PLATFORMS, 12-s PERIOD FOR SENSORS
 NUMBER OF MOTION PLATFORMS = NUMBER OF SENSORS

Figure 1. SPEEDES-based benchmarking results for constructive wargaming simulation for real-time C² training.

Principal Investigator:
 Jeffrey W. Wallace

0601152N
 ZU38

Reflective Memory on Standard Local Area Networks

Objective(s): Apply reflective-memory concepts to distributed computer systems by using standard local area networks rather than proprietary reflective-memory hardware interfaces and protocols.

Accomplishment(s): Created a new computer system local-area-network transport layer protocol and designated the network memory protocol that provides clients with direct access to data within the random-access memories of servers without the overhead of server socket application software.

The network memory protocol is a local-area-network transport layer protocol that provides clients with direct access to data within the random-access memories of servers. The server random-access memories accessed by the network memory protocol are called network memories. A processor implementing a network memory server is called a network memory host.

The network memory protocol, which accesses memory through a local area network, is conceptually similar to direct memory access protocols, which access memory through memory hardware interfaces or through processor backplane busses. Although the formats are different, both the network memory protocol and the direct memory access protocols seek the same goal. They seek to improve performance by accessing processor memory asynchronously, and largely independently, of other activity on the processor.

The motivation for the network memory protocol was the desire to build very efficient real-time databases. A real-time database is a structured collection of data representing the state of a dynamic external environment. Each database entry contains the sampled value of an associated environmental parameter obtained or derived from an external sensor. The network memory protocol provides a means for remote sensor clients distributed over a local area network to broadcast their sample data directly to the memories implementing the real-time databases. The network memory protocol also provides a means for remote user clients distributed over a local area network to obtain data directly from the memories implementing the real-time databases. Figure 1 shows these relationships.

The network memory protocol implements local-area-network access to high-throughput real-time databases more efficiently than servers employing traditional sockets. The efficiency is gained by avoiding unnecessary context switches and data buffer copies. Since the network memory protocol provides random access to data, it is more flexible than socket approaches, which are inherently sequential. The socket approach, on the other hand, does a better job of activating tasks in response to associated message arrivals.

User-defined partitions and overlays can organize the network memory host-user address space independently of the global network memory protocol address space. Partitioning can conserve the amount of kernel memory allocated to network memory. It can also map noncontiguous kernel address spaces for access to different types of memory, such as memory-mapped input/output hardware.

UNIX application software interfaces to the network memory through a network memory character device driver. The first “open” system call allocates the network memory within kernel memory, and the last “close” system call frees it. The “ioctl” system call defines the partitions. The “mmap”

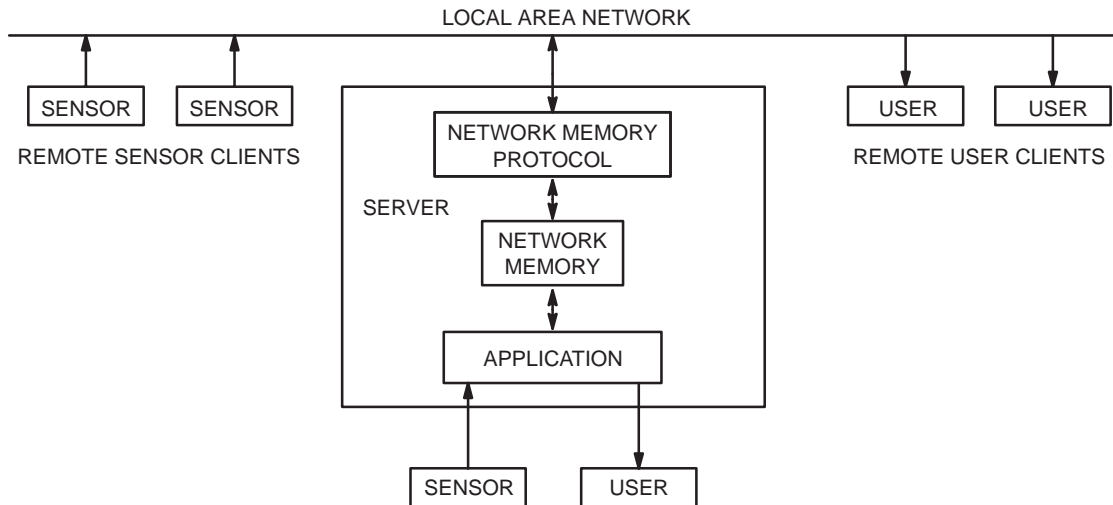


Figure 1. Network memory model.

system call maps the allocated network memory into the application user space. The application then has direct access to the network memory without further system calls.

The network memory protocol server, implemented within the kernel, may access the network memory records while an application task was in the process of accessing the same records. Coordination algorithms, which avoid system calls, have been developed to ensure atomic access to network memory data. The functions required by these algorithms, plus the need for real-time clock synchronization in a real-time system, guided the design of the network memory protocol message format.

Network memory protocol messages are composed of instructions that together form a simple sequential program. The network memory protocol server can be viewed as a very simple processor that executes the program defined by the instructions forming the message. The instructions support both direct and pointer access to data, a few simple logic and arithmetic functions, time stamping, and security keys.

Network memory protocol interfaces to both the Ethernet layer and the Internet Protocol layer have been designed. Immediately above the Ethernet layer, the network memory protocol server was found to execute approximately one-third faster than an equivalent server using traditional sockets to the User Datagram Protocol (UDP).

This research has shown the network memory protocol approach to be both feasible and to offer better access time for real-time database applications. Additional work would be necessary to convert the experimental software into a fully functional product ready for widespread distribution.

This research assumed no special-purpose hardware. It integrates the network memory protocol into the set of existing network software. The simplicity of the network memory protocol instructions suggests that for even greater potential performance, the network memory protocol server could be implemented in a hardware memory system with a local-area-network interface, rather than in software executing within a host processor. This could be an area for possible future research.

Principal Investigator:
Dwight R. Wilcox

0601152N
ZU36

COMMUNICATIONS

Resonantly Enhanced EHF Optoelectronic Transceiver Components

Objective(s): Develop an optoelectronic monolithic-microwave-integrated-circuit (MMIC) module using an electroabsorption (EA) modulator with a novel resonant tuning technique. This module will allow efficient analog photonic link operation out to 50 GHz.

Accomplishment(s): Designed and fabricated discrete modulator on semi-insulating substrate. Designed the MMIC optoelectronic module.

NEED AND BACKGROUND

Photonic links are becoming applicable for future shipboard communication, radar, and electronic warfare systems spanning the HF to EHF frequency range. These photonic links have achieved low RF insertion up to 10 GHz. Above 10 GHz, these links still suffer from poor electrical-to-optical and optical-to-electrical conversion efficiency. More efficient optical modulation and detection techniques are currently being developed for SHF and EHF transmission but are still in the laboratory demonstration phase. In cases where high center frequency and moderate fractional transmission bandwidths are required, impedance matching and resonant driving circuits for modulators and detectors are an attractive option while trading off some microwave bandwidth for enhanced link efficiency. This technique is useful in cases where the bandwidth of the modulator and/or the detector are RC time constant limited where R is the transmission line impedance and C is the optoelectronic device capacitance.

APPROACH

Present low drive voltage electroabsorption (EA) transmit/receive modulator suffers high RF loss (~9 dB) at millimeter wave frequencies (~44 GHz) due to diode capacitive shunting. This capacitive loss can be recovered using a microwave tuning technique for fractional bandwidth, and the performance can be further improved by a novel resonant circuit as shown in figure 1. This resonant tuning circuit offers 16-dB RF loss improvement over the RC limited response and 6 dB over the

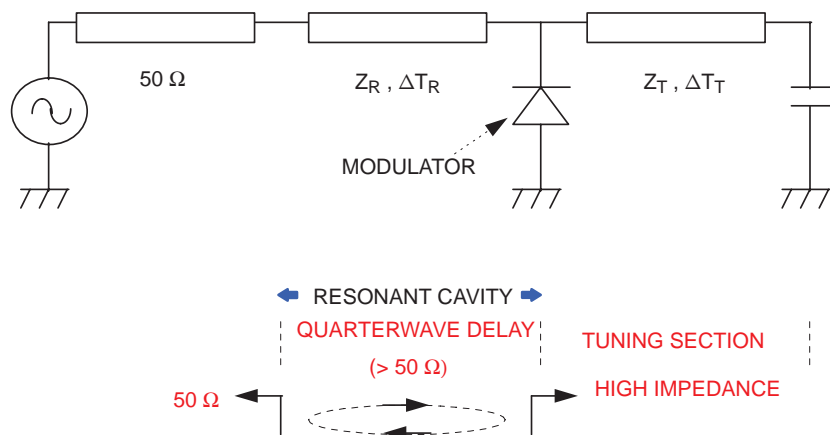


Figure 1. Resonantly tuned modulator circuit layout.

tuning-only case. To reduce parasitics at millimeter wave frequencies, the resonantly tuned circuit and the modulator need to be monolithically integrated.

ACHIEVEMENTS AND ISSUES

To match the coplanar waveguide tuning circuit layout, discrete modulators on semi-insulating substrate were designed and fabricated. The modulator material was grown at the University of California, San Diego (UCSD) by using metal-organic chemical vapour deposition (MOCVD) technology. Based on the discrete modulator data, we designed the monolithic-microwave integrated circuit (MMIC) optoelectronic module using SUPER COMPACT and LIBRA microwave computer-aided-design (CAD) tools. Figure 2 shows the fabricated optoelectronic MMIC module.

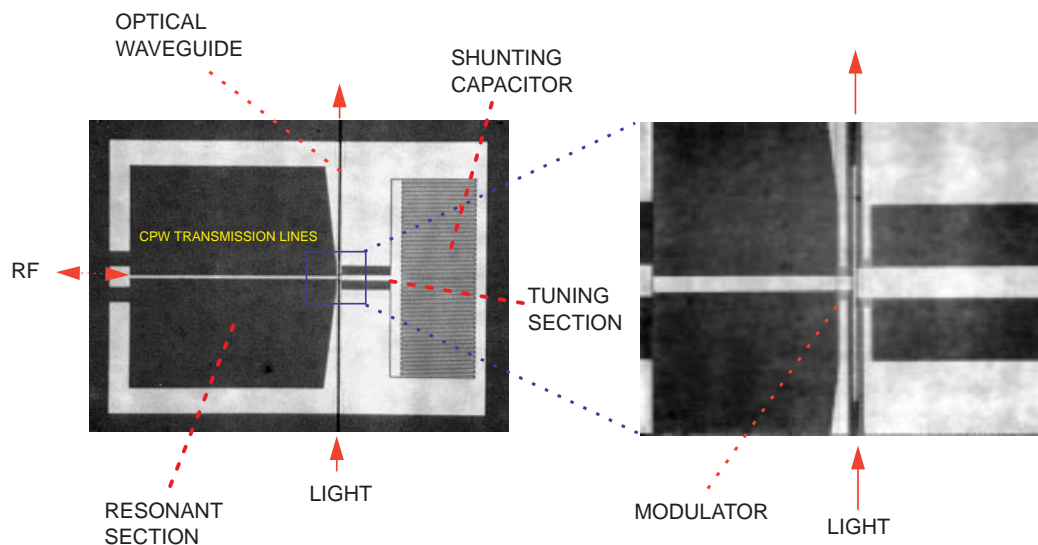


Figure 2. Fabricated modulator module.

Our simulation study predicted that the resonant tuning quality largely depends on the modulator series resistance, R_s , as illustrated in figure 3. For $R_s < 2 \Omega$, enhanced modulator efficiency due to resonant tuning is promised. For $R_s > 5 \Omega$, the peak resonant-tuning efficiency reduces to that of conventional tuning. According to the modulator resistance analysis based on present modulator structure and fabrication quality, we can expect $R_s > 9.5 \Omega$ with P^+ specific contact resistance of $2 \times 10^{-5} \Omega \text{ cm}^2$. To achieve $R_s < 5 \Omega$, we need to (1) reduce both the P^+ contact resistance, (2) reduce the P^+ waveguide thickness, (3) increase both P^+ and N^+ layers doping concentration, and (4) apply a thick ($> 2 \mu\text{m}$) gold plating.

SOLUTION AND CONTINUATION

Since reducing the P^+ contact resistance is not an easy task, an alternative approach to reduce R_s is to use a novel N-P-I-N modulator structure. This structure is designed by forward-biasing the N-P junction while reverse-biasing the P-I-N junction. By changing the waveguide from P^+ layer- P^+ contact to P^+ -N layer- N^+ contact, we can drastically reduce R_s to $1 \sim 2 \Omega$. The new N-P-I-N modulator structure is being investigated in FY 98.

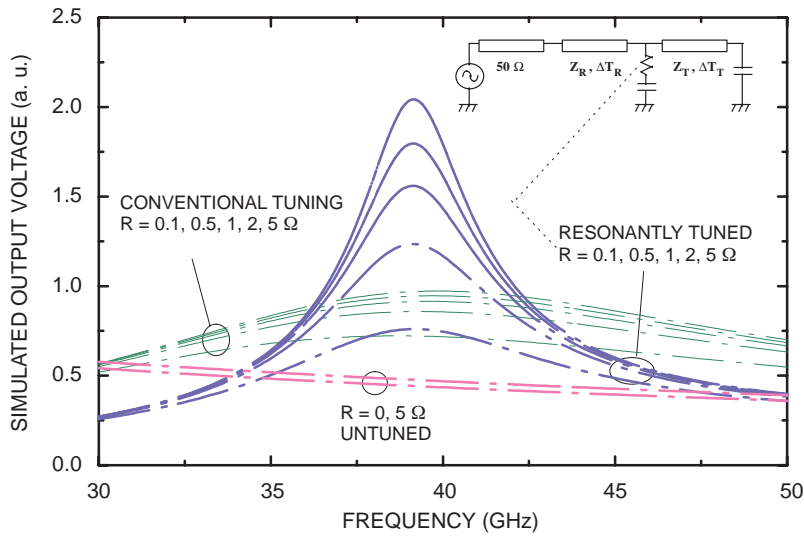


Figure 3. Resonant response degradation due to modulator series resistance.

Principal Investigator:
Dr. Chen-Kuo Sun

0601152N
ZU39

Associate Investigators:
Dr. Steve Pappert

Prof. Paul Yu
University of California, San Diego (UCSD)

H^∞ Waves: A New Approach to Estimating Electromagnetic Fields

Objective(s): Develop an algorithm that is accurate, efficient, and robust in estimating the impedance function of an antenna from a minimal set of samples.

Accomplishment(s): Developed an algorithm that interpolates impedance data and provides a broadband estimate of the impedance function.

This project was inspired by the critical function that electromagnetic (EM) systems have on Navy ships. In the design of these ships, accurate modeling of radar and communication systems reduces cost and increases efficiency. An essential component of these systems is the antenna. The fundamental characteristics of an antenna are its impedance and its radiation pattern. How these characteristics vary with frequency is crucial to analyzing the performance of the antenna. Computing these attributes over frequency bands of interest can be prohibitively expensive. Antenna designers would welcome a method allowing them to estimate the antenna's impedance from a minimal set of computed or measured samples. The goal of this project was to develop such a method.

Our approach was motivated by the conviction that any scheme for interpolating data from a physical system must incorporate knowledge of the system. One way to incorporate knowledge of an antenna into an estimation procedure is to select estimates from a class of functions corresponding to that system. The mathematical properties of the reflectance, W , of an antenna are more amenable to calculation than those of the impedance function, Z .

The reflectance is given by $W = (Z - 1)/(Z + 1)$.

Since the impedance is analytic with a positive real part on the right half of the complex plane, the reflectance will be bounded and analytic on the right half plane. (Here frequency is associated with the imaginary axis by the Laplace transform.) The functions defined on the complex plane that are bounded and analytic in the right half are denoted by H^∞ . Since the reflectance of an antenna is an H^∞ function, our approach uses this class of functions to construct an estimate of the reflectance from samples.

Nevanlinna–Pick (NP) interpolation is a classic H^∞ method that was the basis of this project. The NP operator is defined in terms of a set of complex interpolation data $I = \{(s_1, w_1), \dots, (s_n, w_n)\}$ where the s_n are in the right half plane and the w_n are of norm less than or equal to one.

Given such a data set I , the NP takes a function f in H^∞ of norm 1 and maps it to another function g in H^∞ function of norm 1 that interpolates I as $g(s_n) = w_n$.

For our application, the $\{w_n\}$ are samples of a reflectance at frequencies $\{s_n\}$. Classic NP interpolation requires the $\{s_n\}$ have real part greater than 0, and the $\{w_n\}$ to be in the interior of the unit disk. Recent work extended the interpolation points to the boundary but required that the $\{w_n\}$ values be of norm one.

Our contribution was twofold:

First, we extended NP interpolation by both moving the interpolation points to the boundary while removing the constraint that $\{w_n\}$ be unitary. This was essential for applying this method to

interpolating reflectance data. Second, we created an interpolating function of minimal order so as to incorporate an important engineering consideration.

Figure 1 provides an example of the estimate of the reflectance resulting from our approach. The data set was measured at SSC San Diego's model range from a brass model of a DDG 51. The measurements represent the reflectance of a 35-foot monopole antenna as part of a twin system designed to operate at frequencies between 4 and 12 MHz. The data set consists of 401 reflectance measurements at frequencies equally spaced between 4 and 12 MHz. In the figure, the solid line is formed by interpolating between the 401 frequencies with a cubic spline. The method developed here used 34 evenly spaced samples and computed the dash-dot line. This method interpolates the data set accurately but misses some of the fine structure apparent in the data set. The flexibility in this method is the choice of the "starting" function from which NP produces the interpolant. This flexibility allows a parameterization of all possible solutions. Design requirements will determine the type of interpolant chosen.

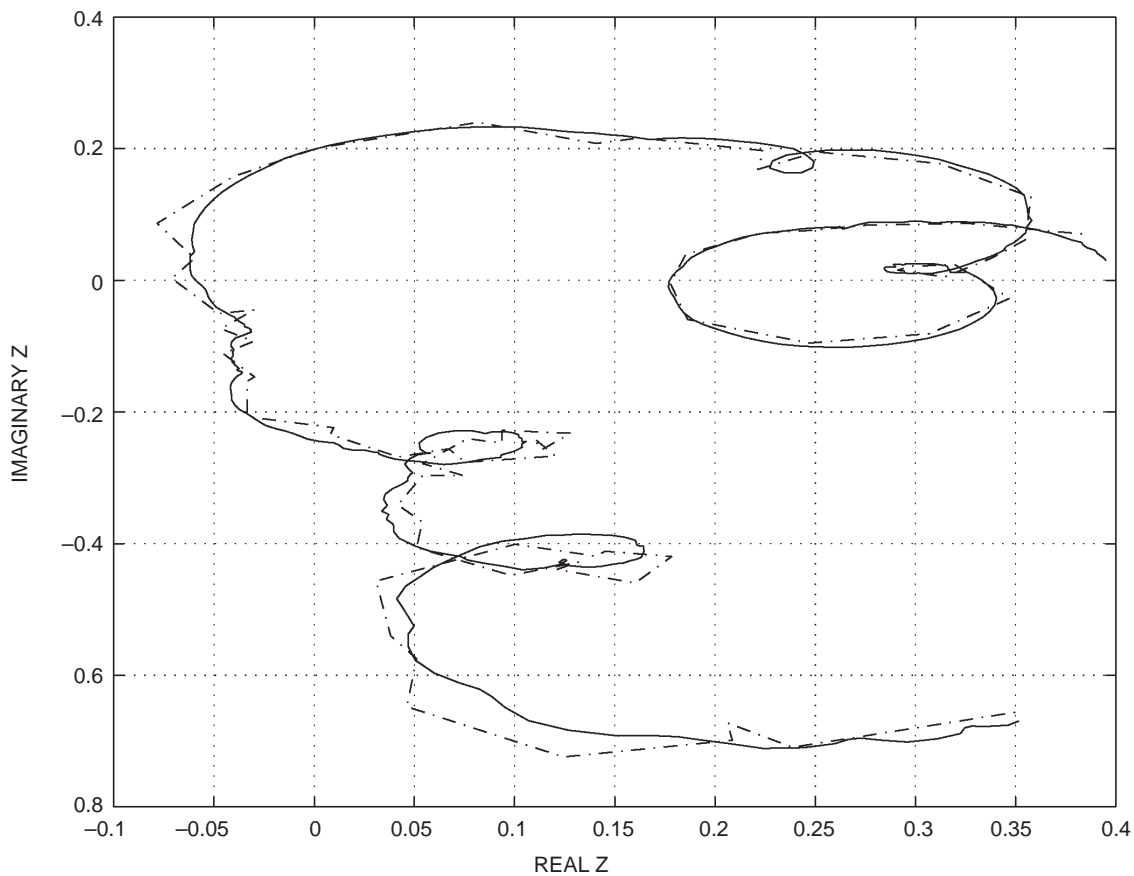


Figure 1. Resulting reflectance estimate.

Principal Investigator:
Dr. David F. Schwartz

0601152N
ZU21

Associate Investigator:
Dr. Jeffrey C. Allen

Algebraic-Geometric Error Control Coding for Improved Performance of Naval High-Data-Rate Line-of-Sight and Satellite Communications Systems

Objective(s): Develop algebraic-geometric (AG) forward-error-correction (FEC) coding techniques and evaluate their performance with respect to coding gain and bandwidth efficiency.

Accomplishment(s): Compiled existing encoding/decoding algorithms for AG codes and identified and analyzed the theoretical performance of promising non-Hermitian AG codes.

Forward error correction (FEC) is an important means of improving the performance of modern digital communications systems. In particular, Reed–Solomon (RS) block codes have a number of desirable characteristics that have made them quite useful, such as a nonbinary alphabet that provides significant burst-error-correcting capability when used alone or as an outer block code concatenated with an inner convolutional code. Such concatenated systems, which may also employ interleaving and soft-decision Viterbi decoding, are used in a variety of applications, including: naval high-data-rate line-of-sight and satellite communications systems subject to error bursts caused by fading or pulsed radar; deep-space exploration systems of the National Aeronautics and Space Administration (NASA) and the European Space Agency, where power savings is the main concern; and the satellite systems of both the International Telecommunications Satellite Organization (INTELSAT) and the European Telecommunications Satellite Organization (EUTELSAT). Similar concatenated systems have also been considered for the transmission layer of the digital television system defined by the Moving Pictures Expert Group (MPEG).

The performance of concatenated systems could be improved by improving the performance of the outer block code. Performance of a block code, measured in terms of probability of decoding error, or as coding gain, can be improved by increasing the code word length relative to the size of the chosen code word alphabet, where the alphabet is assumed to be the finite field containing q elements, denoted as F_q . One of the undesirable limitations of an RS code over a particular finite field is that its code length, n_{RS} , cannot exceed q , the cardinality of the field.

This research is a continuation of an IR project begun in FY 96 to develop algebraic-geometric (AG) codes that improve the performance of naval high-data-rate line-of-sight and satellite communications systems. Using concepts of algebraic geometry, Goppa [1, 2] generalized RS codes over F_q [3] to much longer AG codes ($n_{AG} \gg n_{RS} = q$), which have increased error-correction capability and hence increased coding gain, relative to RS codes. In the context of algebraic geometry, the length of an RS code over a particular finite field is equal to the number of points on a line; therefore, the construction of longer AG codes depends on finding algebraic curves that contain many more points than a line.

During FY 96, we assessed the performance of Hermitian codes over F_{q^2} , i.e., AG codes based on the family of nonsingular Hermitian plane curves given by the equation $y^q + y = x^{q+1}$. Since this family of curves contains the maximum number of points possible over fields of cardinality q^2 , Hermitian codes are the longest AG codes possible over these fields. Our comparisons in [4] of the theoretical performance of Hermitian codes with that of RS codes over a variety of fields demonstrated the

utility of the longer, more powerful Hermitian codes with respect to the trade-offs between coding gain and bandwidth expansion and between bandwidth expansion and complexity of finite-field arithmetic computations. These results show the promise of Hermitian codes if their decoding complexity, presently of order $n^{5/2}$, can be reduced to a level closer to order n^2 , the complexity level already realized for RS codes.

During FY 97, we searched for non-Hermitian singular algebraic curves, which are simpler than Hermitian curves and which, therefore, may produce long AG codes with lower decoding complexity than Hermitian codes. We identified the hyperelliptic family of singular algebraic curves as curves containing more points than a line but fewer points than Hermitian curves. Therefore, hyperelliptic AG codes, based on hyperelliptic curves, are longer and hence more powerful than RS codes, which are associated with lines; while hyperelliptic AG codes are shorter and hence less powerful but also potentially less complex to decode than Hermitian AG codes.

To date we have discovered and tested codes based on the hyperelliptic family of curves given by the equations: (1) $y^2 + y = x^5$ over F_{16} , (2) $y^2 + y = x^9$ over F_{64} , and (3) $y^2 + y = x^{17}$ over F_{256} .

Theoretical performance comparisons for high-rate and low-rate RS, Hermitian, and non-Hermitian (hyperelliptic) codes over these fields are encouraging, showing positive coding gain for the non-Hermitian (hyperelliptic) codes relative to RS codes in all cases (figures 1 through 3).

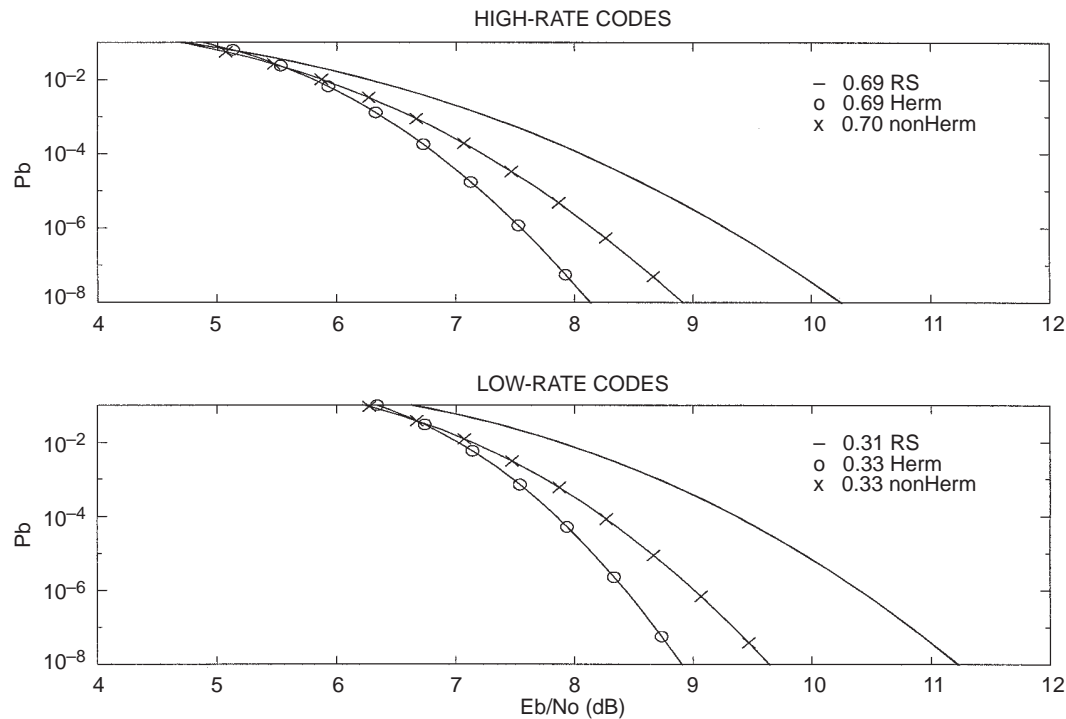


Figure 1. Bit-error probability vs. SNR for RS, Hermitian, and non-Hermitian codes over F_{16} .

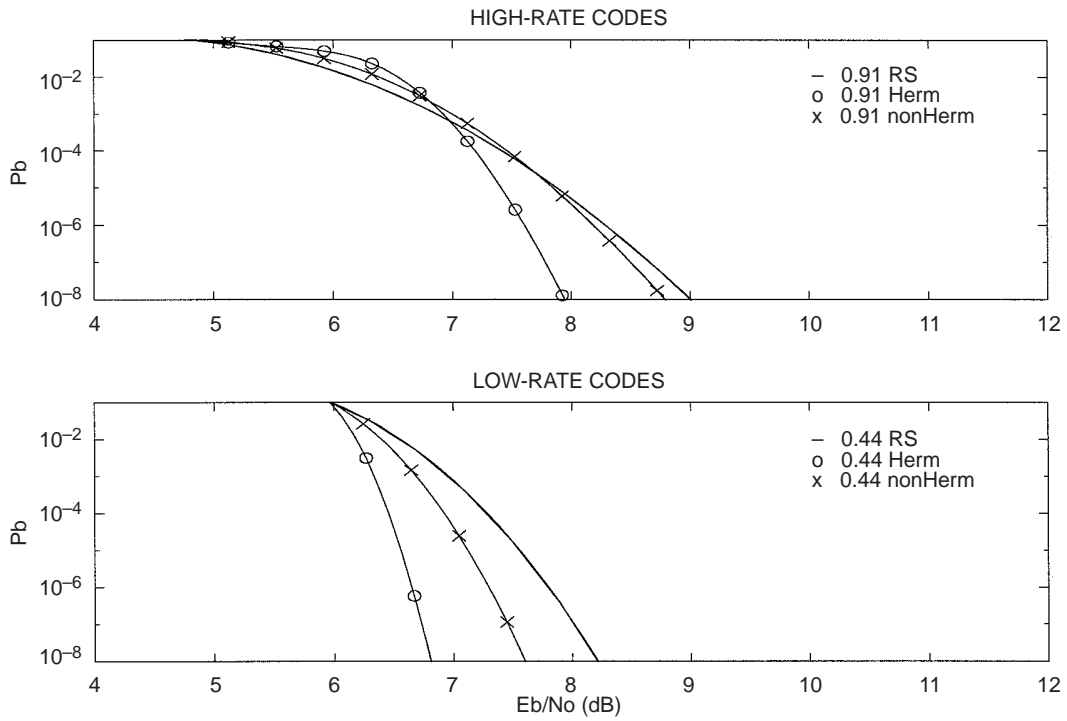


Figure 2. Bit-error probability vs. SNR for RS, Hermitian, and non-Hermitian codes over F_{64} .

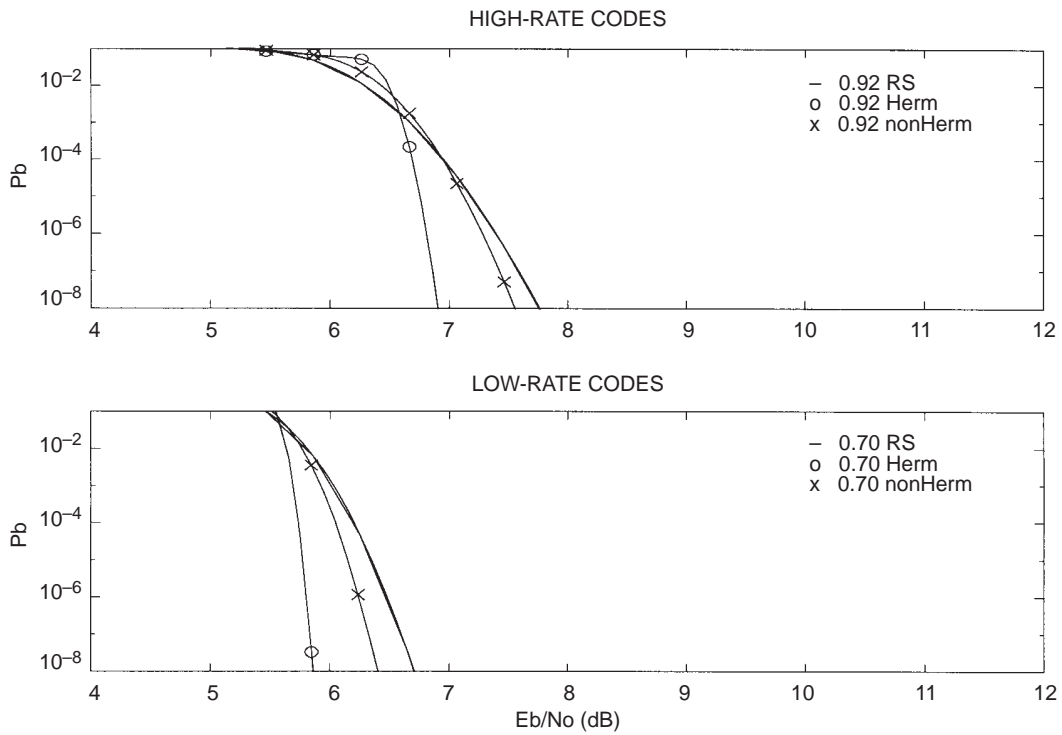


Figure 3. Bit-error probability vs. SNR for RS, Hermitian, and non-Hermitian codes over F_{256} .

REFERENCES

1. Goppa, V. D. 1981. "Codes on Algebraic Curves," *Soviet Mathematics Doklady*, vol. 24, pp. 170–172.
2. Goppa, V. D. 1983. "Algebraic-Geometric Codes," *Math. USSR Izvestiya*, vol. 21, pp. 75–91.
3. Reed, I. S. and G. Solomon. 1960. "Polynomial Codes over Certain Finite Fields," *SIAM Journal of Applied Mathematics*, vol. 8, pp. 300–304.
4. Wahlen, B. E. and J. Jiménez. 1997. "Performance Comparison of Hermitian and Reed–Solomon Codes," IEEE Military Communications Conference (MILCOM 97), 2 to 5 November, Monterey, CA

Principal Investigator:
Dr. Bruce E. Wahlen

0601152N
ZU24

Constant Envelope Modulation Techniques for UHF SATCOM

Objective(s): Investigate modulation techniques that are resistant to the effects of nonlinear amplifiers and communication channels.

Accomplishment(s): Combinations of pulse-shaping and coded-modulation schemes were identified that are highly resistant to the nonlinearities present in the UHF SATCOM communications path, thus enabling a large increase in data-rate capabilities.

Existing systems using ultra-high-frequency satellite communications (UHF SATCOM) have been limited in data throughput by the challenging characteristics of the communications path, which include:

1. **Satellite Transponder:** The UHF satellite transponder contains a hard limiter that removes all amplitude modulation information from the transmitted signal, thus precluding any technique that relies on amplitude modulation, such as quadrature amplitude modulation (QAM). Therefore, only phase and frequency modulation techniques, such as M-PSK (phase shift keying where M is the number of phases) or M-FSK (frequency shift keying where M is the number of frequencies) be considered. A second effect of the hard limiter is spectral re-growth. If the frequency sidelobes of a PSK waveform are suppressed by bandpass filtering, the hard limiter will tend to regenerate the sidelobes.
2. **Nonlinear Amplification:** The nonlinear amplifiers often used in the earth station and satellite High Power Amplifiers (HPAs) can significantly distort the transmitted signal. One way to avoid degradation by the HPA nonlinearity is to select a transmitted signal that is strictly constant envelope.
3. **Link Budget:** Existing systems have relied on binary phase shift keying (BPSK), quaternary phase shift keying (QPSK), or binary frequency shift keying (BFSK). While providing a near constant envelope signal, these techniques allow limited bandwidth efficiency. Greater bandwidth efficiency may be achieved with the use of 8-PSK, but this technique is difficult to implement as a result of the additional power required by 8-PSK to close the link in a system that is already power-limited. In addition, the phase noise requirements placed on the SATCOM radio equipment for 8-PSK are far more restrictive.

One of the ways to achieve greater bandwidth efficiency is to perform spectral shaping on the transmitted signal. Spectral shaping can suppress out-of-band transmission and allow the use of higher signaling rates while still satisfying adjacent channel interference requirements. Typical pulse-shaping techniques for RF transmission have included use of Nyquist pulses such as the raised cosine function applied in the I-Q domain to control spectral spreading. Unfortunately, for distortion-free transmission over the UHF SATCOM channel, a candidate waveform must be phase-modulated and possess a constant envelope. Any spectral shaping must be performed only on the phase to preserve these properties. For an M-PSK signal, the spectral spreading is due to the discontinuities in the phase at symbol transitions. Techniques have been investigated to perform spectral shaping by smoothing out these discontinuities. For example, MIL-STD 188-181 describes a variation on BPSK in which the instantaneous transition between phases is replaced by a linear ramp in phase over a portion of the symbol interval. This technique is described as Shaped BPSK (SBPSK) and can be

easily generalized to M-PSK. Also techniques such as minimum shift keying (MSK) and continuous frequency shift keying (CFSK) remove the phase discontinuity by spreading the transition over the entire symbol interval. All of these methods discussed can be considered as special cases of Continuous Phase Modulation (CPM).

To achieve greater bandwidth efficiency, it is useful to consider higher order modulation schemes in order to obtain a greater number of information bits per transmitted symbol. However, in the UHF SATCOM system, we are power- and bandwidth-limited, and the use of these more bandwidth-efficient modulations requires additional power for similar error-rate performance. A possible solution is a coded modulation system that provides sufficient coding gain to allow increasing modulation complexity without requiring additional power. One candidate technique is Trellis Coded Modulation (TCM).

TCM is a technique in which redundancy is added in the form of a forward error-correction code and the number of bits/symbol is increased by the use of a higher order modulation. This combination can result in a net system gain. For example, in 8-PSK (3 bits/symbol), 2 data bits may be mapped to a symbol by using a rate $\frac{1}{2}$ convolutional coder on 1 bit while leaving the other bit uncoded. In the demodulator, the coded bit is recovered using a Viterbi decoder, with high reliability as result of the redundancy. This simplifies the demodulation of the remaining 2 bits by resolving the 8-PSK constellation into one of four BPSK constellations determined by the coded bits. The coding gain allows use of 8-PSK (at rate $\frac{2}{3}$ or 2 bits/symbol) with up to 3 dB less power than required by uncoded QPSK (also 2 bits/symbol). Thus, TCM can address two of the challenges addressed above: Its structure reduces the sensitivity of the system to phase noise by simplification of the demodulation decision, and it can reduce the power required to close the link relative to other bandwidth-efficient modulation techniques.

By using combinations of the coded-modulation and pulse-shaping techniques discussed above, it is possible to construct a waveform that allows an increase in data throughput without an increase in system power and that also possesses the constant envelope characteristic necessary for successful transmission over the military UHF satellite communications channel (see figure 1).

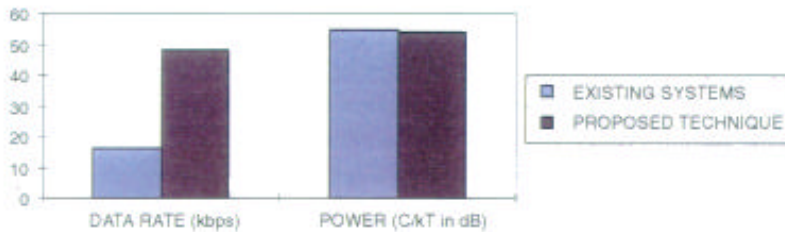


Figure 1. Improved modulation technique for UHF SATCOM.

Principal Investigator:
LCDR Bruce E. Watkins

0601152N
ZU23

SURVEILLANCE

Generalized Higher Order Crossings Theory and Practice

Objective(s): Develop an appropriate mathematical framework for extending and generalizing the theory of Higher Order Crossings (HOCs) and define novel signal/noise analysis tools, based on generalized HOC sequences, for application to detection and estimation.

Accomplishment(s): Proved a central limit theorem for the level-crossings of the envelope of a Gaussian process and obtained an analytic expression for the asymptotic variance [1]. Investigated HOC-based methods for estimating parameters in the spectral density of a normal random process. Examined the power law behavior of the level-crossings for a nonlinear dynamical system [2].

The Navy currently has prototype and fleet operational surveillance systems (e.g., infrared, sonar, and radar) that can produce megabytes of digital information per second. Higher Order Crossing (HOC) sequences are promising for quick classification of background/clutter data from these surveillance sensors [which produce data flow rates on the order of 20 kHz (sonar), 10 mHz (radar), and 50 mHz (infrared search and track) (IRS&T), respectively]. There is a critical need in such systems for fast, efficient methods of first classifying and then further processing (detection and track) data streams from these sensors. Since real-world data can be non-Gaussian as well as spatially and temporally nonstationary, traditional signal- and data-processing methods may fail or at best be suboptimal for a given type of processing. Thus, new data analysis tools, which are computationally efficient and robust to nonstationary regimes, are desirable.

HOCs are the level-crossing counts obtained by repeatedly filtering a time series. Generally, one deals with a zero-mean process with zero-crossing counts being of particular interest. Formulas for the average number of zero-crossings of a random process go back to the pioneering work of S.O. Rice. Explicit formulas were derived by Rice for the case of a Gaussian process, the non-Gaussian case being problematic. Recently, Barnett, and Kedem [3] have derived zero-crossing rates for some non-Gaussian processes and applied HOC to the problem of frequency and power estimation in time series.

The standard HOC theory has provided signal- and data-analysis tools that include: fast spectral estimation, white noise discrimination tests, and fast tests for Gaussianity, with applications in non-destructive testing and speech signal processing. Scattergram methods based on HOC sequences have proven indispensable in various nondestructive evaluation testing. Specific applications in speech processing include online frequency tracking and whale vocal-sound discrimination. Generalized HOC holds the promise of a rigorous non-Fourier-based spectral analysis theory that will provide fast and efficient statistical estimators and novel discrimination metrics for use in exploratory data analyses.

The approach taken in this research has consisted of two parallel efforts:

1. Generalized HOC sequence spaces have been defined. These provide a setting for the use of more general statistics (e.g., parameters of the spectral density of the random process or some nonlinear-based model) to be used in defining other HOC sequences. These new statistics have been exercised on deterministic data sets for classification, detection, and estimation performance evaluation.

2. In the second parallel effort, an appropriate mathematical framework/basis has been established to enrich the new HOC sequences with a full mathematical rigor. An HOC space theory is valuable in that it provides a mechanism for establishing the theoretical convergence properties of the generalized HOC sequences. For this parallel effort, methods from functional analysis, linear operator theory, and fixed-point theory have been used. Theoretical results concerning the statistical nature of level-crossings for some non-Gaussian processes have also been investigated. In particular, we have investigated the level-crossing statistics for envelopes of Gaussian processes and Chi-square processes.

During FY 97, a central limit theorem for the level-crossings of the envelope of a Gaussian process was proved [1] and work began on extending this result to the more general Chi-square process. Figure 1 presents a computer simulation of a continuous-time, ideal, bandpass Gaussian process, sampled at 4 Hz, and its corresponding envelope. Figure 2 is a normal probability plot of the sampled mean level-crossing count and demonstrates the normality of the mean level-crossings count for this particular bandpass process, which is predicted by the theorem.

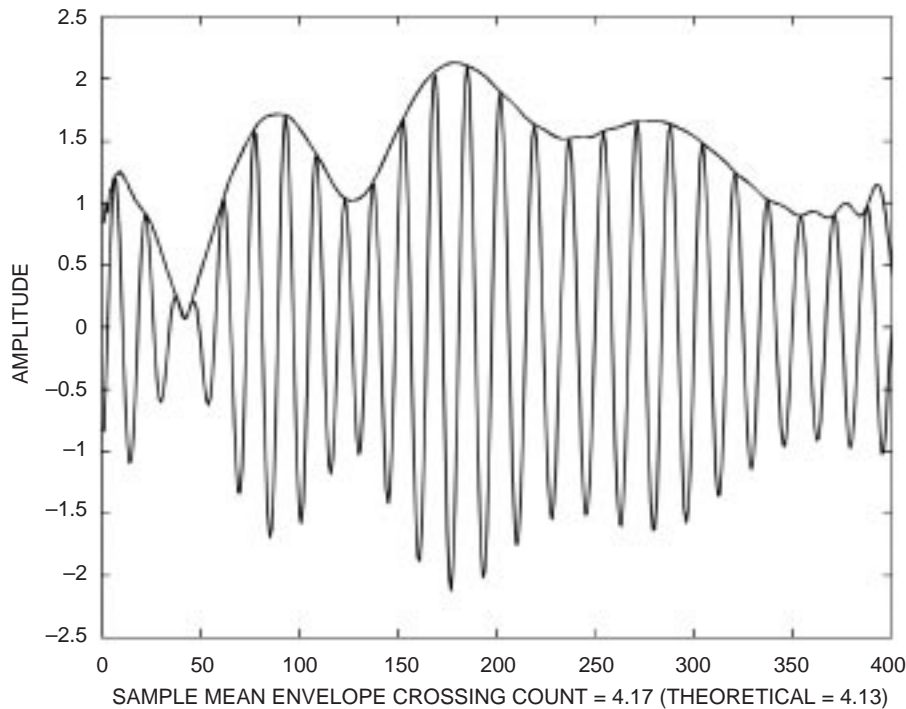


Figure 1. Simulation of a continuous-time, ideal Gaussian process sampled at 4 Hz; $PASSBAND = [0.45 \pi, 0.55 \pi]$.

Theoretical investigations were undertaken with regard to generalizing the theory of Higher Order Crossings to estimating parameters of the spectral density of a random process. In parallel with the general theoretical work on extending HOC, two specific models are being considered for data analysis: a linear family of normal random processes with normal spectral densities and a multiplicative process, which is a normal random process modulated by a deterministic function. The latter nonstationary process is used to model seismic accelerograms. This work is continuing in FY 98. Work began on an infrared clutter background classifier based on crossing counts of filtered background data. This work is also continuing in FY 98.

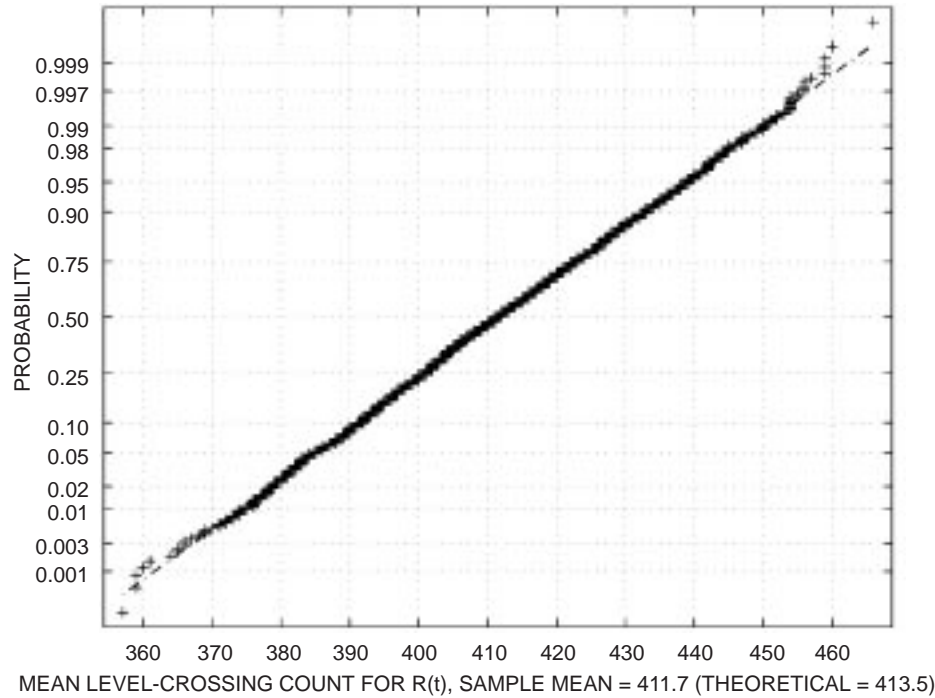


Figure 2. Normal probability plot for level-crossings of envelope of ideal bandlimited Gaussian Noise.

Finally, some theoretical work and numerical experiments were performed involving a nonlinear dynamical system, namely, a generalized tent map driven by different random-noise processes, and the preliminary indication is that the level-crossing statistics behave according to a power law distribution [2].

REFERENCES

1. Barnett, J. T. 1998. "Asymptotic Normality of Level-Crossings for the Envelope of a Gaussian Process with Application to Radar Detection," submitted to the *Journal of Fourier Analysis and Applications*.
2. Hammel, S. M., J. T. Barnett, and N. Platt. 1997. "Diagnosing Intermittency," *American Institute of Physics (AIP) Conference Proceedings*, vol. 411, pp. 51–56.
3. Barnett, J. T. and B. Kedem. 1998. "Zero-Crossing Rates of Mixtures and Products of Gaussian Processes," accepted for the *IEEE Transactions on Information Theory*, to appear in May.

Principal Investigator:
John T. Barnett

0601152N
ZU43

Array Processing with Three-Dimensional Bathymetry

Objective(s): Quantify the effects of the two-dimensional bathymetry assumption on the performance of underwater acoustic array processors (conventional beam-forming and matched-field processing) when the bathymetry is actually three-dimensional. Demonstrate performance improvement by the inclusion of three-dimensional effects into the processor.

Accomplishment(s): A thorough understanding of three-dimensional bathymetric effects on the performance of underwater acoustic array processors has been obtained. Insights into the character and performance improvement obtainable via the inclusion of these effects in the matched-field processor have been obtained. Experimental evidence for the presence of three-dimensional effects has also been observed.

Underwater acoustic propagation in shallow-water, wedge-like environments will experience “bending” out of the vertical plane containing the source and receiver. Consequently, the time for the energy to travel from the source to the receiver will be altered, or some paths may miss the receiver altogether. Localization errors and correlation degradations will result if this horizontal multipath propagation is ignored. This phenomenon was investigated both theoretically, via simulations for an ideal shallow-water wedge, and experimentally, via the analysis of vertical-line-array (VLA) source-to-w data recorded in a steep, wedge-like environment near San Clemente Island during the fourth Shallow Water evaluation cell Experiment (SWelLEX-4).

While FY 96 simulations concentrated on the effect of ignoring the three-dimensional bathymetric effects on array processors (both beamformers and matched-field processors), FY 97 simulations focused on the case where these effects are included in the matched-field processor. Figure 1 compares the 100-Hz matched-field response (correlation between true pressures across the array with those predicted for a source at a candidate source range and cross range) obtained for a 4-degree

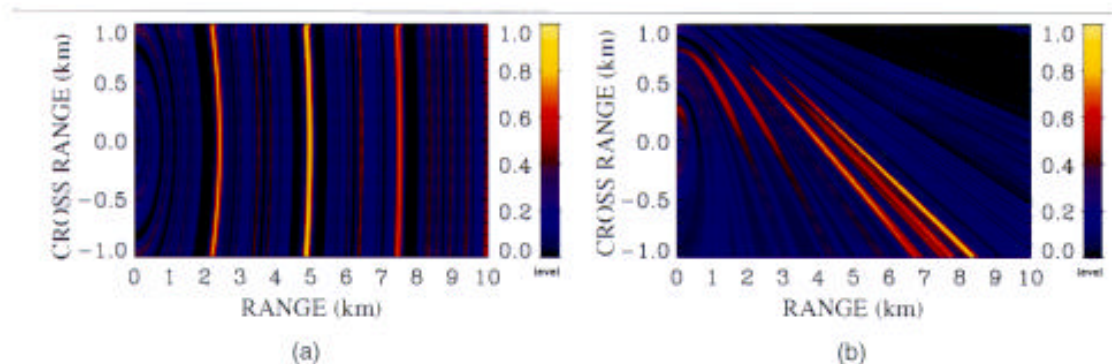


Figure 1. Simulated 100-Hz matched-field range-cross-range (at 10-m candidate source depth ambiguity surface for (a) 100-m water depth flat bottom and (b) 4° wedge with 100-m water depth at zero-cross-range. VLA located at origin. Source range = 5 km. Source cross-range = 0 km. Source depth = 10 m.

wedge with that obtained for a flat bottom. For the wedge result, the water depth is 100 m at the zero-cross-range axis, decreasing in the positive cross-range direction. For the flat-bottom case, the water depth is 100 m everywhere. In both cases, the vertical line array is located at the origin, while the source is located at a range of 5 km and a cross range of 0 km, and the source depth is 10 m. The wedge results exhibit the expected azimuthal discrimination, absent from the flat-bottom case (the arcs in figure 1(a) are actually segments of distorted circles), with the maximum correlation occurring at the true source location. Notice, however, the presence of regions of distinct interference patterns. These regions differ because a different number of modes are surviving in each, as demonstrated by the theoretical caustic lines in figure 2. The caustic lines mark the boundaries beyond which particular modes are stripped out of the energy propagating from a source at the origin. By reciprocity, a source located in a region between the caustics will produce energy containing the stated number of modes for that region at a receiver located at the origin. The higher correlations in the region containing the true source location in figure 1, which clearly corresponds to the region propagating modes 1 through 4 in figure 2, result from the fact that the true and replica pressures contain the same number of modes.

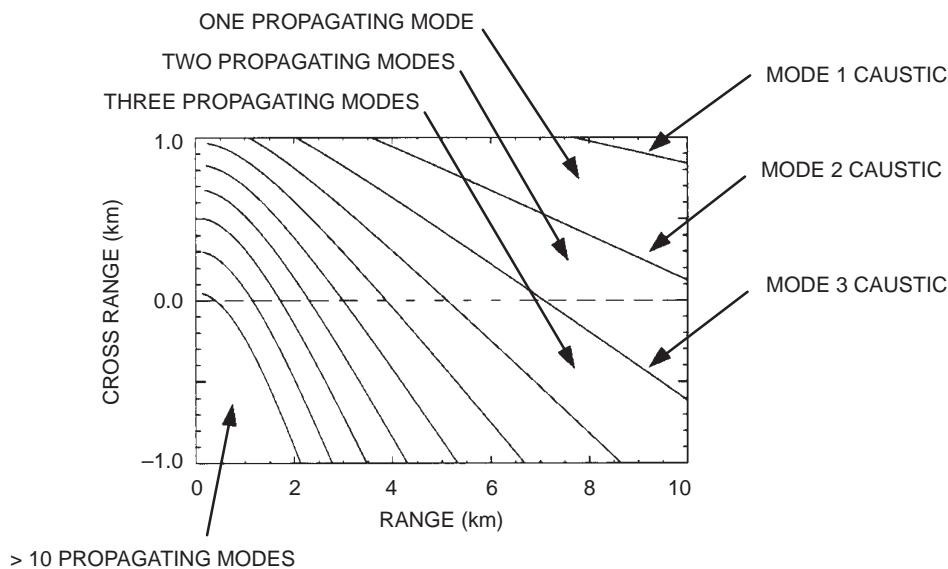


Figure 2. Theoretical 100-Hz caustic lines for 4° wedge with 100-m water depth at zero-cross-range. If source located at origin, caustic lines mark boundaries beyond which particular modes are stripped out.

Experimental evidence for the presence of three-dimensional bathymetric effects was obtained via the analysis of tracks 1 and 2 of the SWellEX-4 test shown in figure 3. Errors in the bathymetry database necessitated the reconstruction of the bathymetry using echosounder data measured during the experiment. Figure 4 compares the 52-Hz power (uncalibrated) measured across the VLA versus time for track 1 with that predicted by a two-dimensional Gaussian Beam model (using the same dynamic range). The coarser, smoother pattern in the data at the later times indicates that more modes have been stripped out than predicted by the two-dimensional model. This effect may be caused by horizontal “refraction” present in the wedge environment.

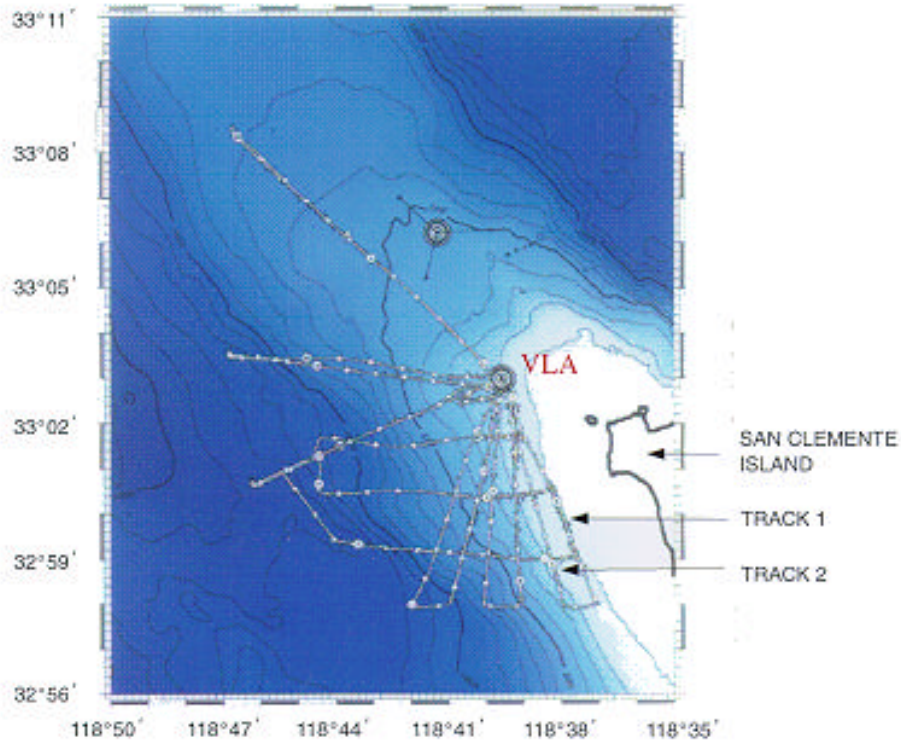


Figure 3. SWellEX-4 test area with source-tow tracks for March 28, 1995. Tracks 1 and 2 considered in this analysis.

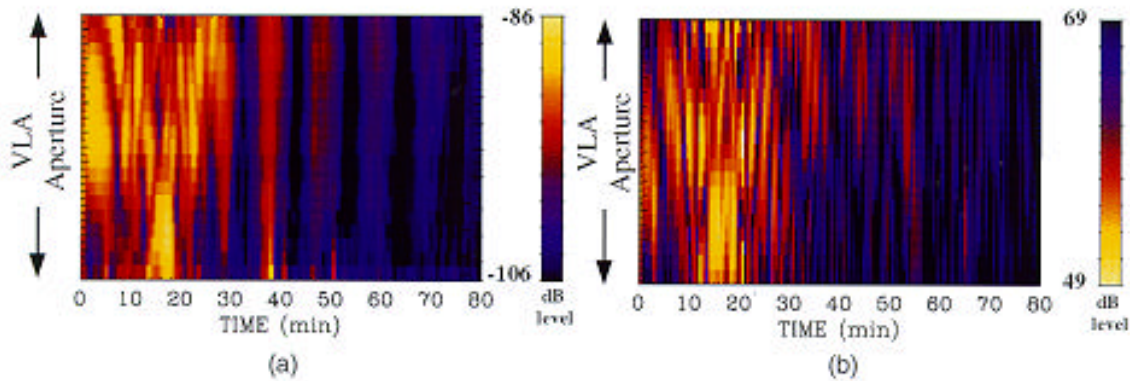


Figure 4. (a) 52-Hz uncalibrated measured power across VLA during Track 1 compared to (b) 52-Hz simulated power (transmission loss) across VLA for Track 1.

Principal Investigator:
 Paul Baxley
 D881
 (619) 553-5634
 baxley@spawar.navy.mil

0601152N
 ZU25

Inverse Synthetic Aperture Radar (ISAR) Scatter Location for Complex Targets via Direction-Finding/Beamforming Methods

Objective(s): Replace the unique one-dimensional (1-D) sequential approach of the TRW/Mark Resources, Inc. (MRI) scatterer location algorithm in the context of Inverse Synthetic Aperture Radar (ISAR) imaging on man-made targets by a representative algorithm from the last 20 years' progress in array processing with an emphasis on matrix-based, multidimensional aspects.

Accomplishment(s): Much progress has been made in identifying and understanding the issues in this connecting attempt, even though the result of this effort is far from being able to outperform MRI's on its simulated data.

A recent book [1] from Mark Resources, Inc. (MRI) outlines the unique TRW/MRI approach to scatterer location in the context of Inverse Synthetic Aperture Radar (ISAR) imaging on man-made targets. During the last 20 years, much progress has been made in array signal processing with an emphasis on matrix-based, multidimensional aspects. This summary documents an effort to connect these two diverse approaches.

For interacting or unresolved cases in which the cross-range resolution is substantially lower than the range resolution, MRI uses a one-dimensional (1-D) Two-Scatterer Algorithm (TSA) [1, pp. 449–475, 505–511] model in its scatterers' localization effort. MRI's two-spatial-dimensional problem is attacked via many 1-D radial cuts. Since MRI has not found a practical way to analyze these surfaces, it has resorted to image cuts and the analysis of the individual image cuts. A general case of a given image peak consisted of two responses in both its range gate and its cross-range gate. The TSA was used in both gates, giving two solutions in one gate and two solutions in the other. These four solutions must be properly paired. The MRI pairing procedure for this nontrivial task is rather *ad hoc* [1, p. 474]. The MRI book stated that there were indications that the (1-D) TSA approach may be extendable to peaks consisting of three responses [1, p. 127]. The pairing would be much more complicated.

Perhaps other candidates could be more efficient in such use of 1-D components to solve an originally two-dimensional (2-D) problem. We surveyed the literature of array processing and beamforming for candidates compatible with MRI's Two-Scatterer Algorithm. The criteria for our candidates included: capable of handling single-snapshot data without spatial smoothing (only 16 cross-range gates available); computationally nonintensive, preferably having closed-form formulas for two and three arrivals; and having automatic pairing worked out if based on 1-D building blocks. The basic premise of the TRW/MRI approach was that no practical and globally valid model exists for man-made targets in the context of ISAR imaging. To conform to the divide and conquer strategy, the candidate approaches must be operating in beamspace. The candidate we tested was by Zoltowski et al. [2].

The result of this limited effort has not outperformed MRI's due to unforeseen hurdles encountered in dividing the global problem into many smaller local ones that fit a two-scatterer model. The problem is not the lack of suitable candidates from array-processing literature to handle *ideal* two-scatterer models. Rather, one difficulty is generalizing MRI's 1-D dividing approach to a 2-D one. More specifically, we found that the support of a rectangular or box-car spotlighting filter of a 2×2

footprint in Nyquist spacing is too small due to the sharp cut-off of the 2-D rectangular window used. (Although MRI did not use the terminology, we borrowed and shortened the term “digital spotlighting” originated for strip map Synthetic Aperture Radar (SAR) [3].) This 2x2 size is the minimum to use the algorithm from [2]. On the other hand, because of the closeness of scatterers, a 3x3 size for box-car spotlighting filters is much too large. Furthermore, many of the peaks we examined call for spotlighting filters with support other than rectangles parallel to the range and cross-range directions.

The sharp cut-off of the 2-D rectangular window, especially at the four corners, counteracts the potential gains from the Hamming window de-weighting in the transform domain (as used successfully by MRI in its 1-D approach). The original 2-D Hamming window is used to control the side-lobes of strong scatterers. The accompanied mainlobe widening of the Hamming window application exacerbates the original lack of mainlobe resolution. After excluding the influence of sidelobe masking by using a spotlight filter on the imaged data for each peak and then converting the spotlighted data back to the transforming domain, a Hamming window de-weighting was used to restore the mainlobe width of a rectangular window. The restoration could indeed be achieved if no sharp cut-off had been used to introduce the severe high-frequency components.

For a single scatterer exactly between two grid points or at the center of the two-gate wide spotlighting filter, the effect of sharp cut-off can be curtailed when over-sampling is used in centering the spotlight filter. Over-sampling is rarely, if ever, considered in super-resolution literature. Fortunately, we found that the formulation in [2] can be easily generalized from the original Nyquist grid to Nyquist spacing. With such sharp cut-off for a given scatterer strength, this is the least damaging location choice because it has the lowest amplitude level possible at the discontinuities.

When out-of-sector interfering scatterers are also present, the sharp cut-off for the nonadaptive spotlight filter occurs at worse amplitude levels. Desirable transform interval determination is more complicated. Compromises need to be made between including (as much as possible) response between the within-sector, two-scatterer response and excluding out-of-sector interference, which may be very close. Such determination should be devised and tested against all scenarios spanning spatial separation, amplitude, and phase separations among the contenders.

After discussion with Professor Merhdad Soumekh of State University of New York (SUNY)/Buffalo (who is currently at Massachusetts Institute of Technology Lincoln Laboratory [MIT/LL]), a 1-D numerical investigation was conducted to assess the amplitude and phase discrepancy from a sharp cut-off spotlighting filter of two-gate width. Phase was found to be more robust than amplitude in this highly mismatched environment. We note that MRI uses only a 1-D approach, so the sharp cut-off is less pronounced compared to a 2-D box-car window use. Furthermore, MRI mainly uses linear phase slopes in the transformed domain to estimate the scatterers’ location in the image domain. This is contrasted to our operation in the beam-space or image domain since the closed-form approach is based on that domain. A single experiment of using phase-only data as input to the closed-form approach did not produce a significant difference in our formulation. This result indicates that the main hurdles of the sharp cut-off issue must be tackled before significant performance can be expected.

In addition to the spotlighting operation, an implicit requirement we tried to meet was a 2-D replacement of TSA. It should be sensitive enough to estimate the location of two interacting scatterers

within a 2×2 footprint of spotlighting filters with power contrast up to 20 dB in difference, yet insensitive to mismatches such as out-of-sector interfering scatterers just outside the 2×2 footprint or high-frequency components from sharp cut-off.

A March 1997 progress report [4] supplied analytic justification for the choices of phase inflection and amplitude minimum locations in setting the boundaries of the transform window. Since MRI uses 1-D techniques to perform an originally intrinsic 2-D task, the justification is based on 1-D as well. To generalize the notion of 1-D amplitude minimum to 2-D is not a trivial problem. We generated figures for individual peaks in which each subplot was centered at the peak location normalized to the peak level. Often, the natural boundary contained saddle-like structures.

Such lessons should be considered in future attempts to make significant component replacements within the framework of MRI's scatterer location context. More documentation is necessary on the description of and the rationale behind the many heuristics in MRI's current 1-D approach.

REFERENCES

1. Rihaczek, A. W. and S. J. Hershkowitz. 1996. *Radar Resolution and Complex-Image Analysis*, Artech House, Norwood, MA.
2. Zoltowski, M. D., M. Haardt, and C. P. Mathews. 1996. "Closed-Form 2-D Angle Estimation with Rectangular Arrays in Element Space or Beamspace via Unitary ESPRIT," *IEEE Transactions on Signal Processing*, vol. 44, no. 2, pp. 316–328.
3. Soumekh, M. 1995. "Reconnaissance with Ultra-Wideband UHF Synthetic Aperture Radar," *IEEE Signal Processing Magazine*, vol. 12, no. 4, pp. 21–40.
4. Hershkowitz, S. J. 1997. "Dominance among Interfering Scatterers," MRI Progress Report 389–1 to ONR on Identification of Moving Ground Vehicles in SAR Imagery, Mark Resources, Inc., Torrance, CA.

Principal Investigator:
Dr. S. I. Chou

0601152N
ZU42

Active Matched-Field Tracking

Objective(s): Develop new method for detecting quiet submarines (i.e., diesel-electric on battery power) in shallow water.

Accomplishment(s): An algorithm has been developed that allows coherent processing of an active sonar system over a 3- to 5-minute period of time. Realistic simulations show reliable shallow-water detection for a low-powered, inexpensive, active shallow-water system at a range of approximately 5 km.

Sonar pulses are collected for an extended period (approximately 3 to 5 minutes), and a set of covariance matrices are calculated. A new set is generated at approximately 10-second intervals. The Active Matched-Field Tracking (AMFT) algorithm calculates the set of tracks that best corresponds to the experimental data set. The algorithm includes the effects of shallow-water, multipath propagation and the calculated echo structure of expected targets.

Figure 1 shows a proposed AMFT system. A seawater battery provides the power for the system and serves as the anchor. A power converter takes the low-voltage output of the battery and generates a 500-V output for use by the transducer. The transducer has 10 elements situated on a rigid vertical line at $\frac{1}{2}$ -wavelength spacing. A tag line connecting the bottom of the transducer array to the power cable is adjusted so that the line source remains vertical. A computer in the upper unit uses the AMFT algorithm to detect possible submarine targets. If a detection is made, the transducer sends an acoustical message to an appropriate data-collection unit.

Advantages of AMFT include automatic target detection, a low false-alarm rate, and good connectivity. The algorithm collects data in approximately 3- to 5-minute segments and, without operator intervention, generates a list of possible targets. Because this list includes target depth, the identification of submarines is greatly simplified. The false-alarm rate tends to be low because of the low output data rate. Obviously, a system that produces output every 5 minutes will tend to have a lower false-alarm rate than one with a 10-second output schedule. Also, connectivity is good because the low data rate simplifies the connection of the signal processor to associated data networks.

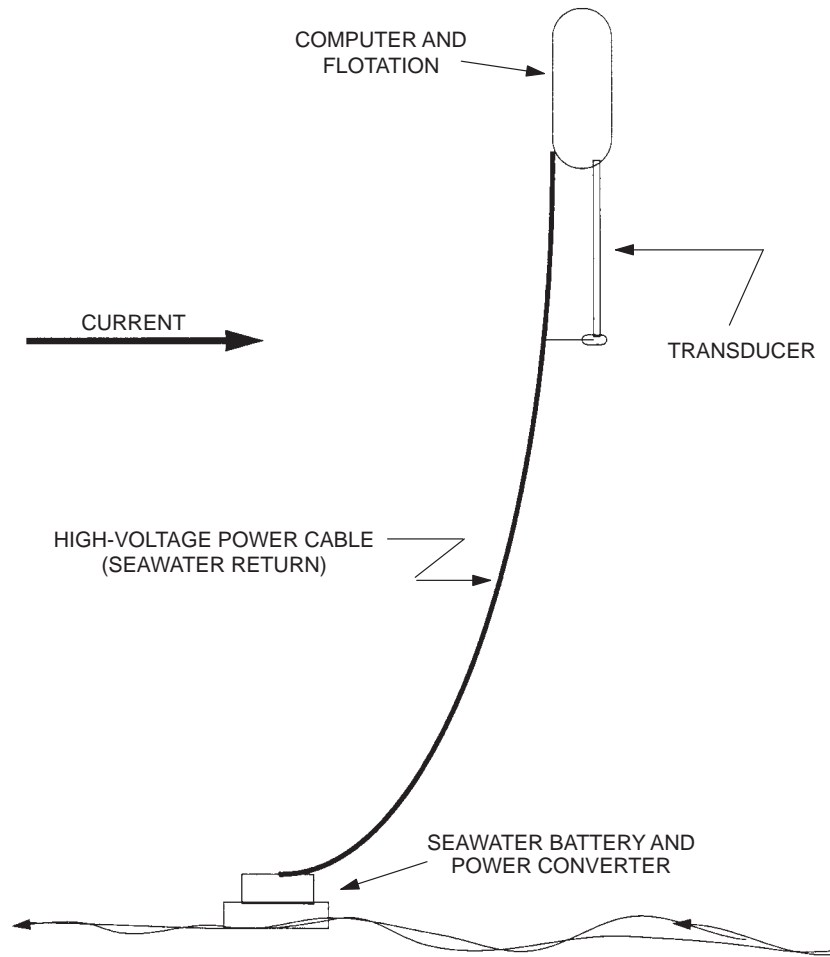


Figure 1. 10-kHz AMFT system.

Principal Investigator:
Dr. Homer Bucker

0601152N
ZU41

Acoustic Data Analysis Using Fourth-Order Cumulants

Objective(s): Gain experience with the use of cumulants of complex Fourier coefficients to analyze acoustic data.

Accomplishment(s): The fourth-order cumulant estimator can sometimes be a sensitive indicator of signals that would generally not be seen in an analysis of second-order moments.

INTRODUCTION AND DATA DESCRIPTION

The proposed procedure differed from previous suggestions in that the data were first Fourier transformed and all computation and testing of the cumulants was done in the frequency domain on complex random variables. In effect, each frequency bin was treated as a separate complex data series.

In the summer of 1996, a rather quiet ship maneuvered over a string of hydrophones in shallow (200-m) water. Recordings of four hydrophones in the string were made to test the system sensitivity. Because the hydrophones were about 300 meters apart, there was little opportunity to correlate the received acoustic pressures. Spectrograms of the sound from the four hydrophones showed that hydrophone number 2 seemed to have some broadband energy that could be attributed to the presence of the ship, but the other hydrophones seemed not to have received significant signal energy. Even in hydrophone 2, the energy level was difficult to distinguish.

The data consisted of four files, one for each of four bottom-mounted sensors. The data were samples from a 16-bit analog-to-digital converter and were sampled at a rate of approximately 4995 samples per second. For this analysis, the data were converted to IEEE double-precision floating-point numbers and written to data files AC1_D, AC2_D, AC3_D, and AC4_D. No calibration information on the hydrophones was used; therefore, none of the results indicate anything about absolute sound levels.

Figure 1 shows the approximate ship track relative to the hydrophones. The data analyzed were from a 5-minute time period in which the ship crossed the array during the third minute.

From an instrumentation point of view, the data were less than ideal. Figure 2 shows a plot of the voltage vs. time for hydrophone 2. Fortunately, the worst instrumentation problems seem to have been confined to the lowest frequencies, as will be seen below.

ANALYSIS PROCEDURE

The analysis was done entirely in the frequency domain. The first step was to compute a set of Fourier coefficients

$$X(m, k) = \sum_{n=0}^{M-1} w(n) x(n + kM/2) e^{i2\pi nm/M}$$

where $w(n)$ is the window function (usually a Kaiser–Bessel window with side lobes about 70 dB down). The product, $kM/2$ gives a 50% overlap of the windows to increase the effective time

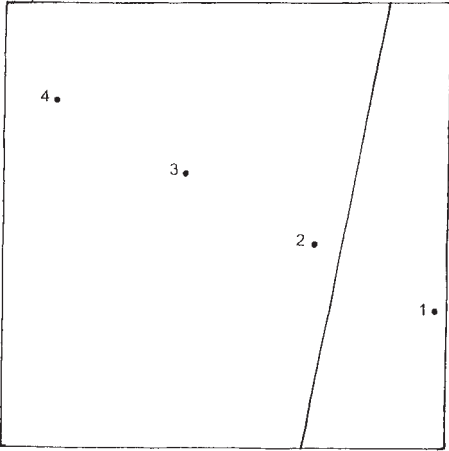


Figure 1. Approximate ship track relative to the hydrophones.

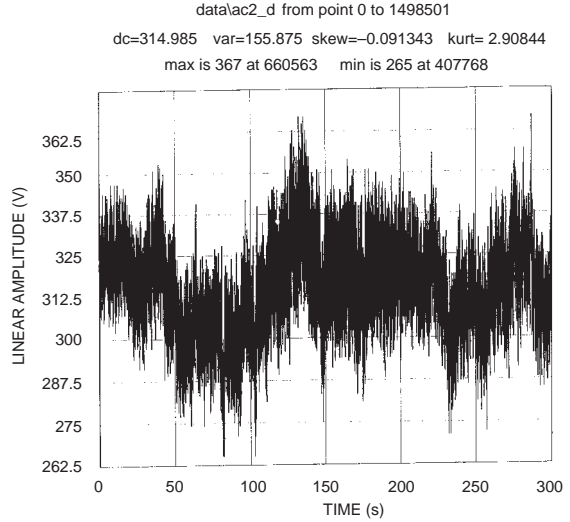


Figure 2. Amplitude vs. time for hydrophone 2.

bandwidth product of the estimates. The Fourier transform length was usually 1024 points. The spectral estimates then were

$$S(m) = \frac{1}{K} \sum_{k=0}^{K-1} X^*(m, k)X(m, k)$$

and

$$C4(m) = \frac{1}{K} \sum_{k=0}^{K-1} (X^*(m, k)X(m, k))^2 - 2S^2(m)$$

(For a real variable analysis, the last term would have been multiplied by 3 instead of 2. This illustrates one of the interesting differences between the real and complex distribution functions.)

For display purposes, the spectrogram, $10 \log(S(m))$, was plotted in the usual manner. The cumulant data were plotted as $5 \log(|C4(m)|)$ on the same scale as the spectral power. The intent was to compare the second-order signal indications with the fourth-order indications. Since the comparison was not always easy to see visually, a third statistic was used:

$$N4(m) = \frac{C4(m)}{S^2(m)}$$

This statistic was especially useful to attempt to find signals that could not be seen with ordinary spectrum analysis. $N4(m)$ is asymptotically -1 for sinusoids, zero for Gaussian noise, and large for highly variable noise.

SPECTRAL PLOTS

Figure 3 shows a plot of the spectrum of the sound from hydrophone 4 during the third minute of the data (at this time, the ship was close to hydrophone 2). This provided an idea of what the noise

background looked like. The heavy upper curve shows the power spectrum, estimated in the usual way. The fine lower curve shows the fourth-cumulant estimator. Both curves show a fairly smooth spectrum plus several tonals. Most of these tonals were harmonics of 60 Hz and were judged to represent instrumentation noise. Exceptions were strong tones at about 162 Hz and 636 Hz. The sources of these tones are unknown. In this plot, the power spectrum and the cumulants appear to tell almost the same story. Figure 4 shows N4 for the same data. Most of the narrow-band components are sinusoids, with the notable exception of 636 Hz. In spite of the approximate coincidence, the 636-Hz sound is evidently not a harmonic of the 162-Hz sound, both because the ratio is not quite 4 and because $N4(162 \text{ Hz})$ is strongly negative while $N4(636 \text{ Hz})$ is positive.

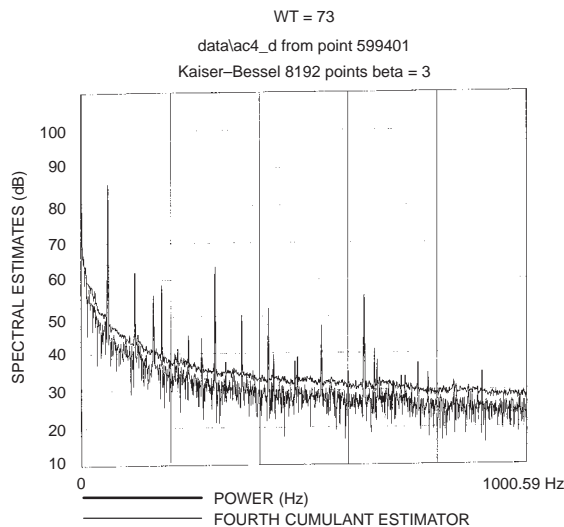


Figure 3. Spectrum plot from hydrophone 4.

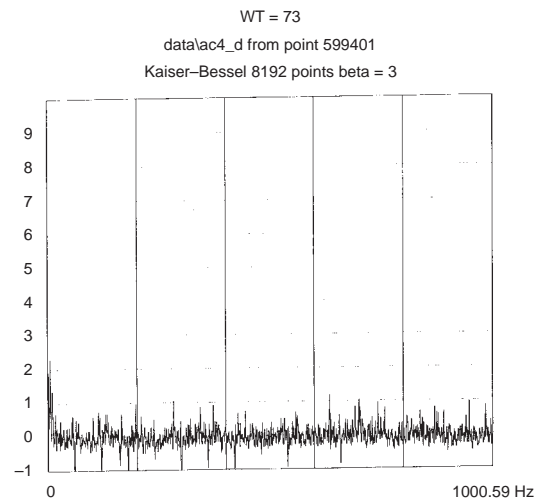


Figure 4. Normalized fourth cumulant (N4) plot for figure 3 data.

Figure 5 shows the key calculation plot of the spectrum from hydrophone 2 during the third minute of the data run, analyzed with a 1024-point Fourier transform. Here, there should be sound from the ship in the hydrophone voltage. Close examination shows that the C4 curve was closer to the power-spectrum curve than in the previous plots in the general range between approximately 200 Hz and 1000 Hz. Closer inspection reveals that at approximately 282 Hz, the C4 curve actually went significantly above the spectral curve. This is more easily seen in the N4 plot in figure 6. The sound has a significantly stronger nonGaussian component below 1000 Hz, and the 282-Hz indication is obvious. It appears that both the broad nonGaussian noise and the 282-Hz component come from the ship.

IMPULSE DISCUSSION

The strong nonGaussian indicator at 282 Hz is probably not as significant an indicator as the broader, though lower cumulants. However, it suggests several questions including the question of what sort of narrow-band signal might have such a large fourth cumulant. To learn more about this signal, a more directed investigation was undertaken.

The data stream was passed through a narrow-band filter centered at 282 Hz and then re-examined. This process revealed several signal peaks. One of the strongest peaks was selected as representative. Figure 7 shows this waveform, which was used as a reference for a correlation against the original

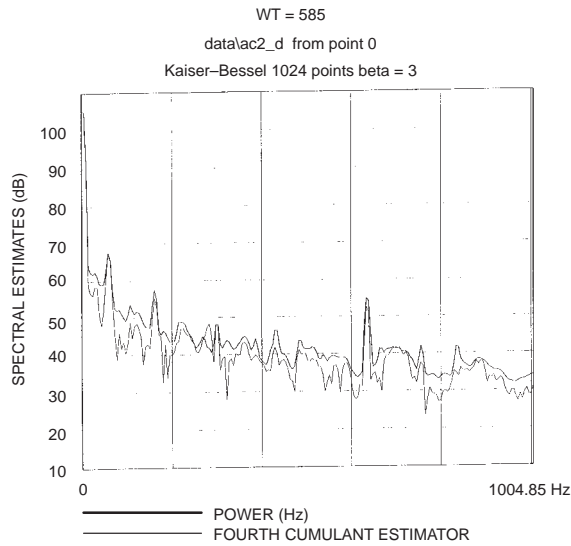


Figure 5. Spectrum plot from hydrophone 2 analyzed with a 1024-point Fourier transform.

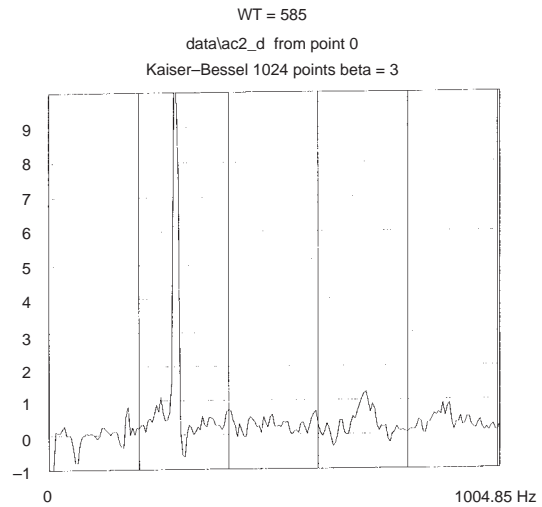


Figure 6. N4 plot for figure 5 data.

data. Figure 8 shows the running correlation coefficient of the impulse with the original waveform. The scale on the left is the correlation coefficient, while the scale on the right shows the corresponding signal-to-noise ratio. The clear indication is that at least six replications of this impulse occurred.

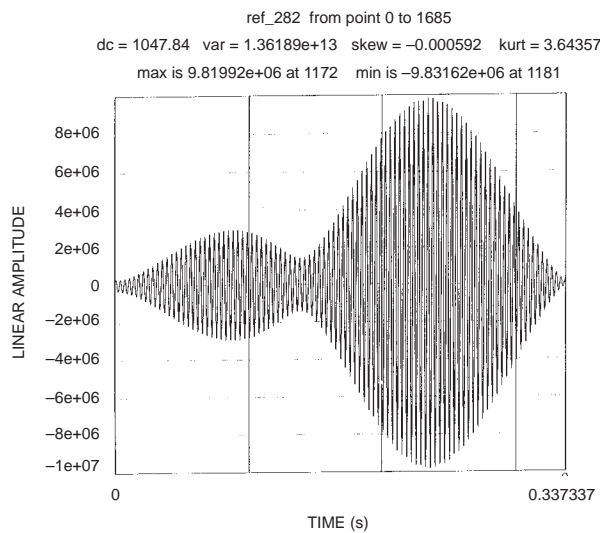


Figure 7. Reference waveform for comparison against original data.

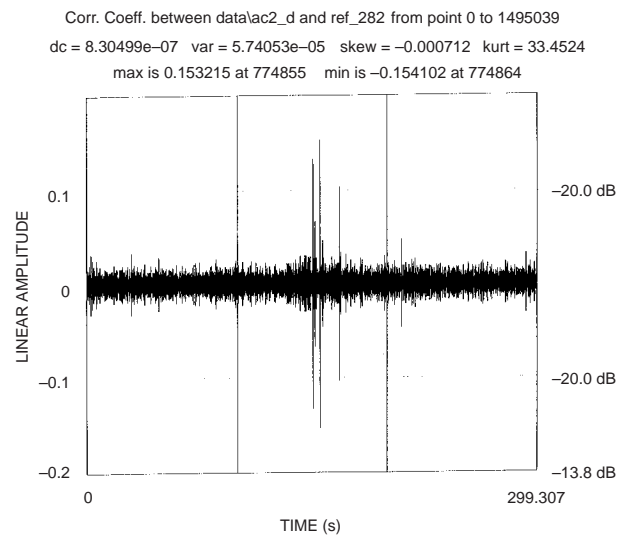


Figure 8. Correlation coefficient of the impulse with the original waveform.

CONCLUSIONS

This analysis reveals several things that were not obvious. The first is that ship noise can have a strong narrow-band nonGaussian component. The analysis also shows that this nonGaussian character can survive considerable filtering including Fourier transforms. The fourth-cumulant estimator

can sometimes be a sensitive indicator of signals that would generally not be seen in an analysis of second-order moments.

From a theoretical standpoint, several important questions remain. In particular, we don't know the detection statistics of fourth-order cumulants. It is possible to define other complex fourth-order cumulants that could be useful in some cases. Some were tried on this data set but without interesting results.

Fourth-order cumulants can complement standard spectral analysis. They can help to separate tonals from narrow-band random noise, and they can serve as indicators of nonGaussian behavior. Fourth-order cumulants provide another way to look at the data, and therefore, a chance to see something new.

Principal Investigator:
David J. Edelblute

0601152N
ZU26

Impulsive Snap-through Acoustic Projector (ISnAP)

Objective(s): Derive “snap-through” analytical expressions representing the kinematics of an impulsive acoustic projector application. Investigate transient (time-domain) acoustic radiation of the Impulsive Snap-through Acoustic Projector’s (ISnAP’s) shell coupled to water to predict the acoustic figures of merit of this impulsive device. Derive expressions for transient, time-domain, acoustic interaction equations. This research is applicable to any impulsive projector (explosives, air-guns, sparkers) where acoustic interaction effects are present, especially when configured in an array.

Accomplishment(s): An analytical acoustic radiation model was derived using a circular piston having a displacement field that simulates a thin shell undergoing snap-through. This math model indicates that the acoustic pressure pulse is better represented by the surface’s acceleration than the velocity. Numerical methods were used to model the transient response of the ISnAP’s hyperelastic shell undergoing snap-through. This model was generated using ABAQUS* explicit and ANSYS**.

The ANSYS and ABAQUS finite-element analysis tools were used to evaluate snap-through of a thick, shallow shell. The shell material modeled uses a hyperelastic formulation that consists of using experimental stress-strain data to determine the strain energy through least-squares methods. The strain energy function is shown below.

$$W = a_{10} (\bar{I}_1 - 3) + a_{01}(\bar{I}_2 - 3) + \beta \left(\bar{I}_3^2 - \bar{I}_3^{-2} \right)^2$$

where

\bar{I}_i = reduced strain invariants in the i^{th} direction that are given by:

$$\bar{I}_1 = I_1 I_3^{-1/3}$$

$$\bar{I}_2 = I_2 I_3^{-2/3}$$

$$\bar{I}_3 = I_3^{-1/2}$$

a_{10}, a_{01} = Mooney–Rivlin material constants

$$\beta = \frac{(1 + \nu) a_{10} + a_{01}}{(1 - 2\nu) 24}$$

ν = Poisson’s ratio

I_i = invariants of the right Cauchy–Green deformation tensor, C_{ij}

Figure 1 shows a numerical solution for the center displacement of the EN-1556 ISnAP for two different scenarios. The MOONEY-2 data pertains to analysis using a two-constant Mooney–Rivlin formulation and 20 stress-strain data points up to a total strain of 100%. This figure shows that the

*ABAQUS is a registered trademark of Hibbitt, Karlsson & Sorenson, Inc. (HKS).

**ANSYS is a registered trademark of SAS IP, Inc., a wholly owned subsidiary of ANSYS, Inc.

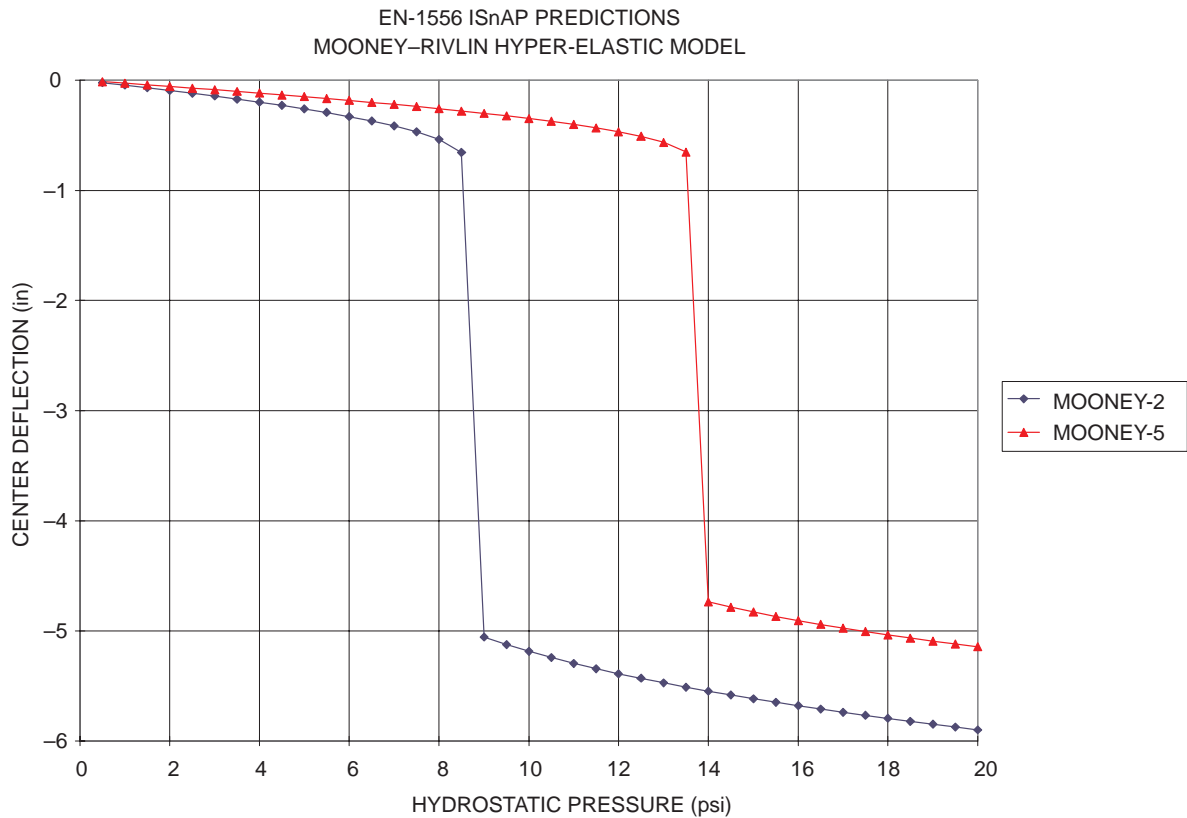


Figure 1. Numerical solution of ISnAP's center deflection.

predicted snap-in pressure is approximately 9 psi. Transducer Evaluation Center (TRANSDEC) testing showed that the required snap-in pressure is actually closer to 20 psi. An improved estimate for snap-through pressure was obtained by using a five-constant Mooney–Rivlin approximation for the stress-strain relation. Using the five-term Mooney–Rivlin solution, figure 1 shows that the calculated snap-through pressure is 14 psi. This pressure is still 43% below that measured at TRANSDEC but is a significant improvement over the previous solution.

The snap-through pressure and resultant displacement fields are critical for determining the mechanical-acoustic response of the ISnAP. The above work indicates that the material model used can be improved. A finer definition of the nonlinear load-displacement relation at small strains is likely to improve this solution technique.

An analytic model was developed to predict the acoustic radiation of the ISnAP. This model was generated to correlate the surface motion of the ISnAP while undergoing snap-through with the pressure pulse, which was measured using a hydrophone. The model assumes that the ISnAP's acoustic loading can be approximated by that of a circular piston. Figure 2 is a schematic representation of the analytical model.

The acoustic radiation model relates the ISnAP's shell force and velocity (F_0 and V) to the radiated acoustic output. The model still requires a well-defined displacement field of the radiating shell as a

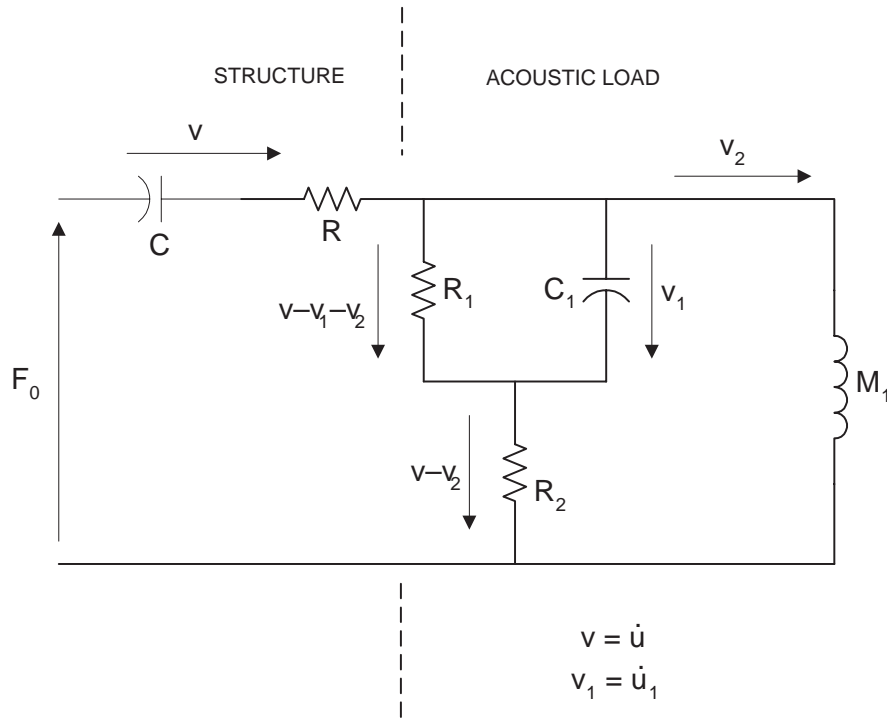


Figure 2. Analytic acoustic radiation model.

function of time. This effort is being continued with the FY 98 IR project. The model can be reduced to a system of differential equations of the form

$$(\dot{u}) + A(u) = F_o(e)$$

where

$$(u) = \begin{bmatrix} u \\ u_1 \\ v_2 \end{bmatrix}, (e) = \begin{bmatrix} \frac{1}{R + R_2} \\ \frac{1}{R + R_2} \\ \frac{1}{M_1(R + R_2)} \end{bmatrix}, \text{ and}$$

$$A = - \begin{bmatrix} \frac{1}{C(R + R_2)} & \frac{1}{(R + R_2)} & \frac{-R_2}{R + R_2} \\ \frac{1}{C(R + R_2)} & \left(\frac{1}{R_1} + \frac{1}{(R + R_2)} \right) \frac{1}{C_1} & \frac{R}{R + R_2} \\ \frac{R_2}{M_1 C (R + R_2)} & \frac{-R}{M_1 C_1 (R + R_2)} & \frac{R_2 R}{M_1 (R + R_2)} \end{bmatrix},$$

which are solved numerically.

Principal Investigator:
Jerome F. DeJaco

0601152N
ZU44

Solid-State Blue Laser Development

Objective(s): Develop a high-repetition rate, solid-state blue laser source for underwater surveillance or communication and also investigate technical issues associated with the efficient operation of a quasi three-level neodymium laser.

Accomplishments(s): Results of a multiple bar diode end-pumped Nd:YAG laser at 946 nm are reported. A pulse energy of 10-mJ has been obtained in long-pulse operation.

Mine detection in coastal waters has been and continues to be an important requirement of regional Navy operations. The Magic Lantern system currently employed on a limited basis by the Navy has demonstrated the capability of a 532-nm pulsed laser radar (ladar) system for mine detection down to keel depths. There are, however, situations where it would be very useful to extend the capability of underwater ladar or communication systems to greater depths for detection of deep submersed mines and submarines and also for submarine communication. With longer path lengths at greater depths, the wavelength variation of irradiance attenuation becomes much more significant. The optical transmission characteristics of seawater have been studied extensively, and over the majority of the ocean surface, the minimum attenuation coefficients occur in the blue-green spectral region [1]. In clean ocean water, the 1/e attenuation length is >50 m at 475 nm, compared with ~20 m at 532 nm. In addition, most waters become cleaner at greater depths so that a blue ladar would have a significantly greater range than a green ladar.

Laser operation of the ${}^4F_{3/2} - {}^4I_{9/2}$ transition in Neodymium with frequency doubling is a promising approach for a simple solid-state laser source in the blue. The transition in Nd:YAG at 946 nm would give 473 nm, which is nearly optimum for transmission in Jerlov Ocean Water Types 1–3 over much of the world's surface. In this work, we investigate issues associated with efficient 946-nm operation of Nd:YAG in pulsed and Q-switched operation, which is relevant for underwater communication and ladar systems. Outputs of 10's of mJ are expected to be required for such applications, and therefore, multiple pump diode bars must be used in an arrangement that maximizes pump brightness and gives high inversion densities. It seems clear that this general approach for developing blue laser sources will become ever more practical with the steady improvement in diode array brightness.

In this work, 20 pulsed diode array bars were used to end-pump a 3-mm-diameter composite Nd:YAG laser rod. All bars were nominally 50 W and configured with a small, coated cylindrical lens to collimate the emission perpendicular to the bar plane. A 10-bar stack from Opto Power Corporation with an ~1-cm by 2-cm aperture was combined with two 5-bar stacks from SDL with a similar combined aperture of ~1-cm by 2 cm. A half-wave plate and polarizing beam splitter was used to superimpose the outputs into a beam ~2 cm high with divergence of ~3 degrees by ~1 cm wide with divergence of ~10 degrees. A 6-cm focal length, horizontal cylindrical lens and an f/0.67 symmetric aspherical lens were then used to focus the pump light into the end of the laser rod.

The composite rod was fabricated by Onyx Optics with a 3-mm-long doped section bonded between undoped ends for a total length of ~25 mm. This arrangement helps to satisfy two conditions that are critical for efficient operation of the quasi three-level 946-nm transition in Nd:YAG. A short doped length consistent with the effective pump absorption length is necessary in order to avoid any length pumped below threshold, and in addition, good heat extraction is required to

minimize the temperature rise with increasing average power. Water cooling, which would be difficult with a 3-mm-long plug, is easily accomplished with the longer rod. In the experiments described below, the water temperature was 20°C.

In previous work, we demonstrated efficient laser operation with a similar geometry but while using only the two 5-bar SDL stacks combined with the beam splitter [2]. The “focal” spot was ~2 mm high by ~4 mm wide, and we found that a 5-mm-diameter rod gave significantly greater efficiency than a 3-mm rod. One reason for this is that if the brightest pump spot is positioned at the doped region of the rod, which would normally be optimum, the aperture at the rod end blocks some of the pump light. In this work we have attempted to scale the pump energy in the laser rod and simultaneously reduce the rod diameter so as to maximize the inversion density and facilitate low-transverse-mode extraction. The rod barrel was polished so that pump light focused on the end would be trapped by total internal reflection and propagate through the doped region. At the YAG/water interface on the barrel, the critical angle is 46.5 degrees to the barrel surface so that any pump ray transmitted through the rod face will therefore be trapped.

Figure 1 shows the pulsed laser performance at 20 Hz with flat 200- μ s pump pulses. Pump energy in this plot represents the measured fluence transmitted through a 3-mm aperture. Both sets of measurements were obtained with a flat 3.7% transmitting output coupler. The most efficient operation was found with a short 2.6-cm cavity and no intracavity lens. This cold cavity had an ~250- μ m TEM₀₀ mode diameter, and consequently, the laser output was highly multimode with a near-field profile ~3 mm wide by ~1 mm high, essentially following the pump distribution. Nearly 10 mJ of output was obtained at a slope efficiency of ~13%. Laser performance is also shown with a slightly longer cavity of 5.5 cm and an intracavity negative lens inserted between the laser rod and flat output coupler. The resulting TEM₀₀ mode diameter at the gain region was then increased to ~850 μ m calculated without any thermal focusing in the laser rod. Laser performance was, however, reduced as shown. Beam quality for both cavities was obtained from second moments of measured intensity profiles [3], and the M² results are indicated in figure 1 for the vertical and horizontal planes,

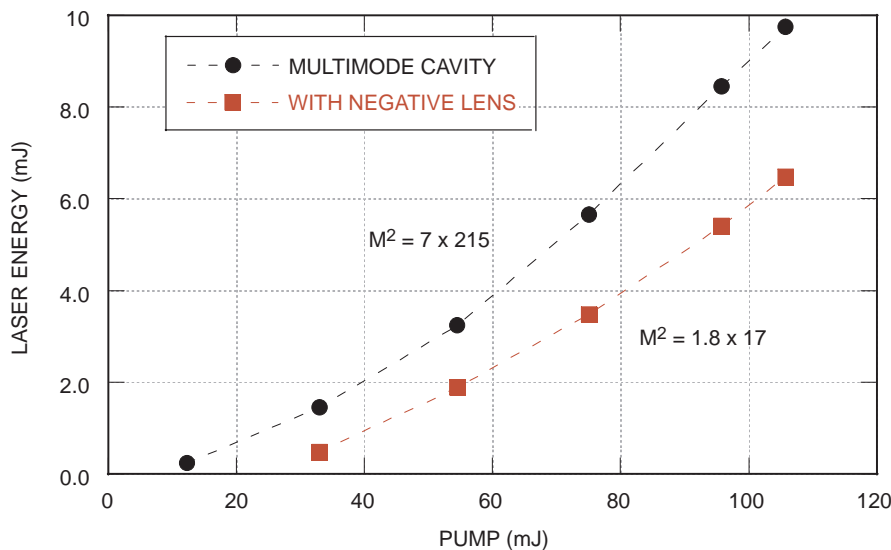


Figure 1. Pulsed laser energy at 946 nm with a highly multimode cavity and with an intracavity negative lens to increase mode size.

respectively. These results indicate a potential method for achieving reasonably good beam quality in at least one plane necessary to satisfy angular acceptance constraints for subsequent frequency doubling.

Efficient Q-switching with low-gain laser materials is difficult because of losses introduced with the additional optical elements in the cavity. Passive Q-switching with Cr:YAG was thought to be promising since a short cavity could be used and because of the large ratio of the cross sections for saturable absorption of the Cr transition to Nd emission at 946 nm. Thin slabs of Cr:YAG were fabricated for use at Brewster's angle so that the internal E-field polarization would be parallel to the (001) axis. Figure 2 shows a representative example of passive Q-switching where four distinct output pulses with successively greater energy were observed. The short cavity was highly multimode, and the unsaturated double-pass transmission in the Cr:YAG was 84% at 946 nm. Unfortunately, the efficiency was low, and attempts to obtain single-pulse output by increasing the loss were not successful. Further work with passive and electro-optic Q-switching is in progress.

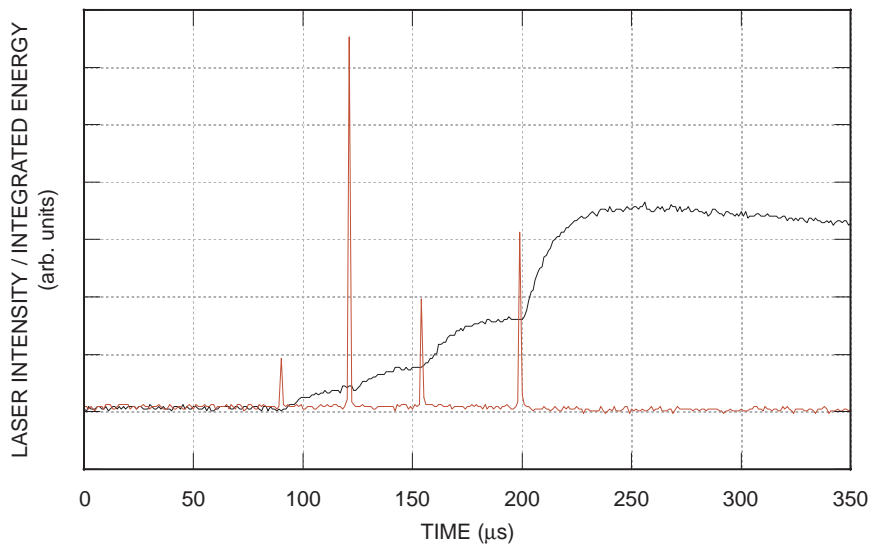


Figure 2. Passive Q-switched behavior at 946 nm with Cr:YAG. Pump pulse was 200 μ s long, and four Q-switch pulses are shown along with a relative measure of the integrated output energy.

REFERENCES

1. Jerlov, N. G. 1976. *Marine Optics*, Elsevier, Amsterdam.
2. Hanson, F. 1995. "Improved Performance at 946 and 473 nm from a Composite Nd: Y3A15O12 Laser Rod," *Applied Physics Letters*, vol. 66, p. 3549.
3. Siegman, A. E. and S. W. Townsend. 1993. "Output Beam Propagation and Beam Quality from a Multimode Stable-Cavity Laser," *IEEE Journal of Quantum Electronics*, vol. 29, pp. 1212–1217.

Principal Investigator:
Dr. Frank Hanson

0601152N
ZU45

High-Modulation-Rate, Solid-State Surveillance Laser

Objective(s): Produce a laser diode-pumped, solid-state dye laser capable of high-modulation frequency.

Accomplishment(s): Laser diode-pumped dye lasers were modulated at rates exceeding 100 MHz.

The goal of this project has been to produce a laser diode-pumped, solid-state dye laser capable of high-modulation frequency. The project was a continuation of research initiated in FY 96. The program approach required the completion of two major tasks. The first was a demonstration of high-modulation-rate laser operation. To this end, we modified our existing, laser diode-pumped, cw dye laser to demonstrate amplitude-modulated output by using a modulated, visible laser diode-pump source (figure 1). By modulating the current drive to the laser diodes, we have demonstrated a directly modulated laser diode-pumped dye laser that produces pulse modulation rates in excess of 100 MHz. Over 0.5 W of visible laser diode power was used to pump the dye.

The second major task was to obtain solid-state dye-laser gain elements that can be used in the high-repetition-rate, modulated dye laser. We evaluated dye laser rods fabricated from modified plastics doped with rhodamine 700 (also called LD700) dye. A modulated argon ion laser was used as the pump source. The pump pulse length used was 50 microseconds, which is over an order of magnitude longer than the excitation pulse duration previously demonstrated for solid-state dye-laser operation. It was found that plastic dye laser rods, while excellent for low-repetition-rate operation, did not perform well at these long pulse lengths and modulation rates. On the other hand, rhodamine 700 dye samples

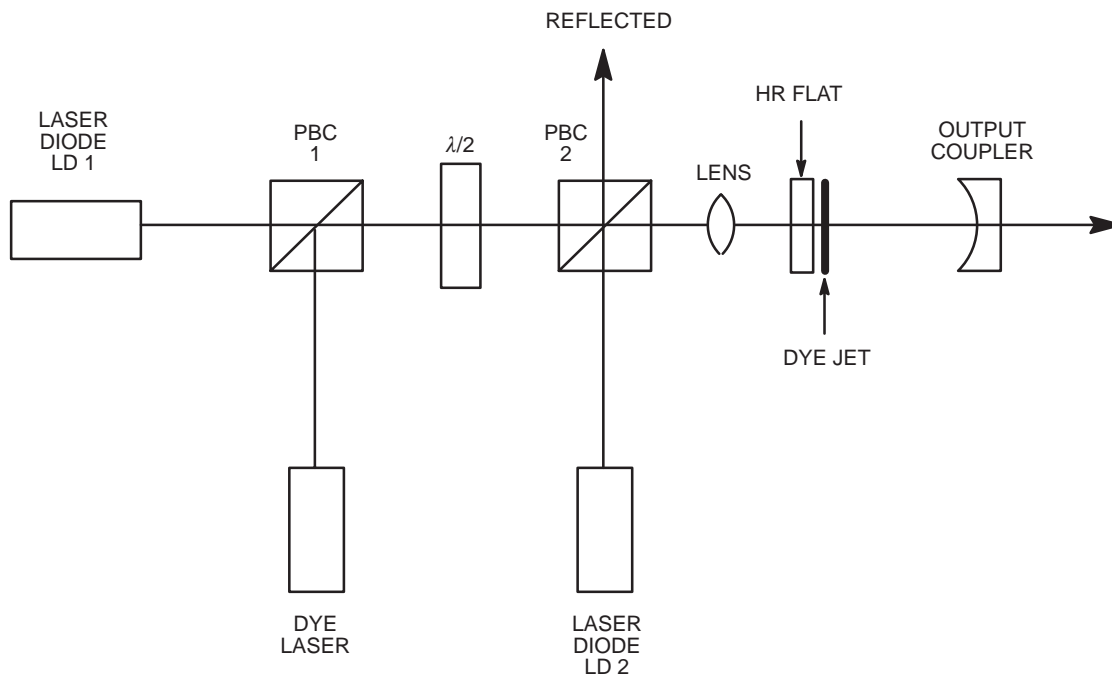


Figure 1. Pump optics and laser resonator configuration for laser diode-pumped dye laser. Polarization beam combiner cubes are labeled PBC.

in glass-like substrates (called organically modified silicates [ORMOSIL]) perform much better at higher repetition rate. We have found that the thermal and optical properties of the glasses are far superior to those of the modified polymers. This evaluation process and the dye-laser-resonator design task have lead to the successful demonstration of a modulated all-solid-state dye laser.

Principal Investigator:
Dr. Richard Scheps

0601152N
ZU14

OTHER LEADERSHIP AREAS

Development of Ultramicroelectrode (UME) Arrays for Use in a Remote Probe

Objective(s): Develop ultramicroelectrode (UME) arrays to perform electrochemistry in the gas phase for use as sensors in a remote probe.

Accomplishment(s): Disk and ring UME arrays have been prepared and have been used to obtain voltammograms of target compounds in the gas phase. Since the electrochemical reactions occur on the outer edges of the electrodes making up the array, sensitivity can be increased by using larger electrodes. However, the spacing between those electrodes must be on the order of 10 to 100 μm . Chemical modification of the electrodes improves selectivity of the arrays as well as increases sensitivity.

Electrochemical detection can be very sensitive. Depending upon the chemical nature of the electrode substrate and the analyte, detection limits in the ppm–ppb range are possible. Figure 1a shows a schematic of the ultramicroelectrode (UME) sensor assembly used to detect volatile organic contaminants in the gas phase. The inner working electrode can be either a wire (disk array) or a thin metal film on a glass fiber (ring array). By design, these electrochemical sensors are chemiresistors. The electrochemical reactions actually occur at the perimeters of the electrodes, and current flows between the electrodes across the insulating layer. Consequently, larger electrodes can be used if a narrow insulating layer, on the order of 10 to 100 μm thick, exists between the inner and outer electrodes of the array. Disk electrode arrays with diameters as large as 500 μm have been prepared and successfully used. Increasing the electrode diameter increases the outer perimeter where the electrochemical reactions occur. In turn, this results in an increase in sensitivity.

These arrays have been shown to respond to volatile organics in the gas phase. The magnitude of the response is dependent upon the chemical nature of both the electrode substrate and the analyte. While the aromatic hydrocarbons exhibit a negligible electrochemical response, the chlorinated and polar solvents are more electrochemically active. Figures 1b, 1c, and 1d summarize the electrochemical response of carbon/gold (C/Au) arrays to acetonitrile in the gas phase. Figure 1b shows voltammetric curves obtained for acetonitrile as it evaporates. However, these voltammetric curves are of limited use in identifying the species causing the electrochemical response. Both static and dynamic exposure tests were done in which the potential between the two electrodes of the array was held constant while measuring current flow. The results, shown in figures 1c and 1d, indicate that the electrode arrays exhibit a good response time, are reversible, and that the arrays can be used in either a flowing stream or in a quiescent environment.

We began looking at schemes to chemically modify the arrays to improve their selectivity. Both silver (Ag) and gold (Au) have been shown to react with thiols to form self-assembled monolayers (SAMs). Analytes that have an affinity for the coating will selectively partition into it. Surface-enhanced Raman spectroscopy (SERS) has been used to evaluate the selectivity of a number of thiol coatings. Figure 2a shows the SERS response of 4-chlorothiophenol on a roughened Ag substrate, as well as the response of methylene chloride as it partitions into the coating. The selectivity of the coatings has been found to be dependent upon the functional groups present on the thiol, as well as sterics. We have prepared SAMs on Ag and Au disk arrays. Figure 2b summarizes the results of static exposure tests of a Au/Au array to methylene chloride before and after chemical modification

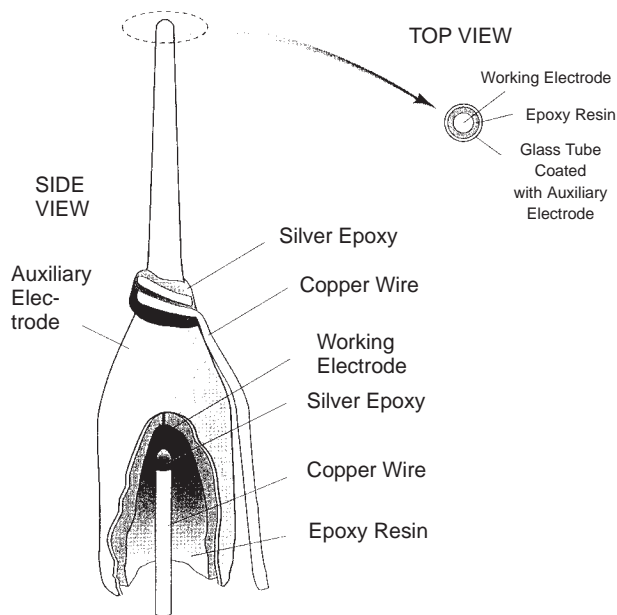


Figure 1a. Schematic of the UME array design.

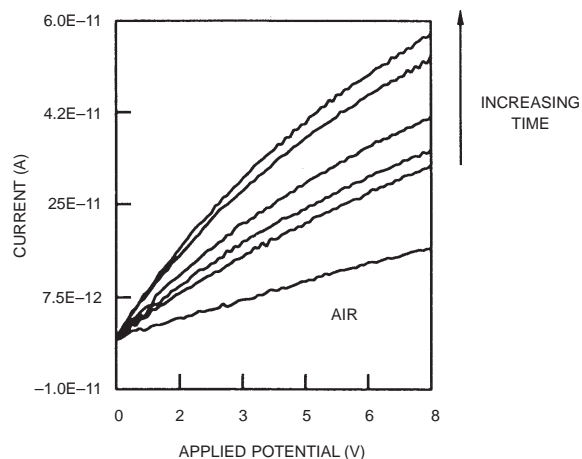


Figure 1b. Electrochemical response of a C/Au disk array to acetonitrile in the gas phase at room temperature. Diameter of the C working electrode was $7\ \mu\text{m}$. A $25\text{-}\mu\text{l}$ aliquot of acetonitrile was injected into a 5-ml glass flask. The evaporation of acetonitrile was monitored electrochemically by sweeping the voltage from 0 to 8 V at a sweep rate of $100\ \text{mV/s}^{-1}$.

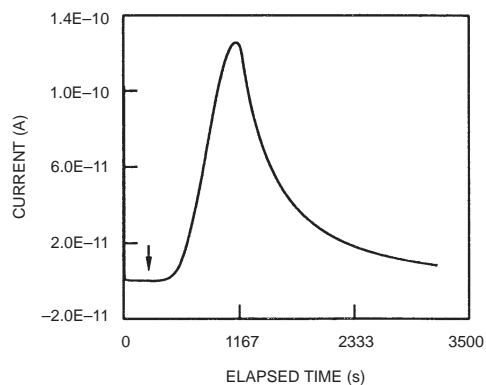


Figure 1c. Static exposure test of the C/Au array. The voltage was held constant at 8 V. The arrow indicates when $2\ \mu\text{l}$ of acetonitrile was placed inside the sample chamber. When volatilized, the total concentration of acetonitrile in the sample chamber was 143 ppm.

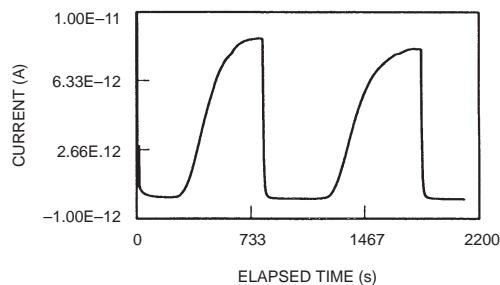


Figure 1d. Dynamic response of the C/Au array as a function of time for acetonitrile vapor. The potential was held constant at 8 V, and the Ar flow rate was $10.9\ \text{ml/min}^{-1}$. The UME array was repeatedly exposed to analyte vapor and then to pure argon and yielded the differential response shown.

Figure 1. Summary of the electrochemical response of the electrode arrays.

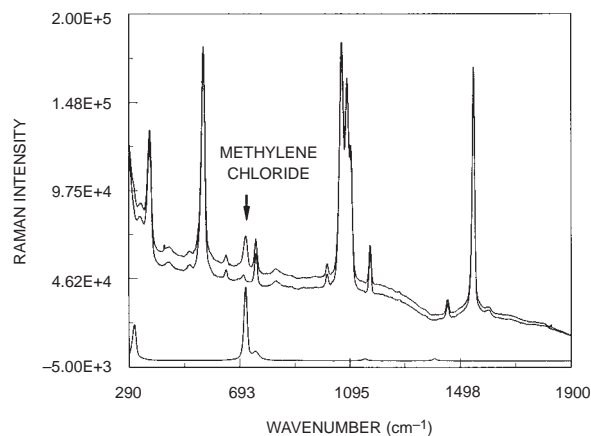


Figure 2a. The bottom Raman spectrum is of pure methylene chloride. The top spectra shows the SERS response of 4-chlorothiophenol on a roughened Ag substrate before and after exposure to methylene-chloride vapor. The spectra clearly show that methylene chloride partitions into the coating from the gas phase.

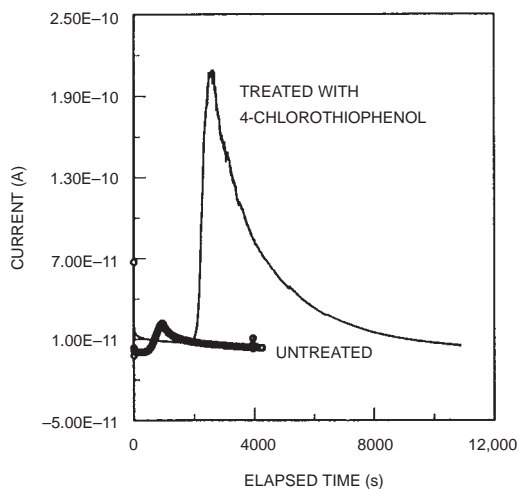


Figure 2b. Static exposure tests of a Au/Au disk array to methylene chloride showing the effect of chemical modification with 4-chlorothiophenol. Diameter of the Au working electrode was 500 μm . The voltage was held constant at 8 V.

with 4-chlorothiophenol. Chemical modification has increased the sensitivity of the array by a factor of 16.6, implying that the coating preconcentrates the analyte, thereby increasing the electrochemical response. To verify that this was occurring, an experiment was conducted that simultaneously recorded the electrochemical response of the array upon exposure to methylene chloride in the gas phase, while obtaining SERS spectra of the surface of the working electrode. The SERS spectra indicate that methylene chloride partitions in the coating as evidenced by the presence of the methylene-chloride Raman peak at 700 cm^{-1} upon exposure. The partitioning of methylene chloride into the coating coincided with an increase in current flow. Besides improving the selectivity of the arrays, the coatings have the added advantage of increasing sensitivity.

Principal Investigator:
Dr. Pamela A. Boss

0601152N
ZU30

Investigation of Shallow Momentumless Wakes

Objective(s): Study the logical hybrid of turbulent jets and wakes: the momentumless wake. More specifically, study the wake's interaction with the propagation of very short (e.g., wind-driven capillary waves) on a free surface with variable surface tension.

Accomplishment(s): A copy of a two-dimensional (2-D) Navier-Stokes equation solver (RIPPLE) was obtained from the NASA COSMIC program repository (COSMIC is the technology transfer organization for NASA.). Modifications to this program were made to initialize a free surface in a 2-D tank to the free surface displacement, fluid velocity, and pressure of linear wave theory. The forces at the free-surface include those of surface tension in addition to gravity force.

A jet is defined as a stream of fluid that has a velocity greater than the ambient fluid that surrounds it. The thrust of the jet is equal to the excess of momentum of the fluid. Likewise, a wake is a flow that has less velocity than ambient. The drag of the object that produced the wake is equal to the integral of the momentum deficit behind the object. Although jet and wake flow sound similar, the scaling laws are quite different. Most fluid-dynamic research in jets/wakes has concentrated on either a jet or a wake. For many problems, this is an appropriate approach (e.g., aircraft, where the wake from a wing is essentially two-dimensional and the thrust from an engine approximates an axisymmetric jet). For other problems, the distinction between a jet and a wake is entirely artificial. The prime example of a "wake" that is neither a jet nor a classical wake is the wake of a fully submerged self-propelled vehicle. For a self-propelled vehicle, traveling at constant velocity, the thrust is equal to the drag. Therefore, the net momentum of the wake is exactly equal to zero; hence the name momentumless wake. Similarly, ship wakes are closer to momentumless wakes than jets because most of the drag is due to skin friction (up to 90 percent) rather than wave drag. The relevance of these types of wake to the Navy is obvious.

A highly observable pattern from Synthetic Aperture Radar (SAR) images of surface ships in motion, is the wake. Distinguishable wakes as long as 40 km have been observed. Conjecture as to the actual mechanism of the bright edges and the darkness (i.e., nonradar return) of the wake centerline has ranged from the Kelvin (gravity) wave train, internal waves (due to density gradients), and the suppression of short wavelength capillary and gravity waves due to bubbles and turbulence in the wake. The most observable portion of the wake is almost always associated with the characteristics of turbulent decay. Current conjecture relates the observable nature of ship wakes to the interaction of organic surfactants that are stirred up by turbulence, and the resulting lower surface-tension suppressing short waves for a period of time related to the ambient sea state.

A numerical study of a momentumless wake has been started. A NASA-developed computer program, available from the COSMIC repository has been obtained and ported to the SSC San Diego HP Exemplar parallel computer. Modification to this program (source code is included) to handle the stated problem is in progress. The program title is "RIPPLE: A computer program for incompressible flows with a free surface." Unfortunately, this program only handles two-dimensional geometries at present. The baseline numerical experiment will be short wave(length) propagation of a wave train on a free surface with no external flows, constant surface tension and density. This can be directly compared to known analytical solutions. The RIPPLE program will be used as the backbone of a

computer program that can solve free-surface hydrodynamic problems of increasing complexity. These problems will always include the effect of surface tension on the flow. Future enhancements to the computer program and effects to be studied include variable (as a function of location) surface tension, turbulence effects on short wave propagation, tangential shear stress (i.e., wind), and density gradient.

Limited funding has resulted in modest progress. The RIPPLE program has been ported to the SSC San Diego HP Exemplar parallel computer. Test cases have been run on initially displaced free surfaces with and without the effects of surface tension included. Figure 1 shows the free surface and fluid (water) pressure in a periodic tank 6 milliseconds after initial displacement. Figure 2 shows the same initial conditions without including the effect of surface tension. The large difference in the computed solutions shows that surface tension is extremely important when wavelength is very short.

The modification of RIPPLE is proceeding. We completed the modification to initialize to the pressure-velocity solution of linear wave theory with an initially displaced free surface. Work is continuing on correcting the implementation of periodic boundary conditions in the program.

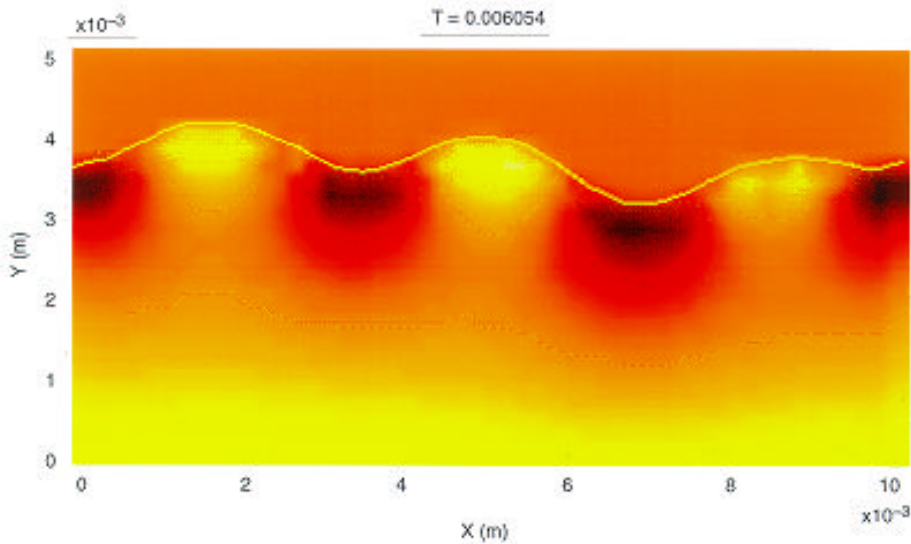


Figure 1. Surface displacement and pressure contours after 6 ms of an initially displaced free surface in a periodic tank. Yellow line is the top of the free surface; brighter areas indicate higher pressure.

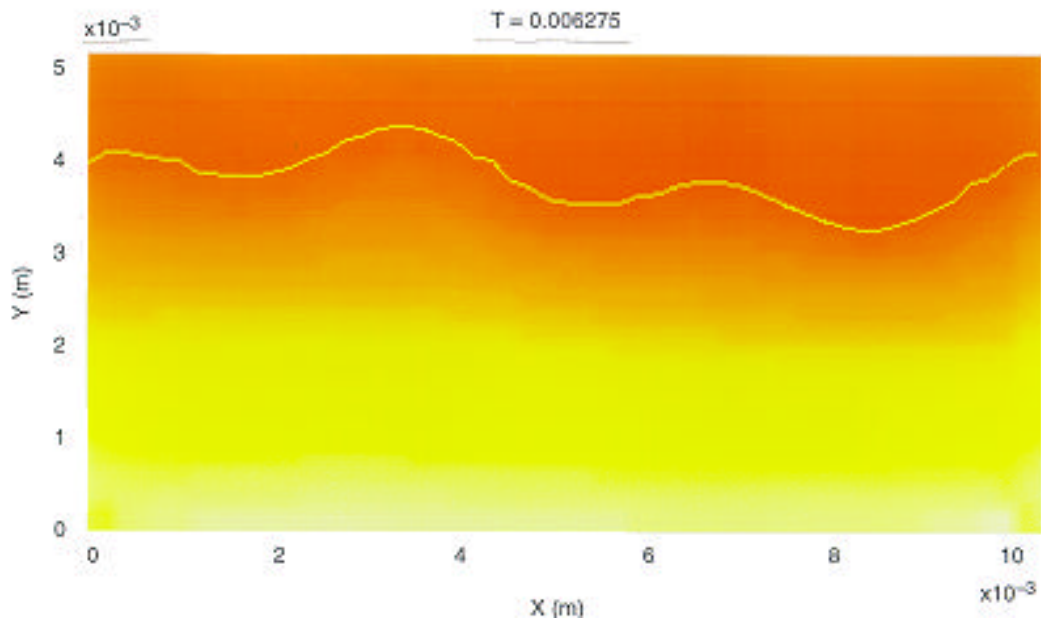


Figure 2. Same conditions as in figure 1, computed without surface tension.

Principal Investigator:
Dan Ladd

0601152N
ZU51

Exact Diagonalization of Many Body Hamiltonians

Objective(s): Develop numerical code to iteratively solve for the relevant eigenvalues and eigenvectors for extremely large sparse matrices representing highly correlated many electron systems.

Accomplishment(s): Code was successfully developed to solve for the ground-state (lowest) eigenvalue and eigenvector. Additional code is under development to obtain the eigenvalues and eigenvectors of additional target states as well as relevant correlation functions.

An iterative scheme starting with a small system size is used to determine final system eigenvectors and eigenvalues. The reduced-density matrix, representing a system of reduced size, is calculated. This reduced-density matrix is then diagonalized, and only those states with a probability density greater than a predetermined cutoff are kept to form a basis for a larger system. Typically, the reduced-density matrix is calculated for a system half as large as the original system. The reduced-density matrix determines which states are most relevant, and an outer product of those states with a mirror-reflected system produces a reduced basis for the original system. The size of the system is then increased by forming an outer product of the reduced basis with a complete basis set for two additional sites. In this way, the system can be iteratively increased to the desired size.

Code has been implemented to accomplish the task described above for a one-dimensional, strongly interacting, many electron system up to 100 sites. To appreciate the accomplishment, the full basis size is on the order of 10^{30} ! Additionally, code is under development to refine these solutions by continuing the iteration process in such a way as to take advantage of earlier results. The code is also being written to allow us to perform both the usual matrix products and outer matrix products, taking advantage of the sparseness of the matrices. The savings in computer memory have been substantial and will enable us to obtain a high degree of accuracy in these calculations.

To obtain information about the low-lying, optically excited states, the dipole operator has been invoked to enable us to target those optical states. A joint-density matrix is formed containing information about both the ground state and the lowest lying optically excited state. The pruning effect described above is not as effective as when you are only targeting a single state, but the additional information is required to describe the optical and nonlinear optical properties of quasi one-dimensional materials. This work is still in progress; however, significant progress has been made. For smaller system sizes (less than 20), the states that play a major role in the optical process have been targeted successfully. The 1-Bu state is the lowest energy state available for a single-photon optical process (absorption); the mAg and nBu are important states for nonlinear optical processes. The energies of these states have been found, and figure 1 plots these energies relative to the ground-state energy.

In addition, the code will eventually be parallelized for applications by using the local Exemplar machine. With increased accuracy from our refinement efforts, reduced memory requirements from code development for sparse matrices, and increased speed from the parallelization, the above results should be extended to 100 sites or more. In addition, code is being developed to calculate relevant correlation functions.

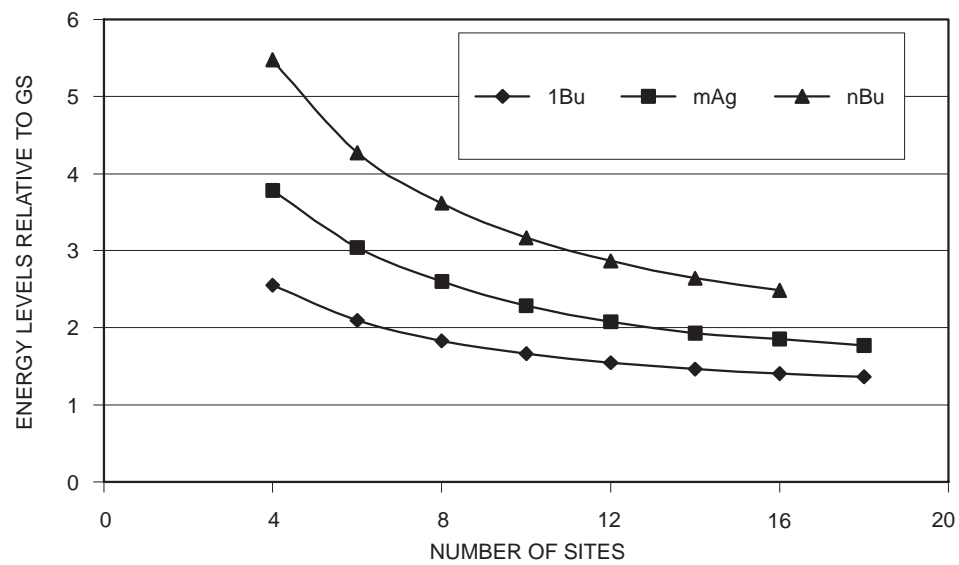


Figure 1. Optical energy levels.

Principal Investigator:
Dr. Charles Hicks

0601152N
ZU53

Sparse Complete Orthogonal Factorization as Applied to Bistatic Target-Strength Prediction

Objective(s): Improve computational efficiency of a method to predict full bistatic target strength from limited measurements.

Accomplishment(s): Algorithmic speedups have enabled the extension of the frequency range in bistatic target-strength prediction models to regions of greater interest to the Navy.

Knowledge of bistatic target strength is of increasing importance in sonar systems. Full-scale measurements of monostatic target strength are expensive and difficult and become impractical for general bistatic geometries. Extending the value of monostatic data by using it to estimate the bistatic target strength is extremely desirable. Previous efforts to do this have had severe limitations or restrictions in their applicability. A numerical method developed at SSC San Diego [1] uses measured monostatic and limited bistatic data to estimate the surface field and propagate it to the far field for full bistatic geometries. The most compute-intensive component in this formulation involves the least-squares solution of large sparse rank-deficient overdetermined system, $Mx = b$. Available conventional algorithms, such as those contained in Linear Algebra PACKage (LAPACK) [2], deal with the rank deficiency, but take no advantage of the sparsity inherent in these models. Therefore, they are very time-consuming, and this severely limits the frequency range of applicability. Existing data sets cannot be fully exploited using present solution techniques.

In the bistatic target-strength prediction model, $Mx = b$, the overdetermined matrix, M , is sparse and rank-deficient. Also, for some permutation matrix, P , PM is a 2-by-1 block matrix

$$PM = \begin{pmatrix} A \\ G \end{pmatrix},$$

where $A = [A_{ij}]$ is a k -by- k block diagonal matrix whose diagonal blocks are overdetermined matrices with identical dimensions and sparsity structure, and $G = [G_{1j}]$ is a 1-by- k block matrix in which every block is nonzero. We will refer to a matrix that has the form in PM as a row-bordered block diagonal matrix.

We have developed a new complete orthogonal factorization method [3] that takes full advantage of the structure and numerical properties of row-bordered block diagonal systems of the type arising in bistatic target-strength prediction models. There are five distinct steps in our method. These are as follows:

1. Apply QR factorization with column pivoting to each of the k diagonal blocks of A individually. At the completion of this step, the overdetermined matrix, PM , takes the form:

$$PMS = Q_1 \begin{pmatrix} U_{11} & U_{12} \\ U_{21} & U_{22} \\ 0 & 0 \end{pmatrix},$$

where S is a permutation matrix, Q_1 is an orthogonal matrix, and U_{11} is an upper triangular matrix and nonsingular. The blocks U_{12} , U_{21} , and U_{22} are nonzero blocks, and the 0s are zero

blocks. We will use s to denote the size of U_{11} in the remaining steps. *Note:* This step is ideally suited for parallel computation since each of the diagonal blocks of A is treated independently of the other diagonal blocks.

2. Use Householder reflections to zero block U_{21} in PMS. At the completion of this step, we have

$$PMS = Q_1 Q_2 \begin{pmatrix} R & B \\ 0 & D \\ 0 & 0 \end{pmatrix},$$

where Q_2 is an orthogonal (or unitary) matrix, R is an s -by- s upper triangular matrix and nonsingular, and B and D are both nonzero blocks.

3. Apply QR factorization with column pivoting to block D in PMS. This gives

$$PMS = Q_1 Q_2 Q_3 \begin{pmatrix} R_{11} & R_{12} \\ 0 & 0 \end{pmatrix},$$

where Q_3 is an orthogonal (or unitary) matrix, R_{11} is an r -by- r upper triangular matrix and nonsingular, and $r = s + \text{rank}(D)$.

4. Use Householder reflections to compute an orthogonal (or unitary) matrix Z such that

$$(R_{11} \ R_{12})Z = (T_{11} \ 0),$$

where T_{11} is an r -by- r upper triangular matrix and nonsingular. Making use of this equality in step 3 gives

$$PMS = Q_1 Q_2 Q_3 \begin{pmatrix} T_{11} & 0 \\ 0 & 0 \end{pmatrix} Z^T.$$

5. By properties of permutation matrices and orthogonal (or unitary) matrices, the minimum norm solution of the rank-deficient bistatic target-strength prediction model, $Mx = b$, can now be written as

$$x = SZ \begin{pmatrix} T_{11}^{-1} c \\ 0 \end{pmatrix},$$

where c consists of the first r elements of the column vector $(Q_1 Q_2 Q_3)^T (Pb)$.

Applying this new decomposition method to a range of highly ill-conditioned, rank-deficient bistatic target-strength prediction models, we have obtained from five- to seven-fold improvement over the compute time required by the linear algebra package, LAPACK, without exploiting any parallelism. By exploiting parallelism in the first step of our method, we have obtained improvements over LAPACK from nine- to fifteen-fold. Further speedups can be realized by exploiting parallelism in all the steps of the new method. Algorithmic speedups of this magnitude will enable the extension of the frequency range in bistatic target-strength prediction models to regions of greater interest to the Navy.

Figure 1 shows the row-bordered block diagonal matrix, PM , for the case where M is a 935-by-300 matrix. Figures 2a through 2d show the matrix, PMS , at the completion of the first four steps of the method.

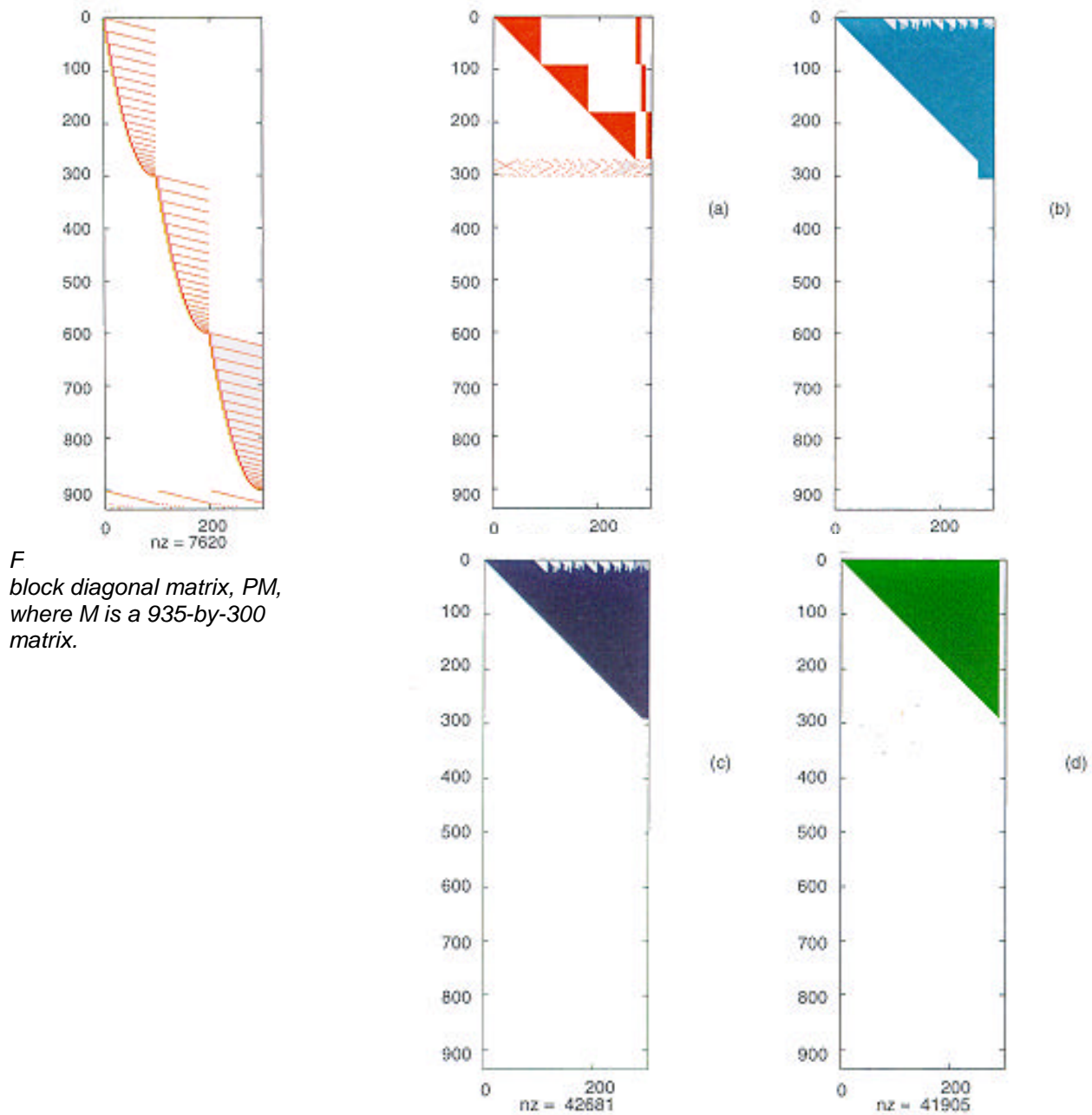


Figure 2. The overdetermined matrix, PMS , at the completion of each of the first four steps in the new decomposition method.

Table 1 summarizes the results obtained from the study of four bistatic target-strength prediction models.

Table 1. Results from four bistatic target-strength prediction models.

Overdetermined Matrix M			Compute Time Improvement Factor over LAPACK	
# rows	# columns	# nonzeros	No Parallelization	First-Step Parallelized
935	300	7620	6.45	14.57
935	900	22,860	5.92	10.61
2046	666	24,840	5.67	14.48
2046	1998	74,520	5.31	9.53

All computer runs were done on the Convex Exemplar at the High-Performance Computing Modernization Program (HPCMP) SSC San Diego Distributed Center.

REFERENCES

1. Schenck, H. A., G. W. Benthien, and D. Barach. 1995. "A Hybrid Method for Predicting the Complete Scattering Function from Limited Data," *Journal of the Acoustical Society of America*, vol. 98, pp. 3469–3481.
2. Anderson, E. et al. 1995. *LAPACK Users' Guide*, Second Edition, Society for Industrial and Applied Mathematics, Philadelphia, PA.
3. Kevorkian, A. K., D. Barach, and G. W. Benthien. 1997. "Sparse Complete Orthogonal Factorization as Applied to Bistatic Target Strength Prediction," *Proceedings of the DoD HPCMP High-Performance Computing Users Group Meeting*, June, San Diego, CA.

Principal Investigator:
Dr. Aram K. Kevorkian

0601152N
ZU35

Segmentation of Independent Motion via Pattern Recognition of Motion Flow in the Log-Polar Transformed Domain

Objective(s): Develop a robust method for segmenting independent motion as observed by a moving camera through the use of pattern recognition of motion flow in the log-polar domain.

Accomplishment(s): We expanded on last year's theoretical results by investigating issues that would allow the techniques to be applied robustly to real-world data.

Segmenting independent motion from a moving background (as observed by a moving camera) has been a difficult problem for computer vision. Inspired by findings on how biological visual systems handle this problem, we developed a mathematical model for a motion-classification method through template-matching the signs of the motion-flow projections on predetermined sets of directional vectors in the log-polar domain. The method potentially can provide magnitudes of improvement over existing methods due to: (1) the data-reduction nature of the log-polar transform, (2) the robustness of employing only the signs (and not the magnitude) of the normal flow (the component of the optical flow perpendicular to the brightness edges—the only motion information that can be extracted by local computations from a sequence of images), and (3) the reduction in the dimensions and complexity of the problem through pattern-matching.

This year, we expanded on last year's theoretical results and studied issues affecting the real-time/real-world data implementation of the method. We examined and compared various models of log-polar receptive fields (circular overlapping fields with uniform averaging, circular overlapping fields with center-weighted averaging, and wedge-shaped receptive fields). Wedge-shaped receptive fields were chosen for implementation.

We also developed further constraints on the parameters of the log-polar transform in order to preserve conformity for the transformation. Real-world data were then obtained and used for testing and evaluating the algorithm. We were able to localize and identify egomotion parameters and determine accuracy measures.

We also noted some weaknesses in the method that still require further refinement. Although the normal flow can be computed more easily than the optical flow, it still inherits some of the errors associated with computing optical flow. Using only the sign and not the magnitude of the normal flow helps to eliminate the errors for larger flow vectors, but it remains a problem for vectors of near-zero magnitude. The problem can be circumvented by using only larger flow vectors, but this tends to reduce the flow image to a sparse set and is difficult to use in pattern-matching. A satisfactory algorithm has not been found to automatically pick the appropriate flow-magnitude thresholds for various real-world conditions. The sparse data sets obtained due to real-world noise also prevent the method from being used recursively to characterize the motion of the independent objects.

There is an additional problem balancing the accuracy obtained and the processing speed. One way to decrease processing time is to reduce the resolution of the patterns. However, this also reduces the accuracy of the results. Accuracy can be increased by using a multiresolution (pyramid) approach at the expense of processing speed. With our existing hardware, we have not found a solution that offered both the necessary accuracy and the real-time speed.

Principal Investigator:
Hoa G. Nguyen

0601152N
ZU34

Broadband-Fiber-Source Power and Spectrum Dependence on Reflectance and Filter Properties

Objective(s): Establish a testbed for rare-earth doped optical-fiber broadband sources and investigate methods of improving the operating performance through the inclusion of novel fiber-optic components.

Accomplishment(s): We demonstrated improved broadband-source operation over a wide temperature range by using filters based on fused-fiber, polarization-independent narrow-channel (PINC) wavelength division multiplexers (WDMs).

The aim of this project was to develop a testbed for rare-earth doped optical-fiber broadband sources, which are becoming the preferred optical source for use in all-optical interferometric fiber-optic gyroscopes (IFOGs) now under development, and to investigate various methods for improving their performance. IFOGs, because of their high sensitivity, robustness, and potential low cost, are one of the leading candidates for the next generation of tactical- and navigation-grade gyroscopes being considered for various platforms throughout the services. One of the key components for these devices is the optical source. Some of the characteristics of an ideal IFOG source would be high power, a wide optical spectrum, wavelength stability, low cost, and small size. Recently developed rare-earth doped optical-fiber amplified-spontaneous-emission (ASE) sources have emerged as the most promising technology capable of meeting all of the IFOG source requirements. The basic components of a fiber ASE source are a length of rare-earth doped optical fiber and a high-power optical pump to excite the fiber. Recent trends have been to use an Erbium-doped fiber, which has a broadband emission in the 1550-nm-wavelength region and can be pumped by commercially available semiconductor lasers at either 980 or 1480 nm.

One area of concern that has emerged with the use of ASE sources in IFOGs is that of the output wavelength stability, particularly over temperature. The scale factor of an IFOG (used to calibrate the output) is directly related to the power-weighted average wavelength of the optical source, given by

$$\int \frac{\lambda P(\lambda)}{P}$$

where $P(\lambda)$ is the power at a given wavelength λ , and P is the total output power. The output spectrum of a rare-earth doped fiber source can vary with pump power and with temperature. With Erbium-doped ASE sources, one of the main causes for this is gain competition between two output peaks located at 1530 and 1560 nm. One of the major thrusts of this project was to demonstrate a simple, potentially low-cost optical filter based upon fused-fiber-coupler technology that could be used to filter out one of the gain peaks and thus result in a more stable source.

To investigate the effect of the fused-fiber filters on ASE source performance, we constructed the testbed shown in figure 1. An ASE source can have one of four basic configurations, which is determined by whether it is forward-pumped (pump light and output signal travel in the same direction) or backward-pumped (pump and output travel in opposite directions), and whether the output is single-pass (no reflections) or double-pass (the output power is reflected on one side). The testbed shown in figure 1 allowed all of these configurations to be tested, with fused-fiber filters inserted just before the mirror and/or just in front of the optical isolator, depending on the configuration under study (the

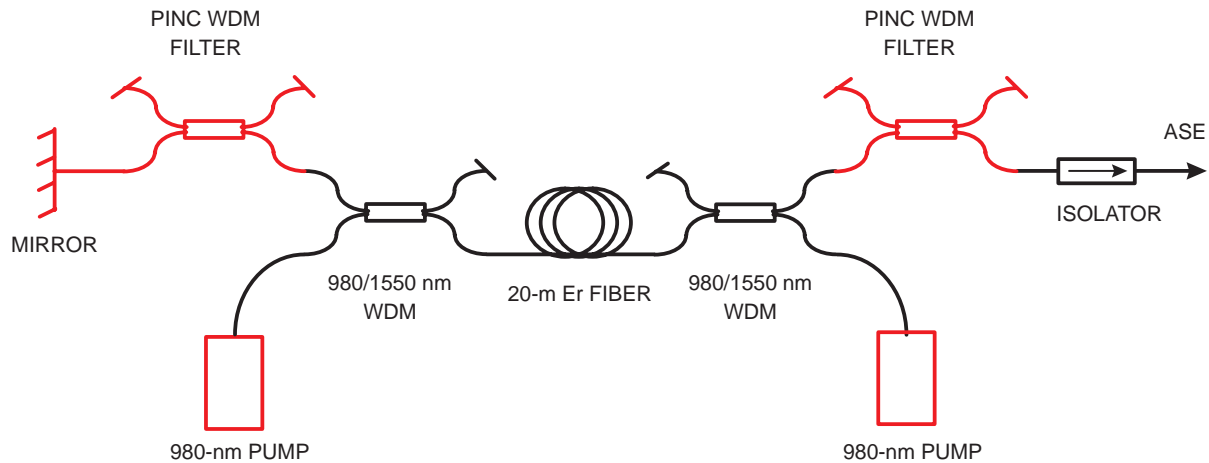


Figure 1. ASE source testbed configuration.

red components in figure 1 indicate items that vary with configuration). The special filters used in the project were developed at SSC San Diego. The filters are a version of our PINC WDM designed to operate at 1530 and 1560 nm. In the experiments conducted, the 1560 port was used to pass the desired wavelength, while the 1530 port was used to filter out light at the unwanted secondary gain peak. These devices were chosen because of their low loss, very low temperature sensitivity, small size, and potential low cost. The polarization-independent operation of these devices is also important in that it allows efficient filtering of the unwanted wavelength from the unpolarized ASE source output.

ASE sources were built and evaluated using all four basic configurations, both with and without the PINC WDM filters inserted. In addition, temperature testing was conducted on the filtered and unfiltered sources. The presence of the filters was found to have very little effect on the output powers obtainable from the ASE source, and only a slight narrowing of the output spectrum was observed. However, there was a noticeable improvement in output spectrum stability with respect to both the pump power and the temperature. Figure 2 is an example of the improved temperature stability of an ASE source, in this case, a double-pass, forward-pumped design with the filter placed next to the reflecting mirror. These experiments have shown that the fused-fiber PINC WDM filters have the potential to reduce the temperature dependence of the average wavelength to the approximately few ppm/ $^{\circ}$ C level necessary for use in high-end, navigation-grade IFOG devices.

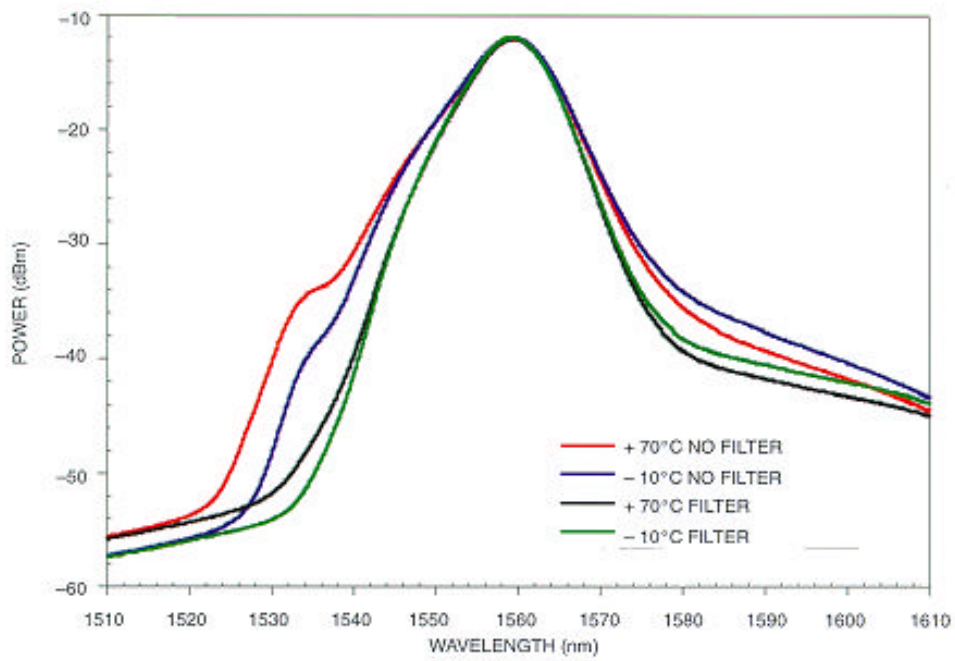


Figure 2. Forward-pumped, double-pass source spectrum temperature dependence with and without filter.

Principal Investigator:
Richard Orazi

0601152N
ZU49

Propwash/Wake Resuspension in San Diego Bay—The Grand Plan

Objective(s): Reliably estimate the resuspension of bottom sediment due to the motion of vessels through San Diego Bay.

Accomplishment(s): We built a flume in which to determine the critical shear stress necessary for resuspension.

The problem of estimating sediment resuspension was divided into four parts:

1. Reliably estimate ship-induced flow field. Due to the complexity of this problem, the ship/propeller flow field has been historically modeled as a simple momentum jet. We proposed to also use the Navy's most sophisticated, ship-wake numerical simulations. Over the last year, Dr. Mark Hyman, Naval Coastal Systems Center (NCSC), has been modifying these codes to include a shallow bottom and to run them for an aircraft carrier and a frigate.
2. Reliably estimate the response of the bottom sediment to the ship-induced flow field. Dr. Scott Jenkins and colleagues, Scripps Institution of Oceanography (SIO), have developed a numerical simulation to predict the transport of cohesive fine sediments, given the hydrodynamic forcing and critical shear stress. Output of the model includes particle size and number distributions at each depth increment throughout the water column, bottom erosion, and deposition patterns, and rates of change of these features. Over the last year, Dr. Jenkins has modified his code to accommodate the output of Dr. Hyman's, which estimates the velocity field throughout the water column and the shear stress at the bottom.
3. Determine the critical shear stress of the bottom sediment necessary to initiate resuspension. For cohesive sediments such as are thought to be in San Diego Harbor, there is presently no way of predicting critical bed shear stress as a function of flow conditions. Consequently, we have built an experimental flume (figure 1) to directly measure the onset of erosive shear stresses as a function of sediment depth. To obtain undisturbed samples of sediment, we have designed and built a sampling tube that can be used in a standard core sampler or directly attached to the flume.
4. Perform field tests to validate model. Using the research vessel (RV) ECOS and associated capabilities (e.g., Acoustic Doppler Current Profiler [ADCP]; conductivity, temperature, and depth [CTD]; transmissometers; and Global Positioning System [GPS]), we completed several preliminary studies showing that we can identify and track the resuspended sediment "footprint" of an aircraft carrier after it passed through the shipping channel to San Diego Harbor.

Knowing the hydrodynamic forcing of the carrier (via Dr. Hyman's model) and the critical shear required for sediment resuspension (experimentally determined in the flume), Dr. Jenkins' sediment transport model can be run and compared with field measurements.

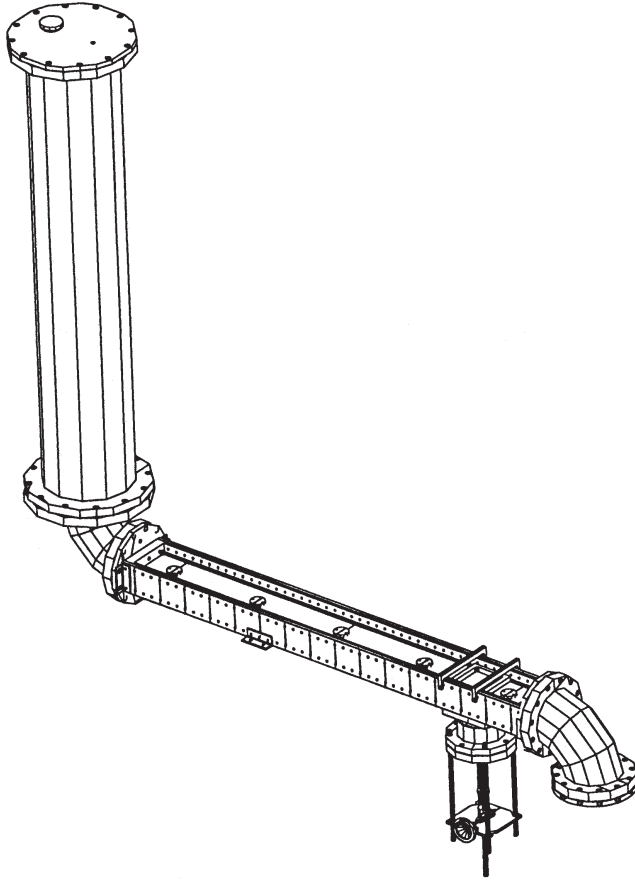


Figure 1. Experimental flume to be used in determining the critical shear stress necessary for resuspension.

Principal Investigator:
Dr. Jim Rohr

0601152N
ZU48

Surface-Plasmon, Flat-Panel Display

Objective(s): Develop components and understand processing techniques required for a novel flat-panel display that uses the surface-plasmon effect for color generation and light modulation.

Accomplishment(s): Demonstrated color-selective absorption by surface plasmons and generated primary colors (cyan, yellow, and magenta) projected from a surface-plasmon tunable filter. Modeled a broadband light modulator and designed and fabricated electrode arrays for gray-scale generation by surface plasmons.

The Navy has an increasing demand for all types of display systems. In particular, command and control requires large-screen, high-density tactical displays. Commercial systems are not yet available that can meet both the cost/performance and size/weight requirements. Established technologies, such as projection cathode ray tubes (CRTs) and active-matrix liquid-crystal devices (AMLCDs), are attempting to fill this void by incremental improvements. In addition, there are several emerging technologies such as plasma discharge, field emission, and the digital mirror device (DMD). However, these display technologies do not meet resolution and brightness requirements for proposed advanced displays (e.g., electronic workstations or [EWS]). This IR project, a collaborative effort with the Jet Propulsion Laboratory (JPL), proposed a new display technology that uses voltage-induced, color-selective absorption by surface plasmons at a metal/liquid-crystal interface. This approach has several potential advantages: increased brightness, improved color purity, higher pixel density, lower cost, and higher reliability.

The first-year effort focused on fabricating an active color filter (using surface plasmons) that was electrically tuned to produce the primary colors (cyan, yellow, and magenta) as shown in figure 1.

Test structures were designed for the surface-plasmon display by using a multilayer mask set with electrodes and integrated spacer structures. Test wafers were fabricated (SSC San Diego Lot #1844 and #1963), and the wafers were sent to JPL for assembly of the prism, top electrode, and liquid-crystal structures. Optical coupling of the broadband light source to the surface-plasmon elements was modeled, and SF-57 Schott glass (refractive index of 1.85) was selected for display/filter assembly. Custom-fabricated SF-57 dove prisms were purchased and received in early October 1997 and are being used to assemble test displays.

Alternate electrode and electro-optic materials also were modeled and investigated. Preliminary tests were completed on the fabrication of semitransparent titanium silicide layers (SSC San Diego Lot# 1953). Initial data showed that obtaining semitransparent silicide films was possible but at a trade-off of low conductivity. Modeling of multilayered top electrodes demonstrated a rhodium/aluminum (Rh/Al) structure that produced the best broadband response in combination with nematic liquid crystals to achieve gray-scale modulation. Two types of solid-state, electro-optic materials were obtained under a nondisclosure agreement with Symetrix Corporation. The optical properties of the proprietary materials, called "Y1" and "YZ," were measured and are under further evaluation as an alternative to nematic liquid crystals.



Figure 1a. Surface-plasmon tunable filter (cyan at 0 V).



Figure 1b. Surface-plasmon tunable filter (magenta at 10 V).



Figure 1c. Surface-plasmon tunable filter (yellow at 30 V).

Principal Investigator:
Dr. Stephen D. Russell

0601152N
ZU47

Associate Investigators:
Dr. Randy Shimabukuro

Dr. Y. Wang
JPL

Biosonar Ensonification of Buried Mines

Objective(s): Record the pattern and spectral composition of biosonar pulses that impinge on buried mines during routine detection and identification by the bottle-nose dolphin (*Tursiops truncatus*).

Accomplishment(s): An underwater instrument package that records the waveforms and rates of biosonar pulses impinging on a mine simulator is in final development and testing. An acoustic data-link that communicates from a buried position to the surface was successfully tested. A surface computer to command the simulator package and receive data from it was developed.

The Navy and Marine Corps have an immediate need to improve mine countermeasures in shallow water/very shallow water (SW/VSW). The reliable detection of buried mines is the most difficult element of that task. The trained dolphin readily solves the buried-mine problem, and future sonar designs could benefit from a more complete understanding of the dolphin's methods. For example, knowing how the animal controls its position and manipulates its biosonar during buried-mine detection, and specifically, knowing the net physical effects of those actions on the energy that actually impinges on the buried mine would provide alternative approaches to test in new sonar designs.

A dolphin that repeatedly detects objects in the water column in fixed positions produces relatively invariant pulse spectra, and that invariance persists even when sediment is suspended between the animal and the objects. However, new findings suggest that the animal's biosonar output is more varied in realistic conditions. A moving animal that searched a large field for objects in the water column in unpredictable locations directed a highly variable number of pulses at objects during identification. Other animals, when searching an open-ocean field for objects on the bottom, showed variability in both the number of pulses-on-object and their pulse spectra. Such variability during detection and identification of buried objects may allow the animal to control bottom penetration or back-scatter while identifying different features of the object.

Measuring the acoustic energy that impinges on a buried mine is done with a self-contained instrument pack that replaces the detonator canister of a realistic Manta mine-simulator. The instrumented simulator will be buried with others in an open-ocean field where trained mine-hunting dolphins will be used to detect and identify them.

The battery-powered instrument pack has a broadband transducer for measuring the biosonar pulse-waveforms and a second transducer for communicating with the surface over an acoustic data-link. The data-acquisition components digitize the waveform of each impinging pulse at 0.9 MHz and store the result along with the interpulse intervals (+/- 0.5 ms). Typically, the dolphin emits a pulse shortly after the receipt of the previous pulse's echo, and thus, the animal's distance from an ensonified object has a high negative correlation with the pulse rate. To conserve power, an onboard clock wakes the unit only at times when animals will be deployed. A surface computer with a compatible underwater modem has been developed to command the underwater package, and after each detection, upload the data from the instrument pack for storage and analysis.

Tests of the data-link were conducted, and final testing of the components is in process. Data collection and its comparison with existing artificial systems are scheduled for FY 98.

Principle Investigator:
Dr. John E. Sigurdson

0601152N
ZU50

Computational Modeling of Sediment Resuspension

Objective(s): Develop and test, computationally, models of sediment resuspension based upon the local shear stress and flow properties at the fluid–sediment interface computed using conditions throughout the entire domain of interest.

Accomplishment(s): Preliminary computations indicate that the current formulation provides both a simple and fast computing platform for developing and evaluating sediment resuspension models. The formulation also allows for easy inclusion of complex sources such as ship wakes and pipe flows.

The growing need to evaluate and control contaminant transport initiated by strong fluid discharges and ship wakes requires detailed understanding of the processes involved in the resuspension of sediments, especially in shallow-water environments. The ability to manage contaminated sediments in naval harbors such as San Diego Bay would be enhanced by an understanding and ability to predict the effects of harbor activity on sediment movement.

Traditionally, models of the boundary shear stress associated with sediments provide a means to estimate the shear stress from conditions outside the bottom boundary layer and to predict the effect it would have on the boundary. The most important variable in sediment transport is probably the boundary shear stress because it provides a link between the momentum and sediment equations. Thus, the boundary shear stress determines the ability of the flow to alter the bottom. It is also known that the influence of the steady component of the bed shear is difficult to estimate from the velocity field at a single level, and that the measurements of unsteady boundary-layer flows over movable beds contain conflicting data. Additionally, the sea-bed turbulent intensities are expected to respond rapidly to the changing flow conditions; thus, the bottom-shear-stress value is required. Implicit in the rapid change of turbulent intensities is the time-varying eddy viscosity that prevents analytical solution of the governing equations. Therefore, it is impossible (or very difficult) to estimate the instantaneous effective bed shear stresses for these flows. The important question is how do we determine the instantaneous effective bed shear stresses under flows of arbitrary form (i.e., discharges, ship wakes). This is a hard question because we know little about the instantaneous stresses on beds; however, total stresses under sine waves have been measured, and there is discussion that the effective stresses may be smaller than the total, even on flat beds. The underlying fact is that sediment transport is a nonlinear problem in two-phase flow which exhibits considerable negative feedback between the sediment and the flow.

Our objective (to develop and test models of sediment resuspension based on the use of fluid flow properties computed throughout the domain of interest) is in contrast with the use of depth-averaged equations or the use of boundary shear estimates based on conditions outside the fluid–sediment interface region. Determining the boundary shear stress required to initiate sediment motion is paramount to our investigation.

To provide a platform for developing sediment resuspension models where the flow field and sediment distributions are computed in a rectangular domain, we computed the two-dimensional, time-dependent, incompressible Navier–Stokes equations by using an explicit second-order, upwind finite-difference representation of the Navier–Stokes equations in vorticity-stream function form. We supplemented the flow-field solution with the Baldwin–Lomax turbulence model and with equations

for the scalar transport of sediment. A second-order, upwind finite-difference formulation was also used to solve the sediment transport equations. All of the computations were made using the Convex Exemplar SPP-1600 at SSC San Diego.

The initial formulation and computations assumed one type of sediment and that the sediment does not influence the velocity field solution. This assumption of small, low-density sediment particles will be removed as the model development continues. Also, the “zero” equation turbulence model will be replaced by a two-equation model.

The fluid–sediment interface at the bottom was modeled using expressions for the deposition and erosion of sediment. The amount of sediment deposited was estimated by using a settling velocity and the sediment concentration adjacent to the fluid–sediment interface. As a starting point, the erosion of sediment was determined by using a modified time-dependent pickup function determined by using local sediment and flow properties and the Shields parameter based on local and critical shear stress values. The amount of sediment transported into the flow is specified to vary exponentially with vertical distance. Inherent in the sediment model is the use of the locally determined wall shear stress and the adjustment of several parameters in the deposition and erosion formulations.

Once the amount of sediment deposition and erosion are determined, the time-dependent location of the fluid–sediment interface is computed. The new interface location is determined by the difference in deposition and erosion and the determination of which vertical cell contains the interface at each horizontal position. Thus, the location of the interface in the output contour data cannot be determined to an accuracy greater than one cell height. However, the actual height of the interface and the local shear stress at the interface are available for examination at each time increment.

Preliminary computations were made using a closed container with the flow driven by a moving (top) surface. At time zero, the bottom region contained a uniform distribution of sediment (red) while the remaining flow field contained an exponential decay of sediment in the vertical direction (yellow for lower sediment concentrations). The four displays in figure 1 represent the time history of the sediment transport and the modification of the bottom boundary fluid–sediment interface. The computed flow-field results show the expected flow rotation found in similar driven cavity flows. The resulting boundary-layer profiles also show a direct correlation between the wall shear stress (rate of change of velocity in the vertical direction) and the change in elevation and motion of the fluid–sediment interface. For nondimensional times less than $t = 7.5$, the results show the bottom erosion and the distribution of sediment in the domain. At $t = 15$, one observes the concentration of bottom sediment (red) along the left wall which, with increasing time and stabilization of the flow, begins to settle along the bottom.

The preliminary computations indicate that this formulation provides a simple and fast computing platform for developing and evaluating sediment resuspension models. Additionally, the model would allow more detailed analysis of wake effects from ships and inflows from discharge pipes, thus providing additional information for sediment-management programs.

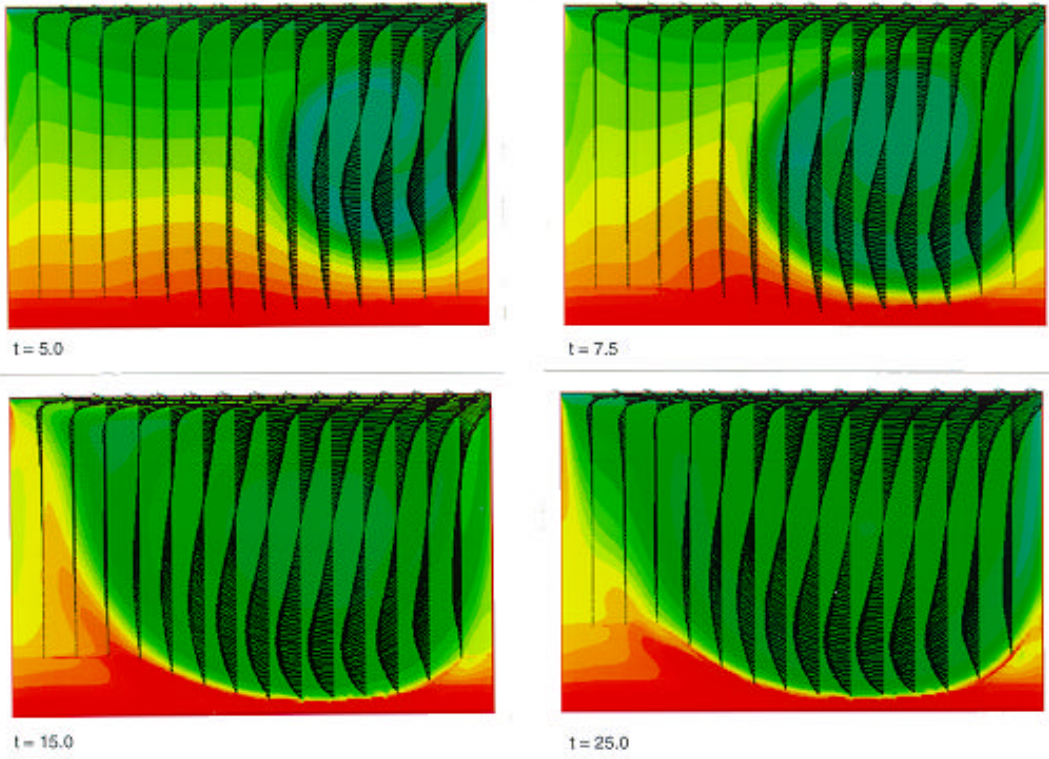


Figure 1. Time history of the sediment transport and the modification of the bottom boundary fluid–sediment interface.

Principal Investigator:
Dr. Tom Mautner

0601152N
ZU52

**PUBLICATIONS
AND PRESENTATIONS**

REFEREED JOURNALS, BOOKS/CHAPTERS, AND DISSERTATIONS (PUBLISHED/ACCEPTED)

Refereed Journals

- Barnett, J. T. and B. Kedem. 1998. "Zero Crossing Rates of Mixtures and Products of Gaussian Processes," *IEEE Transactions on Information Theory*, to appear in May.
- Bulsara, A. and A. Zador. 1996. "Threshold Detection of Wideband Signals: A Noise-Induced Maximum in the Mutual Information," *Physical Review E*, vol. 54, no. 3, pp. R2185–2188.
- Bulsara, A. R., T. C. Elston, C. R. Doering, S. B. Lowen, and K. Lindenberg. 1996. "Cooperative Behavior in Periodically Driven Noisy Integrate-Fire Models of Neuronal Dynamics," *Physical Review E*, vol. 53, pp. 3958–3969.
- Bulsara, A. R., S. B. Lowen, and C. D. Rees. 1994. "Cooperative Behavior in the Periodically Modulated Wiener Process: Noise-Induced Complexity in a Model Neuron," *Physical Review E*, vol. 49, pp. 4989–5000.
- Edelblute, D. J. 1996. "Non Circularity," *IEEE Signal Processing Letters*, vol. 3, no. 5.
- Goodman, I. R. 1998. "New Homomorphic-Like Random Set Representations for Fuzzy Logic Models Using Exponentiation with Applications to Data Fusion," *Information Sciences*, to appear.
- Hanson, F. 1995. "Improved Performance at 946 and 473 nm from a Composite Nd:Y3Al5O12 Laser Rod," *Applied Physics Letters*, vol. 66, p. 3549.
- Inchiosa, M. and A. R. Bulsara. 1995. "Coupling Enhances Stochastic Resonance in Nonlinear Dynamic Elements Driven by a Sinusoid Plus Noise," *Physics Letters A*, vol. 200, pp. 283–288.
- Inchiosa, M. E. and A. R. Bulsara. 1998. "DC Signal Detection via Dynamical Asymmetry in a Nonlinear Device," *Physical Review E*, in press.
- Inchiosa, M., A. Bulsara, A. Hibbs, B. Whitecotton. 1998. "Signal Enhancement in a Nonlinear Transfer Characteristic," *Physical Review Letters*, vol. 80, 16 February, pp. 1381ff.
- Johnson, R. A., P. R. de la Houssaye, M. E. Wood, G. A. Garcia, C. E. Chang, P. M. Asbeck, and I. Lagnado. 1997. "A Silicon-on-Sapphire MOSFET Transmit/Receive Switch for L and S Band Transceiver Applications," *IEEE Electronics Letters*, vol. 33, no. 15, pp. 1324–1326.
- Kevorkian, A. K., D. Barach, and G. W. Benthien. 1998. "Bistatic Target Strength Prediction from Limited Data," to appear in *High-Performance Computing Modernization Program (HPCMP) DoD Mission Success Stories*.
- Marchesoni, F., L. Gammaitoni, and A. R. Bulsara. 1996. "Spatiotemporal Stochastic Resonance in a ϕ^4 Model of Kink–Antikink Nucleation," *Physical Review Letters*, vol. 76, no. 15, pp. 2609–2612.
- Reuter, M. 1997. "Numerically Efficient Fourier-Based Technique for Calculating Error Probabilities with Intersymbol Interference," *IEEE Transactions on Communications*, vol. 45, no. 6, pp. 629–632.
- Rohr, J., J. Allen, J. Losee, and M. I. Latz. 1997. "The Use of Bioluminescence as a Flow Diagnostic," *Physics Letters A*, vol. 228, pp. 408–416.

Rohr, J., M. I. Latz, S. Fallon, J. C. Nauen, and E. Hendricks. 1998. "Dolphin-Stimulated Bioluminescence," *Journal of Experimental Biology*, vol. 201, May, pp. 1447–1460.

Schwartz, D. F. 1997. " H^∞ Approximation with Point Constraints Applied to Impedance Estimation," *Circuits, Systems, and Signal Processing*, vol. 16, no. 5, pp. 507–522.

Books/Chapters

Goodman, I. R. and G. F. Kramer. 1997. "Extension of Relational and Conditional Event Algebra to Random Sets with Applications to Data Fusion," in book *Random Sets: Theory & Applications* (IMA volume in Mathematica & Its Applications #97), J. Goussias, R. P. Mahler, and H. T. Nguyen, eds., Springer-Verlag, Berlin, pp. 209–242.

Goodman, I. R., R. P. Mahler, and H. T. Nguyen. 1997. *Mathematics of Data Fusion*, Kluwer Academic Publishers, Dordrecht, The Netherlands.

REFEREED JOURNALS, BOOKS/CHAPTERS, AND DISSERTATIONS (SUBMITTED)

Refereed Journals

Bamber, D. E. "Entailment with Near Surety of Scaled Assertions of High Conditional Probability," submitted to the *Journal of Philosophical Logic*.

Barnett, J. T. "Asymptotic Normality of Level-Crossings for the Envelope of a Gaussian Process with Application to Radar Detection," submitted to the *Journal of Fourier Analysis and Applications*.

Edelblute, D. J. "Complex Cumulants and Spectral Analysis," submitted to the *Journal of the Acoustical Society of America*.

Freund, R. F., M. Gherrity, S. Ambrosius, M. Campbell, M. Halderman, D. Hensgen, E. Keith, T. Kidd, M. Kussow, J. Lima, F. Mirabile, L. Moore, B. Rust, and H. J. Siegel. "Scheduling Resources in Multi-User, Heterogeneous, Computer Environments," submitted to the *Journal of Parallel and Distributed Computing*.

Inchiosa, M. and A. Bulsara. "Nonlinear SQUID Signal Detection," submitted to *Physical Review E*.

Lorincz, K., Z. Gingl, L. Kiss, and A. Bulsara. "Higher Order Stochastic Resonance in a Level Crossing Detector," submitted to *Physical Review E*.

Reuter, M. and J. Zeidler. "Nonlinear Effects in LMS-Implemented Adaptive Equalizers," submitted to *IEEE Transactions on Signal Processing*.

Stein, D. W. J. "Computing K-Clutter-Plus-Gauss Distributions," submitted to *Society on Industrial and Applied Mathematics (SIAM) Journal on Applied Mathematics*.

Stein, D. W. J. "Robust Implementations of an Exponential Mixture Detector with Applications to Radar," submitted to *IEE Proceedings on Radar, Sonar, and Navigation*.

Vu, T. T., R. J. Orazi, and M. N. McLandrich. "Four-Channel Fused-Fiber Mux/Demux Couplers and Add/Drop Filters in the 1300- and 1550-nm Regions," submitted to *Electronics Letters*.

SSC SAN DIEGO (FORMERLY NRaD) PUBLICATIONS

DeJaco, J. F. and W. F. Rask. 1997. "Impulsive Snap-through Acoustic Projector (ISnAP) FY 96 Demonstration Prototype, Final Report," TD 2941 (March). Naval Command, Control and Ocean Surveillance Center, RDT&E Division, San Diego, CA.

Wilcox, D. R. 1997. "Network Memory Protocol," TR 1757 (Sep). Naval Command, Control and Ocean Surveillance Center, RDT&E Division, San Diego, CA.

PRESENTATIONS TO PROFESSIONAL MEETINGS

- Baxley, P. 1997. "Matched-Field Processing in a Wedgelike Ocean," 133rd Meeting of the Acoustical Society of America, 16 to 20 June, Penn State, State College, PA, *Journal of the Acoustical Society of America*, vol. 101, no. 5, pt. 2, p. 3047.
- Baxley, P. 1998. "Experimental Investigation of Matched-Field Processing in a Wedgelike Shallow-Water Environment," accepted for presentation at the 135th Meeting of the Acoustical Society of America/16th International Congress on Acoustics, 20 to 26 June, Seattle, WA.
- Bucker, H. 1997. "Active Matched-Field Tracking," Conference on Environmentally Adaptive Sonar Technology (EAST), 27 to 31 January, Applied Physics Laboratory (APL), University of Washington, Seattle, WA.
- Bulsara, A. R. 1996. "Stochastic Resonance: Tuning in to Noise," University of Ottawa, 11 October, Ottawa, Canada.
- Bulsara, A. R. 1997. "Stochastic Resonance," (invited presentation), International Conference on Dynamical Systems, 14 January, Bangalore, India.
- Bulsara, A. R. 1997. "Stochastic Resonance," Tata Institute of Fundamental Research, 20 January, Bombay, India.
- Bulsara, A. R. 1997. "Stochastic Resonance: Tuning in to Noise," Boston University, 27 March, Boston, MA.
- Bulsara, A. R. 1997. "Stochastic Resonance and Signal Processing," Office of Naval Research, 8 August, London, England.
- Bulsara, A. R. 1997. "Stochastic Resonance, Parts I, II, and III," (three invited presentations), International Summer School on Randomness and Nonlinearity, Uppsala University, 21 August, Uppsala, Sweden.
- Bulsara, A. R. 1997. "Signal Enhancement in SQUIDs," University of Perugia, 29 August, Perugia, Italy.
- Bulsara, A. R. 1997. "Stochastic Resonance: Signal Processing with Noise," Istituto Nazionale di Ottica, 16 September, Florence, Italy.
- Bulsara, A. R. 1997. "Signal Enhancement Using Stochastic Resonance," University of Marburg, 22 September, Federal Republic of Germany.
- Bulsara, A. R. 1997. "Signal Enhancement in SQUIDs Using Stochastic Resonance," University of Augsburg, 26 September, Federal Republic of Germany.
- Bulsara, A. R. 1997. "Stochastic Resonance and Its Applications," (invited presentation), International Meeting on Neural Coding, 30 September, Versailles, France.
- Bulsara, A. R. 1997. "Stochastic Resonance: Taking Advantage of Noise in Nonlinear Dynamics," Yale University, 20 October, New Haven, CT.

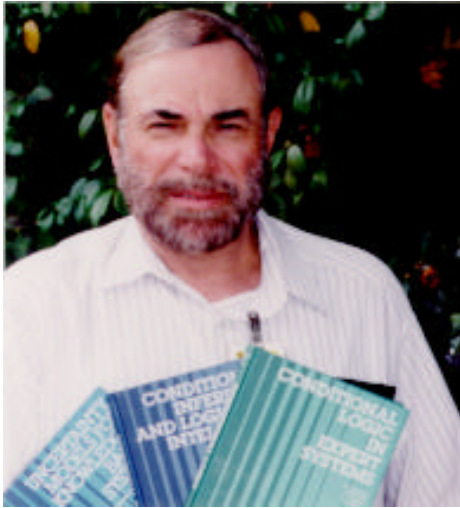
- Bulsara, A. R., M. E. Inchiosa, J. F. Lindner, B. K. Meadows, and W. L. Ditto. 1995. "Noise-Induced Synchronized Switching in Coupled Bistable Systems," *Proceedings of the Second New Zealand International Two-Stream Conference on Artificial Neural Networks and Expert Systems*, (November), Dunedin, New Zealand.
- DeJaco, J. F. 1996. "Impulsive Snap-through Acoustic Projector," invited presentation at the Third Joint Meeting of the Acoustical Society of America (ASA) and the Acoustical Society of Japan (ASJ), 2 to 6 December, Honolulu, HI.
- Freund, R. F., M. Gherrity, S. Ambrosius, M. Campbell, M. Halderman, D. Hensgen, E. Keith, T. Kidd, M. Kussow, J. Lima, F. Mirabile, L. Moore, B. Rust, and H. J. Siegel. 1998. "Scheduling Resources in Multi-User, Heterogeneous, Computer Environments," invited paper, 1998 Heterogeneous Computing Workshop, 30 March, Orlando, FL.
- Goodman, I. R. 1997. "Homomorphic-Like Random Set Representations for Fuzzy Logic Models Using Exponentiation with Applications to Data Fusion," *Proceedings of the Third Joint Conference on Information Sciences*, 1 to 5 March, Research Triangle Park, NC, pp. 271–274.
- Goodman, I. R. 1997. "Two New Results in Product Space (PS) Conditional Event Algebra: A Characterization Relating All Three Major CEAs through Deduction and a New Family That Extends PS and Includes Locally Dependent Densities for the Limiting Case of Point-Nested Antecedents," presented at the Department of Electrical and Computer Engineering, 15 April, University of Massachusetts at Amherst, MA.
- Goodman, I. R. (prepared also by G. F. Kramer). 1997. "Combination of Evidence and Deduction Corresponding to Collections of Events Which Are Not Initially Probability Represented," invited presentation at the 35th Annual Bayesian Research Conference, 19 to 22 February, University of Southern California (USC), Los Angeles, CA.
- Goodman, I. R. and G. F. Kramer. 1997. "Decision-Making Relative to Functionally Expressed Information in Terms of Probabilities or Possibilities," *Proceedings of the 1997 Infrared Information Symposium (IRIS) on Sensor and Data Fusion*, MIT Lincoln Laboratory, 14 to 17 April, Lexington, MA, vol. 1, pp. 89–108.
- Goodman, I. R. and G. F. Kramer. 1997. "Comparison of Incompletely Specified Models in C4I and Data Fusion Using Relational and Conditional Event Algebra," *Proceedings of the Third International Command and Control Research and Technology Symposium*, National Defense University, 17 to 20 June, Washington, DC, pp. 193–215.
- Hammel, S. M., J. T. Barnett, and N. Platt. 1997. "Diagnosing Intermittency," *American Institute of Physics (AIP) Conference Proceedings*, vol. 411, pp. 51–56.
- Hanson, F. and P. Poirier. 1998. "Long-Pulse and Q-Switched Operation of Diode-Pumped Nd:YAG at 946 nm," *Advanced Solid-State Lasers*, Technical Digest, Topical Meeting of the Optical Society of America, February, Washington, DC.
- Hicks, C. 1997. "Exact Diagonalization of Many Body Hamiltonians," workshop at Los Alamos National Laboratory, July, Los Alamos, NM.
- Inchiosa, M. E. 1997. "Stochastic Resonances in Asymmetric Nonlinear Systems," American Physical Society Annual Meeting, 21 March, Kansas City, MO.

- Inchiosa, M. E. 1997. "Signal Enhancement in SQUIDS Operated in the Non-Hysteretic Regime," International Conference on Applied Nonlinear Dynamics near the Millennium, University of California at San Diego (UCSD), 9 July, La Jolla, CA.
- Inchiosa, M. E. 1997. "Stochastic Resonance in Arrays, Signal Processing, and High Performance Computing, Parts I and II," (two invited talks), International Summer School on Randomness and Nonlinearity, Uppsala University, 20 August, Uppsala, Sweden.
- Inchiosa, M. E. 1997. "Parallel Simulation of Coupled Nonlinear Sensors," Computational Electronics and Nanoelectronics Workshop, National Center for Supercomputer Applications, Beckman Institute, University of Illinois, 21 October, Urbana, IL.
- Inchiosa, M. E. 1997. "Nonlinear Response in a SQUID Magnetometer: Above and Beyond Stochastic Resonance," Georgia Institute of Technology, 24 October, Atlanta, GA.
- Kevorkian, A. K., D. Barach, and G. W. Benthien. 1997. "Sparse Complete Orthogonal Factorization as Applied to Bistatic Target Strength Prediction," *Proceedings of the DoD HPCMP High-Performance Computing Users Group Meeting*, June, San Diego, CA.
- Kevorkian, A. K. 1997. "Sparse Complete Orthogonal Factorization as Applied to Bistatic Target Strength Prediction," invited lecture, Mathematics and Scientific Computing Seminar, Naval Postgraduate School, 9 July, Monterey, CA.
- Latz, M. I., J. Nauen, and J. Rohr. 1996. "Interspecific Variation in the Sensitivity of Dinoflagellates to Hydrodynamic Stimulation of Bioluminescence," *Transactions of the American Geophysical Union, Eos 76, Ocean Sciences (OS)81*.
- Latz, M. I., A. Juhl, S. E. Elghobashi, A. M. Ahmed, and J. Rohr. 1997. "Response of Dinoflagellates in Well-Characterized Laminar and Turbulent Flows: Differentiating the Effect of Shear and Acceleration," Meeting of the American Association of Limnology and Oceanography, Santa Fe, NM.
- Nauen, J. C., G. A. Rebstock, M. I. Latz, and J. Rohr. 1996. "Is the Bioluminescence of Dinoflagellates Stimulated by Fluid Shear Stress or Shear Rate?" *Eos 76, OS81*.
- Reuter, M. and J. Zeidler. 1997. "Non-Wiener Effects in LMS-Implemented Adaptive Equalizers," *Proceedings of the 1997 International Conference on Acoustics, Speech, and Signal Processing (ICASSP-97)*, 21 to 24 April, Munich, Germany, pp. 2509–2512.
- Rohr, J., S. Fallon, and M. I. Latz. 1996. "When Do Dolphins Stimulate Plankton Bioluminescence?" *Eos 76, OS81*.
- Scheps, R. 1997. "Laser Diode-Pumped Dye Laser," Photonics West, Society of Photo-Optical Instrumentation Engineers (SPIE), 8 to 14 February, San Jose, CA.
- Stein, D. W. J. 1997. "Detection of Small Targets in Clutter Modeled as a Gaussian Mixture or Hidden Markov Process," *Proceedings of the SPIE Signal and Data Processing of Small Targets*, 29 to 31 July, San Diego, CA.
- Stein, D. W. J. 1997. "Computing K-Clutter-plus-Gauss-Distributions," *Radar 97*, IEE Conference Publication 449, 14 to 16 October, Edinburgh, Scotland, pp. 194–198.

- Stein, D. W. J. and G. M. Dillard. 1997. "Applying Hidden Markov Models to Radar Detection in Clutter," *Radar 97*, IEE Conference Publication 449, 14 to 16 October, Edinburgh, Scotland, pp. 586–590.
- Wahlen, B. E. and J. Jimenez. 1997. "Performance Comparison of Hermitian and Reed–Solomon Codes," IEEE Military Communications Conference (MILCOM 97), 2 to 5 November, Monterey, CA.
- Wallace, J. and R. A. Whitehurst. 1997. "Using IMPORT to Implement Complex Behaviors in Simulations," *Proceedings of the 1997 Object-Oriented Simulation Conference*, Society for Computer Simulation (SCS) International's Western Multiconference for Simulations, 12 to 15 January, Phoenix, AZ.
- Wallace, J. W., G. E. Leonard, L. J. Peterson, A. Vagus, and C. L. Kropp. 1998. "Using IMPORT to Develop Wargames," *Proceedings of the 1998 Object-Oriented Simulation Conference*, SCS International's Western Multiconference for Simulations, 11 to 14 January, San Diego, CA.
- Wang, Y., S. D. Russell, and R. L. Shimabukuro. 1997. "Surface Plasmon Tunable Filter and Spectrometer-on-a-Chip," *Proceedings of SPIE*, Imaging Spectrometry III Session, International Symposium on Optical Science, Engineering, and Instrumentation, 27 July to 1 August, San Diego, CA, vol. 3118, pp. 288–294.
- Yu, P. K. L., R. B. Welstand, G. L. Li, W. X. Chen, J. T. Zhu, S. A. Pappert, C. K. Sun, R. Nguyen, and Y. Z. Liu. 1998. "Recent Progress on the Enhancement of SFDR in Electroabsorption Modulators and the Dual-Use Modulator/Detector," Eighth Annual DARPA Symposium on Photonic Systems for Antenna Applications, 13 January, Naval Postgraduate School, Monterey, CA.

**HONORS
AND AWARDS**

HONORS AND AWARDS



Dr. I.R. Goodman published his latest book, *Mathematics of Data Fusion*, (Kluwer Academic Publishers, 1997), together with coauthors Dr. R. P. Mahler (Lookheed Martin) and Professor H. T. Nguyen (New Mexico State University). This book clarifies the way data-fusion problems are treated by providing a general and rigorous conceptual framework. Dr. Goodman and his colleagues have extended their previous work on the links between probability theory and the modeling of natural language information through Zadeh's fuzzy logic. These links use random sets, generalizing the ordinary idea of point or vector-valued random variables, and integrate with conditional and relational event algebra. The new book also features several other applications of random set techniques to data-fusion problems.

The theory of fuzzy sets and conditional logic has found numerous commercial applications in monitoring and automating management of electronic and mechanical systems. Small appliances, automobile engines, missile guidance systems, robotics, etc., have all benefited from these new logic extensions that can handle situations and operations that cause traditional software based on formal logic to fail. Applications of particular interest to SSC San Diego include data-fusion techniques and uncertainty management in naval command and control systems.

During FY 91, a major result from Dr. Goodman's research was a demonstration that all unconditional linguistic information (modeled initially through fuzzy sets and some choice of associated logical operators and relations) can be naturally and fully imbedded into a Boolean algebra-probability measure context. More recent research, some of which is described in this IR report, has demonstrated that probability metrics can be applied to relational event algebras in order to quantitatively test similarities and differences between different probability-functional models.

Dr. Goodman's work was supported by the Office of Naval Research through SSC San Diego's Independent Research Program. Dr. Goodman credits the general environment of the Center and specifically a number of colleagues here for helping stimulate his interest in these areas. Colleagues include Fred Kramer, who coauthored a number of papers; Dr. Phil Calabrese, one of the pioneers in conditional event algebra and a consultant to SSC San Diego; and Dr. Don Bamber, a former Independent Research principal investigator, who is developing probabilistic approaches to nonmonotonic logic.

Dr. Goodman, a mathematician, has long considered problems in the modeling of command, control, communications, and information (C³I) processes. In 1989, he received both the Technical Director's Award and the Center's highest honor, the Lauritsen-Bennett Award. Dr. Goodman has authored or coauthored approximately 100 publications in the open literature. He has also served as guest

coeditor and author for a conditional event algebra edition of *IEEE Transactions on Systems, Man, and Cybernetics*. Additionally, he has chaired a number of special meetings devoted to these subjects in the U.S. and abroad and has made and contributed presentations at over 60 internationally recognized conferences.

Dr. John T. Barnett received one of SSC San Diego's 1997 Exemplary Achievement Awards for technical leadership in the algorithms processing task on the surface Navy's infrared search and track programs. He has also served as an occasional referee for *IEEE Transactions on Information Theory*. Dr. Barnett's work on extending S. O. Rice's formula for products and mixtures of Gaussain processes and Dr. Barnett's central limit theorem for envelope crossings were presented by University of Maryland Professor Benjamin Kedem as an invited speaker at the International Summer School on Randomness and Nonlinearity, 18 to 27 August 1997, in Uppsala, Sweden.

Paul Baxley continues as President of the San Diego Chapter of the Acoustical Society of America (ASA). He is Chairman of the ASA Public Relations Committee, a Member of the ASA External Affairs Committee, and Co-Chair of the ASA Home Page Committee. He developed ASA's scientific web page as a tool for science writers, students, and members of the scientific community interested in current developments and state-of-the-art research in acoustics.

Dr. Adi Bulsara was co-winner of SSC San Diego's Publication of the Year Award for Open Literature for his combined work in two articles: "Tuning in to Noise," *Physics Today*, March 1996, and "Scaling Laws for Spatiotemporal Synchronization and Array Enhanced Stochastic Resonance," co-written with Dr. Mario Inchiosa and others, for *Physical Review E*, vol. 53, no.3. Dr. Bulsara also received an SSC San Diego Publication Award of Merit for his 1996 co-written article entitled, "Spatiotemporal Stochastic Resonance in a ϕ^4 Model of Kink-Antikink Nucleation," *Physics Review Letters*, vol. 76, no. 15, and an SSC San Diego Publication Award of Excellence for "Noise-Controlled Resonance Behavior in Nonlinear Dynamical Systems with Broken Symmetry," *Physics Review Letters*, vol. 77, no. 11, co-written with Dr. Mario Inchiosa and L. Gammaitoni. Besides making several presentations in the United States and Europe, Dr. Bulsara also organized the International Conference on Applied Nonlinear Dynamics near the Millennium (ANDM97) held at the University of California, San Diego (UCSD), 7 to 11 July 1997.

Bart Chadwick and **Dr. James Rohr** received an SSC San Diego Distinguished Publication Award for their multi-authored technical report entitled, "Environmental Analysis of U.S. Navy Shipboard Solid-Waste Discharges: Report of Findings and Appendices A-L," NRaD (now SSC San Diego) TR 1716, (Feb 1996).

Jerome DeJaco received a 1997 Exemplary Achievement Award for serving as coordinator and technical supervisor for all Office of Naval Research 6.2 transducer engineering projects at SSC San Diego.

Hoa Nguyen received SSC San Diego's Publication of the Year Award for Technical Documents for the multi-authored NRaD TD 2914 entitled, "Air-Mobile Ground Surveillance and Security System (AMGSSS) Project Summary Report," (Sep 1996).

Dr. Stephen Russell is a journal referee for *Physical Review B* and *Physical Review Letters* and was an invited participant at the Industrial Affiliates Meeting on Materials Chemistry at the University of California, San Diego, on 27 September 1997.

Dr. Richard Scheps was co-winner of SSC San Diego's Publication of the Year Award for Open Literature for his article entitled, "Upconversion Laser Processes," *Progress in Quantum Electronics*, vol. 20, no. 4. He was appointed Symposium Chair for the Society of Photo-Optical Instrumentation Engineers (SPIE) LASE '98 and was Conference Chair for the SPIE Solid-State Lasers Meetings in 1997 and 1998. In addition, he was Program Chair, Laser Source Engineering, for OE Lase '97 and is Associate Editor of *IEEE Photonics Technology Letters*.

Dr. Chen-Ko Sun received a 1997 Exemplary Achievement Award for developing advanced photonic techniques for radio-frequency signal generation, distribution, and switching. His work resulted in the success of several Office of Naval Research photonics-related projects.

Jeffrey Wallace was the Industrial General Chairman for the Society for Computer Simulation (SCS) International's 1997 Object-Oriented Simulation Conference. He has also been nominated to SCS International's Board of Directors; elections will be held this summer.

LCDR Bruce Watkins served as Navy representative to the UHF SATCOM Standard Modem Committee, conducted by the Defense Information Systems Agency (DISA) Joint Interoperability Engineering Organization (JIEO) to incorporate advanced technology for improvements in UHF SATCOM data throughput.

PATENT ACTIVITY

INDEPENDENT RESEARCH

Patents Issued

Michael R. Brininstool

**“Fiber-Optic Self-Multiplexing Amplified
Ring Transducer and Force Transfer Sensor
with Pressure Compensation”**

This invention provides a system of multiplexed-array fiber-optic sensors with force transfer transducers for detecting the presence of an environmental field condition, such as underwater acoustic pressure perturbations. The invention can be deployed in a single multiplexed-array system with incoherent light and at various depths or altitudes with a hydrostatic-pressure equalizer enabling the isolation of dynamic external perturbations from other pressure variations.

Patent 5,589,937 Navy case 75,649 (Serial 08/434,366) filed 2 May 1995; issued 31 December 1996.

**David M. Bullat
Po-Yun Tang**

**“Fiber-Optic Self-Multiplexing Amplified
Ring Transducer and Force Transfer Sensor
with Pressure Compensation”**

Note: Same title as above patent but covers different invention.

A fiber-optic sensor is also disclosed for measuring or detecting the presence of an environmental field condition, such as underwater acoustic perturbations. The sensor includes a force transfer transducer, which is enclosed within a shell, with a pressure equalizer for equalizing the interior and exterior shell pressures. An optical fiber is coiled about the transducer. An optical detector detects stress or strain in the optical fiber, resulting from external perturbations. The sensor is able to operate at various depths or altitudes. Pressure equalization enables the isolation of dynamic external perturbations from other pressure variations. For this purpose, a pressure-equalizing valve may be used to allow the equalization of slow changes in static pressures and the detection of higher frequency perturbations that might emanate from a target source.

Patent 5,637,865 Navy case 77,786 (Serial 08/668,620) filed 11 June 1996; issued 10 June 1997.

**Paul G. Kennedy
Willard Stevenson**

“Fiber-Optic Cable Junction”

A fiber-optic cable junction for joining the ends of two fiber-optic cables comprises the steps of inserting a tube fastener over each cable end and inserting a protective sleeve and a splint fastener over either cable end. The cable ends are then spliced together. The protective sleeve is positioned over the splice and is supported by fastening an inner splint rod to the cable buffer with the tube fasteners. The cable buffer is supported by an outer split rod fastened to the tube fasteners by the splint fastener.

Patent 5,642,451 Navy case 76,880 (Serial 08/579,711) filed 28 December 1995; issued 24 June 1997.

Richard J. Orazi

**“Method for Tuning Fiber-Optic
Couplers and Multiplexers”**

This patent application describes a way of tuning the wavelength response of fused and tapered optical-fiber couplers by exposing the fused region to high-intensity ultraviolet light, which permanently changes the index of refraction in the fused region and so alters the wavelength response of the device.

Patent 5,652,819 Navy case 77,012 (Serial 08/538,432) filed 9 August 1995; issued 29 July 1997.

**Wadad B. Dubbelday
Randy L. Shimabukuro
Stephen D. Russell**

**“Electroluminescent Devices
in Porous Silicon on Sapphire”**

This invention describes an electroluminescent Schottky or p-n diode device on silicon on sapphire and a method of manufacturing this device.

Patent 5,661,313 Navy case 75,291 (Serial 08/614,783) filed 8 March 1996; issued 26 August 1997.

Richard Scheps

“Er:YALO Upconversion Laser”

A novel technique for upconversion pumping is described that uses intracavity absorption to get 100-percent conversion efficiency.

Patent 5,682,397 Navy case 76,005 (Serial 08/565,075) filed 30 November 1995; issued 28 October 1997.

David W. J. Stein

**“A Method for Detecting Signals in
Non-Gaussian Background Clutter”**

This device detects (using only amplitude data) signals in nonstationary, non-Gaussian noise that may be modeled by using exponential mixture distributions.

Patent 5,694,342 Navy case 77,579 (Serial 08/742,413) filed 24 October 1996; issued 2 December 1997.

INDEPENDENT RESEARCH

Statutory Invention Registration (SIR) Issued

Frank E. Hanson

**“Cooling Device for
Solid-State Laser”**

A solid-state laser comprises a composite solid-state laser gain element. The gain element comprises an undoped section and a doped section having a concentration of dopant ions for absorbing pumping radiation. The doped section is diffusion-bonded to the undoped section to form an active region in the gain element. A cooling jacket conducts flowing coolant around the circumference of a portion of the gain element surrounding the active region.

SIR H1673 Navy case 76,103 (Serial 08/581,699) filed 29 December 1995, published 5 August 1997.

INDEPENDENT RESEARCH

Claims Allowed; Notice of Allowance

Richard Scheps

**“Laser Diode Wavelength and
and Beam Homogenizer”**

A laser-diode power combiner comprises a dye laser operably coupled to an array of laser diodes for combining optical power from the laser diodes into a single, coherent laser beam.

Navy case 77,221 (Serial 08/572,828) filed 14 December 1995; Notice of Allowance 31 October 1997.

Howard L. Dyckman

**“Spread Spectrum Modulation Using
Time-Varying Linear Filtering”**

This method for transmitting information by radio over a wide bandwidth comprises the following steps: inputting a data signal into a time-varying filter modulator; spreading the data signal in time and in frequency to produce a wide-band signal; modulating the sideband signal onto an RF carrier to provide an RF output signal; and transmitting the RF output signal. This step of spreading includes performing a series of linear transformations to the data signal.

Navy case 77,685 (Serial 08/621,400) filed 25 March 1996; Notice of Allowance 21 July 1997.

INDEPENDENT RESEARCH Patent Applications Filed

**Stanislaw J. Szpak
Pamela A. Boss**

**“Electrode and Method for Preparation of
Electrode for Electrochemical Compression
of Deuterium into a Metal Lattice”**

This invention provides an electrode and method for preparing the electrode that may be employed to electrochemically compress deuterium into a metal lattice of the electrode. An electrochemical cell is constructed that includes an electrolyte solution comprising a metallic salt and a supporting electrolyte. The metallic salt, when in a reduced state, absorbs deuterium. Both the electrolytic solution and supporting electrolyte are dissolved in heavy water. An anode and cathode are immersed and stable within the electrolytic solution. The anode is stable when polarized. A voltage is applied across the anode and cathode while a constant potential is maintained at the cathode. The constant potential is measured with respect to a reference electrode immersed within the electrolytic solution so that deposition of metallic ions occurs in the presence of evolving deuterium during electrolysis of the electrolytic solution. By this method, the cathode is transformed into the electrode.

Navy case 73,311 (Serial 07/632,896) filed 24 December 1990; pending.

**Stanislaw J. Szpak
Pamela A. Boss**

**“Electrochemical Cell Having a
Beryllium Compound Coated Electrode”**

This invention describes a procedure to modify metal-hydride electrodes so as to increase hydrogen storage capabilities as well as increase the cycling lifetime of the electrode. Such an invention improves the performance of fuel cells and/or rechargeable metal-hydride batteries.

Navy case 76,707 (Serial 08/969,175) filed 12 November 1997; pending.

Stephen D. Russell

**“Energy-Converting Porous Silicon
Optical Element”**

This invention describes an optical element made of porous silicon on a transparent substrate for converting light of an incident energy to that of a lower emitted energy. This invention may be used for the efficient detection of normally invisible and undetectable wavelengths.

Navy case 76,947 (Serial 08/812,680) filed 6 March 1997; pending.

Stephen D. Russell
Robert C. Dynes
Paul R. de la Houssaye
Wadad B. Dubbelday
Andrew Katz
Randy L. Shimabukuro

**“Silicon Nanostructures in
Silicon on Insulator”**

This invention discloses a variety of electrical, optical, mechanical, and quantum-effect devices on an insulating substrate and their method of fabrication for advanced electronic, optoelectronic, optical computing, and flat-panel display applications.

Navy case 76,969 (Serial 08/528,386) filed 13 September 1995; pending.

Richard Scheps

**“Underwater Imaging Technique for the
Detection of Shallow Submerged Objects”**

This high-resolution underwater imaging and ranging device scans an area underwater with a pulsed laser and records the reflected signal from the illuminated area with a gated photomultiplier.

Navy case 77,222 (Serial 08/908,778) filed 7 August 1997; pending.

Jerome F. DeJaco
Willard F. Rask

**“Impulsive Snap-through
Acoustic Projector (ISnAP)”**

An impulsive snap-through acoustic pulse generator may be used to generate an acoustic pulse in an aqueous environment without gas bubbles. The impulsive snap-through acoustic pulse generator includes a support structure having an open end, a resilient shell mounted to the support structure to define a chamber, and a gas vent in fluid communication with the chamber through which a gas passes for changing the pressure in the chamber so that the resilient shell transitions from a first stable state to a second stable state, thereby generating an acoustic pulse.

Navy case 77,245 (Serial 08/955,339) filed 21 October 1997; pending.

Allen Shum

**“Asynchronous Transfer Mode Cell
Loss Estimation Algorithms”**

A software program for estimating traffic loss of an asynchronous transfer mode (ATM) statistical multiplexer comprises a communication channel having traffic sources and a buffer. Traffic is generated by the traffic sources and removed by the communication channel. When total traffic exceeds the capacity of the communication channel, excess traffic is stored in the buffer. When the buffer is full, excess traffic is lost. Estimating the amount of traffic that will be lost by an ATM statistical multiplexer, therefore, has application in the design of ATM networks.

Navy case 77,443 (Serial 08/707,284) filed 3 September 1996; pending.

Michael J. Winton
Stephen D. Russell

**“Method of Making Improved
Electrical Contact to Porous Silicon”**

This is an improved method of making electrical contact to porous silicon and porous silicon device structures by controlling the global or large-scale surface morphology. The inventive process uses the supply of holes, ions of other charged species to control the etching dynamics of the porous silicon formation. The intensity of the light emitted by porous silicon layers and devices can therefore be increased by the improved electrical interconnection between the mechanically, chemically, and thermally fragile porous silicon and the device electrodes.

Navy case 77,603 (Serial 08/944,746) filed 6 October 1997; pending.

Monti E. Aklufi
Stephen D. Russell

**“Thin-Film Improvement Method
and Apparatus”**

This invention provides a novel apparatus and an improved method by using a contoured laser beam to improve the electrical, optical, and material properties of thin films.

Navy case 77,921 (Serial 08/934,037) filed 19 September 1997; pending.

Adi R. Bulsara
Mario E. Inchiosa
Luca Gammaitoni
Frank E. Gordon

**“Detector of Weak Signals Based on
Noise-Controlled Resonance Behavior in Nonlinear
Dynamic Systems with Broken Symmetry”**

This device exploits the dynamical symmetry-breaking property of a weak dc signal in an *a priori* symmetric nonlinear dynamic device, to detect and quantify the dc signal. Simultaneously, the technique offers a novel way to circumvent detector low-frequency noise constraints by shifting the detection to a more acceptable part of the frequency spectrum.

Navy case 78,154 (Serial 08/917,655) filed 25 August 1997; pending.

**Parviz Soltan
John A. Trias
Weldon J. Dahlke
Robert V. Belfatto
Frank Sanzone
Christopher J. Poulos
Neil P. Acantilado**

**“Computer-Controlled
Three-Dimensional
Volumetric Display”**

A three-dimensional display system comprises a display volume selectively partitioned into distinct display regions: a display surface for scattering light beams from the display volume; at least two optical scanners for modulating the light beams and for directing the light beams to the display surface within each distinct display region, respectively; and a display controller. The display controller comprises a world-coordinate interface for inputting world coordinates, a data processor for transforming the world coordinates into view coordinates and device coordinates, and an optical-scanner controller for sensing and controlling the motion of the display surface and for outputting the device coordinates to the optical scanners to generate a three-dimensional image within the display volume.

Navy case 78,445 (Serial 08/926,854) filed 10 September 1997; pending.

**Gregory A. Theriault
Leonard J. Martini
Leon V. Smith**

**“A Translation System
for Directing an Optical Signal
to Predetermined Coordinates”**

A translation system for directing an optical signal through predetermined coordinates of a window mounted in a soil penetration probe includes a tube having a sidewall and an aperture through said sidewall; an optically transparent window mounted in said aperture; an optical system for emitting an optical signal through said aperture; and a translation mechanism mounted within said tube. The translation mechanism may be selectively operated to translate independently and simultaneously the optical system along two orthogonal vectors so that the optical signal scans across the window. Scanning the optical signal extends the useful life of the window before its transmissibility becomes too impaired by damage caused from the optical signal.

Navy case 78,881 (Serial 09/015,431) filed 29 January 1998; pending.

INDEPENDENT RESEARCH Invention Disclosures Authorized

Willard M. Cronyn

**“Compact, Phasable, Multioctave,
Planar, High-Efficiency Spiral-Mode
Antenna”**

The antenna consists of eight planar windings, each one of which is an exponential spiral. The windings are connected in groups of three to a balanced transmission line, with a “floating” winding between each of the two groups. For the purpose of phasing elements together for directional-beam control, the particular grouping of windings can be changed. A sinuous variation is imposed on the spiral windings to increase the path length for each winding rotation so that the circumference through which the phase increases by 360 degrees is correspondingly decreased. This element integrates a planar structure, wide-band compact design, and phasability into a single physical structure.

Navy case 76,188; authorized for preparation of patent application 30 April 1997.

**Steven D. Russell
Shannon Kasa
Howard W. Walker**

**“Chemical Sensor Using Ring-
Oscillator Thermometry”**

This invention describes a novel structure using ring-oscillator thermometry for use as a chemical or biological sensor. Combustible gas sensors based on thermal sensors have been demonstrated in the prior art. These sensors, called pellistors, depend on a rise in temperature at a catalytic surface due to catalytic oxidation of the combustible gas. The pellistor measures this rise in temperature with a thermistor. The novel gas sensor incorporates a catalytic platinum layer deposited on top of a ring oscillator. Combustible gases will be catalytically oxidized at the platinum surface. The heat released by the reaction will cause local heating of the ring oscillator and thus, affect its frequency.

Navy case 76,462; authorized for preparation of patent application 11 July 1995.

Stephen M. Hart

**“Optoelectronically Controlled
Frequency-Selective Surface”**

A photovoltaic field-effect transistor (PVFET) is used to control the impedance, scattering frequency, and scattering cross-section of the scattering elements on a Frequency-Selective Surface. The PVFETs are implanted in the arms of either wire or slot scatterers to make their scattering properties adjustable. The resulting Optoelectronically Controlled Frequency-Selective Surface (OCFSS) becomes a programmable electromagnetic shield or pattern control device.

Navy case 76,915; authorized for preparation of patent application 26 March 1996.

Stephen M. Hart

“Optoelectronically Controlled Waveguide”

An Optoelectronically Controlled Waveguide (OCW) is composed of a metallic waveguide, a finline, and a PVFET. (A PVFET is a field-effect transistor with a gate controlled by a photovoltaic cell.) The finline is inserted into the waveguide making electrical contact, and the PVFET is affixed to the finline in a shunt configuration. The resulting device is capable of attenuating the energy propagating in the waveguide to any desired degree. In this fashion, the OCW can function as an attenuator or a switch.

Navy case 76,916; authorized for preparation of patent application 26 March 1996.

INDEPENDENT RESEARCH Invention Disclosures Submitted

Thomas W. Schlosser

**“A Spherical Coordinate Algorithm for the
Detection of Collisions between Three-
Dimensional Objects in Computer Models”**

This invention describes an algorithm for collision detection between three-dimensional objects in computer models that is more efficient and simpler than current algorithms. Current collision-detection algorithms rely either on testing for polygon intersections or attempt to solve multiple simultaneous polynomial equations to test for collision between surface patches on a three-dimensional model. All algorithms rely on Cartesian representations of the objects. A method using spherical coordinates, based on the relatively simple test for collision between spheres, provides a more efficient means of testing for collisions and is simple to calculate and implement after multiple rotations of the model.

Navy case 77,771; disclosure submitted 18 April 1996.

**Stephen D. Russell
Philip R. Kesten**

“Interactive Display Device”

This invention is a monolithically integrated display and sensor array that provides for interactive real-time changes to the display image.

Navy case 78,287; disclosure submitted 24 October 1996.

Stephen D. Russell
Randy L. Shimabukuro
Yu Wang

**“Transmissive Surface-
Plasmon Light Valve**

The invention provides a light valve or optical modulating device that exploits color-selective absorption at a metal-dielectric interface by surface plasmons. The invention includes an electrode layer formed of an optically transparent substrate. A layer of electro-optic material is formed on the electrode. The electro-optic material has an index of refraction that may be modulated by an electrical bias. A second electrode is formed over the electro-optic material. Changes in a voltage bias across the electrodes modulate the index of refraction of the electro-optic material so that it selectively absorbs light (at different wavelengths) that passes through the light valve, depending on the index of refraction. The electrodes are made of a transparent or semitransparent material, such as indium tin oxide. Multiple light valves may be arranged in an array to form a flat-screen video display.

The novelty of the invention is that it provides a new mode of operation in that it is a transmissive device, rather than a reflective device.

Navy case 78,518; disclosure submitted 18 April 1997.

Pamela A. Boss
Stephen H. Lieberman

**“The Use of Microelectrode
Arrays for the Detection of
Volatile Organic Contaminants
in the Air”**

The invention is used to detect organic contaminants in the gas phase. The invention comprises a working electrode separated from an auxiliary electrode by an insulator. The electrodes are coated with self-assembled monolayers, and a voltage bias is applied across the electrodes while the resulting current is measured. The electrode materials and monolayers are selected so that when a gaseous analyte of interest contacts the electrodes, the current changes by a detectable amount. Multiple microelectrodes may be configured into arrays whereby each microelectrode is responsive to a particular analyte. In this way, many different gaseous contaminants may be detected with a single instrument. The microelectrodes may be fabricated onto chips using photo-lithographic techniques.

An important novelty of the invention is that it provides an instrument capable of monitoring contaminants over time and provides the real-time detection of drugs and explosives. The use of the self-assembled monolayers as a coating to enhance the response of the electrodes is novel.

Navy case 78,928; disclosure submitted 1 December 1997.

David W. J. Stein

“Coherent Hidden-Markov Detector”

This method for processing coherent radar-return data detects targets in nonstationary radar clutter. Advantages and new features of this method over Doppler processing include modeling the clutter using Markov models and applying a phase-coherent detection statistic based on a likelihood ratio that allows for the clutter level to fluctuate over the duration of the time series being analyzed.

Navy case 78,933; disclosure submitted 17 December 1997.

**Stephen D. Russell
Randy L. Shimabukuro
Yu Wang**

“Microdynamic Optical Device”

This invention describes a light valve, display, optical modulating device or optical filter that uses a microdynamic construction to exploit the color-selective absorption at a metal-dielectric interface by surface plasmons.

Navy case 78,968; disclosure submitted 19 November 1997.

Carol A. Becker

“Light-Activated Polymeric Actuators”

Visible light causes a pH charge *in situ* to the polymer backbone. The pH charge expands and contracts the polymeric actuator in a timeframe suitable for robotics. A mechanism is provided for reversible dissipation of any heat produced by the light.

Navy case 78,990; disclosure submitted 13 January 1998.

**Stephen D. Russell
Randy L. Shimabukuro
Yu Wang**

“Solid-State Light Valve and Tunable Filter”

This invention describes an all solid-state light valve, optical modulating device or optical filter that uses color-selective absorption at a metal-dielectric interface by surface plasmons.

SSC SD-283; disclosure submitted 3 November 1997.

David W. J. Stein

“Hidden-Markov Amplitude Detector”

This invention provides a means of detecting incoherent signals in non-Gaussian noise.

SSC SD-293; disclosure submitted 17 December 1997.

Richard Scheps

“Compact Solid-State Dye Laser”

This invention describes a compact solid-state dye laser that is diode-pumpable. The laser in its preferred embodiment consists of a monolithic state of materials including a solid-state 1- μ -emitting laser gain element, a passive Q-switch, a second-harmonic doubling crystal, and the solid-state dye gain element.

SSC SD-294; disclosure submitted 12 January 1998.

INDEPENDENT EXPLORATORY DEVELOPMENT
Claims Allowed; Notice of Allowance

Everett W. Jacobs
Roger D. Boss
Yuval Fisher

**“Method of Encoding a
Digital Image by Using Adaptive
Partitioning in an Iterated
Transformation System”**

This invention is a new adaptive method for partitioning an image, resulting in efficient encoding by using the iterated transformation image-compression technique.

Navy case 74,198 (Serial 07/859,782) filed 30 March 1992; Notice of Allowance 15 May 1996.

Stephen D. Russell
Wadad B. Dubbelday
Randy L. Shimabukuro
Paul de la Houssaye
Diane M. Szarflarski

**“Photonic Silicon on a
Transparent Substrate”**

This invention describes light-emitting (photonic) silicon on a transparent substrate and its method of fabrication.

Navy case 75,292 (Serial 08/118,900) filed 9 September 1993; Notice of Allowance 4 September 1996.

INDEPENDENT EXPLORATORY DEVELOPMENT
Patent Applications Filed

Neil P. Acantilado

**“Computer Program for a Three-
Dimensional Volumetric Display”**

This method for transforming world coordinates into device coordinates comprises the following steps: inputting a set of world coordinates to be displayed; scaling the world coordinates into view coordinates bounded by a display volume; finding a control memory location of a light-beam deflector corresponding to a Y-axis position for each of the view coordinates; calculating X-axis and Z-axis device coordinates from the view coordinates for deflecting a light beam to a selected point within the display volume, corresponding to each of the view coordinates; and loading the device coordinates into the control memory locations corresponding to the Y-axis position for each of the view coordinates, to cause the light beam to be deflected to each selected point.

Navy case 77,782 (Serial 08/726,305) filed 2 October 1996; pending.

**Pamela A. Boss
Roger D. Boss**

**“Versatile, Thin-Layer Cell for
In-Situ Spectroelectrochemistry”**

This invention describes the design of a low-volume, thin-layer cell constructed of chemically resistant materials capable of performing spectroelectrochemistry. Such a cell can be used as a flow-through cell to continuously monitor manufacturing processes.

Navy case 77,803 (Serial 08/900,983) filed 25 July 1997; pending.

PROJECT TABLES

**NRaD (now SSC San Diego) FY 97 Independent Research Database
0601152N**

Work Unit Identification		Project Title	Principal Investigator			ONR SE#	DoD MA	JMA	DoD CT	Keywords	FY 96 Funds \$K	FY 97 Funds \$K	Status/Planned FY 98 Funds \$K
NRaD PROJ #	DTIC DN#												
ZU43	306750	Generalized Higher Order Crossings Theory and Practice	Barnett, J.T.			14	MWT CCC	4	6	level-crossings; higher order crossings; parametric filtering; fixed-point theory	0	93	110
ZU25	305519	Array Processing with Three-Dimensional (3-D) Bathymetry	Baxley, P.			31	ASW OSV	3	19	array processing; underwater acoustic propagation; matched field	65	66	60
ZU20	305514	Important Perceptual Features for Speaker Identity	Bemis, S.			42	CCC INT	4	6	speaker identity	97	89	COMPL
ZU30	305524	Development of Ultramicroelectrode (UME) Arrays for Use in a Remote Probe	Boss, P.A.			13	FSO	7	12	UME array; gas phase; sensors; electrochemistry	102	82	60
ZU41	306763	Active Matched-Field Tracking (AMFT) for Automatic Detection of Sonar or Radar Targets	Bucker, H.			14	OSV ASW	3	19	underwater sound	0	73	COMPL
ZU03	305312	Stochastic Resonance Detectors	Bulsara, A.			14	ASW	3	19	stochastic resonance; detection probability	78	115	TRANS
ZU42	306751	ISAR Scatter Location for Complex Targets via Direction-Finding/Beamforming Methods	Chou, S.I.			14	OSV AAW	3	19	array processing; scatterer location; radar target imaging	0	86	COMPL
ZU44	306749	Impulsive Snap-through Acoustic Projector (ISnAP)	DeJaco, J.			11	OSV ASW	3	19	impulsive acoustic force; snap-through	0	88	55
ZU26	305520	Acoustic Data Analysis Using Fourth-Order Cumulants	Edelblute, D.			14	ASW OSV	3	19	cumulant procession; higher order moments	63	69	COMPL
ZU06	305322	Enhancing SmartNet for Scheduling Network Traffic	Freund, R.			15	CCC	4	7	heterogenous computing; code profiling; algorithmic analysis; smartnet	146	142	COMPL
ZU07	305301	Relational Event Algebra Extensions	Goodman, I.R.			14	CCC	4	6	data fusion; event metrics; decision theory; relational event algebras	199	148	COMPL
ZU45	306755	Solid-State Blue Laser Development	Hanson, F.E.			11	MIW CCC	3	19	lasers; nonlinear optics; neodymium	0	83	70

NOTES: SE = Subelement (codes); MA = Mission Area; JMA = Joint Mission Area (codes); CT = Critical Technology (codes); COMPL = Completed; TRANS = Transitioned
See Glossary for numbered codes and other abbreviations.

**NRaD (now SSC San Diego) FY 97 Independent Research Database
0601152N (continued)**

Work Unit Identification		Project Title	Principal Investigator			ONR SE#	DoD MA	JMA	DoD CT	Keywords	FY 96 Funds \$K	FY 97 Funds \$K	Status/Planned FY 98 Funds \$K
NRaD PROJ #	DTIC DN#												
ZU53	306770	Exact Diagonalization of Many Body Hamiltonians	Hicks, C.			11	MWT CCC	4	6	high-performance computing; large matrix diagonalization	0	27	40
ZU35	305529	Solution of Sparse Indefinite Systems in Least Squares and Optimization	Kevorkian, A.			14	MWT	3	22	least squares; sparse matrices; indefinite systems; nonlinear programming	74	99	84
ZU51	306761	Investigation of Shallow Momentumless Wakes	Ladd, D.			31	FSO MWT	7	19	free surface hydrodynamics; momentumless wakes	0	45	COMPL
ZU52	306759	Determination of the Boundary Shear Stress Required for Sediment Resuspension	Mautner, T.			35	FSO MWT	7	12	sediment; shear stress	0	45	80
ZU34	305528	Segmentation of Independent Motion via Pattern Recognition of Motion Flow in the Log-Polar Transformed Domain	Nguyen, H.G.			15	MWT FSO	7	19	pattern recognition; motion segmentation; log-polar mapping	111	69	COMPL
ZU49	306754	Photonic Switching Based on Index of Refraction Changes in Highly Overcoupled Fused-Fiber Couplers	Orazi, R.			11	CCC	4	6	fiber gyroscopes; amplified spontaneous emission; wavelength stability	0	51	TRANS
ZU12	305318	Performance Analysis of Multichannel Adaptive Equalization for Line-of-Sight (LOS) Digital Radio	Reuter, M.			14	CCC	4	6	adaptive equalization; interference suppression; channel fading; jamming	78	114	COMPL
ZU48	306760	Propwash/Wake Resuspension in San Diego Bay—The Grand Plan	Rohr, J.			35	FSO MWT	7	12	critical shear stress; resuspension	0	76	80
ZU47	306756	Surface Plasmon Flat-Panel Display	Russell, S.D.			21	CCC	4	6	flat-panel display; surface plasmon	0	137	135
ZU14	305320	High-Modulation-Rate, Solid-State Surveillance Laser	Scheps, R.			11	MIW CCC	2	19	dye lasers; diode-pumped; polymers; solid-state lasers	97	24	COMPL
ZU21	305515	H [∞] Waves: A New Approach to Estimating EM Fields	Schwartz, D.F.			12	CCC FSO	4	6	H-infinity methods; antenna design; impedance estimation	140	117	105
ZU50	306762	Biosonar Ensonification of Buried Mines	Sigurdson, J.			11	MIW	2	19	biosonar; detection; mines	0	63	35

NOTES: SE = Subelement (codes); MA = Mission Area; JMA = Joint Mission Area (codes); CT = Critical Technology (codes); COMPL = Completed; TRANS = Transitioned
See Glossary for numbered codes and other abbreviations.

**NRaD (now SSC San Diego) FY 97 Independent Research Database
0601152N (continued)**

Work Unit Identification		Project Title	Principal Investigator			ONR SE#	DoD MA	JMA	DoD CT	Keywords	FY 96 Funds \$K	FY 97 Funds \$K	Status/Planned FY 98 Funds \$K
NRaD PROJ #	DTIC DN#												
ZU39	306758	Resonantly Enhanced EHF Optoelectronic Transceiver Components	Sun, C.K.			11	CCC MWT	4	6	fiber-optic link; optoelectronic transceiver	0	123	115
ZU24	305518	Algebraic-Geometric Error Control Coding for Improved Performance of Naval High-Data-Rate Line-of-Sight and Satellite Communications Systems	Wahlen, B.E.			14	CCC	4	6	error control coding; algebraic curves; error bursts	97	112	COMPL
ZU38	306748	Faster-Than-Real-Time Synthetic Forces (FTRT SF) Simulation	Wallace, J.W.			15	FSO MWT	8	24	parallel processing; modeling and simulation; time warp; synthetic forces	0	124	TRANS
ZU23	305517	Constant Envelope Modulation Techniques for UHF SATCOM	Watkins, B.E.			12	CCC	4	6	RF amplifier; neural networks; amplifier predistortion	97	83	TRANS
ZU36	306757	Reflective Memory on Standard Local Area Networks	Wilcox, D.R.			15	CCC	4	6	reflective memory; local area networks	0	79	COMPL

NOTES: SE = Subelement (codes); MA = Mission Area; JMA = Joint Mission Area (codes); CT = Critical Technology (codes); COMPL = Completed; TRANS = Transitioned
See Glossary for numbered codes and other abbreviations.

**SSC San Diego FY 98 Independent Research Database
0601152N**

Work Unit Identification		Project Title	Principal Investigator			ONR SE#	DoD MA	JMA	DoD CT	Keywords	FY 96 Funds \$K	FY 97 Funds \$K	Planned FY 98 Funds \$K
SSC SD PROJ#	DTIC DN#												
ZU54	307777	3-D Propagation in Shallow Water Overlaying an Elastic Bottom	Abawi, A.			14	ASW OSV	2	19	propagation; parabolic equation model; coupled mode	0	0	80
ZU43	306750	Generalized Higher Order Crossings Theory and Practice	Barnett, J.T.			14	MWT CCC	4	6	level crossing; higher order crossing; parametric filtering; fixed-point theory	0	93	110
ZU25	305519	Array Processing with 3-D Bathymetry	Baxley, P.			31	ASW OSV	3	19	array processing; underwater acoustic propagation; matched-field processing	65	66	60
ZU30	305524	Development of Ultramicroelectrode (UME) Arrays for Use in a Remote Probe	Boss, P.A.			13	FSO	7	12	UME array; gas phase; sensors; electrochemistry	102	82	60
ZU55	307778	Environmentally Adaptive Autonomous Matched-Field Tracking	Bucker, H.			14	OSV ASW	3	19	underwater sound; signal processing	0	0	68
ZU65	307790	Stochastic Resonance for Communications	Bulsara, A.			14	CCC	4	6	stochastic resonance; receivers	0	0	130
ZU44	306749	Impulsive Snap-through Acoustic Projector (ISnAP)	DeJaco, J.			11	OSV ASW	3	19	impulsive acoustic source; snap-through	0	88	55
ZU56	307779	Robust Control and Identification of Multiclass Queuing Systems for C4I	Freund, R.			15	CCC	4	7	distributed computing; scheduling; multiclass queuing	0	0	187
ZU57	307780	Anti-Ice Coatings: New Low-Surface, Free-Energy Coatings for Easy Ice Release	George, R.D.			13	MOB	8	17	polymers; coatings; ice-release; environmental; anti-ice	0	0	90
ZU58	307781	Algebraic Estimation of Multivalued Phenomena with Applications to Data Fusion	Goodman, I.R.			14	CCC	4	6	data fusion; expectation of random sets; generalized estimation; relational event algebras	0	0	185
ZU45	306755	Solid-State Blue Laser Development	Hanson, F.E.			14	MIW CCC	3	19	lasers; nonlinear optics; neodymium	0	83	70
ZU53	306770	Exact Diagonalization of Large Sparse Matrices	Hicks, C.			11	MWT CCC	4	6	high-performance computing; large matrix diagonalization	0	27	40

NOTES: SE = Subelement (codes); MA = Mission Area; JMA = Joint Mission Area (codes); CT = Critical Technology (codes); COMPL = Completed; TRANS = Transitioned
See Glossary for numbered codes and other abbreviations.

**SSC San Diego FY 98 Independent Research Database
0601152N (continued)**

Work Unit Identification		Project Title	Principal Investigator			ONR SE#	DoD MA	JMA	DoD CT	Keywords	FY 96 Funds \$K	FY 97 Funds \$K	Planned FY 98 Funds \$K
SSC SD PROJ#	DTIC DN#												
ZU35	305529	Sparse QR Factorization with Column Pivoting as Applied to Target-Strength Prediction	Kevorkian, A.			14	MWT	3	22	least squares; sparse matrices; indefinite systems; linear and nonlinear programming	74	99	84
ZU52	306759	Determination of the Boundary Shear Stress Required for Sediment Resuspension	Mautner, T.			35	FSO MWT	7	12	sediment; shear stress	0	45	80
ZU59	307782	Fiber-Optic Add/Drop Multiplexers Produced by Writing Gratings on Fused-Fiber Tapered Couplers	Orazi, R.			11	CCC	4	6	wavelength division multiplexing; Bragg gratings; fused-fiber couplers	0	0	90
ZU60	307783	Performance Analysis of Single and Multichannel Adaptive Equalizers	Reuter, M.			14	CCC	4	6	adaptive equalization; line-of-sight digital radio; multichannel equalization; channel fading; interference	0	0	105
ZU61	307784	Telesonar Channel Measurements and Models	Rice, J.A.			31	CCC	2	19	underwater acoustic propagation; transmission channels; propagation models; telesonar; sound scattering	0	0	105
ZU48	306760	Propwash/Wake Resuspension in San Diego Bay—The Grand Plan	Rohr, J.			35	FSO MWT	7	12	critical shear stress; resuspension	0	76	80
ZU47	306756	Surface-Plasmon, Flat-Panel Display	Russell, S.D.			21	CCC	4	6	flat-panel display; surface plasmon	0	137	135
ZU21	305515	H [∞] Impedance Matching Broadband Antennas	Schwartz, D.F.			12	CCC FSO	4	6	H-infinity methods; antenna design; impedance estimation	140	117	105
ZU50	306762	Biosonar Ensonification of Buried Mines	Sigurdson, J.			11	MIW	2	19	biosonar; detection; mines	0	63	35
ZU39	306758	Resonantly Enhanced EHF Electroabsorption Modulator with a Novel Back-to-Back Diode Structure	Sun, C.K.			11	CCC MWT	4	6	fiber-optic link; optoelectronic transceiver	0	123	115
ZU62	307785	Pixon-Based Image Reconstruction from Inverse Synthetic Aperture Radar Data	Trischman, J.			14	OSV	3	19	radar; ISAR; imaging; PIXON; Bayesian; target identification	0	0	90

NOTES: SE = Subelement (codes); MA = Mission Area; JMA = Joint Mission Area (codes); CT = Critical Technology (codes); COMPL = Completed; TRANS = Transitioned
See Glossary for numbered codes and other abbreviations.

**SSC San Diego FY 98 Independent Research Database
0601152N (continued)**

Work Unit Identification		Project Title	Principal Investigator			ONR SE#	DoD MA	JMA	DoD CT	Keywords	FY 96 Funds \$K	FY 97 Funds \$K	Planned FY 98 Funds \$K
SSC SD PROJ#	DTIC DN#												
ZU63	307786	Development and Analysis of Turbo Codes for Navy Applications	Wahlen, B.E.			14	CCC	4	6	forward error correction; turbo codes; trellis-coded modulation	0	0	105
ZU64	307787	Using IMPORT to Implement Complex Behaviors in Simulations	Wallace, J.			15	CCC	4	7	modeling and simulation forces	0	0	187

NOTES: SE = Subelement (codes); MA = Mission Area; JMA = Joint Mission Area (codes); CT = Critical Technology (codes); COMPL = Completed; TRANS = Transitioned
See Glossary for numbered codes and other abbreviations.

GLOSSARY

GLOSSARY

ADCP	Acoustic Doppler Current Profiler
Ag	silver
AG	algebraic-geometric
AIP	American Institute of Physics
AMFT	active matched-field tracking
AMGSSS	Air-Mobile Ground Surveillance and Security System
AMLCD	active-matrix liquid-crystal device
ANDM	Applied Nonlinear Dynamics near the Millennium
AODS	All-Optical Deployable System
APL	Applied Research Laboratory
ASA	Acoustical Society of America
ASE	amplified spontaneous emission
ASJ	Acoustical Society of Japan
ASTO	Advanced Submarine Technology Office
ASW	antisubmarine warfare
ATM	asynchronous transfer mode
Au	gold
AWGN	additive white Gaussian noise
BPSK	binary phase shift keying
C ²	command and control
C ³ I	command, control, communications, and information
CAD	computer-aided design
CAOTA	Common All-Optical Towed Array
C/Au	carbon/gold
CFSK	continuous frequency shift keying
COASTeR	Collaborative, Object-oriented Advanced Simulation Technology Research
COTS	commercial off-the-shelf
CPM	continuous phase modulation
CPU	central processing unit
CRADA	Cooperative Research and Development Agreement
CRT	cathode ray tube
CTD	conductivity, temperature, and depth
1-D	one-dimensional
2-D	two-dimensional
DARPA	Defense Advanced Research Projects Agency
dc	direct current
DDR&E	Director, Defense Research and Engineering
DISA	Defense Information Systems Agency
DMD	digital mirror device

DoD CT	Department of Defense Critical Technology
Codes	
1	Aerospace Propulsion and Power
2	Air Vehicles
3	Space Vehicles
4	Chemical and Biological Defenses
5	Clothing, Textiles, and Food
6	Command, Control, and Communications
7	Computers
8	Conventional Weapons
9	Electronics
10	Electronic Warfare
11	Directed Energy Weapons
12	Environmental Quality
13	Civil Engineering
14	Battlespace Environments
15	Human–System Interfaces
16	Manpower, Personnel, and Training
17	Materials, Processes, and Structures
18	Biomedical
19	Sensors
20	Surface/Undersurface Vehicles
21	Ground Vehicles
22	Software
23	Manufacturing Science and Technology
24	Simulation and Modeling Technology

DoD MA	Department of Defense Mission Area
AAW	Anti-Air Warfare
AMW	Amphibious Warfare
ASU	Anti-Surface Ship Warfare
ASW	Anti-Submarine Warfare
CCC	Command, Control, and Communications
ELW	Electronic Warfare
FSO	Fleet Support Operations
INT	Intelligence
LOG	Logistics
MIW	Mine Warfare/Mine Countermeasures
MOB	Mobility
MWT	Multi-Warfare Technology
OSV	Ocean Surveillance
PMD	Personnel/Medical
SBS	Sea-Based Strategic Warfare
SPW	Special Warfare

STW	Strike Warfare
TNG	Training
EA	electroabsorption
EAST	Environmentally Adaptive Sonar Technology
EHF	extremely high frequency
EM	electromagnetic
ETDM	extension of the standard theory of decision making
EUTELSAT	European Telecommunications Satellite Organization
EWS	electronic workstations
FEC	forward error correction
FTRT SF	Faster-Than-Real-Time Synthetic Forces
GGP	GPS Guidance Package
GOTS	Government-Off-The-Shelf
GPS	Global Positioning System
HF	high frequency
HOCs	Higher Order Crossings
HP	Hewlett-Packard
HPA	high-power amplifier
HPCMP	High-Performance Computing Modernization Program
HT	high temperature
ICASSP	International Conference on Acoustics, Speech, and Signal Processing
IED	Independent Exploratory Development
IEE	Institution of Electrical Engineers (British)
IEEE	Institute of Electrical and Electronic Engineers
IFOG	Interferometric Fiber-Optic Gyroscope
ILIR	In-house Laboratory Independent Research
INTELSAT	International Telecommunications Satellite
IR	Independent Research
IRIS	Infrared Information Symposium
IRS&T	infrared search and track
ISAR	Inverse Synthetic Aperture Radar
ISnAP	Impulsive Snap-through Acoustic Projector
IT-21	Information Technology for the 21st Century
JIEO	Joint Interoperability Engineering Organization
JMA	Joint Mission Area
Codes	
1	Joint Strike
2	Joint Littoral Warfare
3	Joint Surveillance
4	Joint Space and Electronic Warfare/Intelligence
5	Strategic Deterrence

6	Strategic Sealift and Protection
7	Forward Presence
8	Readiness, Support, and Infrastructure
9	Manpower and Personnel
JPL	Jet Propulsion Laboratory
JSIMS	Joint Simulation System
ladar	laser radar
LAPACK	Linear Algebra PACKage
LOS	line of sight
MAEQ	multichannel adaptive equalization
MANTECH	Manufacturing Technology
MFP	matched-field processing
MILCOM	Military Communications
MMIC	monolithic microwave integrated circuit
MMSE	minimization of the mean square error
MOCVD	metal-organic chemical vapro deposition
MPEG	Moving Pictures Expert Group
M-PSK	M-ary phase shift keying
M-QAM	M-ary quadrature amplitude modulation
MRI	Mark Resources, Inc.
MSK	minimum shift keying
NASA	National Aeronautics and Space Administration
NAVAIR	Naval Air Systems Command
NAVSEA	Naval Sea Systems Command
NCSC	Naval Coastal Systems Center
NIST	National Institute of Standards and Technology
NP	Nevanlinna-Pick
NRL	Naval Research Laboratory
NUWC	Naval Undersea Warfare Center
OCFSS	optoelectronically controlled frequency-selective surface
OCW	optoelectronically controlled waveguide
ONR	Office of Naval Research
ONR SE	Office of Naval Research Subelement
Codes	
11	General Physics
12	Radiation Sciences
13	Chemistry
14	Mathematics
15	Computer Science
21	Electronics
22	Materials
23	Mechanics

24	Energy Conversion
31	Ocean Sciences
32	Ocean Geophysics
33	Atmospheric Sciences
34	Astronomy and Astrophysics
35	Environmental Science
41	Biological and Medical Sciences
42	Cognitive and Neural Sciences
52	Multidisciplinary Support
ORMOSIL	organically modified silicates
OS	ocean sciences
PC	personal computer
Pe	probability of error
PINC	polarization-independent narrow-channel
PS	product space
PVFET	photovoltaic field-effect transistor
QAM	quadrature amplitude modulation
QPSK	quadrature phase shift keying
QTSR	Quick Threads Simulation Runtime
RF	radio frequency
Rh/Al	rhodium/aluminum
RS	Reed–Solomon
RV	research vessel
SAIC	Science Applications International Corporation
SAM	self-assembled monolayer
SAR	Synthetic Aperture Radar
SATCOM	satellite communications
SBIR	Small Business Innovation Research
SBPSK	shaped binary phase shift keying
SCS	Society for Computer Simulation
SERS	surface-enhanced Raman spectroscopy
SHF	super high frequency
SIAM	Society of Industrial and Applied Mathematics
SIO	Scripps Institution of Oceanography
SIR	signal-to-interference ratio
	Statutory Invention Registration
SPEEDES	Synchronous Parallel Environment for Emulation and Discrete-Event Simulation
SPIE	Society of Photo-Optical Instrumentation Engineers (also known as The International Society for Optical Engineering)
SQUID	Superconducting Quantum Interference Device
SR	stochastic resonance

SSC San Diego	Space and Naval Warfare (SPAWAR) Systems Center, San Diego
STO	Sensor Technology Office
STOW	Synthetic Theater of War
SUNY	State University of New York
SURTASS	Surveillance Towed Array Sensor System
SW/VSW	shallow water/very shallow water
TCM	Trellis Coded Modulation
TRANSDEC	Transducer Evaluation Center
TSA	Two-Scatterer Algorithm
UCSD	University of California at San Diego
UDP	User Datagram Protocol
UHF SATCOM	ultra-high-frequency satellite communications
UME	ultramicroelectrode
USC	University of Southern California
VLA	vertical-line array
WDM	wavelength division multiplexer

Public reporting burden for this collection of information is estimated to average 1 hour per response, including the time for reviewing instructions, searching existing data sources, gathering and maintaining the data needed, and completing and reviewing the collection of information. Send comments regarding this burden estimate or any other aspect of this collection of information, including suggestions for reducing this burden, to Washington Headquarters Services, Directorate for Information Operations and Reports, 1215 Jefferson Davis Highway, Suite 1204, Arlington, VA 22202-4302, and to the Office of Management and Budget, Paperwork Reduction Project (0704-0188), Washington, DC 20503.

1. AGENCY USE ONLY (Leave blank)		2. REPORT DATE April 1998	3. REPORT TYPE AND DATES COVERED Final: October 1996 through September 1997	
4. TITLE AND SUBTITLE INDEPENDENT RESEARCH 1997 ANNUAL REPORT			5. FUNDING NUMBERS In-house	
6. AUTHOR(S)				
7. PERFORMING ORGANIZATION NAME(S) AND ADDRESS(ES) Space and Naval Warfare Systems Center San Diego, CA 92152-5001			8. PERFORMING ORGANIZATION REPORT NUMBER	
9. SPONSORING/MONITORING AGENCY NAME(S) AND ADDRESS(ES) Office of Naval Research 800 North Quincy Street Arlington, VA 22217-5000			10. SPONSORING/MONITORING AGENCY REPORT NUMBER TD 2987	
11. SUPPLEMENTARY NOTES				
12a. DISTRIBUTION/AVAILABILITY STATEMENT Approved for public release; distribution is unlimited.			12b. DISTRIBUTION CODE	
13. ABSTRACT (Maximum 200 words) The work detailed in this report was carried out in FY 97 as part of the Office of Naval Research In-house Laboratory Independent Research (ILIR) program. Summaries of the projects are presented, and three projects are described in detail: Magnetic Signal Detection Using Stochastic Resonance in a Radio Frequency (rf) Superconducting Quantum Interference Device (SQUID); Decision Theory Augmented by Natural Event Metrics with Applications to Data Fusion; and Performance Analysis of Multichannel Adaptive Equalization (MAEQ) for Line-of-Sight Digital Radio.				
14. SUBJECT TERMS AND MISSION AREAS command and control communications surveillance other leadership areas in-house laboratory independent research (ILIR)			15. NUMBER OF PAGES 212	
			16. PRICE CODE	
17. SECURITY CLASSIFICATION OF REPORT UNCLASSIFIED	18. SECURITY CLASSIFICATION OF THIS PAGE UNCLASSIFIED	19. SECURITY CLASSIFICATION OF ABSTRACT UNCLASSIFIED	20. LIMITATION OF ABSTRACT SAME AS REPORT	

EXTERNAL DISTRIBUTION

Air Force Office of Scientific Research
Bolling AFB, DC 20332-0001

Center for Naval Analysis
Alexandria, VA 22302-0268

Coastal Systems Station
Panama City, FL 32407-7001

Defense Advanced Research
Projects Agency
Arlington, VA 22203-1700

Defense Research and Engineering (3)
Washington, DC 20301-3030

Defense Technical (2)
Information Center
Fort Belvoir, VA 22060-6218

Federal Contracts Research Center
Ft. Monmouth, NJ 07703-5027

Government-Industry Data Exchange
Program (GIDEP) Operations Center
Corona, CA 91718-8000

Naval Air Warfare Center
Aircraft Division
Patuxent River, MD 20670-1161

Naval Air Warfare Center
Weapons Division
China Lake, CA 93555-6001

Naval Facilities Engineering Service Center
Port Hueneme, CA 93043-4370

Naval Medical Research and
Development Command
Bethesda, MD 20889-5606

Navy Personnel Research and
Development Center
San Diego, CA 92152-6800

Naval Postgraduate School (6)
Monterey, CA 93943-5001

Naval Research Laboratory
Washington, DC 20375-5320

Naval Sea Systems Command
Arlington, VA 22242-5160

Naval Surface Warfare Center
Arlington, VA 22242-5160

Naval Surface Warfare Center
Carderock Division
West Bethesda, MD 20817-5700

Naval Surface Warfare Center
Carderock Division Detachment
Annapolis, MD 21402-1198

Naval Surface Warfare Center
Dahlgren Division
Dahlgren, VA 22448-5100

Naval Undersea Warfare Center
Newport, RI 02841-1708

Naval Undersea Warfare Center Division
Newport, RI 02841-5047

Navy Acquisition, Research and Develop-
ment Information Center (NARDIC)
Arlington, VA 22214-5114

Office of Naval Research (24)
Arlington, VA 22217-5660

Space and Naval Warfare Systems (2)
Command
San Diego, CA 92110-3127

SPAWARSYSCEN Washington Liaison
Office
Arlington, VA 22202-4804

U. S. Army Laboratory Command
Ft. Monmouth, NJ 07703-5302

U.S. Naval Academy
Annapolis, MD 21402-5000